The University Of Sheffield.

AN EXPERIMENTAL STUDY ON THE FRACTURE BEHAVIOUR OF TOUGHENED RESINS UNDER MIXED MODE LOADS

By:

Nithiananthan Kuppusamy

A thesis submitted in partial fulfilment of the requirements for the degree of Doctor of Philosophy

The University of Sheffield

Department of Mechanical Engineering

February 2021

Abstract

Improving the fracture toughness of materials particularly by particulate toughening mechanisms is an area that has generated a lot of commercial interest in the recent years. Reports have shown that infusion of particles in the inter-laminar and intra-laminar region improves material performance by several orders of magnitude. However, detailed characterisation of particle induced toughening mechanisms in mixed-mode remains complex and calls further exploration.

The sponsoring organization of this project (Cytec Engineered Materials Ltd) conducts advanced research in developing methodologies that characterize fracture behaviour of particulate toughened polymers. This study has developed a novel, repeatable pre-crack initiation tool that produces a consistent, sharp pre-crack of a specified length, orientation and crack front in a consistent and safe manner. This tool facilitates high through-put characterisation of fracture behaviour in toughened polymers. The Compact Tension Mixed Mode modified (CTMMM) specimen and grips designed in this study provide less constraint at the pin loading points and hence facilitate ‘pure’ mode I, mode II and mixed mode I&II testing. A range of unmodified and particle toughened resins were subjected to fracture testing in these loading modes. Displacement fields around the tip of the crack were determined by 2D Digital Image Correlation (DIC) and fracture parameters were evaluated using in-house software (DICITAC).

The combined preparation and testing methodology using 2D DIC and the fracture parameter extraction methods have proved to be an efficient and effective way to screen different resin formulations. Results show that in unmodified and particle-modified resins, the type and concentration of particle (% weight loading) influences fracture toughness of a resin and determines its behaviour in mixed mode I and II. Further, it is shown that strain energy and

behaviour of resin modified composites are also influenced by particle weight loading concentrations of the resin systems incorporated in them.

Acknowledgements

Firstly, I want to express my deepest gratitude for my supervisor, Dr Rachel A Tomlinson; for her undivided attention, tireless support and guidance. I want to thank her for providing me support that is above and beyond what I can imagine and training me into a scientist. Rachel has been the greatest mentor for me, and I feel privileged with great pleasure to have worked with.

Secondly, Mr Richard Kay for helping me with specimen preparation and support with all my experimental work. I have learned a lot from him and gained a high level of fabrication knowledgeable. Thank you, Richard, for being patient with me and in machining countless specimens and grips, and for dealing with all the work I've lumbered you with over the last three years. I would like to thank my other supervisor Dr Joel Foreman, for imparting his knowledge and supporting me. I would like to thank Dr Mohammed Mostafavi, for imparting his knowledge and support during my Ph.D.

I would like to thank Dr Stephen Jones for imparting his knowledge and training me on experimental techniques and engaging in scientific discussions. Thank you for all the help in getting the project started and for all the tips and tricks that you have helped me.

I would like to thank all the people who helped me throughout this project.

I would like to thank Dr Mohammed Zanganeh for providing me the developed tools and if not this project would be very different. I would like to thank my research group, the Composite Systems Innovation Centre, for the interesting discussion and a joyous time in the office; Panos, Alon, Teddy, Mulyadi, Ioannis, Khaled, Diyar and everyone else.

I would like to thank the Department of Mechanical Engineering, Cytec Engineered Materials and the EPSRC for the continuing to fund.

I would like to thank my best friends Michael Lee for putting up with my whining and believing in me.

I would like to thank my father Vejayan, mother Saraswathy and Grandmother Meenachi for their support on every aspect of my life.

Lastly, I would like to thank my wonderful wife Sadhvi and loving son Mitunand, words cannot express how grateful I am for all their support.

Contents

List of Figures

Acronyms

ASTM	American Society for Testing and Materials
BS ISO	British and International Standard Organisation
CAD	Computer Aided Design
CFRP	Carbon Fibre Reinforced Plastic
CNC	Computer Numerical Control
CT	Compact Tension
CT-MMM	Compact Tension Mixed Mode Modified
CTOA	Crack Tip Opening Angle
CTOD	Crack Tip Opening Displacement
DIC	Digital Image Correlation
ILS	Interlaminar Shear
LEFM	Linear Elastic Fracture Mechanics
NK-Arcan	modified Arcan grips and modified Arcan specimen
SJ-Arcan	Stephen Jones Arcan testing grips and modified Arcan specimen
2D DIC	2-Dimensional Digital Image Correlation of in plane (x & y)
S3D DIC	3-Dimensional Digital Image Correlation in and out of plane (x, y & z)

Nomenclature

a	Crack Length	mm
A	Constant	-
b	Absolute Specimen Width	mm
B	Constant	-
E	Young's Modulus of Elasticity	Pa
G	Elastic Energy Release Rate	J/m^2
h	Specimen Thickness	mm
K	Stress Intensity Factor	$Pa\sqrt{m}$
K_I	Mode I Stress Intensity Factor	$Pa\sqrt{m}$
K_{II}	Mode II Stress Intensity Factor	$Pa\sqrt{m}$
L	Length	mm
O	Order symbol	-
r	Distance	mm
t	Thickness	mm
T	T-Stress	Pa
w	Specimen Width	mm
α	Crack length to width ratio, a/w	-
ε	Strain	-
θ	Angle	°
γ	Shear strain	-
ν	Poisson's ratio	-
σ_{xx}	Stresses in the xx direction	Pa
σ_{yy}	Stresses in the yy direction	Pa
τ_{xy}	Shear stress in the xy direction	Pa

CHAPTER 1

Introduction

1.1 Introduction

This chapter gives an overview into the developments and challenges in utilising composite technology within the aerospace and automotive industry. A brief history into the development of composites is given; inclusive of frontier composite technology application.

1.2 Industrial development and uses of composites

Polymer science began in the early 1930's. Research in this discipline has generated a lot of interest [1] and has been integrated as an essential component in our lives and many industries. The aviation sector is one such thriving industry that uses polymer composite materials based on their high performance to weight ratios.

Boeing's recent 787 Dreamliner is 80 % composite by volume and 50% composite by material weight [2]. It is the highest amount of composite material used to date in commercial aerospace. The Airbus flagship A380-800 currently uses 23 % of composites by weight. The flagship A350 XWB (to be launched in the near future) is expected to use more than 53 % composite by weight [3, 4]. Other aircraft manufacturers such as Bombardier and Cormac also focus research for development of new components using Carbon Fibre Reinforced Polymer (CFRP) composites. CFRP's are predominantly used due to their characteristics in strength and very high modulus. CFRP's when compared to metals have lower density and better specific stiffness and strength characteristics. Commercial vendors from the automotive industry have sought to integrate desirable properties of a composite for manufacturing high end motor sports such as Formula One cars [5-9]. With increased use of polymer composite there arises a need to understand mechanical properties of resin systems and composites. Amongst the varied CFRP's the application of thin ply laminates is becoming more desirable in many industries. The reduction in ply thickness increases the capability to enhance design structures, since more ply stacking orientations can be selected to optimise mechanical properties in the desired

direction with increased load capacity. The ability to increase the ply thickness is very important in thin-structures and sandwich skins for improving mechanical properties. A key advantage of this enhancement is the increased Ultimate Tensile Strength (UTS) and ability to delay the start of damage of thin ply laminates when compared with traditional bulk composites. This composite sizing effect is attributed to the changes of failure mode from compounded damage in brittle failure [10, 11].

There are several reasons to why cracks occur in composites. One of the most significant damages or defects during fabrication processes is in-plane and out-of-plane loading, cyclic loading fatigue damage, material discontinuities such as stress concentrations or residual stresses. In unidirectional composite laminates, cracks can grow in three basic directions namely interlaminar, intralaminar, and translaminar (Figure 1.1).

Interlaminar fracture is commonly known as delamination which is the debonding between two plies (fibre layer) and generally caused by out-of-plane loading. Interlaminar fracture is one of the main problems faced when designing and manufacturing composite structures. Intralaminar fracture is where a crack propagates parallel to the fibres in ply laminate, it can be caused by impact to the surface of the composite and occurs commonly together with interlaminar fracture. Translaminar fracture occurs perpendicular to the fibres and requires much greater energy to propagate than intralaminar and interlaminar fracture.

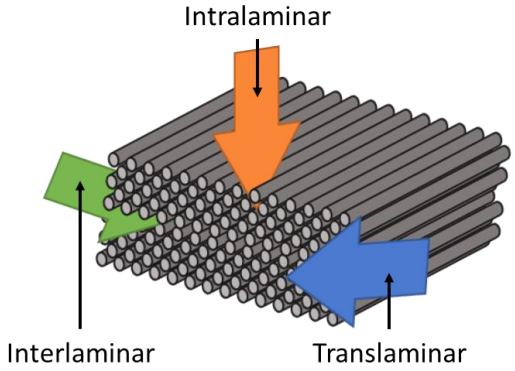

Figure 1.1 - Representation of different laminar terminology

However, the improvement in composite strength is accompanied with a decrease in toughness due to the absence of delamination in a quasi-brittle fracture behaviour. Material design selection methods for a complex advanced structure or component is predominantly driven by stress or strain criteria where the resistance to fracture is vital for assessing the safety of such structures.

Currently, the development of composites has been influenced by the tailoring of directional toughness by introducing particles into the interlayer and /or intra-layer of the resin system. Introduction of particles in the resin systems is believed to improve resin toughness and consequently improve composite fracture toughness. The different size, shape, orientation and physical structure of particles is expected to change fracture toughness of the resin systems but details on inclusion of particles to improve resin toughness are a closely-kept industrial secret. The particle inclusion in a resin system makes a particulate toughened resin. The contribution of a particle toughened resin to a composite requires further scientific experimental study before being applied to composite component structures. Therefore this study looks to provide a standardised mode I, mode II and mixed mode I and II experimental technique for characterisation of particulate toughened resin system that can be used to accurately predict and evaluate the resin performance in small scale resin for relating to bulk material property (composite laminates) and provide insight into material performance when subjected to real life failure conditions.

1.3 Research aims and objectives

Mechanical behaviour of standard resin systems is considered to be of paramount importance in understanding improved fracture performances in modified formulated resin systems. It is essential to identify methods to distinguish fracture behaviour of a formulated resin with particles in addition to studying the behaviour of a formulated resin system as part of a composite.

This research is unique because it takes on a comprehensive optimised approach to investigating failure scenario in mode I, mode II and mixed mode I&II behaviour of toughened and untoughened resin materials systems used as a part of composite.

Findings from this study will be useful for accurate characterization and response analysis. Additionally, providing data in resin enhancements or reduction leading to catastrophic failure and providing a prognosis of bulk material limitation, removing the need to conduct extensive time conducive and expensive experimentations.

This research is designed to study a range of particle-toughened materials and investigate experimental deformation mechanisms around the particles, thus discriminating potential methods of failure for the determination of material fracture parameters of particular importance.

This research aims to accomplish the following main objectives:

I. Conduct experimental investigations to characterize different material behaviour over a wide range of particulate toughened resin systems provided by sponsoring organisation.

II. Develop a novel method to investigate the behaviour of polymer matrix materials under mode I, mode II and mixed mode I&II loading using a simple unsophisticated specimen geometry and loading test fixture with optimised specimen manufacturing, preparation, and pre-cracking techniques.

III. Investigate the effect of out-of-plane loading conditions in brittle polymeric structures subjected to loading to failure.

IV. Investigate the effect of weight loading (wl) in brittle specimens with in-plane deformation.

1.4 Summary of the research programme

1.4.1 Chapter 2: State of the art research

This chapter aims to review literature on the effect of mixed mode behaviour and its effects in material behaviour in the context of linear elastic fracture mechanics. It also includes a review of crack path identification and stability, and application of 2D and 3D digital image correlation.

1.4.2 Chapter 3: Optimisation of specimen manufacturing, polishing, pre-crack application and speckle pattern painting

This chapter includes various approaches adopted in optimisation of specimen manufacturing, polishing, speckle pattern painting with special focus on the development of an accurate, repetitive and novel pre-cracking technique developed in this study.

1.4.3 Chapter 4: Design and development of testing grips and specimen geometry

This chapter describes experiments involving evaluation of current testing grips and development of grips to ensure that 'pure' mixed mode I & II testing method is used for characterising material parameters.

1.4.4 Chapter 5: Mixed Mode testing of toughened unmodified resins (F-Formulation)

This chapter describes the findings obtained from testing of toughened unmodified resins in mode I, mode II and mixed mode I&II testing and analysis using the Digital Image Correlation stress analysis technique.

1.4.5 Chapter 6: Mixed Mode testing of toughened modified resins (S-Formulation)

This chapter summarises the findings obtained from testing of toughened modified resins in mode I, mode II and mixed mode I&II testing and analysis using the Digital Image Correlation stress analysis technique. Strain energy of resin modified composites was subjected to analysis. This chapter also discusses results obtained and provides a good understanding on the role of particulate toughening in enhancing material toughness.

1.4.6 Chapter 7: Discussion of findings

This chapter discusses key findings obtained from this study from an industrial perspective and the role of particle toughening in modifying the behaviour of composites.

1.4.7 Chapter 8: Conclusions

This chapter includes concluding remarks with the overall findings of the study, comments on limitations and suggested work for the future.

CHAPTER 2

State of the art

2.1 State of the art: Introduction

This chapter introduces the state of the art techniques used in linear elastic fracture mechanics (LEFM), fracture testing of resin, crack path identification and stability, 2D and 3D digital image correlation. Firstly, this chapter introduces the epoxy (resin system) and toughening mechanisms that influences change in toughness.

2.2 Unmodified Resin Systems

Resin systems are manufactured by a process of polymerisation (curing) process with hardeners and or catalysts. This results in an unmodified resin (epoxy) system that depends on a combination of the selected base resin chemistry, hardeners and or catalysts, curing temperature, curing time and cross-linking density which determines the effective toughness of the resin system. Therefore, understanding the mechanical properties of the unmodified resin system is important to study toughening mechanisms of modified epoxies.

2.2.1 Relationship of composite and resin systems

It is well established that improvements to a resin system's property does not guarantee a direct improvement to a composite performance. However, it has been observed in many studies that some composite performance has improved due to an increased Mode I fracture toughness of the resin system. Researchers Hsieh et al. [12] provided an insight into a variety of different toughening methods and a figure from this research is reproduced in Figure 2.1.

Another compilation of mode I composite and resin toughness comparison with similar trend can be found in Kim et al. [13].

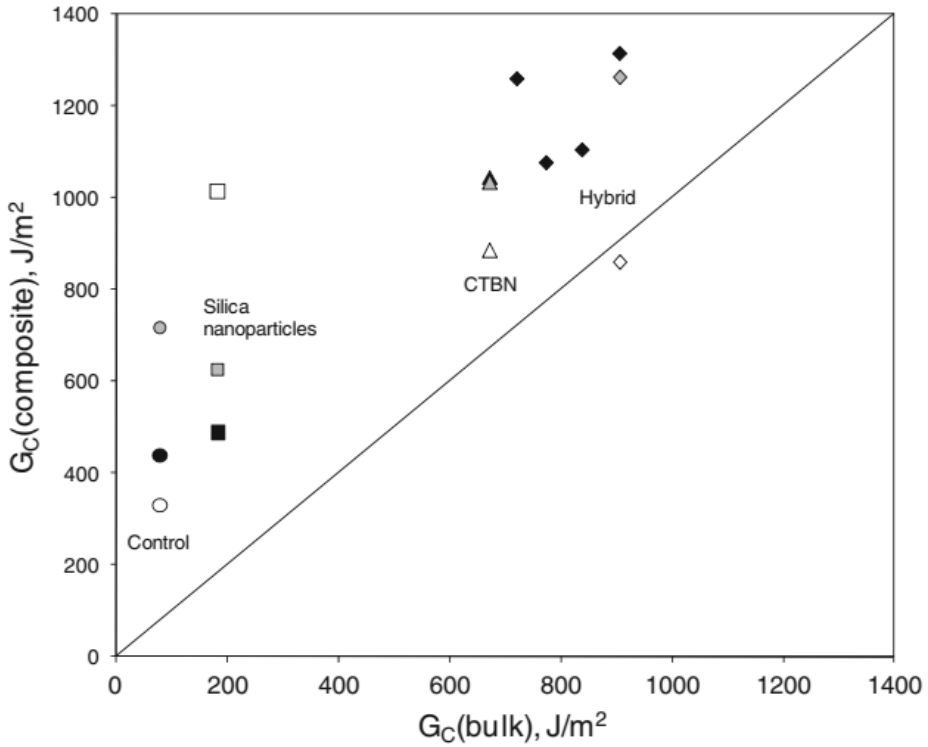

Black-filled symbols are for CFRP; unfilled symbols are for UD GFRP; and grey-filled symbols are for QI GFRP. Unmodified epoxy polymer (i.e. 'control'): ●; with silica nanoparticles: ■; with CTBN: ▲; 'hybrid': ◆.

Figure 2.1 - Shows the relationship between resin mode I toughness and composite mode I toughness in epoxy composites, taken from Hsieh et al. [12]. Strong epoxies with good performance and ideal for aerospace application are the ones closest to the line.

Figure 2.1 is reproduced from Hseih et al. [12] Interlaminar fracture energy, G_c (composite), for the composite versus the corresponding bulk resin fracture energy, G_c, for the epoxy polymers. (The 1:1 line is shown to for visual interpretation of the data.)

2.2.2 Early Work in Toughening Mechanism for Epoxies

Research work in the past has provided valuable insight on characteristics contributing to toughening mechanisms and assists in developing tougher epoxies which can be used for strengthening composites.

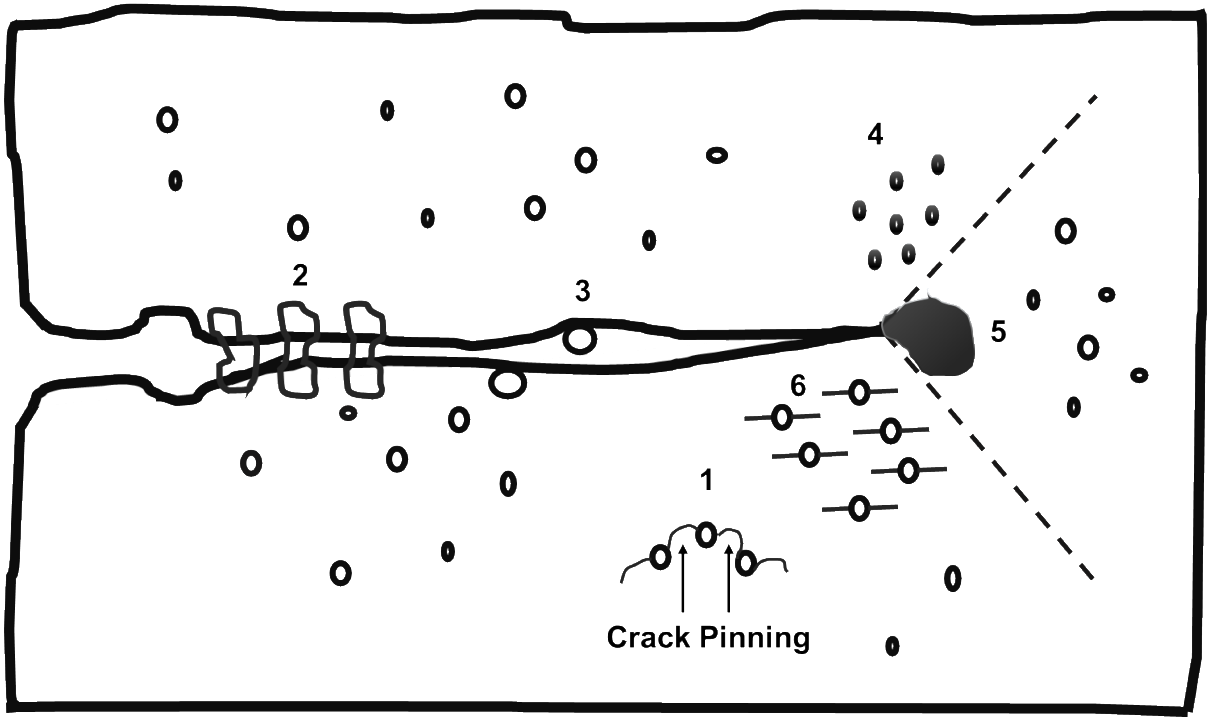

1. Crack Pinning
2. Particle Bridging
3. Crack Path Deflection
4. Particle Yielding
5. Particle Yielding Induced Shear Banding
6. Micro Cracking

Figure 2.2 - A schematic diagram depicting a modified view of toughening mechanism from Raymond A Pearson [14]

Several toughening mechanisms contribute to the increase in toughness of constituent materials and are known by different terms in research work (Figure 2.2). Pearson et al. [14] and Withers [15] have analysed the mechanism involved in toughening characteristics and defined the process of particle bridging (also referred as fibre bridging or particle cavitation depending on the material constituents). Although the material constituents of fibre bridging and particle bridging are different, the effect is the same. When the crack is obstructed by particles or fibres the cohesiveness binds the fracture together by redirecting the energy required to propagate the crack. Initial stages of cracking often occur at microscopic level around the particle. The initial

crack conjoins with other micro cracks to form a macro crack. Research work has established micro cracks are pinned around the particle, which is referred as crack pinning. Crack pinning occurs when a particle (hard filler particles) obstruct propagation of the crack. The crack is pinned against the particles. Crack pinning has a bowed crack front at the time of breaking point. If the particle is not present on the other side, then the crack is diverted away from its original path.

The effect of particle yielding near the crack tip arises from crazes or cavitation, voiding, shear banding and the occurrence of a plastic zone. Further, the particle yielding effects on toughness is not observed until the critical plastic zone size or the critical opening displacement at the crack tip has been accomplished. The induced shear banding results from the effect of narrow zones of intense localised shearing strain and can be inferred from particle yielding.

2.2.3 Toughening Polymers

A reason for toughening polymers is to improve the low interlaminar properties. The use of fibre reinforced composites in safety critical structures have created a necessity for tougher, high damage resistant polymer resin/matrix composites. They play a major role in inducing material toughness. Improving high performance composite toughness beyond the standard approach is possible through modifying epoxy chemical composition thus enhancing toughness of composite materials shown in Figure 2.3.

In a composite made up of fibres and untoughened resin (Figure 2.3a), the area within the resin matrix is known as the intralayer and an area of resin separating laminates is known as the interlayer. This interlayer may be unmodified resin or be modified with particles (Figure 2.3b). Both interlayer and intralayer resin may be modified with particles (Figure 2.3c & 2.3d). Figure 2.3 shows that cracks may occur in all of these regions and in different directions.

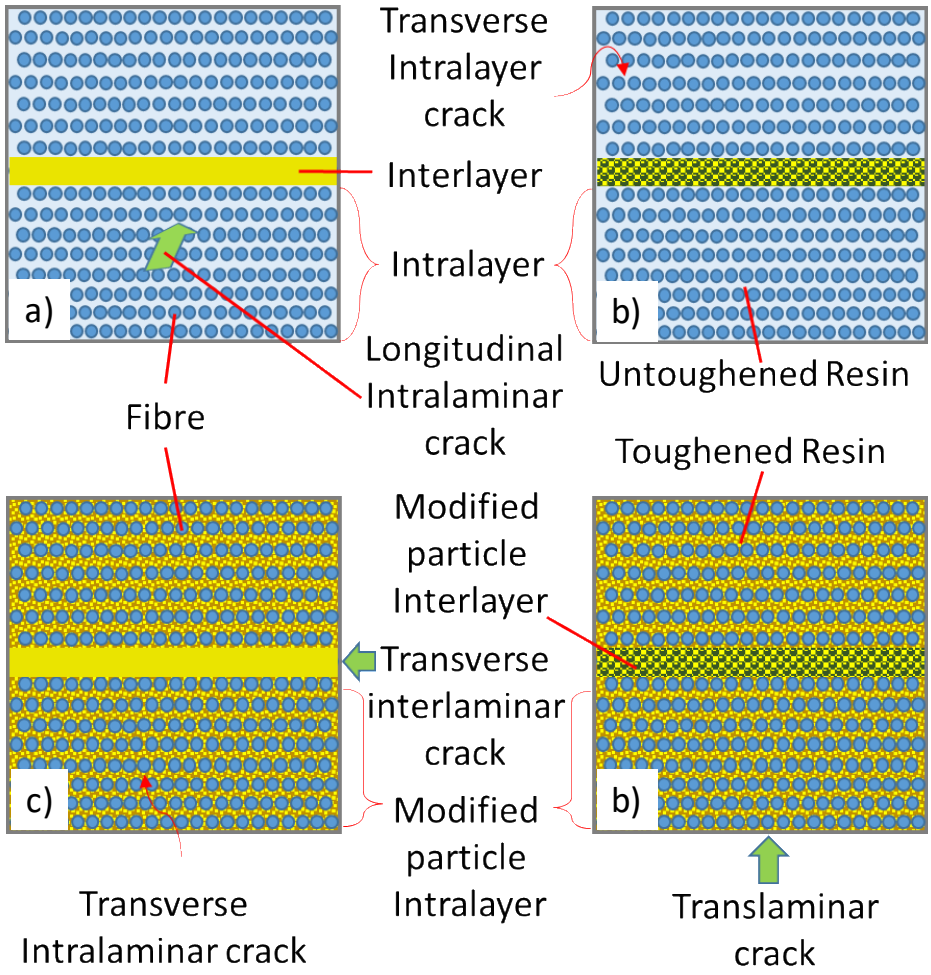

Figure 2.3 - Methods of inter/intra layer toughening system, a) Untoughened resin and fibres with resin interlayer, b) Untoughened resin and fibres with modified particle interlayer, c) Modified particle intralayer and fibres with resin interlayer, d) Modified particle intralayer and fibres with modified particle interlayer.

Without improving the toughness of the resin, the addition of a modified interlayer to a laminate can contribute to increase in material performance and tolerance to damage [6, 16, 17]. The interlayer toughening process uses a stacking sequence to apply layers of material with normal resin and a modified resin is included as an interlayer to enhance the toughening properties. The interlayer materials considered are thin thermoplastic sheets with modified resin and are tougher compositions compared to the standard layers in the stacking. The application of pre-impregnated (Pre-preg) material with inter layer toughening is limited due to constraints in processing of composite structures [17, 18].

2.2.4 Toughening Epoxy Resin

Rubber modified epoxy resin is a well-established technology and has been around since the late 1960's. Early studies indicate a moderate increase in material toughness can contribute to the creation of micro voids to mimic material toughness. Of all of research studied on micro void toughening, study conducted by Pearson is highly significant [14, 19]. This study was conducted by varying four modifiers with different sized hollow plastic particles employed as toughening agents infused with resin system. These particles induced cavitation or voids in the resin. The study reported that the variation of cavitation sizes altered the material toughness.

Later work conducted by Bagheri and Pearson in 2000 indicated that a rubber / micro void toughened epoxy varies in toughness with the increase / decrease in the distance between the micro voids [19, 20]. Their study revealed a transition from brittleness to toughness when the inter particle distance is decreased and it demonstrated the change from a plane strain to a plane stress state. This study also establishes the role of the cavitation in relieving plane strain constraints of the resin. Further, whenever there was variation in the size of the particle, it was observed that a larger particle requires greater inter particle distances to achieve inter laminar toughness and vice versa [20, 21].

Crack pinning in toughening mechanism can be observed from the scanning electron microscope (SEM) micrographs (Figure 2.4). The direction of crack migrating around the particle reveals the advantages of redirecting the path of the crack and emphasises on reducing failure in composite materials (Figure 2.4).

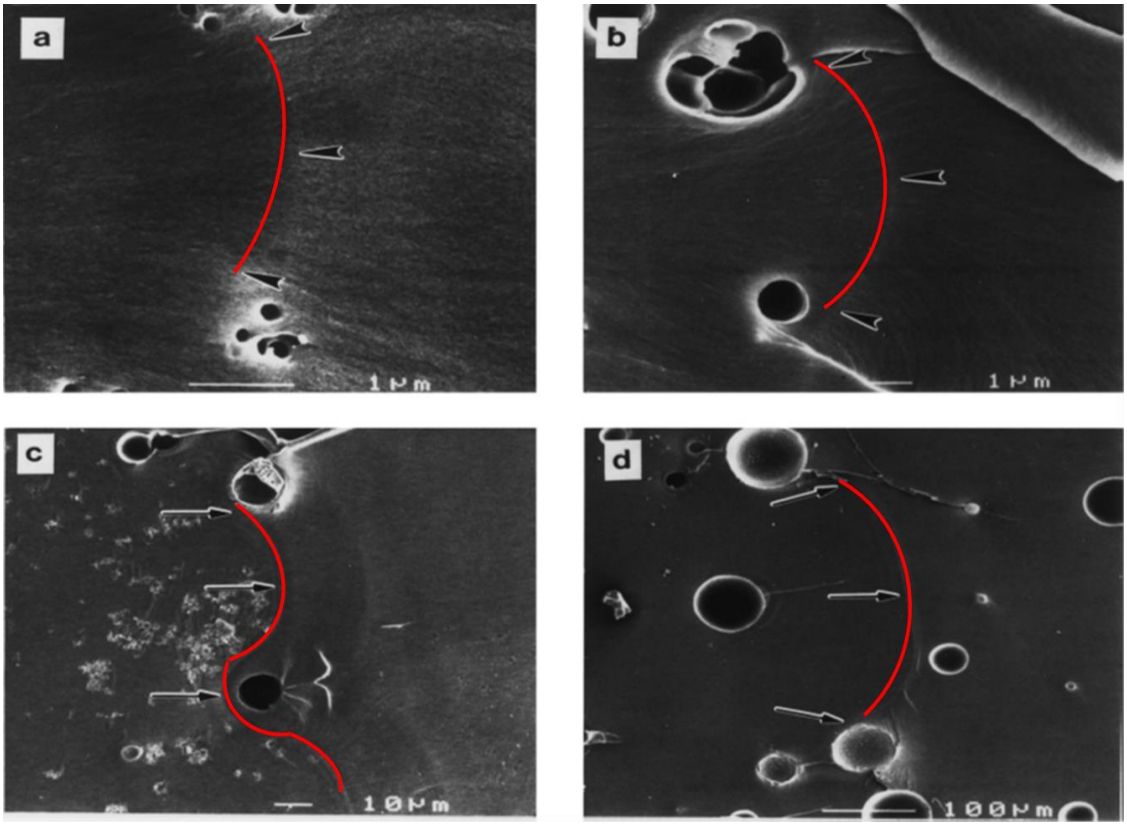

Figure 2.4 - SEM micrographs from the fracture surface of epoxies toughened by (a) 0.5 vol% Modified Particle (MBS-COOH), (b) 1 vol% Modified Particle (HLP-1.0), (c) 1 vol% Modified Particle (HLP-15), and (d) 5 vol% Modified Particle (HLP-40) particles. Crack tip bowing between neighbouring particles was observed in all [20]

Yahyaie and co-workers observed that the introduction of core shell rubber (CSR) particles reduce Young's modulus (E) and tensile strength without affecting the glass transition temperature [12, 21-23]. The study strengthened previous findings and reported that improvement in mechanical properties was mainly due to shear yielding and crack jump/arrest between particles. It indicates the presence of possible drawbacks in modifying a resin formulation for increasing material toughness. It can be inferred that the particles infused with resin in a microscopic level provides a good platform for material toughness. These findings could also be extrapolated to create a similar effect with nano particles.

A composite is a combination of two or more materials. Carbon fibre combined with resin makes a carbon fibre composite. The type of resin system used determines the type of

application of the composite. There are different types of resins such as polyester, vinyl ester, cyanate esters, bismaleimides (BMIs), epoxy, benzoxazines and phenolic. Manufacturing of carbon fibre composites or other types of composites is a relatively complex process and usually involves multiple steps. The two types of matrix (resin) used in composites are thermoplastic and thermosetting. The adhesive and cohesive characteristics of these resins serve as a binder for fibres in keeping them together for transferring load to and between fibres. Further, they act to protect the fibres from environmental conditions.

Epoxies are formed by polymerising or curing viscous liquid with hardener and/or catalyst. Their properties are determined by the ratio of the base resin, hardener, catalyst, the time and temperature to cure. Based on chemical composition, epoxies can be broadly classified as two types – unmodified and modified epoxies.

Toughened epoxies that do not have any particles are known as unmodified epoxies. Very few experimental studies have been conducted on mixed mode fracture of toughened epoxies [24]. Majority of them focus on factors such load data, crack length and geometry factors by fitting the fourth order polynomial to finite element analysis to obtain stress intensity values. Toughened epoxies embedded with particles are categorized as modified epoxies. These epoxies find a wide range of application in the composites industry due to their ability to redirect and absorb energy and delay failure of composite material.

Numerous reports suggest that mere introduction of particles in a resin system enhances fracture toughness further and recently a lot interest has been focused towards modifying toughening systems to develop composites with greater strength. Characterisation of composite strength has a major bearing on the understanding of toughening mechanisms in resin.

2.2.5 Toughening by rubber particles

In recent years, rubber particles are commonly investigated as a toughening mechanism to modify epoxy. The most common mechanisms reported in literature are void growth, particle cavitation and localised shear banding [19, 20, 25, 26]. However, particle cavitation occurs at low stresses before shear band yielding (particle yielding induced shear banding) and the plastic deformation zone is surrounded by large rubber particle cavitation zone ahead of the crack tip leading to unstable crack growth [20]. Pearson reported that the size of the cavitation zone and initiation could depend on rubber particle's resistance to cavitation. Further, higher cavitation resistance with rubber particles would store greater elastic energy before the occurrence of cavitation, thus resulting in shear band yielding. Therefore, it could be inferred that greater the plastic zone deformation, the higher the fracture toughness of the material. Other toughening mechanisms of rubber particle modified toughened epoxy was also was indicated, such as particle bridging, crack separation and/or deflection [14, 27]. Other types of particles exist that can enhance toughened epoxy with the addition of particles such as Nano particles.

2.2.6 Toughening by Nano Particles

Recent research has developed novel methodologies to modified resin, by combining small quantities of Nano size particles to attain tougher epoxy systems. Nano particles, such as Nano-Silica (Nano clay), carbon black (Bucky ball) and graphene carbon nanostructures (carbon nanotubes) are being experimented with as toughening mechanisms [23].

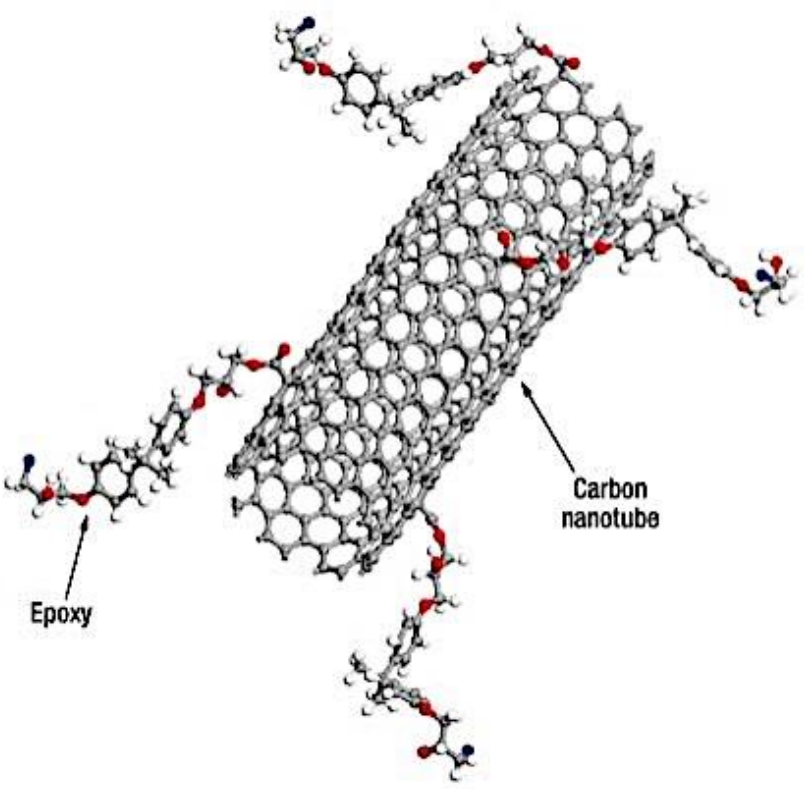

Figure 2.5 - A schematic representation of Carbon Nanotube (CNT) reinforced epoxy [28]

Due to the strong bonding between functionalized carbon nanotubes and epoxy, single and multi-walled Carbon Nanotubes (CNT) are commonly used in combination with epoxies to reinforce toughness (Figure 2.5). When used as part of a composite, it results in improving mechanical properties significantly. Industries such as aerospace, sports equipment manufacturers, and construction organizations pursue advanced research on nano composites for manufacturing critical components. Their observations suggest that carbon nanotube modified epoxy system contributes to the material to become stiffer, lighter, and stronger structures [28].

Toughening systems that improve material strengthening properties share an equal characteristic trait. All toughening systems aim to inhibit and control the direction of crack propagation and its path around the toughening system. They also assist to increase material strength. Identification of the type and direction of crack is crucial when toughened systems are used in aerospace components.

Study conducted by Kinloch et al. investigated silica nanoparticles and CTBN rubber particles effect on fracture toughness [26]. Their results indicate that the fracture toughness for 9% Weight Loading (WL) CTBN toughened epoxies increased when more silica Nano-particles was introduced.

2.3 Fracture Mechanics Theory

To determine if a material will fail or not for a given load, usually requires the stress state in the material to be analysed and stress is defined as applied load over a given area. Stress is defined as:

$$\sigma = \frac{P}{A} \tag{2.1}$$

where P is the applied load, A is the cross-sectional area and σ is the stress. A typical failure condition assumes testing of a flawless material, but this will fail to predict what happens to a component already with a crack in it. Fracture mechanics, a study of crack initiation and propagation subjected to failure in solid materials, recommends two fracture criteria; (1) stress field (local) at the tip of a crack and (2) the energy balance method (global) [29, 30].

2.3.1 Stress Intensity Factor Approach

In engineering, strength of a material is seen as a typical a failure property and can either be yield stress or ultimate stress. However, when an interface or a crack is concerned, yielding of a material is not observed in a conventional way, but instead as a separation of molecules that makes up the interface via localised stresses. Experimentation indicate that the start of crack propagation does not occur the same way as theoretical estimates indicated by calculations and typically occur lower than the theoretically value. This is due to a magnification of stresses in the area surrounding the crack and is known as stress concentration [31]. This is the foundation of fracture mechanic's concept. To predict the failure accurately the stress intensity factor K_I (SIF) must be calculated and compared against the material property known as critical stress

intensity factor K_{Ic}. Employing the parameter (K_I) we can fully understand the stress fields in a linear elastic material around the crack tip. For example, the relationship between stress and SIF for an edge crack specimen with a crack length of a subject to a stress is defined as:

$$K = Y\,\sigma\sqrt{\pi\,a} \tag{2.2}$$

where K is the stress intensity factor, Y is the stress concentration factor dependant on the crack and specimen shape, σ is the applied stress, and a is the length of edge crack length [31].

With the onset of tensile failure during experimentation the critical stress intensity factor can be calculated (i.e., $K_I = K_{Ic}$) at failure. Essentially, K_{Ic} is a measure of fracture toughness and a material property which is independent of the crack size or specimen size.

Furthermore, the energy balance theory indicates that the fracture (i.e., crack extension) occurs only when there is sufficient energy to overcome the resistance of the material. The material resistance can be surface energy, plasticity or other forms of energy required for arresting crack [32, 33].There are two main methods to describe this phenomenon: (1) linear elastic fracture mechanics (LEFM) and (2) nonlinear fracture mechanics. The LEFM approach is a good approximation when there is small volume of plastic deformation or brittle fracture occurs in the vicinity of the crack tip. However, nonlinear elastic fracture mechanics is necessary if there are viscous effects or the appearance of considerable volume of plasticity at the crack tip.

The earliest approaches to formulate fracture problems were identified by Inglis (1913), Griffith (1920), Westegaard (1939), Irwin (1948) and Williams (1957), relating to the stress at the crack tip region (local approach) and relating to energy (global approach). The approach by the researchers were equivalent and due to their assumptions of linearity, thus coined the term linear elastic fracture mechanics (LEFM). The linear elastic fracture mechanics (LEFM) conditions are satisfied, when the plastic zone is comparatively small to the singular stress field, the stress field around the crack (local) is defined as:

$$\sigma_{ij}\,(r,\theta) = \mathrm{K}(2\,\pi\,r)^{-\frac{1}{2}}\;\; f_{ij}(\theta) + \dots\,, \tag{2.3}$$

where $f_{ij}(\theta)$ is a dimensionless function of the angle θ, r is the radial distance from the tip of the crack and *K* is the stress intensity factor (SIF) dependant on applied load and crack geometry. A crack propagates when the stress intensity factor *K* grows to equal of critical stress intensity factor which can be determined experimentally and also known as fracture toughness K_c (MPa√m) [34].

A global approach looks at the energy required to create a new surface and equates to the decrease in potential energy, proposed by Griffith [35]:

$$G = -\frac{1}{b}\frac{d\Pi}{da} = 2\gamma \tag{2.4}$$

where a is the crack length, Π is the potential energy of the system or elastic body and γ is the surface energy. The drop in potential energy is defined as the energy release rate (ERR) by Irwin, also known as crack driving force. Irwin modified Griffith's Theory [34] and proposed a practical approach for solving engineering problems and proposed the following equation:

$$G = \frac{\pi\sigma^2 a}{E} > G_c = R = 2\gamma_e \tag{2.5}$$

The left side of the equation defines *G* and the right side defines the crack resistance, *R*, the increase in surface energy per unit crack area. A crack propagates when the *G* ERR grows to equal or greater than of critical ERR G_c (J/m2) or R. In situations where LEFM is not valid and nonlinear effects must be accounted for, a different fracture parameter can be used proposed by Rice: J-integral[36]. The path independent contour integral is an extension of ERR and used for nonlinear and elastic plastic deformation and equals to ERR *G* when LEFM is verified to check for validity.

2.3.2 Key Fracture Mechanics Concepts

Brittle fracture denotes a rapid and aggressive crack propagation due to presence of microscopic flaws or defects in the material which enables a fast propagation. As a result, a relatively small amount of energy is absorbed without any appreciable plastic deformation.

Ductile fracture is the converse of brittle fracture and involves large plastic deformation (necking) requiring more energy before the material is separated by a crack. Thus, ductile fracture occurs slower than brittle fracture.

Fracture toughness is the resistance to crack propagation in a material. Several approaches exist to identify and measure fracture toughness properties. For example, the energy release rate (G), and stress intensity factor (K) and the J-integral.

Figure 2.6 shows different modes of failure; a real material fracture can occur simultaneously in a combination of multiple modes. There are three modes of failure denoted by subscript I, mode I or opening mode, when a required load or energy is applied perpendicular to the surface of the crack (tension), a crack propagates. The propagating crack direction will reorient until being perpendicular to the load and often requires the smallest of load to propagate crack. In mode II or sliding mode fracture, the required load or energy is applied parallel to the surface of the crack (in-plane shear). However, in mode III or tearing mode, the required load or energy is applied orthogonally to the crack surface.

Inter-laminar fracture and delamination play an important role in determining macroscopic mechanics in failure mechanisms of composites.

Delamination is a recurrent feature which causes very high out of plane loading in the absence of fibres (Figure 2.6).

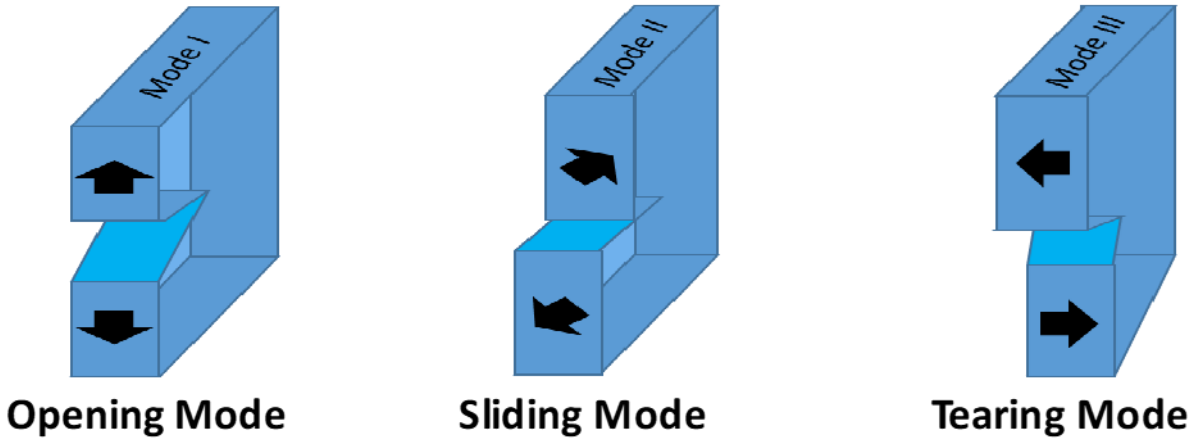

Figure 2.6 - Representation depicting of different modes of fracture.

To summarise:

1. Mode I Fracture or Opening Mode (TENSION)
2. Mode II Fracture or Sliding Mode (IN PLANE SHEAR)
3. Mode III Fracture or Tearing Mode (OUT OF PLANE SHEAR)
4. Mixed mode can be of any combination of Fracture Modes
5. Measuring mechanical properties.

Several different methods and parameters exist to aid in measuring mechanical parameter to calculate material properties. The common parameters used to measure and quantify fracture toughness of a material are:

- Stress intensity factor (*K*): the intensity of stresses in the vicinity of the crack tip.
- Energy release rate (*G*): the energy required to propagate the crack "a" unit area.
- J-integral: used for elastic-plastic fracture mechanics, it could be considered as a more general form of *G*.
- CTOD: Measures the line between the intersection between the sides of 90° vertex in the original crack and crack flanks.
- The CTOA: Used to measure fracture of a stable crack extension in a thin-walled material.

During the life of an aerospace component, loading does not occur in a singular mode and often is subjected to multiple modes of loading. Moreover, the components can be engineered to either change or fail in different modes of failure to that of the loading path during service or crack growth.

The area surrounding the crack front (at the tip of a crack) is known as plastic zone and its size plays a vital role in linear elastic fracture mechanics (LEFM). The plastic zone differs with the micro or nanoscale material atomic structure. For example, the deformations in metals occur plastically resulting in crack tip blunting by process of dislocation between planes. However, a polymer's structure is very different in micro or nanoscale since a shear yielding and crazing process occurs at the centre of crack tip resulting in disentanglement of interconnected layers of polymer bond chains. The behaviour of fracture at the process zone and its resistance to fracture cannot be fully described with traditional solid mechanics theory. When describing resistance to fracture by LEFM, it must be assumed that the process zone is small at the region of fracture which is otherwise known as the tip of the crack (i.e. stress or strain field at the crack tip).

The size and shape of the plastic zone (Figure 2.7) can be different between modes of failure as plasticity changes. Furthermore, the plastic zone (plasticity) region changes are dependent on the plane strain and plane stress conditions of a specific material. Measurement of fracture toughness dependent on plain strain condition is known as plain strain fracture toughness and fracture toughness measurement dependent plane stress condition is known as plane stress fracture toughness. Whilst fracture toughness is a material property, it depends on whether a plane stress or plane strain condition exists in test specimen. Plane strain fracture toughness is the most conservative approach to take.

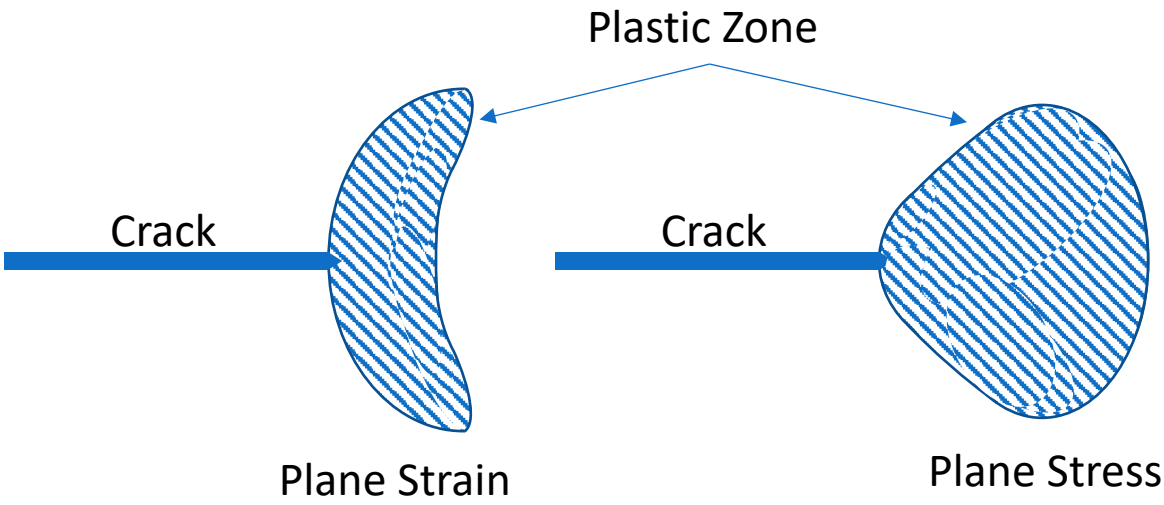

Figure 2.7 - Representation depicting different plastic zones in metals

Brittle materials are defined as materials whose fracture process involve little or no energy absorption by plasticity. However, ductile materials plastically deform substantially. In polymers and other amorphous materials, plasticity does not occur with the same dislocation and slip based microstructural behaviour as in metals. Instead shear-yielding or crazing processes occur.

However, the effect of irreversible strain energy-absorption processes can be viewed as similar and comparable to true plasticity processes [6]. Although the current study on brittle materials is performed from a fracture mechanics perspective, use of the term 'brittleness' does not imply that these are "low-toughness" materials. The sponsoring organization Cytec industries emphasize that they are extremely tough aerospace epoxies.

2.3.3 Measuring Fracture Toughness

A material exhibiting a linear elastic behaviour up to failure such as a comparatively small plastic zone to the specimen dimension, then a critical value of Mode I SIF can be considered as a suitable fracture parameter. This technique provides a quantitative measure of fracture toughness for critical plane strain stress intensity factor. However, the test should be validated once to assure that the results are meaningful. The specimen size should be adequately large enough for plane strain conditions at the crack tip. Moreover, the specimen thickness influences the amount of constraint at the crack tip which influences the fracture toughness value, and the fracture toughness reduces with increasing specimen size until it reaches the plateau (Figure 2.8)

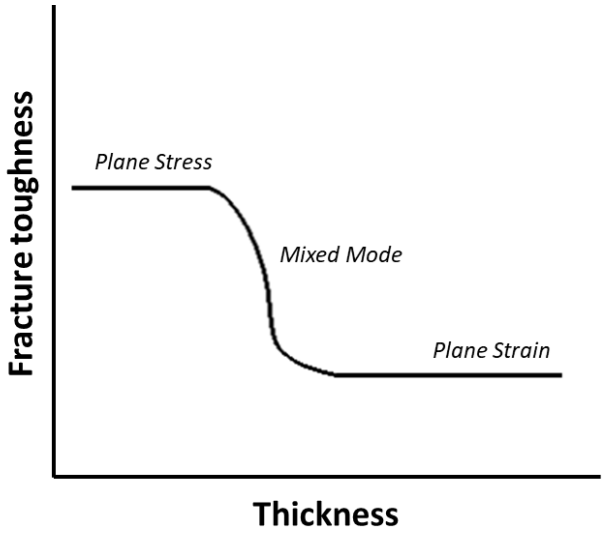

Figure 2.8 - Influence of specimen thickness on fracture toughness [37]

When testing for plane strain fracture toughness, it is important to validate steps to ensure that the specimen tested experiences plane strain condition. This is very important for Aerospace materials such as epoxies tested commonly associated with reduced thickness due to the nature of the material. The preparation of aerospace grade epoxy test specimens with high cure temperatures poses great difficulty for manufacturing thicker material without incurring thermal-runway.

Requirements of specimen size in International Standard BS EN ISO 13586:2000 are intended to assure that K_{Ic} and G_{Ic} measurements relate to the plane strain plateau by making sure that the specimen fractures under linear elastic conditions [38]. This means that the plastic zone must be comparably smaller to the specimen cross section. Two testing specimen configurations are permitted by the current version of BS EN ISO 13586:2000: the compact tension (CT), and the 3-point bending specimens. Specimens for K_{Ic} tests are usually fabricated with the overall width W equal 1.25 of width w and the thickness h lies between 0.4 and 0.6. They are razor blade pre-cracked so that the crack length/width ratio (a/W) lies between 0.45 and 0.55. Testing has shown that plane-strain conditions generally occur when:

$$h, a, (W - a) > 2.5 \left(\frac{K_Q}{\sigma_Y}\right)^2 \tag{2.6}$$

where a is the initial crack, h is the minimum necessary thickness, W-a is the ligand length, σ_Y is the yield strength of the material K_Q the fracture toughness of the material and σ_Y is the material yield strength [38]. Test specimens that are not adequately brittle or large enough to exhibit predominantly linear elastic behaviour, K can be calculated using the same method, although the result will be described as K_{mat} or K_Q as a material toughness instead of K_{Ic}. Therefore, K_{mat} or K_Q can referred to as a valid K_{Ic} value if the test specimen dimensions the fulfil the condition in equation 2.6.

A crack undergoing a complex state of stress in combination of Mode I, Mode II and Mode III, this is referred to as mixed mode. The combinations of fracture modes are mixed mode I & II, mixed mode I & III, mixed mode II & III or mixed mode I & II & III and this study will be focused on mixed mode I & II. Complex fracture modes occur when the crack changes direction and does not grow in its original plane and also because the two fracture modes do not act independently, instead interact together. Performing a test equivalent to a K_{Ic} test to determine K_{IIc} and K_{IIIc} are difficult to conduct accurately, not standardised and toughness values differ with many different approaches ultimately unknown [39]. Although several different mixed mode fracture criteria exist, thus far there is no consensus on which approach is the best. An elliptical curve could be used as an empirical fit to describe mixed mode where K_{Ic} and K_{IIc} are known as shown in equation 2.7a [40].

$$\left(\frac{K_{IQ}}{K_{IC}}\right)^{m} + \left(\frac{K_{IIQ}}{K_{IIC}}\right)^{n} = 1 \tag{2.7a}$$

It is possible to determine K_{IIc} by choosing suitable power terms m and n in the fitting of the elliptical. Many studies have used many different mixed mode failure criteria to compare with experimental data [41, 42], however the simplest failure criteria is referred to as Mixed Mode Failure Envelope (MMFE) where mode I, mode II and mode III and acceptable power terms m, n and o are considered as shown in equation 2.7b.

$$\left(\frac{K_{IQ}}{K_{IC}}\right)^{m} + \left(\frac{K_{IIQ}}{K_{IIC}}\right)^{n} + \left(\frac{K_{IIIQ}}{K_{IIIC}}\right)^{o} = 1 \tag{2.7b}$$

The key assumption of the MMFE is that failure occurs when a material critical energy release rate G_c and a combination of the three failure modes each contribute to failure relative to the toughness in the individual failure mode. Therefore, the failure can be separated into three groups, one per failure mode. The MMFE criteria is widely used in Virtual Crack Closure Technique (VCCT) for the assessment of delamination in component design [43].

2.3.4 Validity of Linear Elastic Fracture Mechanics (LEFM) Assumptions

In order for LEFM conditions to be met, it is important to ensure the size of the process zone (Area where plasticity or energy absorption mechanism such as shear yielding occurs) is small compared to the width or ligand length and specimen thickness.

The thickness of the specimen was limited to the thickness limits of casting resin, due to the high exothermic reactions of curing the resin a maximum thickness of 5.5mm was possible. Therefore, a compromise is needed to be made between using thick, small specimens versus thinner, non-standard larger specimens. The CT specimen thickness advised by the standards to ensure plane strain conditions for every type of material that might be studied is unusually thick. It is left to the user to check the evaluate the assumptions and the validation check can be found in section 4.2.5.

2.3.5 Characterisation of near Crack Tip condition using Linear Elastic Fracture Mechanics (LEFM)

The Stress Intensity Factor (SIF), *K*, is an important Linear Elastic Fracture Mechanics (LEFM) parameter used for the assessment of structural integrity of structures containing cracks and singular stress fields. The SIF provides a measure of stress field intensity surrounding the crack tip. The parameter '*K*' detects crack growth when a given load is applied to a material and could be obtained by numerical analysis or experimental techniques. Early work conducted by Williams [44] and Westergaard [45] provide preliminary information on understanding the behaviour of stresses and strains near the crack tip. State and distribution of stress around a crack tip as is described in polar and Cartesian coordinates (Figure 2. 9).

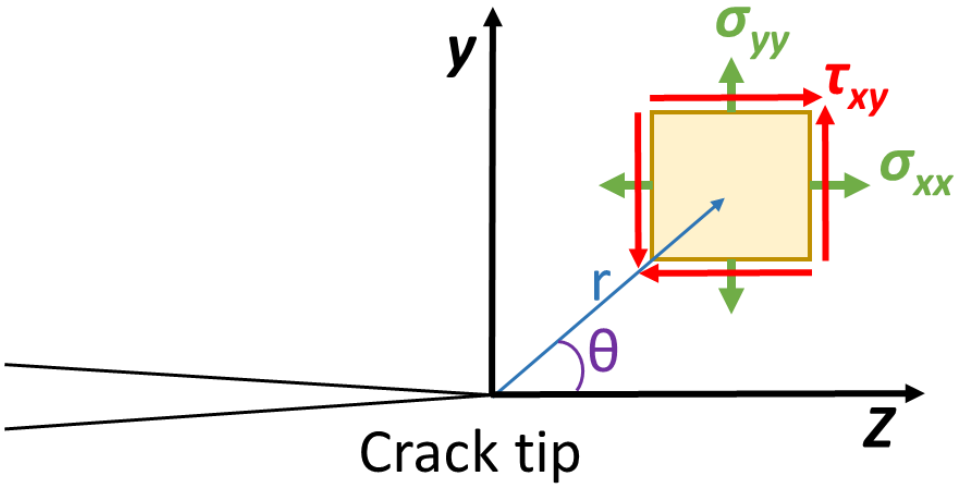

Figure 2.9 - Stress state around a crack tip

The stress intensity factors K_I and K_{II} may be evaluated from the first term of the Williams [44] asymptotic crack tip behaviour solution in Cartesian coordinates described in equation 2.7a and 2.7b.

Mode I

$$\sigma_{xx} = \frac{K_I}{\sqrt{2\pi r}}\cos\frac{\theta}{2}\left(1 - \sin\frac{\theta}{2}\sin\frac{3\theta}{2}\right) + T + A\sqrt{\boldsymbol{r}}\cos\frac{\theta}{2}\left(1 + \sin^2\frac{\theta}{2}\right) + O(r)$$

$$\sigma_{yy} = \frac{K_I}{\sqrt{2\pi r}}cos\frac{\theta}{2}\left(1 + sin\frac{\theta}{2}sin\frac{3\theta}{2}\right) + A\sqrt{r}cos\frac{\theta}{2}\left(1 - sin^2\frac{\theta}{2}\right) + O\left(r^{3/2}\right)$$

$$\tau_{xy} = \frac{K_I}{\sqrt{2\pi r}}cos\frac{\theta}{2}sin\frac{\theta}{2}cos\frac{3\theta}{2} - A\sqrt{r}sin\frac{\theta}{2}cos^2\frac{\theta}{2} + O(r)$$

(2.7a)

Mode II

$$\sigma_{xx} = \frac{-K_{II}}{\sqrt{2\pi r}}sin\frac{\theta}{2}\left(2 + cos\frac{\theta}{2}cos\frac{3\theta}{2}\right) + B\sqrt{\boldsymbol{r}}sin\frac{\theta}{2}\left(2 + cos^2\frac{\theta}{2}\right) + O(r)$$

$$\sigma_{yy} = \frac{K_{II}}{\sqrt{2\pi r}}sin\frac{\theta}{2}cos\frac{\theta}{2}cos\frac{3\theta}{2} - B\sqrt{r}sin\frac{\theta}{2}cos^2\frac{\theta}{2} + O\left(r^{3/2}\right)$$

$$\tau_{xy} = \frac{K_{II}}{\sqrt{2\pi r}}cos\frac{\theta}{2}\left(1 - sin\frac{\theta}{2}sin\frac{3}{2}\frac{\theta}{2}\right) + B\sqrt{r}cos\frac{\theta}{2}\left(1 + sin\frac{\theta}{2}sin\frac{3\theta}{2}\right) + O\left(r^{3/2}\right)$$

(2.7b)

There are three terms of the Williams solution and the distribution of the stress at the tip of the crack is able to be expanded as a power series. The first term is normally known as the stress intensity factor that calculates the amount of fracture in a brittle material. The second term makes sure that the direction of the crack remains stable, whereas the third term controls the propagation of the crack to ensure its stability.

The expanded form of the Williams solution into the second term with a remote normal stress σ_a applied in one direction, results in the formation of uniaxial normal stress T at 90 degrees relative to the crack (Figure 2.9). The high order terms in the series expansions indicated by $O(r)$ which is considered to be negligible near the crack tip. Here, T (T-Stress) represents the uniform stress acting parallel to the crack tip or the equivalent expression the second term of Williams's solution [46, 47]. Although T-Stress was initially detected by researchers Maccagno and Knott [48], its significance was understood only after the derivation of William's solution. They investigated the pure relationships between critical K_I and K_{II}, with K_{Ic} and material properties as the key parameters and deemed undesirable for any additional effects arising from higher order terms during testing. It was understood that it was necessary to ensure T-stress was almost zero to perform experimentation in pure mode I for investigating PMMA.

Literature suggests that the behaviour of the crack path in a crack kinking (Figure 2.10) could be closely related to crack path stability and T-Stress. Literature suggests that the direction of the crack propagation is influenced by presence of the mode II SIF and results in angled deviation from the direction of the crack. However, the crack is dominated by mode I [49, 50].

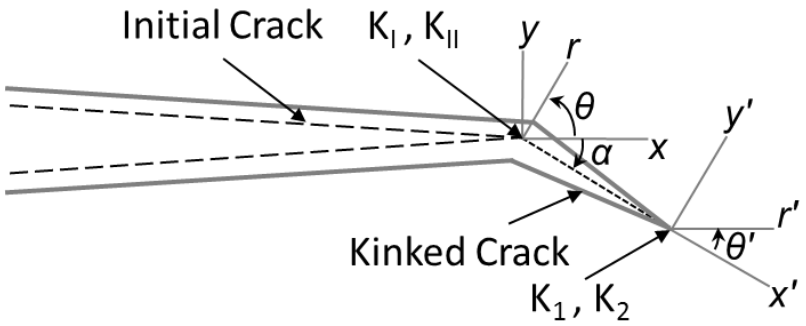

Figure 2.10 - Crack kinking characteristics

Cotterell and Rice looked at slightly curved and kinked cracks (Figure 2.10) [47]. This implies that it is possible to accurately determine the crack path when K_{II}=0 and a crack opening of 30°. Studies conducted by Fleck indicate that cracks have a tendency to be directionally stable

when T-Stress is negative (compressive), and directionally unstable when T-Stress is positive (tensile) [50]. The research reveals that the length of the initial crack influences the final shape of the fracture if the direction of the growth post initiation is rapidly changing. Complementary work by Yates et al indicates that the crack path is influenced by pure mode I SIF dominance and virtually no Mode II SIF, indicating possible crack stability [51].

Research work conducted by Tomlinson and co-workers strengthens previous findings in investigating the non-singular term or T-Stress [51-56]. Further, it strengthens previous work by Maccagno [48]. Jones and Tomlinson explored the crack path behaviour and identified that crack path stability is closely related to the variation in T-Stress [56]. In previous studies the thermoelastic stress analysis technique was employed and the evaluation of T-Stress was determined by a series expansion of the two original high order mode I and II terms [52, 54, 55]. Zanganeh et al [57] reported while extracting T-stress from displacement field data at the crack tip, identifying the correct crack tip location accurately is difficult and as a result can lead to extracting inaccurate T-stress values.

Despite these findings, the current study hypothesizes that the evaluation of stress intensity factor *K* would help towards characterisation of failure in toughened resins with and without particles. This is a simple approach with less uncertainty in experiments. Hence, the literature review is driven with a focus on evaluating stress intensity factors (SIF) at fracture.

Measuring fracture toughness parameter is a complex process and a methodical experimental approach is required to achieve optimum results. Of the different failure modes of engineering components, mode I (tension) fracture testing is more commonly used than mode II or mode III. This is because international standard testing exists only for mode I, thus ensuring accuracy of results. However, other fracture modes (mode II, mode III and mixed mode I and II) are important to investigate, but they are relatively more complex and there is no standardised international test method for these modes.

2.3.6 Crack Path Identification and Stability

A flawless crack free manufacturing of safety critical composite components is impossible; the propagation of a crack will greatly reduce the life of the composite components and cause unexpected failure. Therefore, understanding the behaviour of crack propagation is an important element in evaluating the performance of composite component.

Fracture mechanics theory defines the onset of fracture for a crack characterized by a single variable. Isotropic and linear elastic material characteristic identifies Linear Elastic Fracture Mechanics (LEFM). LEFM Elastic theory is used to calculate stress fields near the crack tip. When stresses near or at the crack tip exceed the material fracture toughness *K*, or energy release rate G the crack will propagate. However, the variable can also be either J-integral or the crack opening displacement (COD) when yielding is more dispersed [7]. In order to understand crack propagation better, characterisation of stress conditions at the crack tip is needed [47, 58, 59]. The stress intensity of a crack propagation in a homogenous elastic material at the tip is characterised by William's series asymptotic solution [47, 59] as explained in section 2.3.

Furthermore, the Cartesian coordinates at the crack tip in the x-axis, along the direction of crack for mode I and mode II is assessed by non-singular stress intensity factors for the Williams series solution. The direction of cracks in homogenous materials is influenced by the stress intensity factor or energy release rate at the crack tip and this has been widely investigated [47, 60-64].

The direction of crack propagation has been studied widely by various laboratories [61, 65]. Erdogan and Sih in 1963 developed the maximum opening stress criteria reporting that the direction of the crack is perpendicular to the maximum opening stress at the tip of crack [62]. Mode I dominance was first suggested in [62] looking at cracked plates undergoing transverse shear and in-plane loading where the crack growth is nearly in the direction perpendicular to

maximum tangential stress (MTS) radiating from the tip of the initial crack. This approach is one of the widely exploited theory used for mixed mode crack growth. This approach assumes that the crack propagation starts in the direction on which MTS reaches a maximum, the shear stress should be zero and the occurrences of principle stresses. The occurrence of fracture is observed when MTS reaches a critical stress for the material equal to tensile (uniaxial tension) fracture stress. Furthermore, Sih proposed the theory of core region (fracture dominant region) surrounding the crack tip [39, 66, 67].

The concept of fracture mechanics approach and experimental measurement stops at a distance ahead from of the crack tip. The distance functions as a measurement scale of analysis at a fracture level. This approach has been widely used due to its simplicity and supported by many experimental studies. The use of this approach can be found applied by several authors, in particular by Ayatollahi and co workers where they have expanded to a sharp and blunt V notches with consideration to singular and non-singular terms [68-74].

Knauss and Palaniswamy developed a method by applying the maximum energy release rate as a function of crack kinking angle to detect the direction of the crack propagation [63]. In 1980, Cotterell and Rice proposed the Mode I fracture criteria, when $K_{II} = 0$ at the crack tip, a crack propagates along the pure mode I path [47].

The criteria of crack propagation developed for characterising homogenous materials should be used with care especially when there is changes in the interface crack and fracture toughness differences around the interface. The three criteria indicate similar results with little or no change experimentally. Furthermore, the directionally stable crack propagation depends on the ratio between mode I and mode II components at the tip of crack or the crack will deviate from the straight path due to influences of mixed mode loading. Applying the criteria to a resin system, the failure occurring at the centre of fracture is strongly dependant on the global mixed mode influence. The root failure in the specimen begins at the notch tip of the test specimen

occurs predominantly in mode I loading. Further, the crack is predicted to propagate towards the path of least resistance when loaded under mixed mode. However, since the resin systems are designed with toughened particles to reduce "normal" crack behaviour, it is hypothesised that the crack propagation behaves like fracture between two interfaces. Further, if the chemistry of the resin is tougher than the embedded particle, then the toughening mechanism will change the crack path with respect to the type of reinforcement used.

Early work by Cotterell in 1966 and Rice in 1968 on investigating slightly curved or kinked cracks in homogenous materials reported that the T-stress plays a major role in directional stability for crack propagation. [46, 75]. If the T-stress is negative (-), then the curved and kinked crack in a homogenous material will return to the original crack path when loaded in predominantly mode I or result in a directionally stable crack path. However, if the T-stress is positive (+), then the curved and kinked crack path of a homogenous material will deviate further away from the original crack path or result in a directionally unstable crack path (Figure 2.11).

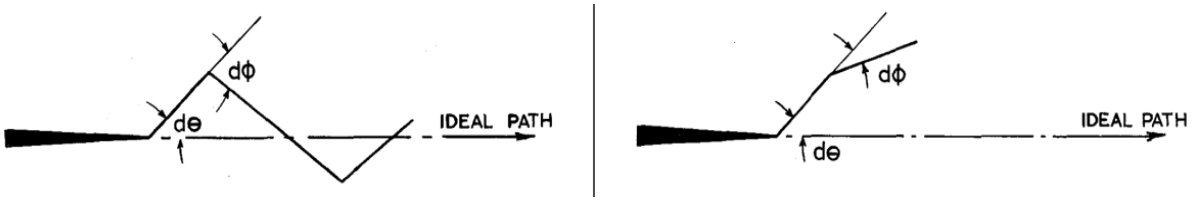

a. Negative T-stress: Stable crack path b. Positive T-stress: Unstable crack path

Figure 2.11 - Crack path stability captured from Notes on the path and stability of cracks [59]

The directional stability is investigated analytically by Fleck, Hutchinson, and Suo in 1991 indicated homogenous material cracks in joints with adhesive bonding are more directionally stable if T-stress is negative and directionally unstable if T-stress is positive and depends largely on the magnitude of T-stress [59].

Chao et al. in 1996 investigated the influence of T-stress on crack propagation [76, 77] using the William's high order asymptotic stress expansion for a crack in a homogenous material

[44]. The study provides an insight on directional stability of cracks for homogenous materials and role of T-stress. Results indicated that the direction of crack propagation and the direction of maximum opening stress criterion at the crack tip varies with T-stress. Prediction of T-stress dependence of crack path stability in adhesive bonded DCB test specimens was experimentally verified by Chen and Dillard in 1999 [78].

Other reports revealed that T-stress is directionally proportional to the thickness of the adhesive layer [59]. T-stress value changes with specimen thickness suggesting a change in directional stability of the crack. These findings warrant further studies on the geometry and geometry constraints that influence T-stress values. Literature has shown that the predicted crack path is an independent process that occurs until mode II SIF disappears, suggesting that the crack is guided by mode II failure [49]. Further, findings also report that the length of the initial crack influences the final shape of the fracture if the direction of the growth post initiation changes rapidly. Complementary work by Yates suggested that crack path is influenced by pure mode I dominance and no Mode II SIF suggesting stability [51]. Figure 2.12 indicates variation in plastic zone shape for different modes of failure.

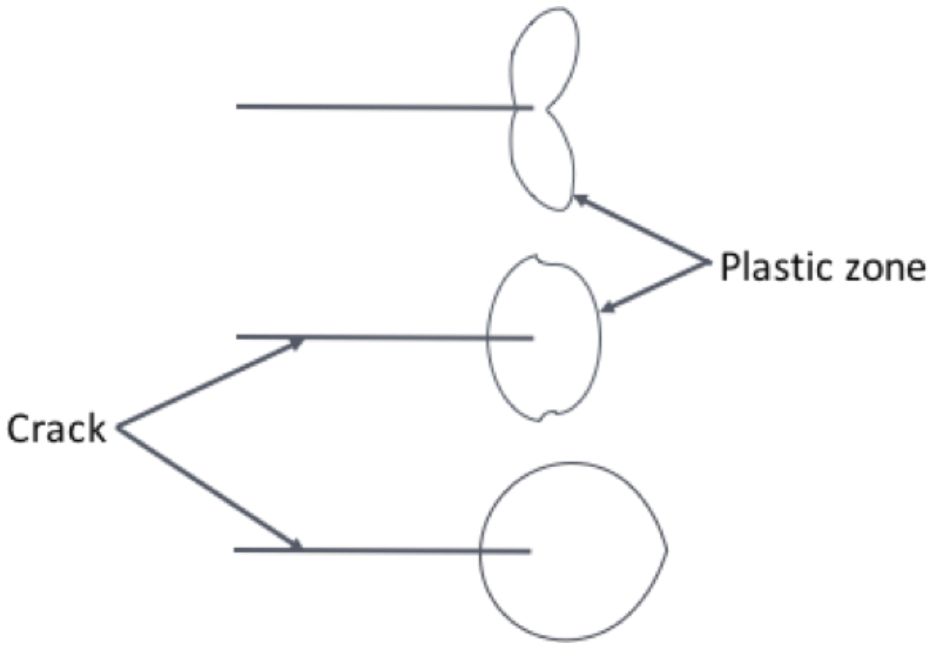

Figure 2.12 - Variations of plastic zone shape from pure mode I (top), $K_I/K_{III} = 1.5$ (middle) and $K_I/K_{III} = 0.5$ (bottom).

Subsequent studies that were conducted by Tomlinson and co-workers with thermoelastic stress analysis techniques used to evaluate T-Stress by a series expansion of the two original High Order Mode I and II Terms showed that if only two terms were used, an undesirable difference in sign and magnitude of T-Stress could be observed and revealed that the crack path stability is closely related to variations in T-Stress.

2.3.7 Fracture Testing of Resins – Mode I Testing

There are two main testing specimens for loading material in pure mode I. The single edge notched beam specimen (SENB or 3-point bend specimen) is loaded in a 3-point bend (3PB) configuration as shown in figure 2.13a and the compact tension (CT) as shown in figure 2.13b. Both specimens and configuration approach are explained in detail in the British and International Standard(BS ISO) [38] and in the American Standard International (ASTM) [79].

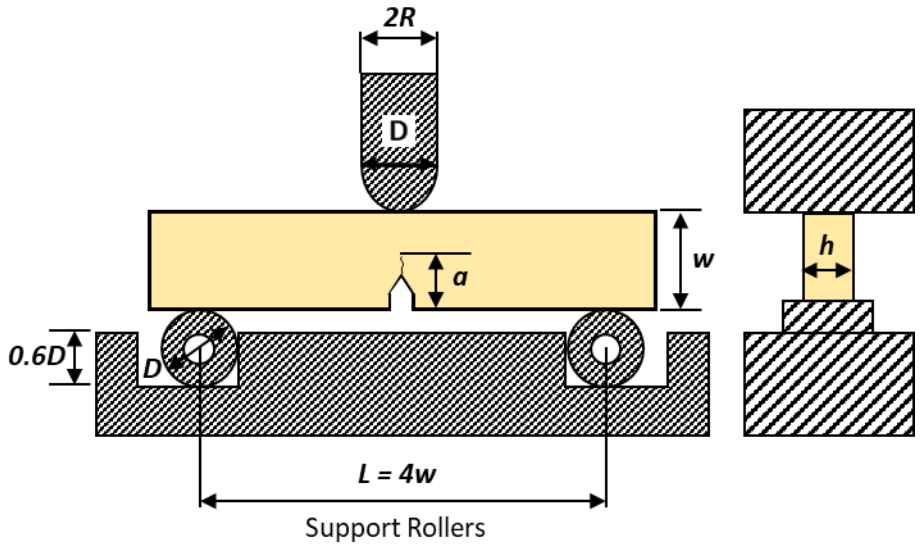

a. SENB (3-Point Bend Specimen or 3BPS) specimen loaded in a 3PB setup

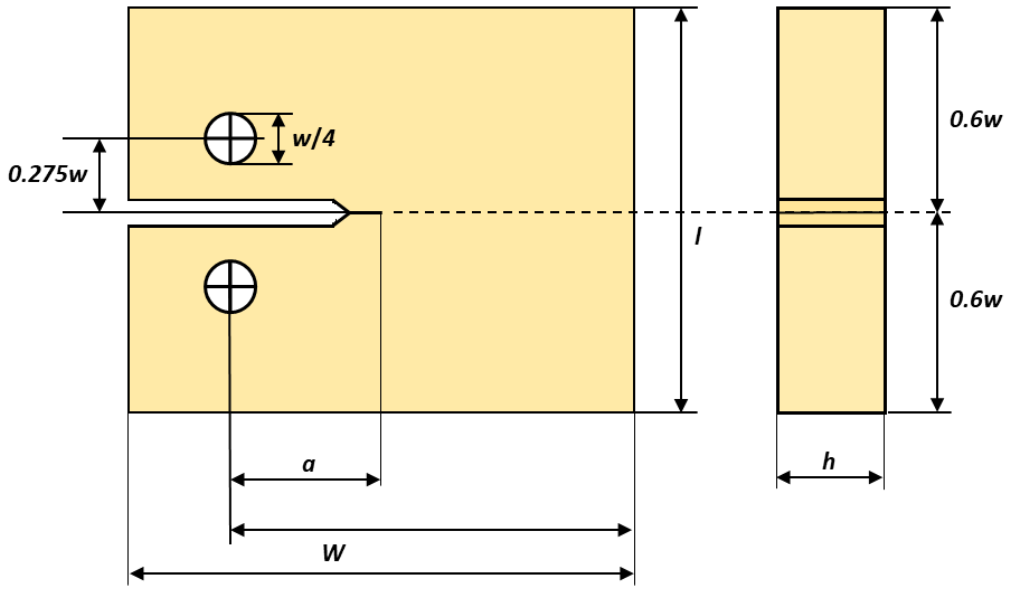

b. CT specimen loaded in standard 2 pin loading grips

Figure 2.13 - The two standard specimen and configuration for evaluating K_{Ic}, created from BS ISO 13586:2000 [38]

2.3.8 Fracture Testing of Resins – Mode II and Mixed Mode (I/II) Testing

Fracture in composite materials can be due to individual modes and the combination of mode I (opening) and mode II (shearing). The blend of two modes of fracture is termed mixed-mode fracture. While mode I fracture toughness may identify a conservative value to use in a mixed-mode case, it is more appropriate to measure the actual mixed-mode fracture toughness as this will give accurate overall design. There are different experimental testing and sample configurations for mixed-mode testing of materials which have been proposed in the past.

Suresh et al. investigated in the early 1990's a test method which can be used to apply mixed mode loading to the centre of a pre-cracked beam specimen is by using a four-point bend tests fixture (4PB) [80]. The 4PB mode II and mixed mode I &II loading configuration is expressed by the loading points P on the specimen (Figure 2.14).

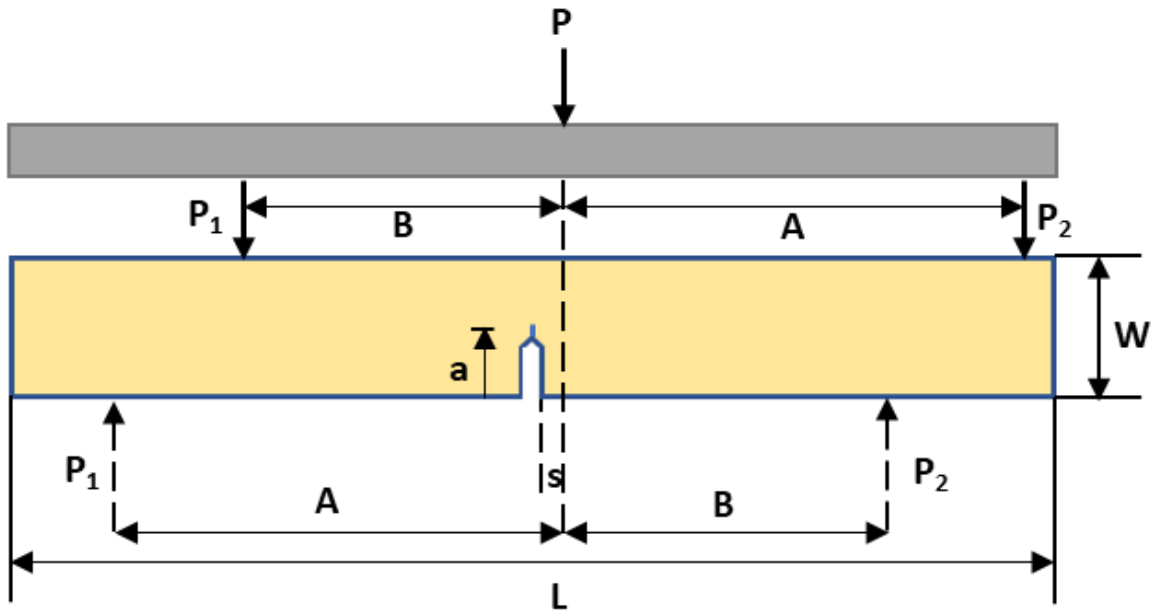

Figure 2.14 - Mixed-mode I&II loading arrangements – Four Point Bending (4PB)

The Mixed-Mode Bending (MMB) test has distinctive advantages over other testing techniques for testing composites.

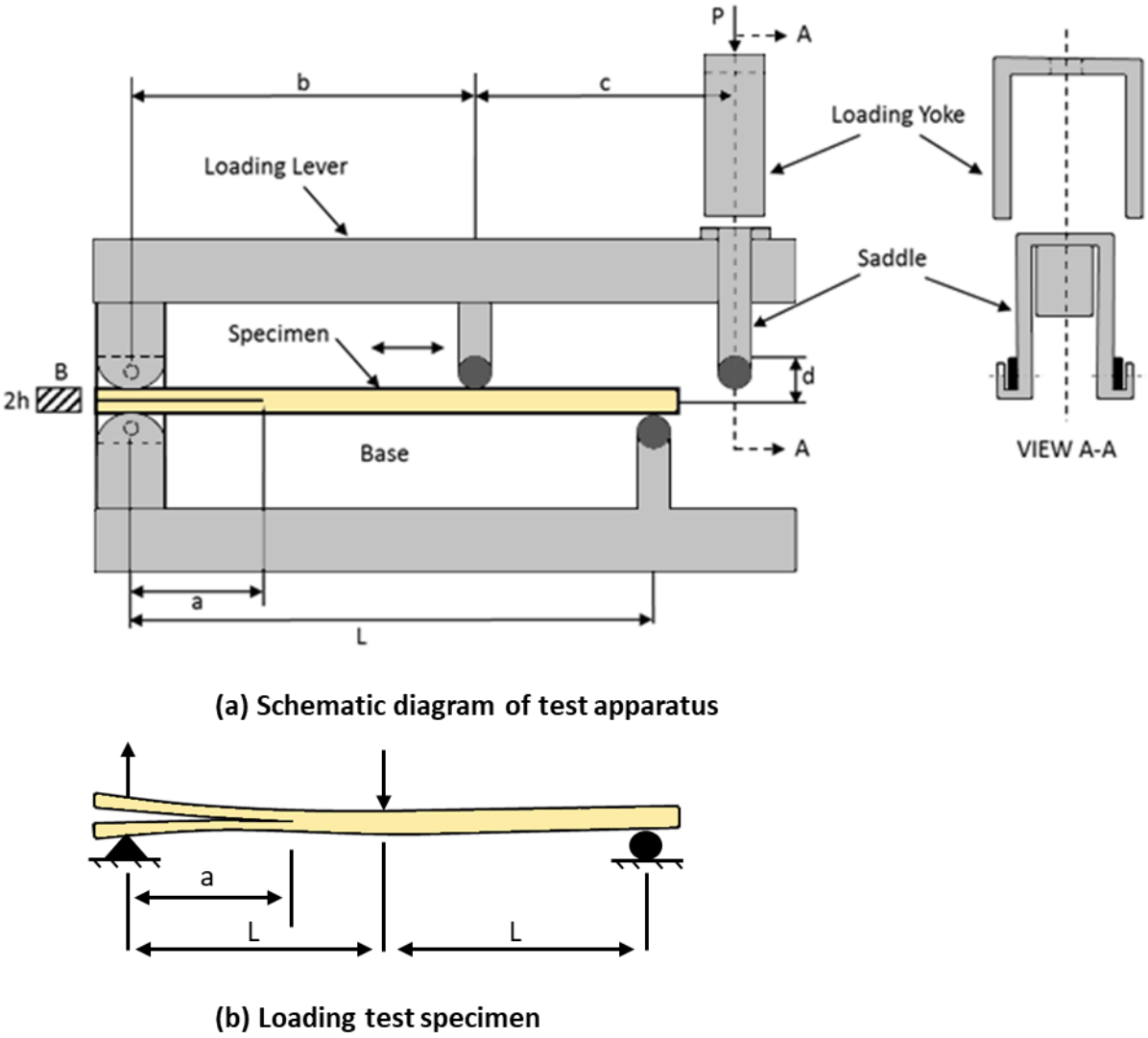

Figure 2.15 - Mixed-mode I&II loading arrangements – Mixed-Mode Bending (MMB) [81]

The MMB test (Figure 2.15) is a combination of the Double Cantilever Beam (DCB) test (standard mode I test for fracture toughness), with the End Notch Flexure (ENF) (mode II test for fracture toughness) specimen. Although this test was designed for testing static delamination of composites, researchers have also used this method for fatigue testing. MMB testing is performed by applying an opening mode load to the mid-span of the ENF specimen (Figure 2.15b). The applied load separates arms of the split unidirectional composite DCB testing. The proportionate magnitude of the two applied loads at the front of the delamination determines the mixed mode I & II ratio. The applied two loads through the hinge and loading lever is shown in Figure 2.15a and the testing is performed by applying a single load via the

loading yoke. The position c denotes to the proportionate magnitude of the resulting two loads applied onto the specimen and determines the composite mixed mode I & II delamination ratio. Pure mode I loading is achieved by removing the loading leaver beam and pulling on the attached hinges on the test specimen. Pure mode II loading is achieved by applying load directly above the beam (c=0). The geometry of test samples used for MMB are same as the DCB or 4ENF according to international standard ASTM D6671M. Studies by Kinloch, Wang, Williams and Yayla indicate that this experimentation method is in its primary stages[81]. Therefore, the results obtained required an additional evaluation of global or a local singular field analysis. Alternative approaches to obtain mixed-mode I & II include sample modified tensile testing as shown in Figure 2.16.

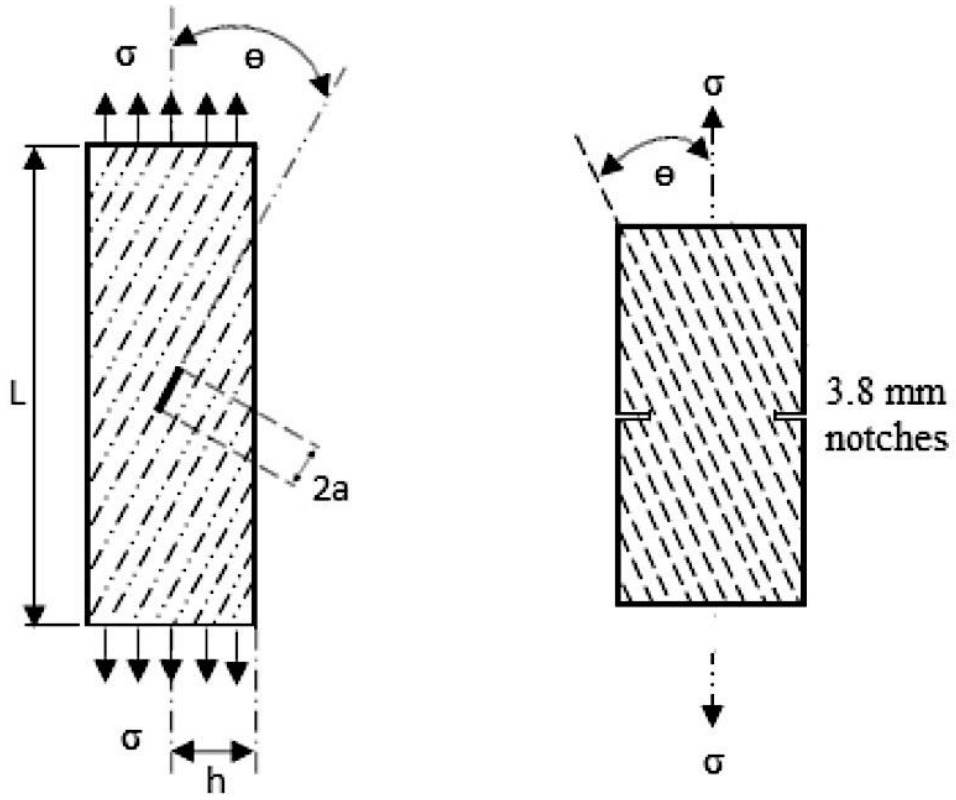

(a) Off-Axis Tensile Test (b) Double Edged Notched Tensile Test

Figure 2.16 - Mixed-mode I&II loading arrangements – two types of sample orientation [82]

It is to be observed that both test samples in Figure 2.17 are the same setup in principle when loaded in tension, but differ in geometric orientation and both types of tensile configuration can obtain values for the critical stress intensity factors [82].

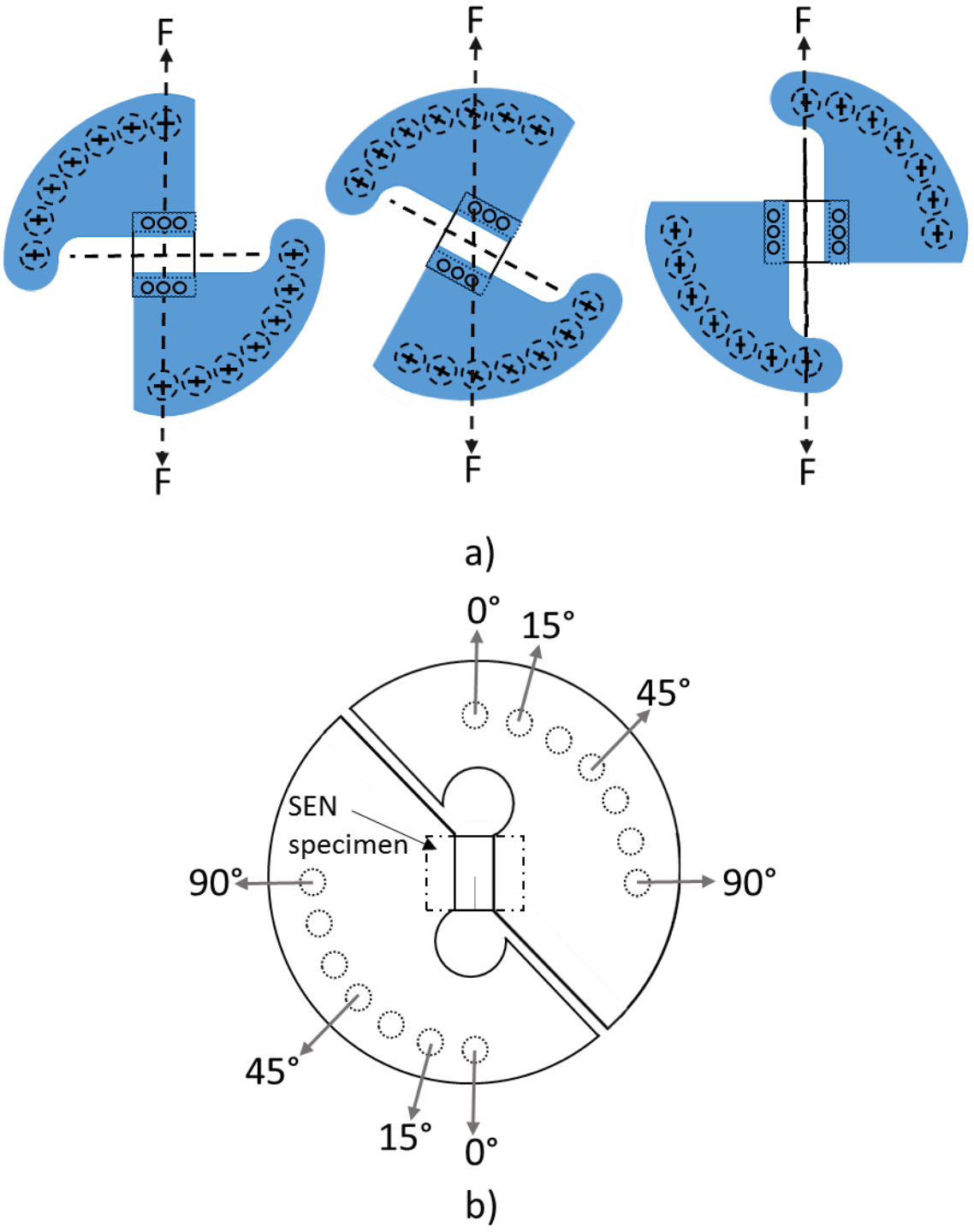

Figure 2.17 - Mixed-mode I&II loading arrangements a) Richard compact tension shear (CTS) test fixture and b) single edge notch Arcan test fixture

The CTS fixture [83] (Figure 2.17a) was initially designed to determine the critical shear stress intensity factor and later modified to be used in mixed-mode sample configurations at fifteen degree intervals between 0º and 90º. The compact tension shear fixture is mounted with a pre-cracked sample and then fixed with pins to the required angle, before loading the sample.

The Arcan single edge notch (SEN) specimen (Figure 2.17b) [82] was made for the mixed-mode fracture test of small specimens which allows mode I, mode II and mixed-mode I & II to be tested with the same test specimen configuration [84, 85]. The Arcan test fixture (Figure 2.17b) gives more variation in the orientation of sample geometry and the application of different angles in testing. The single edged notch Arcan test fixture is identical to the CTS fixture in the loading angle variations, but the difference lies in the way the sample is mounted. (Figure 2.17b). The sample must be bonded to the test fixture with adhesive before it is attached to the testing frame. This can cause great inaccuracies by residual stresses due to the effect of misalignment caused by the samples bonded to the surface of the test fixture and can cause undesired out-of-plane bending resulting in a mode III presence to the propagating fracture stress intensity [86].

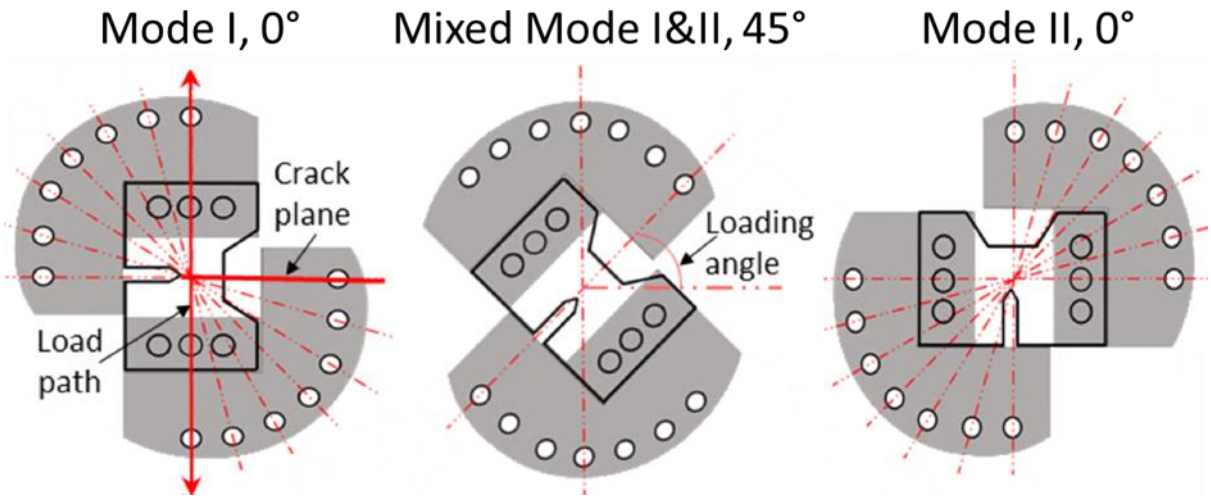

Figure 2.18 - Loading arrangements of the SJ Arcan test fixture

The SJ Arcan test fixture is a hybrid of the CTS fixture loading arrangement and the Arcan test rig can be loaded in mode I (0°), mode II (90°) and mixed mode I&II (45°) (Figure 2.18). The SJ Arcan test fixture is considered to be significantly better when compared to the other mixed-mode testing mentioned in this section, because it has variable loading angles like the Arcan and the CTS. However the specimens are not required to be adhesively bonded to the surface of the SJ Arcan test rig, as is required for the Arcan test fixture [56]. The Arcan method can become a complex process when aiming to ensure accuracy of the overall position, angle, and bonding of specimen before testing. The SJ Arcan is also an improvement on the CTS because the CTS is prone to out-of-plane displacements whilst loading.

The need for further study of the crack growth behaviour has been acknowledged in recent works, since available concepts and present findings are inadequate to fully describe the crack path under mixed mode I&II loading conditions. A review of test methods provides insight into the problems associated with inelastic material behaviour, large displacements, and abrasive frictional forces between two surfaces associated with mixed-mode I & II experimental setup which will be valuable in designing tests in the future [87].

However, considering the current available techniques it was decided that the ideal testing configuration and specimen geometry for conducting experimental study in brittle epoxies is to utilise the SJ Arcan to measure and characterise near the crack tip condition.

2.4 Experimental Image Analysis Techniques

Experimental image analysis is a technique that uses the properties of light captured from an unloaded or loaded specimen to determine the relative change in a material to establish strain and/or stress fields. Cloud describes comprehensively a range of optical strain measurement techniques, each of which has relative merits for different applications [88]. The technique used in the current work is primarily digital image correlation. Photoelasticity is used as a secondary technique.

2.4.1 Digital Image Correlation (DIC)

Digital image correlation (DIC) is a widely accepted experimental technique that facilitates identification of inherent material fracture parameters. It is a technique developed in the 1980's by Sutton et al. [89]. It uses a computer vision to extract the full field displacement data. Subset features from pairs of digital images of a specimen surface before and after deformations are compared. The specimen surface is prepared with a high-contrast, random, grey scale speckle pattern which is illuminated to prevent shadows. These patterns are often black painted dots on a white paint background. The grey scale images of the specimen are recorded digitally and cross-correlation algorithms are performed, thus producing a vector displacement field. This vector field is then differentiated to produce a strain field [90-93].

2D DIC (Figure 2.19a) utilises only one camera and 3D DIC (Figure 2.19b) uses two or more cameras (stereoscopic). The term 2D and 3D refers to spatial referencing points of the imaging system. Essentially capturing 2D displacement images, the 2D DIC method identifies a reference to change in spatial mapping in the direction of x and y. 3D DIC's spatial difference lies in identifying the displacement measurement with an additional z-axis component which signifies the ability to achieve displacement measurement for in-plane and out-of-plane deformation.

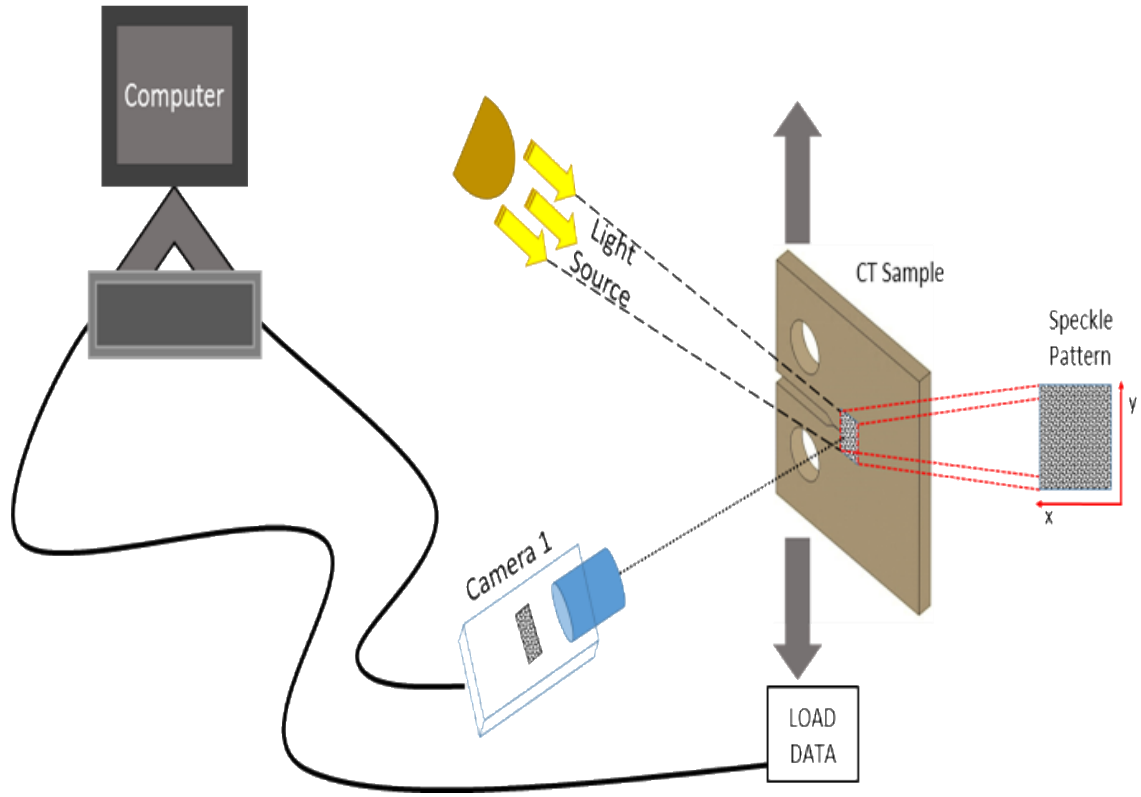

(a)

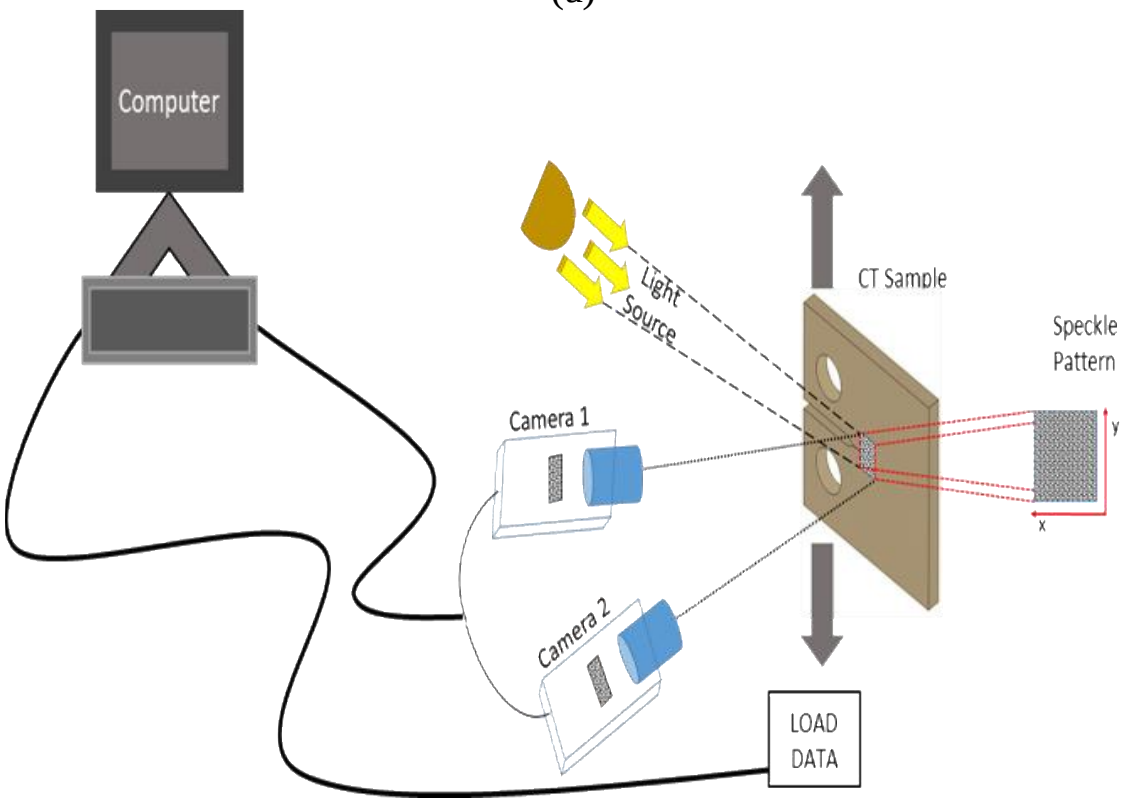

(b)

Figure 2.19 - a) 2D DIC and b) 3D DIC standard experimental setup

Analysis of displacement in the z-axis (out-of-plane), as well as in the x and y-axis (in-plane) during the fracture process gives comprehensive information about the fracture. Some materials can exhibit out-of-plane deformation at the crack tip and if a 2D DIC system is used, then the information gained will only indicate in-plane strain. However, if the material exhibits out-of-plane behaviour, 2D DIC generated data will be subject to error with incorrect strain fields determined [94]. Therefore, validation of out-of-plane effects is vital to ensure accuracy in displacement data.

In-plane tensile testing for mode I is conducted with a compact tension specimen geometry, and mode II shear testing conducted with a shear notch rail (Iosipescu) [95, 96] or the (CTS) compact tension shear test [83], or the Arcan test fixture [97].

For the fracture mechanics investigation, we are assuming that it is completely in-plane and only at high magnification of the crack tip, it could be possible to observe some out of plane behaviour. The test configuration is selected on the assumption that the specimen will predominantly undergo in-plane behaviour and therefore the samples 2D DIC configuration could be used. However, if a material behaviour is not known, investigating the effects of out-of-plane first with a 3D DIC experimental setup ensures accuracy of results with minimal errors.

As a general practice, the 3D DIC system is used as a default experimental technique for material characterisation. The 3D DIC system has added complication of calibration and experimental setup. 2D DIC (Figure 2.19a) systems are simpler to set up and calibrate, easily available and economical. Therefore, the 2D DIC system is more desirable than the 3D DIC, only if relative out-of-plane deformation (z-axis displacement) errors are within acceptable levels.

2.4.1.1 Digital Image Correlation Errors

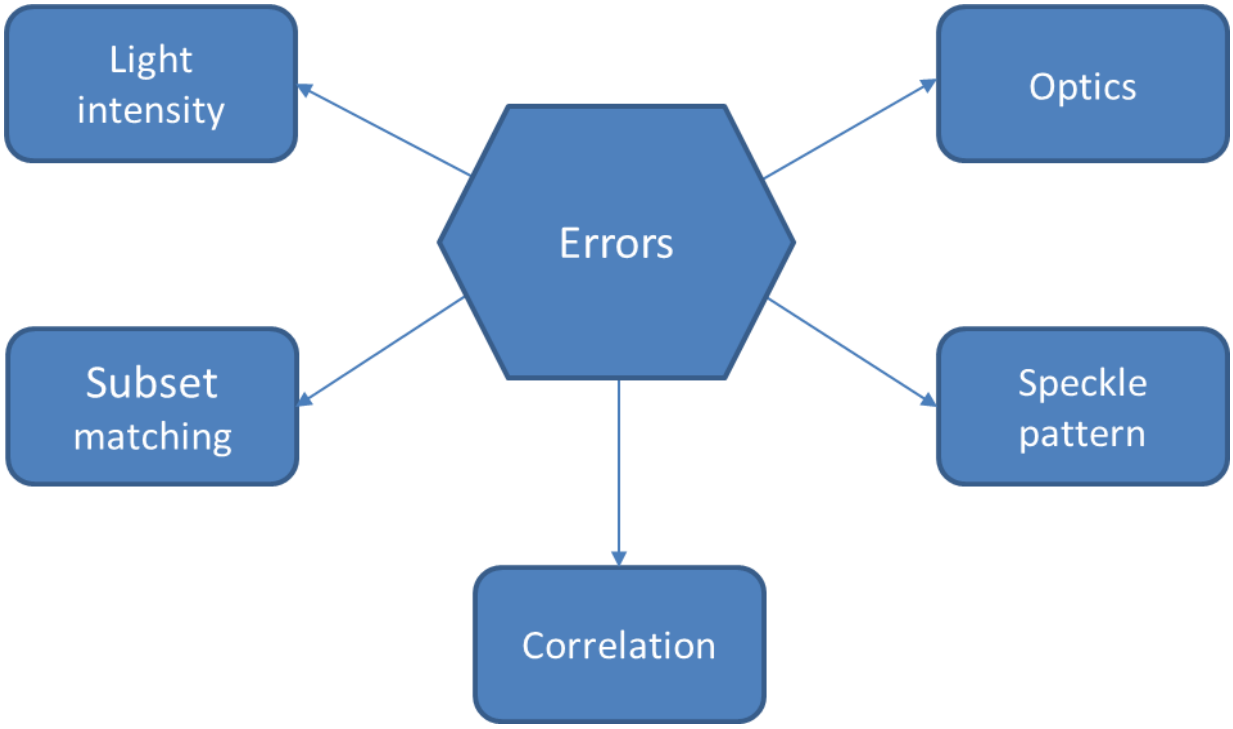

Figure 2.20 - Representative errors associated with using either and or both 2D and 3D DIC systems

Currently, there are numerous challenges encountered whilst optimising accuracy in experimental investigation (Figure 2.20). Therefore, it is vital to evaluate and minimise the effects of these errors when designing an experimental investigation.

2.4.1.2 Light Intensity (Illumination)

Illumination setup plays a vital role in achieving optimum lighting conditions and hence selection should be considered with care. If a DIC lighting setup emits fluctuating light and or generates heat on to the specimen during an investigation, then such environment will accrue detrimental effects onto the experimental investigation where the captured and processed successive images translated into displacement vectors that are subject to induced errors. The fluctuating light intensity emitted onto the specimen causes variations in the light contrast of the speckle-patterned image captured during an experimentation and subsequent processing will result in altered displacement vectors [98, 99]. Similarly, heat generating floodlights alter

the environment of the experimental investigation where the specimen is subject to change over time. The floodlights expose the area of the specimen and speckle pattern with heat, resulting in either ageing or drying of the paint applied to the specimen during an experiment. The drying or aging of the paint result in movement of the pattern and an inaccurate surface strain measurement or DIC image decorrelation [100].

2.4.1.3 Speckle Pattern

The speckle pattern used with a DIC system for measuring deformation should be of high quality, many criteria exist for evaluating optimum speckle patterns, such as ensuring that the whole image has a higher mean gradient and a good contrast ratio [101, 102]. These criteria indicate change in the DIC algorithm calculations, but the users must be able to produce a high quality speckle pattern to facilitate the evaluation criteria.

Creation of an optimum speckle pattern is dependent on application, time and accuracy. Every pattern depends on the experimental condition and if the condition changes, then the speckle pattern will change accordingly. A speckle pattern's characteristics can vary based the size of the speckle [103-108]. Producing similar and consistent speckle patterns by improving the paint flow from an airbrush requires careful consideration. Further details on speckle pattern optimisation are discussed Chapter 3. The camera optics play a vital role in visualising, correlation and subset matching of the applied speckle pattern.

It is very important to select an optically effective camera that complements scale of the applied speckle pattern to accurately capture displacements during a DIC experiment. The selection of an optical lens depends on variables such as focal length and distance between camera and test specimen. Focal length is the distance between the centre of the lens and the focal point on the surface of the camera's sensor when the test specimen is in focus. There are several different types optical lens, such as standard lens (focal length is between 35mm-70mm), wide-angle lens (focal length is less than 35mm), telephoto lens (focal length is between 135-300+

mm), tele-centric lens (constant) and macro lens (focal length greater than 35 mm-100mm). The closer the object, the greater the focal length and greater the distance between the centre of the lens and specimen and vice versa. The focal length varies with every setup and configures differently each time to get the specimen in focus with the camera. If the distance between the camera and the specimen needs to be greater, the image observed through lens is focused with a longer focal length and vice versa. Similarly, if the specimen dimension is greater than the focal area, the focal distance between the lens and the specimen is increased to capture the entire focal area.

2.4.1.4 Optics

Optical lenses are encumbered with distortional effects that alter the image on the outer edge of the lens producing an imperfect image. Conventional optics such as standard, wide angle, telephoto and macro lenses have angular fields of view where the distance between the specimen and the lens increases as the magnification decreases [109]. It is possible to eliminate the lens distortion exhibited due to the aspherical shape of a conventional lens configuration by using a tele-centric lens. The tele-centric lens is also aspherical in nature but the lens configuration produces the field of view image with negligible parallax and distortional error. Therefore, the distortional problem exhibited by a conventional lens is not present in a tele-centric lens and the information captured on the outer edge can be used error free. Although the tele-centric lens eliminates distortional effects, there are inherent disadvantages to using a tele-centric lens such as a relatively close lens position is required (small distance between the camera lens setup and the specimen) and is very expensive when compared to a conventional lens setup. Thus, the experimental environment, budget and specimen dimensions will dictate the use of a tele-centric lens with either 2D or 3D Digital Image Correlation. Using conventional macro lens by keeping the image located towards the centre of field of view is a simpler alternative to reduce distortional effects. The macro lens is less expensive than the

tele-centric lens with additional benefits such as providing a higher magnification at a smaller field of view. Experiments conducted in this study require high magnification and small field of view from macroscopic to microscopic scale study. Therefore, it is beneficial to use a high magnification macro lens configuration, to capture a defined high quality speckle pattern with a reproduction image ratio of 1:1. Once a suitable optical lens is identified, the image is acquired and the field of view configured with subset matching for image correlation post processing.

2.4.1.5 Subset Matching

The image correlation is application based and involves comparing two acquisitioned images prior to and after deformation. A field of view subset masking is applied to two or more matching subsets above and below a location of failure to occur. The DIC correlation application software has a built-in correlation algorithm that detects local displacement vectors ‘v’ and ‘u’ by comparing the two or more image subsets. The point of interest in the subset reference image is characterised by the selected square subset pixels per area. The algorithm has a fine search routine to scan and subset matches pixel by pixel of the deformed image, at a certain location with in subset mask against the previous image resulting in a mean displacement.

The mean displacement often identifies a sinusoidal bias error because of interpolation and standard deviation indicates the displacement noise. The interpolation and displacement noise errors are primarily attributed to noise and contrast conditions [110, 111].

Any filtering effect of the aperture change will decrease the contrast conditions if the speckle pattern is not adequately sized. Therefore, for the same field of view, it necessary to either increase the speckle size or use a higher resolution camera system to maintain the same contrast ratio. There is some evidence that by decreasing the subset size and applying minimal filtering by changing aperture and slightly defocussing the lens benefits greatly in reducing matching

errors. However, the opposite is true, too much filtering can increase subset matching errors [112]. All of the errors discussed above contribute towards correlation error.

2.4.1.6 Correlation

The determination of coordinates of a specimen can be classified as the identification of corresponding points in the cameras and the reconstruction of the projected points in space. Different types of error sources that effect the accuracy of the image correlation are correlation errors and calibration error which directly impacts reconstruction of coordinates of the correlated image. The correlation error can be categorised into statistical and system errors. Statistical errors consist of noise with camera images, limited number of grey scale pixels and the field of view positioning accuracy. The noise is influenced by several environmental conditions such as light intensity, optical distortion, speckle pattern, subset matching and hardware configuration error. Other than statistical errors, system error can contribute to correlation errors such as a curved specimen attributing towards lens distortion [113]. Current commercial imaging system provide noise level limits to correlation errors depending on the type of digital camera.

Before identifying displacement of the DIC image analysis, the intrinsic parameters such as subset characterisation must be identified. The image analysis software usually selects subset characterisation automatically. However, it could be altered when the subsets need to be identified individually. This depends on the type of image analysis package used. The other intrinsic parameter is the type and size of speckle pattern applied to a sample and most test equipment requires a grey scale speckle pattern. One needs to randomise the speckle pattern with no uniformity as the image recognition correlates via subset variations. Figure 2.21 illustrates a randomised speckle pattern and indicates a typical subset size and strain measurement region required for correlating images.

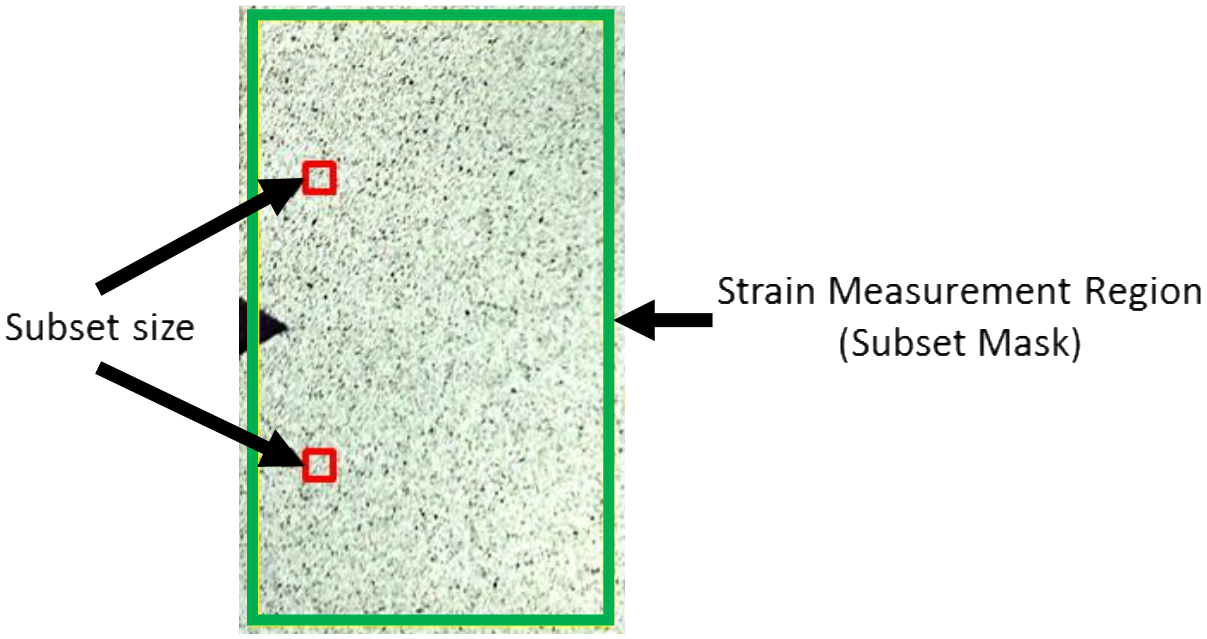

Figure 2.21 - 2D DIC Subset Characterisation

Significant progress has been made in the area of digital correlation and image capture systems, out of which there are numerous customizable optic systems and always improving with technological developments. Generally, improvement is focussed on the hardware of optics in sensor technology between image capture systems and the lens magnification system. However, until date there has been little change in improving algorithms that contribute to image analysis for a stereoscopic camera system [93, 111, 114-116].

2.4.2 Photoelasticity

Photo-elasticity is an experimental image analysis technique where polarised light is propagated through transparent specimens [117-131]. The transparent material exhibits temporary birefringence under load. When observed under polarised light, an interference pattern is revealed which represents contours of maximum shear stress. A schematic of a standard polariscope for studying this photoelastic effect is shown in Figure 2.22

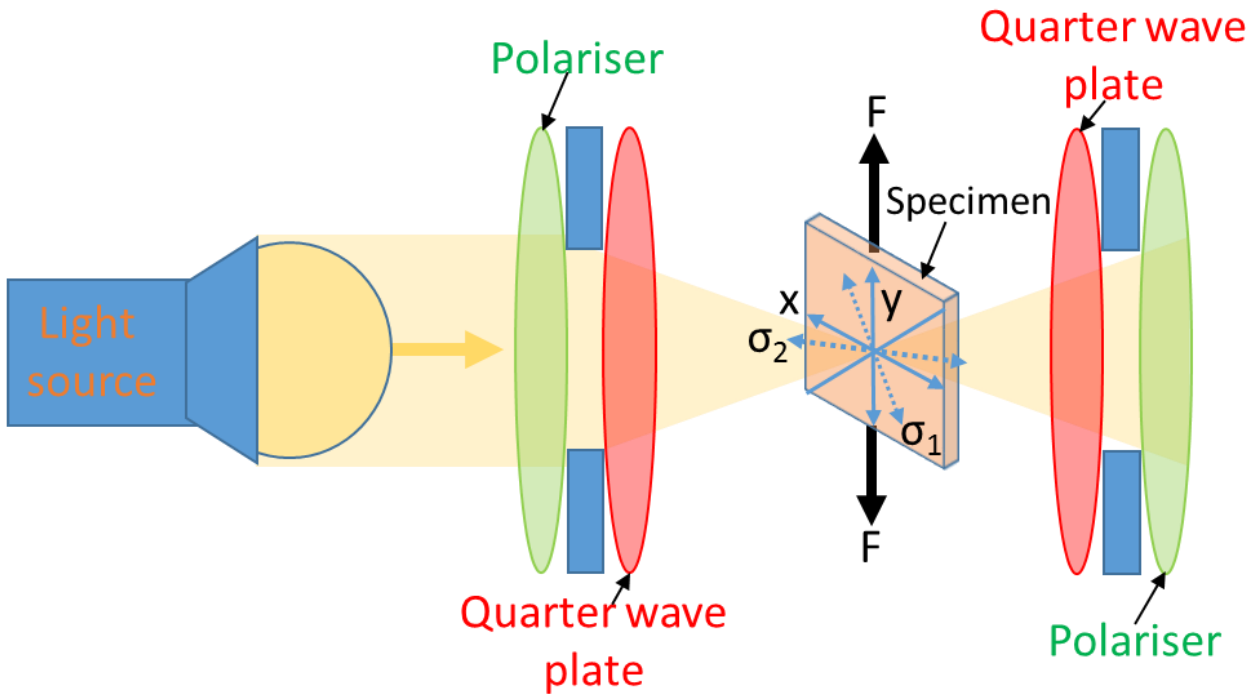

Figure 2.22 - A schematic representation of a polariscope

Light passes through the polariser to transform to polarised light and then through the specimen. The birefringence effect in the specimen causes the light entering the stressed body to divide into waves whose vibrations are parallel to the principal stresses and velocities are proportional to the principal stress magnitudes. Hence, when emerging from the stressed body the light waves have a phase retardation or phase difference. The second polariser combines the waves along its axis producing an interference pattern (isochromatics) except where the waves were vibrating parallel or perpendicular to its axis (isoclinics). The isochromatic fringes represent the magnitude of the maximum shear stress which is equal to the difference in

principal stresses. The isoclinic fringes provide the direction of the principal stresses relative to the polariser. The introduction of the two quarter wave plates optically removes the isoclinic fringes to allow observation of the isochromatics only. This method was applied in the current study since only the magnitude of the stresses was of interest and the isoclinic fringes tend to mask the isochromatics.

The magnitude of retardation under plane stress may be assessed by the stress optic law equation:

$$\Delta = \frac{2\pi}{\lambda} * C(\sigma_1 - \sigma_2) \tag{2.8}$$

where Δ = relative retardation, λ= wave length of light, C = stress optic coefficient of the material and (σ_1-σ_2) equals the difference in principle stresses. In a state of stress, a loaded body held between polarising lenses shows interference fringes (Figure 2.23).

Photoelasticity has been adopted as a technique to measure crack tip stresses and mixed mode data. However, in the current study this technique has been adopted only to observe residual stresses in specimens.

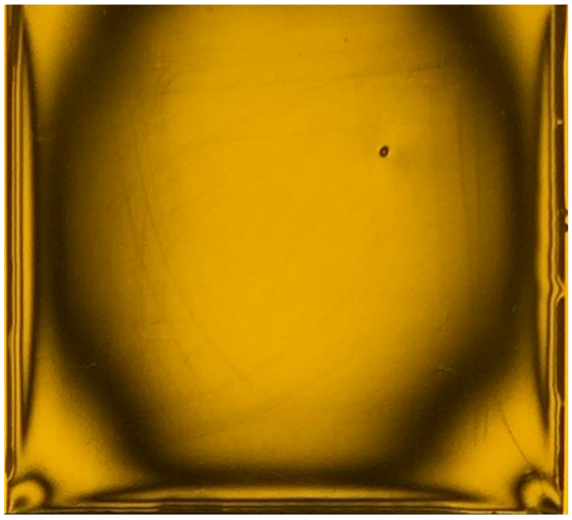

Figure 2.23 - S1 resin specimen viewed in a polariscope. The isochromatic fringe pattern represents residual stress from the fabrication process.

Figure 2.23 shows the localised photoelastic response used to determine the residual stress present in the resin specimen. Observations of the images indicate that areas under stress can be inspected visually and quantitatively under high magnification or with other experimental stress analysis techniques. The difference in the sum of principle stress $\sigma_1 - \sigma_2$ can be quantified from the fringes.

Investigation into crack propagation has been based on characterising the displacement field. Photoelastic stress analysis has been the centre of successful characterisation of stress fields around the crack. However, these techniques are not able to take into consideration plasticity effect. The increased interest in this field has led to the development of experimental techniques for characterising crack tip stress field from displacement field measurements. Recent advancements in high resolution digital camera technology provided the ability to utilise the full field elastic displacement field measurement to directly measure and given rise to the possibility of investigating the influence of plastic deformation around the crack tip during crack growth. Digital image correlation (DIC) is relatively straight forward, cost effective technique to employ and the chosen mode for characterising displacement fields.

2.4.3 Parameter extraction and digital image correlation studies in mixed mode fracture experiment

Mechanical experimental testing techniques enable scientists to measure fracture mode and material characteristics by measuring fracture parameters. A singular fracture parameter is not sufficient in many cases to accurately describe fracture behaviour or crack tip stress fields, mainly where it is predominantly plastic [132]. A number of parameters can be evaluated such as *K* (stress intensity factor), G (strain energy release rate), J (the energy contour integral), T (T-stress), CTOA (crack tip opening angle) and CTOD (crack tip opening displacement) can be measured within reasonable accuracy (these parameters are further detailed and explained in chapter 5.5).Measurement of Crack Tip Opening Displacement (CTOD) is achieved by measuring two displacement subsets and then evaluating the position of the reference to the original. Figure 2.24 illustrates the crack tip opening displacement measurement technique by characterising the DIC image subset. 3D digital image correlation is almost identical to 2D DIC with differences in the reference and origin subset [90, 92].

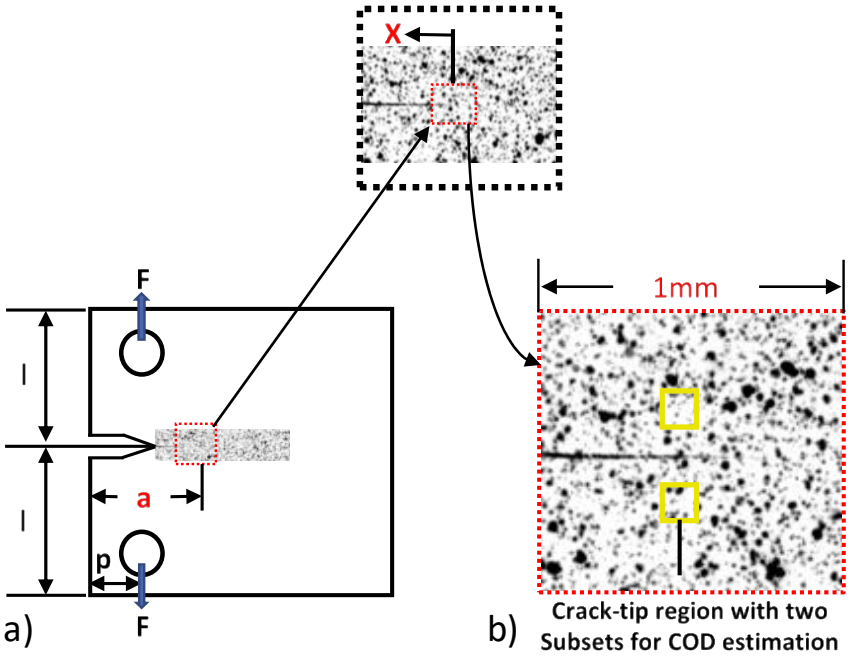

Figure 2.24 - a) 2 mm thick extended compact tension specimen and the CTOD two subset location of the pattern and b) 2D DIC Subset Characterisation

Early work conducted at the University of Sheffield [133] provides a way to achieve material characterisation by examining extracted fracture toughness parameters at the point of failure. Very few studies have attempted to characterise mode II (shear) or mixed mode I&II (tension/shear) composite fracture by analysing measurement made by extracted parameters from a composite matrix and experimental optimisation is very important.

Although experiments undertaken in this project uses almost brittle materials and studies related to elastic solution are well described [29, 30], the extraction of multiple parameters and crack tip stress field measurement are greatly preferred over load based and numerical equation approaches. The materials tested in this project have a very low plasticity, brittle composition and interest of crack behaviour in epoxy resins in Mode II and Mixed Mode I & II loading leads to SIF K_I and K_{II} and T-stress parameters to be extracted with high concern. DIC is a useful tool for obtaining displacement fields around the crack tip. Using the displacement fields, key fracture parameters can be evaluated and extracted. There has been a lot of work undertaken on extracting mixed mode SIF from DIC displacement field data [134-140]. In general the extraction involves fitting of displacement field into the Williams' stress field solution [134, 135] (shown in equation 2.7a and 2.7b) or the Muskhelishvili approach [141, 142]. A number of different methods have been used, in particular the Westergaard crack tip stress solutions for predominantly Mode I fractured cracks only [143, 144], however the Westergaard crack tip method is less accurate and more limited than the Muskhelishvili and Williams' approach. Applying Williams approach for extracting requires fitting strain or displacement fields, stress to a suitable form of the Williams stress solutions; which is an infinite series solution (as shown in equation 2.9a and 2.9b), usually by using either the Newton-Raphson or least-squares iterative methods.

Mode I

$$\sigma_{xx} = \sum_{n=1}^{\infty} \frac{n}{2}\, r^{\frac{n}{2}-1} a_n \left\{ \left[2 + \frac{n}{2} + (-1)^n\right] \cos\left[\left(\frac{n}{2}-1\right)\theta\right] - \left(\frac{n}{2}-1\right) \cos\left[\left(\frac{n}{2}-3\right)\theta\right] \right\}$$

$$\sigma_{yy} = \sum_{n=1}^{\infty} \frac{n}{2}\, r^{\frac{n}{2}-1} a_n \left\{ \left[2 - \frac{n}{2} - (-1)^n\right] \cos\left[\left(\frac{n}{2}-1\right)\theta\right] + \left(\frac{n}{2}-1\right) \cos\left[\left(\frac{n}{2}-3\right)\theta\right] \right\}$$

$$\tau_{xy} = \sum_{n=1}^{\infty} \frac{n}{2}\, r^{\frac{n}{2}-1} a_n \left\{ \left(\frac{n}{2}-1\right) sin\left[\left(\frac{n}{2}-3\right)\theta\right] - \left[\frac{n}{2} + (-1^n)\right] sin\left[\left(\frac{n}{2}-1\right)\theta\right] \right\}$$

(2.9a)

Mode II

$$\sigma_{xx} = \sum_{n=1}^{\infty} \frac{n}{2}\, r^{\frac{n}{2}-1} b_n \left\{ \left[2 + \frac{n}{2} - (-1)^n\right] \sin\left[\left(\frac{n}{2}-1\right)\theta\right] - \left(\frac{n}{2}-1\right) \sin\left[\left(\frac{n}{2}-3\right)\theta\right] \right\}$$

$$\sigma_{yy} = \sum_{n=1}^{\infty} \frac{n}{2}\, r^{\frac{n}{2}-1} b_n \left\{ \left[2 - \frac{n}{2} + (-1)^n\right] \sin\left[\left(\frac{n}{2}-1\right)\theta\right] + \left(\frac{n}{2}-1\right) \sin\left[\left(\frac{n}{2}-3\right)\theta\right] \right\}$$

$$\tau_{xy} = \sum_{n=1}^{\infty} \frac{n}{2}\, r^{\frac{n}{2}-1} b_n \left\{ \left(\frac{n}{2}-1\right) cos\left[\left(\frac{n}{2}-3\right)\theta\right] - \left[\frac{n}{2} + (-1^n)\right] cos\left[\left(\frac{n}{2}-1\right)\theta\right] \right\}$$

(2.9b)

Early method by Muskhelishvili [145], requires two complex functions to be applied to the stress field around the crack tip, a complex Fourier transformation series and boundary conditions in order to define the crack . The method is then solved for determining K_I and K_{II}. An exhaustive review of the following approach, design and testing of crack tip fracture parameter extraction techniques utilised in this project is available in [57].

An alternate technique, apt for material study in fatigue, thermoelastic stress analysis (TSA) has been used to determine fracture parameters and stress fields, applying both Muskhelishvili and Williams solution method [55, 57, 135].

Before the use of DIC was a widely accepted tool, Nurse and Patterson used photoelastic fringe patterns surrounding a notch cracks on the attaching end (firtree like shape) of turbine blade to extract mode I SIF under compression [144] with applying the Westergaard stress calculation. In later study [141] four-point bending (4PB) shear loading was used to extract mixed mode SIF using the Muskhelishvili approach.

Dally and Sanford were the first in the 1970s to use Williams approach taking into account the non-singular T-stress term to extract SIF from photoelasticity fringe patterns. Furthermore,

they only needed to use two terms of the Taylor series of Williams solution; achieving errors of ± 10 % for K_I and ± 13 % for K_{II}. Commonly, more than the first two terms of the series using the Williams stress solution is required for achieving an accurate fracture parameter extraction results.

Zanganeh observed that using three terms of the series using Williams stress solution was used to measure K_I and K_{II} to achieve ± 13 % accuracy and convergence occurred at 15 or more terms with an accuracy of ±7% [57]. Using Zanganeh's Matlab algorithm based on current computing hardware to calculate SIF using the Williams solution expanding for 20-50 series terms takes between 0.5-1 second and it is not computationally demanding.

An advantage of using the Williams approach over the Muskhelishvili's is the ability to extract the T-stress from displacement field data, a difficulty of this was shown by Zanganeh et al. [134], in particular the crack tip location needs to be accurately identified. It was shown that a poorly defined crack tip with just a few pixels away from the actual crack tip location, produced accurate K_I and K_{II} values by using either Muskhelishvilli or Williams solution. However, both approaches gave variable T-stress values. Assessment of crack tip location sensitivity is discussed in section 2.52. It would be beneficial to utilise a robust algorithm that can locate the crack tip from displacement field data. An established parameter for crack path stability is T-stress [146, 147] and an essential parameter for considering Mode II experimental evaluation [148], T-stress is explained further in section 2.14.

López-Crespo et al. used DIC to successfully measure mixed mode I and II SIF in a fatigue induced cracked test specimens using the Muskhelishvili's method [142]. The test specimen was lightly scratched on the surface region of interest to define a speckle type pattern for determining DIC displacement field measurement. Crack tip was discovered by using the Sobel–Feldman operator for edge detection and adequately identified accurate extracted K values. Additionally, the same research team in [134] advises the use of a more advanced crack

tip identification algorithm for determining displacement fields at the crack tip, where the accurately selected location is used to extract T-stress.

An interesting study by Du at al. [140] shows the use of DIC to extract fracture parameters of mixed mode I and II applied to a specimen from an aircraft panel. Using the López-Crespo's method [142] and the Muskhelishvili's approach [145].

Furthermore, Hild and Roux in numerous research article [136, 138, 149, 150] showed the Applicability of the Sobel–Feldman edge detection algorithm combined with the Muskhelishvili approach for addressing challenges relating to large displacement fields and tough materials. An in-house modular DIC system was later developed by the researchers [150], CORRELLIQ4, to integrate finite element analysis (FEA) with DIC system in attempts to reduce noise and simplify processing of displacement field data. The tool enables the integration of displacement field, geometry and any other known material behaviour included into the algorithm for post processing. Benefits include advantages of integrated displacement field calculation in single tool, applying crack tip detection algorithm and enable extraction of fracture parameters. However, the CORRELIQ4 tool is not a commercial of the shelf tool and unavailable for public and commercial use.

Yates et al. conducted a review into the assessment of fracture problems using DIC [151], notably the study of more complex problems with anisotropic and plasticity. A key finding identified some differences between T-stress values extracted using Williams approach with Zanganeh's DICITAC tool and T-stress values acquired from FEA [152]. The differences in T-stress values observed was due to a number of factor attributed to FEA limited capability to asses such features as crack front curvature, surface residual stresses, non-planar crack, crack closure and anisotropic material properties affecting t-stress observed in physical mechanical specimen testing. DICITAC is further detailed and explained in section 2.5.

2.5 DICITAC

A Matlab based standalone tool (Figure 2.25) developed as part of PhD thesis [57] by Dr Mohammad Zanganeh at University of Sheffield called DICITAC (Digital Image Correlation Intensity factor and T-stress Analyser Code) [152] was used extract fracture parameters from displacement field of processed individual frames captured during DIC experiments.

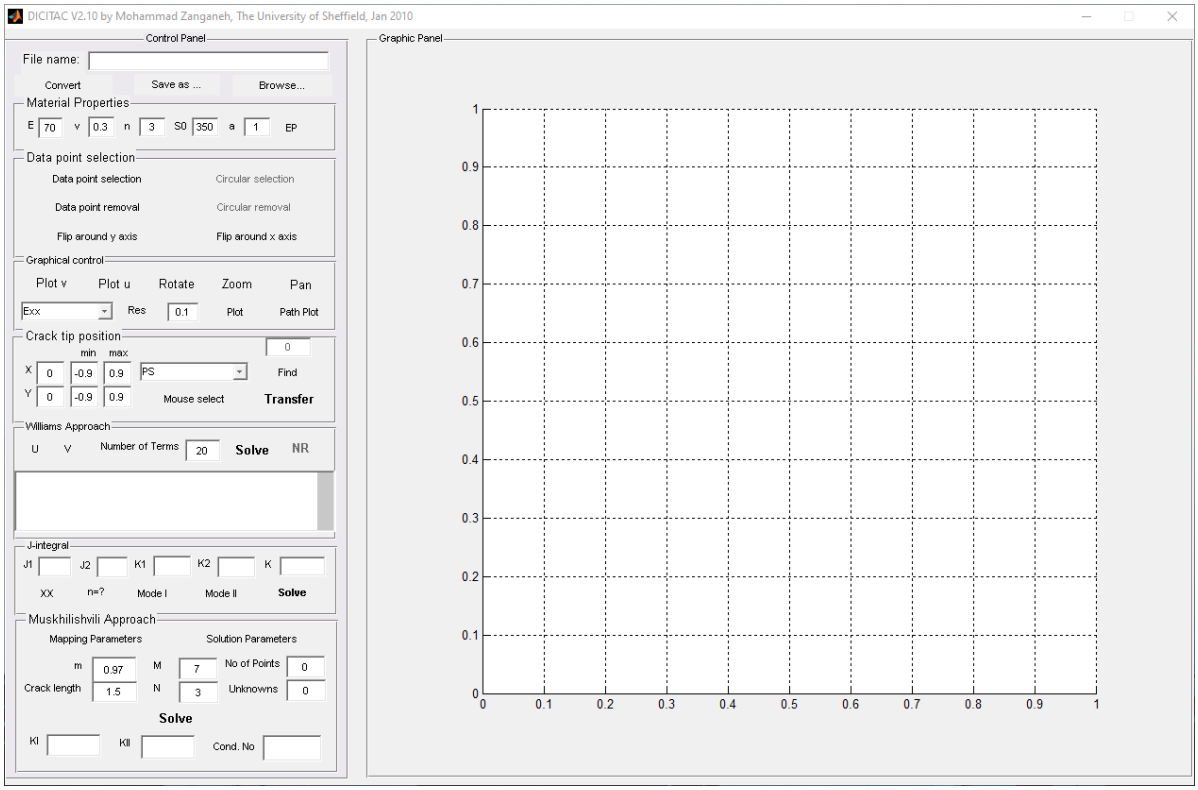

Figure 2.25 - DICITAC standalone tool

DICITAC requires two elastic moduli inputs for calculating the stress intensity factors (SIF) from displacement fields using the Williams series stress solutions. Poisson's ratio and Young's modulus (E) are entered into DICITAC prior to implementation. Due to proprietary reason the values were provided from Cytec Engineered Ltd to be used for the parameter extraction. These values are listed in section 5.1 (F-Formulation) and section 6.2 (S-Formulation).

2.5.1 Using DIC displacement fields to extract fracture parameters with DICITAC

The captured DIC images during experiment are recorded until loaded to failure with a single camera setup, cross-correlation algorithms are performed to produce displacement vector field. The vector field is converted and saved into strain fields, using 'DICITAC' (Developed at the University of Sheffield by Zanganeh) to fit the Williams series equation to the experimental data to extract crack tip parameters K_{IQ}, K_{IIQ}, T-stress (Figure 2.26).

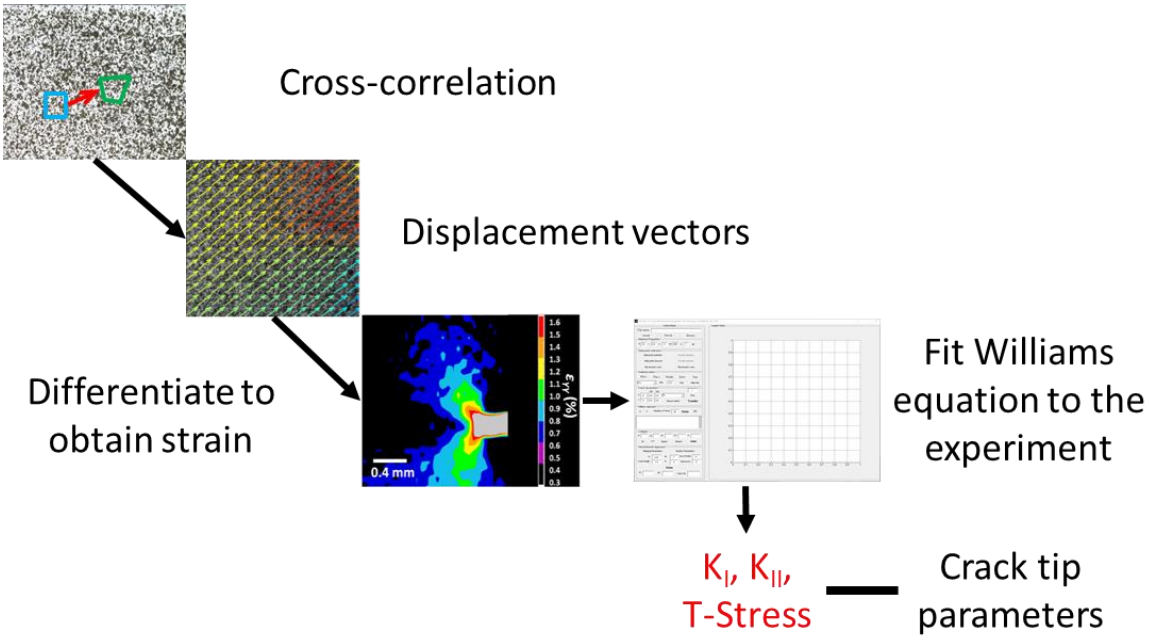

Figure 2.26 - Data extraction with DICITAC

The tool provides different options to the user for extracting K_{IQ} and K_{IIQ} using either the Williams series [44] or the Mukshilisvilli [145] crack tip stress solution. However, using the William series crack tip stress solution provides the user an additional option to extract T-stress. DICITAC tool uses the Williams stress infinite series solution equation to solve in a cartesian displacement form (equation 2.7a and2.7b) to find unknown constant values for each displacement field with elastic properties input using a Moore-Penrose pseudoinverse least square method [74].

$$mode\ I \begin{cases} u_1 = \sum_{n=1}^{\infty} \frac{r^{\frac{n}{2}}}{2\mu} a_n \left\{ \left[\kappa + \frac{n}{2} + (-1)^n \right] \cos\frac{n\,\theta}{2} - \frac{n}{2}\cos\frac{(\mathrm{n}-4)\,\theta}{2} \right\} \\ v_1 = \sum_{n=1}^{\infty} \frac{r^{\frac{n}{2}}}{2\mu} a_n \left\{ \left[\kappa - \frac{n}{2} - (-1)^n \right] \sin\frac{n\,\theta}{2} + \frac{n}{2}\sin\frac{(\mathrm{n}-4)\,\theta}{2} \right\} \end{cases} \quad (2.10a)$$

$$mode\ II \begin{cases} u_{11} = -\sum_{n=1}^{\infty} \frac{r^{\frac{n}{2}}}{2\mu} b_n \left\{ \left[\kappa + \frac{n}{2} - (-1)^n \right] \sin\frac{n\,\theta}{2} - \frac{n}{2}\cos\frac{(\mathrm{n}-4)\,\theta}{2} \right\} \\ v_{11} = \sum_{n=1}^{\infty} \frac{r^{\frac{n}{2}}}{2\mu} b_n \left\{ \left[\kappa - \frac{n}{2} + (-1)^n \right] \cos\frac{n\,\theta}{2} + \frac{n}{2}\sin\frac{(\mathrm{n}-4)\,\theta}{2} \right\} \end{cases} \quad (2.10b)$$

$\kappa = 3 - 4\,\nu$ for plane strain condition

$\kappa = \frac{(3-\nu)}{(1+\nu)}$ for plane stress condition

$\mu = \frac{E}{2(1+\nu)}$ where μ is the shear modulus

ν is the Poisson's ratio and a and b are constants

The Williams infinite series solution expressed in equations (2.10*a*) and (2.10*b*) is reproduced directly from Mohammed Zanganeh PhD thesis [57]. Expansion of the equations (4*a*) and (4*b*) provides $\kappa_{\mathrm{I}} = \frac{a_1}{\sqrt{2\pi}}$, $\kappa_{\mathrm{II}} = \frac{-b_1}{\sqrt{2\pi}}$ and $\mathrm{T} = 4a_2$, therefore by solving a_1, b_1 and a_2, the fracture parameters can be obtained. Previous studies at the university of Sheffield by S. Jones [56] identify that solving the first fifteen terms was required for converging results and the computational time required is minimal hence 20 terms of the Williams stress solution expansion was used.

Work conducted by Jones [34] reveals that when the load cell data around the critical region is corrected for the increasing crack length values up to failure, there is a close similarity between load cell and DICITAC obtained *K* values. However, observations indicate limitations when using the William's method or other similar methods for measuring critical toughness values (K_c) in materials that exhibit unstable crack propagation prior to failure. The use of load based measurement technique with uncorrected propagating crack length provides maximum *K* values which is representative of a typical material plane strain fracture toughness, *K*.

Furthermore, using the Williams series technique indicates no such failure problems and by extracting individual stress intensity factor immediately before failure will not always provide a critical, static, stress intensity factor but instead a dynamic stress intensity factor. Care must be taken to ensure the correct SIF values are measured and recorded as “critical” when growing cracks.

The material investigation in this study is not using “standard” specimen geometry in order to induce plane strain conditions as indicated in BS ISO 13586 or ASTM D5045. This work is measuring the material fracture toughness for a specimen of a specific thickness (4 mm) with a specific pre-crack length (2 mm) to compare the relative fracture behaviour of the materials. Therefore, DICITAC / Williams approach can be used to extract SIF ‘*K*’ material fracture toughness values.

2.6 Conclusion

This chapter has introduced linear elastic fracture mechanics (LEFM), fracture testing of resin and the experimental image analysis techniques to be used in this work. The current study aims to evaluate the stress intensity factor using digital image correlation.

Amongst the two types of digital image correlation (DIC) systems, 3D DIC is a common choice for investigation purposes since it provides the capability of assessing both in-plane and out-of-plane deformation. However, complexity in configuring and calibrating negates its use in the current study. It is quick, simple and easy to configure and calibrate a 2D DIC for investigation provided that the out-of-plane errors are negligible. Although it is imperative to consider out-of-plane deformations and that measurements to assess the level of out-of-plane influence before using a 2D DIC system, experimental time is notably lesser when compared with 3D DIC. The current study aims to improve the efficiency of experimentation to evaluate fracture mechanics of composite materials and enable qualitative material characterisation in an industrial environment.

Although T-stress is discussed in this chapter as a fracture parameter of interest, it has been established that it is a relatively changing parameter to measure. The second order nature of the term becomes significantly more difficult to measure than SIF's. The sensitivity and application of DIC methods to measure T-stress in relatively brittle materials such as resins is unknown; previously T-stress have only been measured by DIC in much tougher materials with larger displacements and T-stress measurement will not be investigated as a main parameter. Instead, the focus will be driven towards looking at stress intensity factors and calculating the fracture toughness of the material from the SIF.

In the next chapter, a series of experimental optimisation techniques will be described, which will be critical for the use the DIC fracture parameter extraction technique on resin specimens to assess the applicability and limitations of the testing method.

CHAPTER 3

Optimisation of specimen manufacturing, polishing, pre-crack application and speckle pattern painting

3.1 Introduction

Materials used in this research for the assessment of fracture toughness was sponsored by Cytec Industries. Proprietary rights inhibit the disclosure of material composition and hence, the materials are represented as the F-Formulation and S-Formulation for study purposes. Both material chemistries have a neat resin referred to as F1 and the particulate toughened resins are referred to with increasing numerals as F2, F3, F4 and so on.

Measuring fracture toughness parameter is a complex process and a methodical experimental approach is required to achieve optimum results. Of the different failure modes of engineering components, mode I (tension) fracture testing is more commonly used than mode II or mode III. This is because international standard testing exists only for mode I, thus ensuring accuracy of results. However, other fracture modes (mode II, mode III and mixed mode I and II) are important to investigate, but they are relatively more complex and there is no standardised international test method for these modes.

When measuring fracture toughness parameters of a toughened material with a test coupon, it is important to have an optimum geometry for the specimen to achieve an accurate material intrinsic value. Therefore, it is essential to select or tailor close to a specified standard testing method which can optimise experimentation in achieving high levels of accuracy with results obtained. There are several different types of experimental methods, as discussed in section 2.4, which can be used to identify intrinsic parameters. In consideration, testing standards from ASTM D5528-01 [153] and BS ISO 13586:2000 [38] were reviewed to tailor an appropriate testing method for evaluation of fracture toughness parameters.

The LEFM approach would be the appropriate testing solution for the identification of K_{Ic}, K_{IIc} and T-Stress [38]. Although three-point bending system (3PBS) or 3ENF or SENB, four-point bending system (4PBS) or 4ENF, can be used to identify the intrinsic parameters, it would not

be suitable for tailoring experiments to include DIC. This is due to the focal point of the field of view, where the grey scale CCD camera will focus ahead of the crack. When the 3ENF or 4ENF is tested, the movement of the sample will be far greater than the field of view leading to inaccurate results.

A recent study conducted at the University of Sheffield by Jones and Tomlinson [56], identified the intrinsic parameters by modifying the standard testing method for fracture toughness (BS ISO 13586:2000 Plastic-Determination of Fracture Toughness (G_{IC} and K_{IC}) - Linear Elastic Fracture Mechanics (LEFM)) [38]. This was achieved with the use of DIC, a modified Arcan test rig and applying LEFM to the third term of the Williams solution to obtain the intrinsic parameters. There are three terms of the Williams solution and the distribution of the stress at the tip of the crack is able to be expanded as a power series. The first term is normally known as the stress intensity factor that calculates the amount of fracture in a brittle material. The second term makes sure that the direction of the crack remains stable, whereas the third term controls the propagation of the crack to ensure its stability. This methodology has many advantages over other mixed mode testing as it can identify more than a single fracture toughness parameter and would be the ideal approach to observe effect of particulate toughening and crack path stability in resins and composites.

One drawback to Jones' methodology is the time taken to prepare the specimens for DIC fracture testing. Technique used to date for specimen preparation and their limitations are summarised in Table 3.1

Techniques for Optimisation	Time Taken	Problems / Disadvantages
Traditional manufacturing of one plaque specimen	2 weeks	Traditional manufacturing techniques introduces residual stresses
Manually polishing by hand	30 min / specimen	Time consuming, can hazardous if the user is not wearing a mask.
A standard blade utilised to grow a pre-crack manually	10 min / specimen	Very difficult to achieve identical pre-crack length repeatedly
Old spray paint gun	10 min / specimen	A reasonable controllable fine speckle pattern can be achieved

Table 3.1 - Sample preparation techniques used to date and their limitations.

The improvement of the preparation techniques can increase overall experimental efficiency and lead to a more standardised approach of fracture analysis. This could be a significant step in optimisation of the overall testing method and thus provide an improved understanding of the processes that leads to occurrence of fracture.

This chapter aims to optimise preliminary steps involved in enhancing experimental accuracy for studying fracture behaviour and material properties of different resin materials. The various fabrication methods to be considered for optimisation are specimen preparation, manufacturing, polishing, pre-crack application and speckle pattern painting.

3.1.1 Specimen Manufacturing

Optimisation of specimen fabrication techniques streamlined the process involved in experimentation, with the aim of achieving an efficient and safe method of sample preparation before testing. Specimens are generally manufactured from plaques of resin and machined by using a saw cutter and / or a milling machine and a pillar drill to generate a shape such as that of the SJ Arcan specimen as shown in Appendix 1 (Figure 1 c).

Precise dimensions are essential with minimal residual machining stresses [154]. These traditional manufacturing methods are labour intensive. The machine operator must be highly skilled to perform manufacturing of specimens to a high standard and the entire process is often time consuming and poses a health risk. Additionally, there is a risk of introducing residual stresses if adequate coolant is not used, if feed speeds are incorrect [155].

In this study, research was focussed on the introduction of residual stress in resin specimens during drilling, using a pillar drill with and without coolant, and using the CNC. The specimens were made from the same sheet of F1 formulation neat resin and viewed in a polariscope to visualise the residual stresses. The isochromatic fringes represent contours of maximum shear stress, thus the greater the number of fringes, the greater the residual stress. Figure 3.1 shows images of three F1 formulation (neat resin) viewed in the polariscope after drilling the material under the three different conditions.

The material drilled with the drilling machine revealed an extended isochromatic fringe pattern of the surrounding area of drilling hole observed in the polariscope (Figure 3.1 a). The material drilled with the drilling machine in presence of water shows a small fringe pattern in the surrounding area of the drilled hole observed in a polariscope (Figure 3.1 b). The material

drilled with the CNC machine in presence of coolant shows no isochromatic fringe pattern in the surrounding vicinity of the drilled hole (Figure 3.1 c).

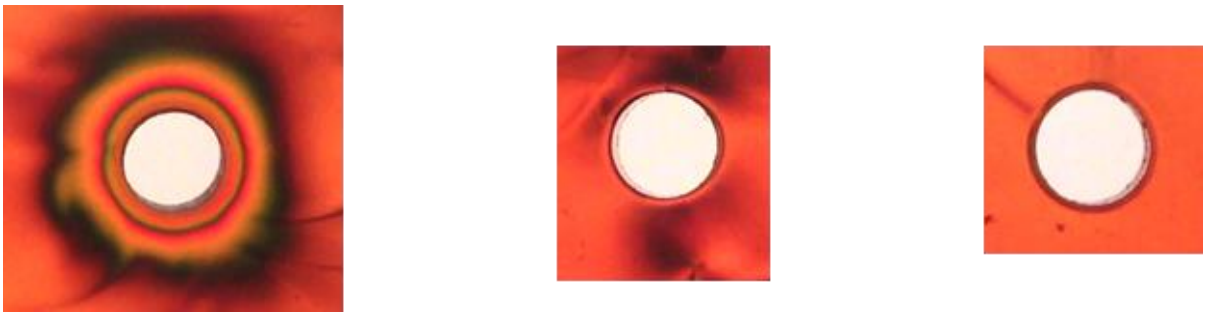

(a) *(b)* *(c)*

Figure 3.1 - Visual representation of Residual Stress of F1-NEAT specimen subjected to machining, (a) Pillar drilled without a coolant, (b) Pillar drilled with water and (c) CNC drilled with a coolant.

Therefore, CNC machining is the best approach to manufacture specimens and all the specimens required for experiments in this study will use CNC machining.

3.1.2 Polishing specimens

The plaques of formulated resins are manufactured in a steel mould tool and the curing of the resin occurs in different stages and final curing performed in an oven controlled environment. The resin chemistry is mixed in the state of the art vacuum mixing chamber unit (industrial proprietary technology). The resin mixture is poured into an oven preheated mould tool with an inner surface of 150mm x 100mm and left to cure in a temperature controlled oven. The cured resin takes the form of the rectangle plaque (Figure 3.2).

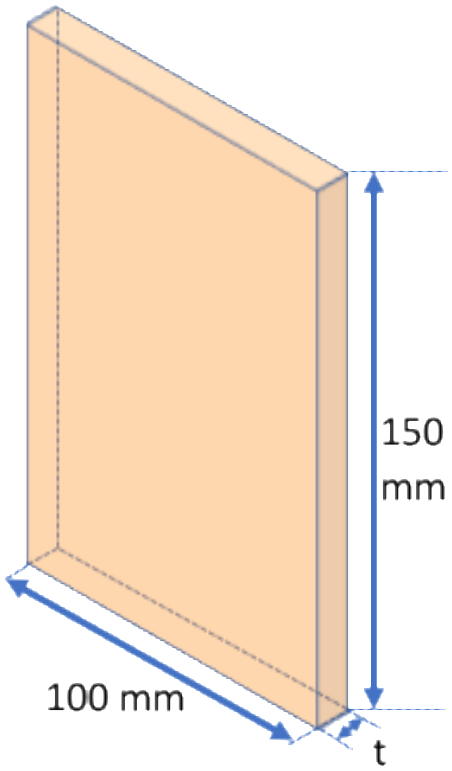

Figure 3.2 - A schematic drawing of the material plaque and dimensions.

Conventional methods for achieving uniform specimen thickness and removing the resin-rich layers require the specimens to be manually sanded with a fine grit/sand paper. Often, the manual polishing process requires a lot of care and time for achieving a uniform thickness of each specimen. Hence, it is difficult to yield repeatable results. Further, employing the conventional method in an industrial testing environment is not an adequate and consistent sample preparation technique. Therefore, it is important to develop an accurate repeatable efficient specimen preparation method. Repeatability of specimen preparation can be achieved by automating the process that resembles conventional polishing techniques by using different fine grit/sand paper. Often using a sand paper to achieve adequate thickness is difficult, time consuming and can be harmful if the dust particles are accidentally inhaled. Furthermore, using an automated polisher to achieve controlled and repeatable conditions for specimen thickness is an optimum method that can be implemented.

Recent work conducted by Jones and Tomlinson [56] discovered bowing on both sides of surfaces of the manufactured plaques and indicated a partial contribution to erroneous results. Their specimen manufacturing technique was adapted by automating to minimise sample preparation time and loss of material. Research conducted by Savabi et al shows that post curing contraction occurred when manufacturing resin samples [156]. This suggests that the rate of curing in resins affects overall bulk resin volume, thereby causing shrinkage. Cunha et al indicate the change in post polymerisation rate effect the level of shrinkage that induces stress into a composite [157]. Therefore, it is important to ensure good practices when preparing specimens for fracture testing to ensure minimal residual stresses in the resin. The shrinkage in the curing process can cause uneven thickness of the resin plaque.

A sample preparation rig was designed to optimise the sample polishing. The polishing machine has an automated polisher with an extended arm for the sample rig to attach (Figure 3.3). Since the sample rig available was not able to accommodate large specimens, a customised sample rig was designed (Figure 3.4 a). Based on previous findings, it was decided that polishing the specimens after the CNC process was more efficient. Only the cut specimen is required polishing and not the specimen with the waste material. If the six or more specimens are to be machined from a single plaque these need to be of the uniform thickness to provide a repeatable, identical sample geometry. Additionally, the surface of the plaque tended to exhibit a resin-rich layer of up to 3 mm, where the particle distribution was not uniform. So, the plaque or cut specimens had to be polished to achieve a uniform thickness and remove resin rich layer and any surface abnormalities such as bubbles.

It is also important to remove any unwanted surface abnormalities, such as bubbles formed in the surface and any resin rich formation on the surface of the material. The sample preparation rig will ensure that all the test samples are similar in dimension without removing excessive

material volume. The steps involved in designing a tool for optimising test sample dimensions is a complex process, due to the variation in samples dimensions, to which there are many techniques and process that are required to be incorporated.

The polisher plate revolves counter clockwise to the sample rig and conversely, the sample rig revolves clockwise. The speed of both the sample rig and polisher plate can be adjusted individually while a steady flow of water over the polisher plate is maintained. Moreover, findings suggested that improper sample orientation could result in occurrences of residual stress in the samples.

The automated sample polisher houses the material in the holder block inside the sample rig (Figure 3.4 b) developed in house. The holder block can accommodate different specimen geometries (Figure 3.5). The sample rig remains attached to the arm of the polisher and locks in place before moving the arm in line with the polisher plate. Samples prepared with this approach achieve a uniform thickness throughout the sample with a minimal average difference of ±0.01 mm.

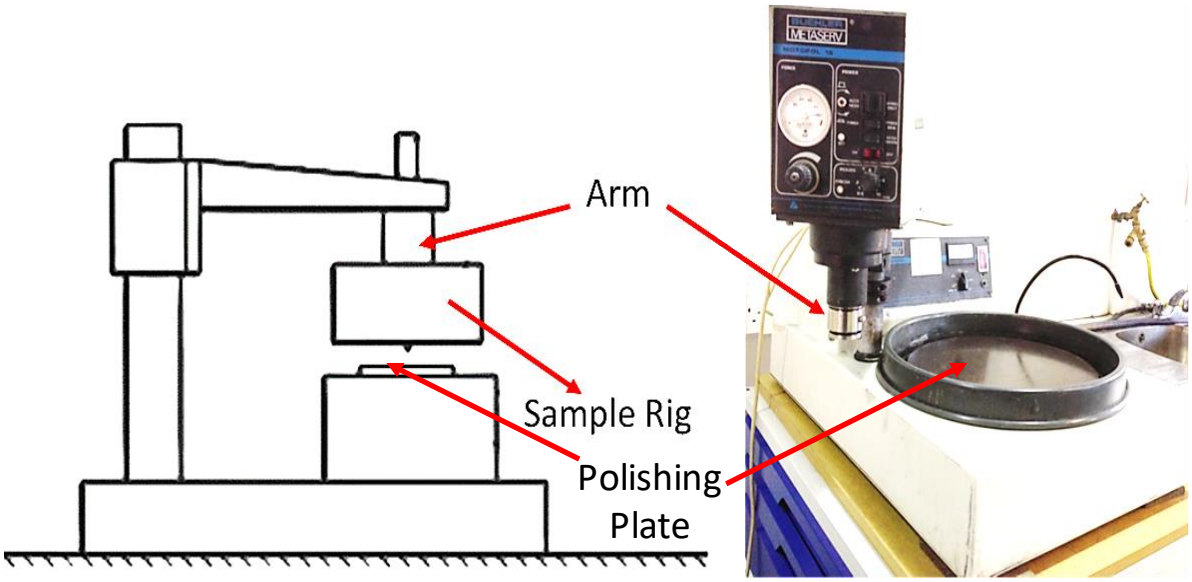

Figure 3.3 - Image and schematic diagram of the polishing unit at University of Sheffield (Buehler Metaserv Motopol 12).

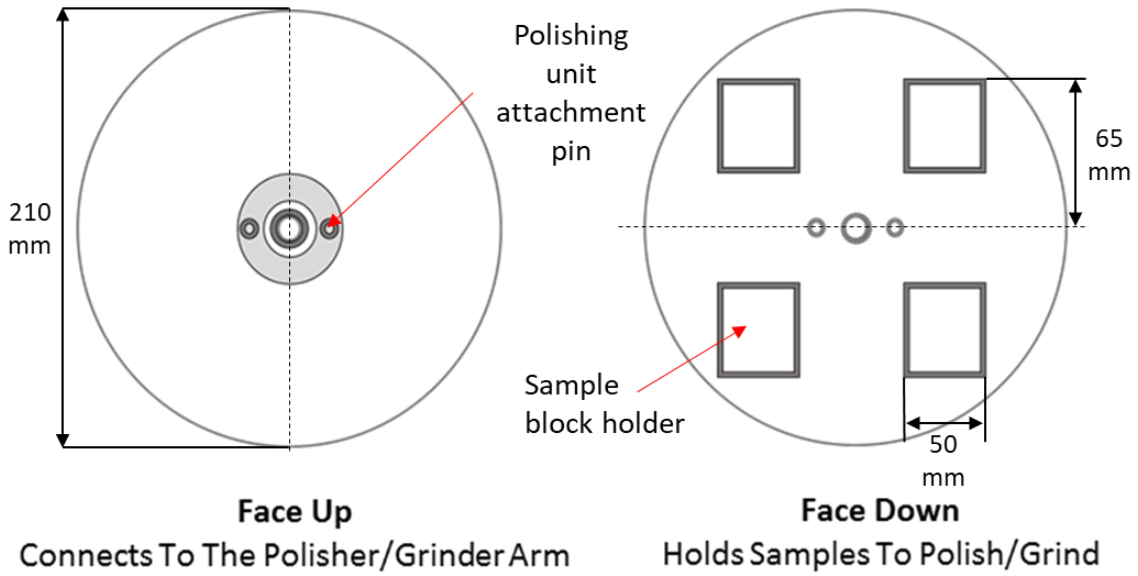

(a) (b)

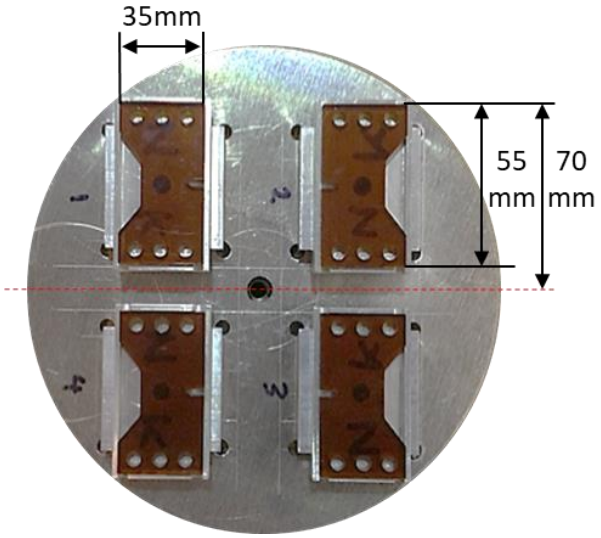

(c)

Figure 3.4 - Schematic of the designed sample preparation rig, a) Front face of the polishing rig that connects to the arm b) bottom face of the polishing rig c) Specimen block holder attached to the bottom face of polishing rig.

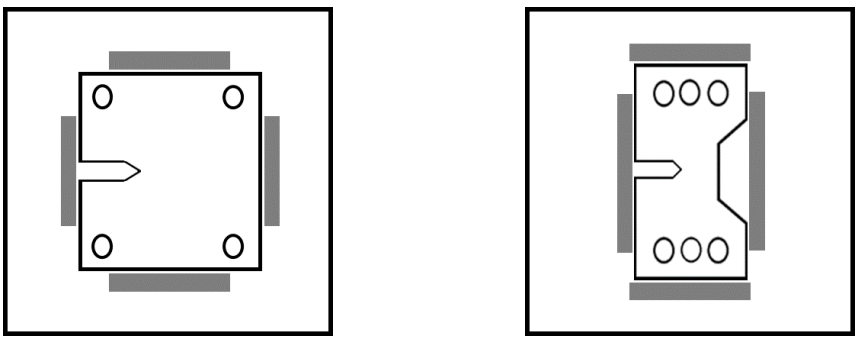

(a) CT Sample Block (b) Modified Arcan Sample Block

Figure 3.5 - Schematic of different sample block utilised in the sample rig

3.1.3 Initiation of Pre-crack in specimens

A fracture toughness test requires a number of notched specimens all containing a pre-crack, of known length, which is introduced to simulate a natural crack into the material. Both the British International Standard (BS ISO) 13586:2000 [38] and American Standard Test Method (ASTM) D5045 [79], which guide testing for the plane strain fracture toughness of polymers, indicate that the pre-crack should be created naturally by tapping at the centre of the notch with a new razor blade (Figure 3.6). The standards alternatively suggest creating a pre-crack by sliding a new razor blade in either a sawing motion (side-to-side) or slicing repeatedly in a single direction. If it is not possible to create a pre-crack using the above methods, the standards warn not to apply pressure to the new razor blade on to the centre of the notch, since this could introduce residual stresses at the tip of the natural crack and effectively alter the measured K_{Ic} values [103, 109]. It is suggested in the ASTM D6068 [158], that pre-cracking may be performed by induced fatigue cycles, however this is time consuming and it is quite difficult to achieve a fatigue crack in a brittle material without unwanted fast fracture.

Additionally, for testing of plastics (E1820), the shape of the notch is strictly defined, whereas in fracture testing of metals (ASTM E399 [159] and ASTM E1820 [160], the production of the notch is less restrictive. If the notch and the pre-crack are not introduced correctly and consistently then this has a detrimental effect on the fracture parameters determined, therefore accurate, repeatable specimen preparation is vital. Fracture specimen preparation is more challenging in brittle, polymer materials, since very little energy is required to propagate a crack in such materials, thus more controlled procedures are needed.

Generating the crack using a razor blade (Figure 3.6) is unpredictable and can result in the range of shapes of pre-crack front as shown Figure 3.7. These shapes are influenced by material properties. A notched groove created by a sharp diamond saw does not provide a natural crack

condition for investigation. Figure 3.8 illustrates that an applied cut notch does not have a natural sharp crack tip.

There is a lack of study involved in looking at the structure of the 3-dimensional crack front and the identification and analysis can be beneficial in the study of crack propagation behaviour. It is observed that this phenomenon occurs with different loading condition and stress/strain state at the point of crack initiation with respect to the homogenous nature of the material. Although, the presence of this phenomena observed, the linear elastic testing standards only requires a near flat crack front condition. Therefore, it is important to manufacture an accurate flat pre-crack front for all testing specimens.

Although it is possible to possess the necessary skill to propagate a pre-crack, it is still very difficult to achieve a repeatable natural crack length using a razor blade. Figure 3.6 shows how the blade is positioned by the operator into the machined notch and tapped vertically to propagate a crack. The tapping force needed is very subjective depending on the material and the operator. The following procedure requires good coordination and bi-lateral stable positioning to achieve a natural crack. Holding a razor blade at the correct angle and tapping the hammer simultaneously is challenging and has associated risks. Therefore, a prototype rig was designed to introduce some control into the procedure. Figure 3.7 shows the observation of different crack fronts (Figure 3.7c) during the evolution of pre-crack tool development, a Tipped cracked front (Figure 3.7a) and a Pyramid crack front (Figure 3.7b).

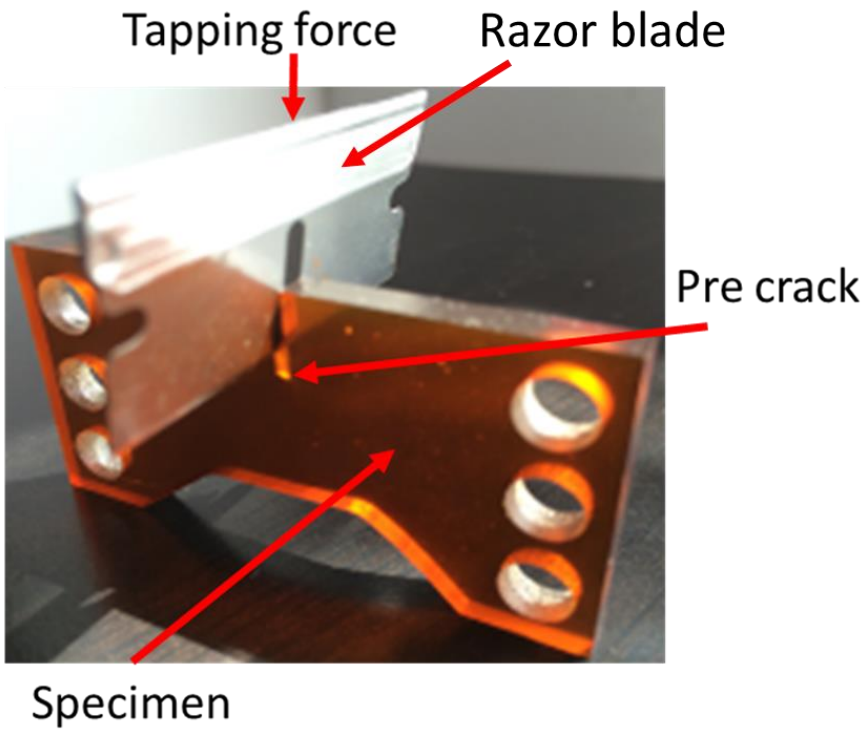

Figure 3.6 - Pre- Crack created by a razor blade.

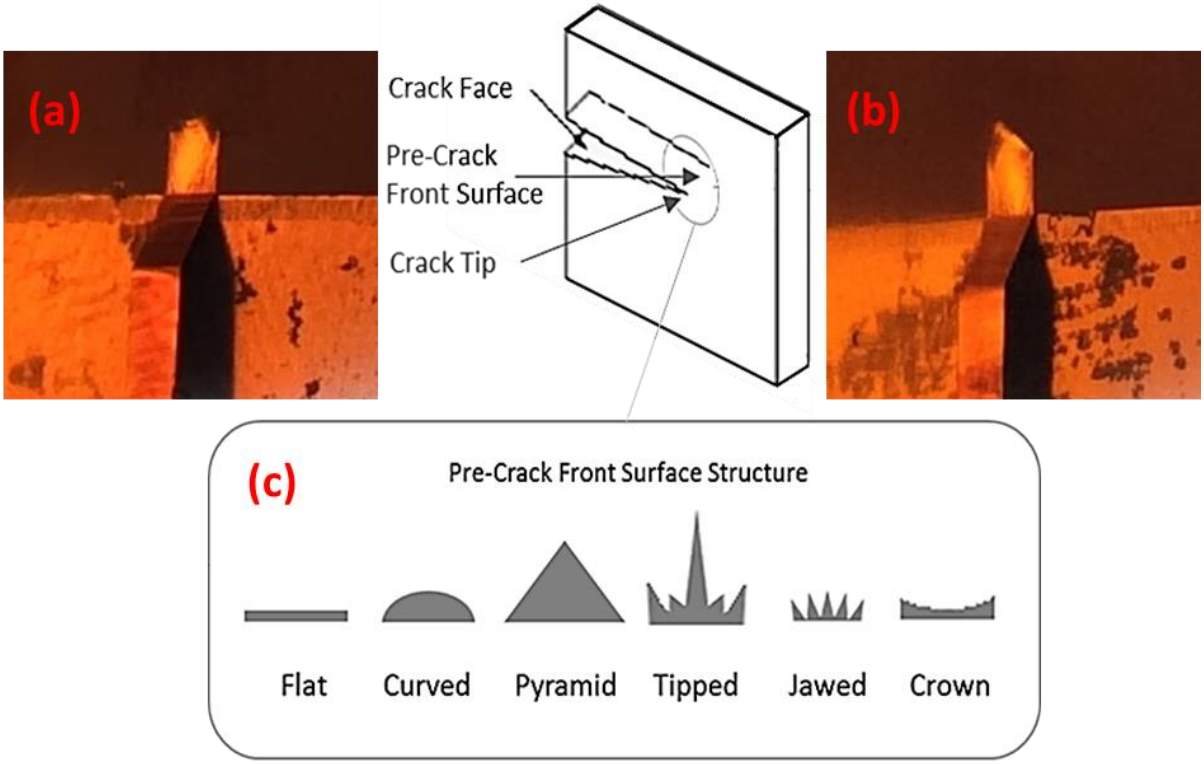

Figure 3.7 - Macroscopic view of a pre-crack front shape – (a) Tipped crack front shape, (b) Pyramid crack front shape and (c) other observed crack front shapes.

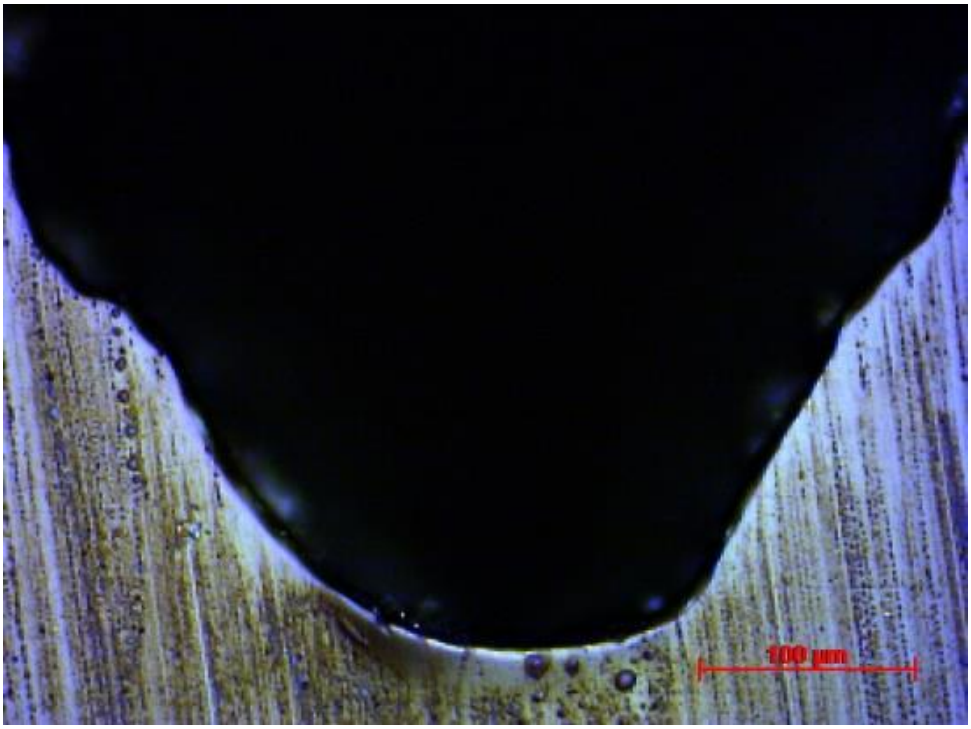

Figure 3.8 - Microscopic image of a slot created by a cutting tool (F3 specimen)

The prototype pre-crack rig was designed to create a natural crack onto the test specimen using a computer aided designing (CAD) software (Figure 3.9a). This design was developed further to control the force required to initiate crack. CAD Model Type B (Figure 3.10) was embedded within a tensile testing machine to initiate a pre-crack.

The rig clamps the specimen and holds the razor blade within the notch fixed in the x–y plane (Figure 3.9b). The razor blade is positioned just touching the tip of the notch, then the top of the fixture is tapped with a hammer by the operator. The guide springs ensure that there is no rotation of the razor blade about the z axis or y axis and also ensures that no compressive force is applied to the notch surface apart from the operator's tapping force.

Although the pre-crack rig was able to tackle the operator's coordination problems, and hence out-of-plane cracks are prevented, it was not possible to achieve complete control of the length of the pre-crack produced using this rig. The applied tapping force still depends on the operator's consistency and the material properties. Additionally, producing a repeatable pre-crack is more challenging in polymers containing toughening particles or short fibres due to

the unpredictability of such material. Finally, the risks of using a razor blade have been reduced, but not completely eliminated. Therefore, an alternative method was investigated.

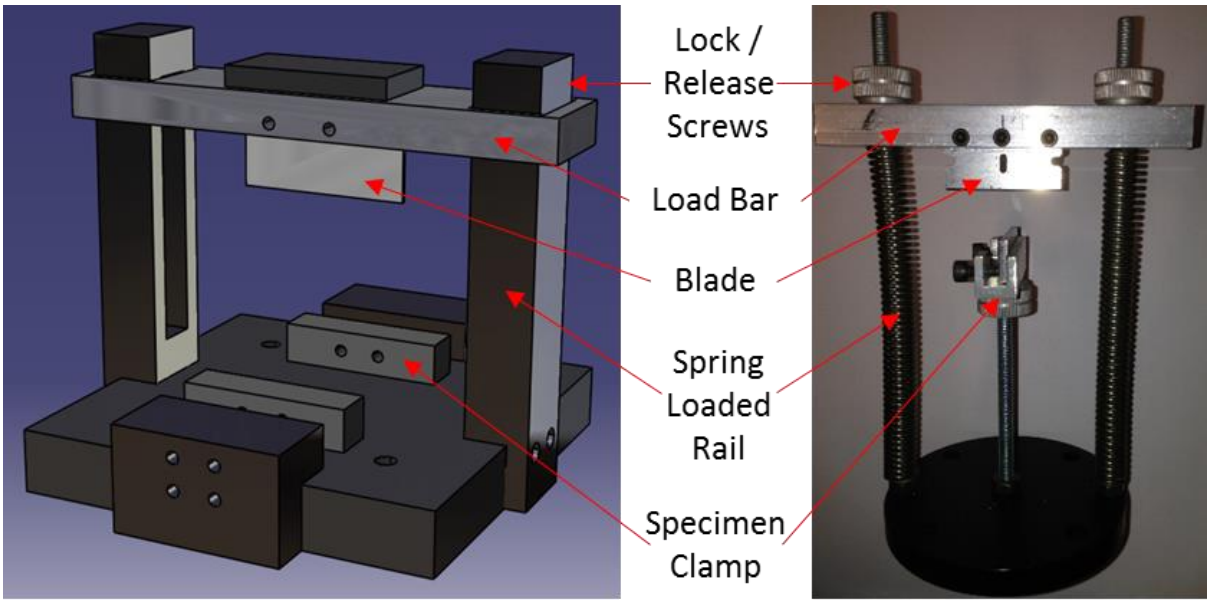

(a) (b)

Figure 3.9 - Design of the pre-crack rig (a) CAD model Type A, (b) prototype model

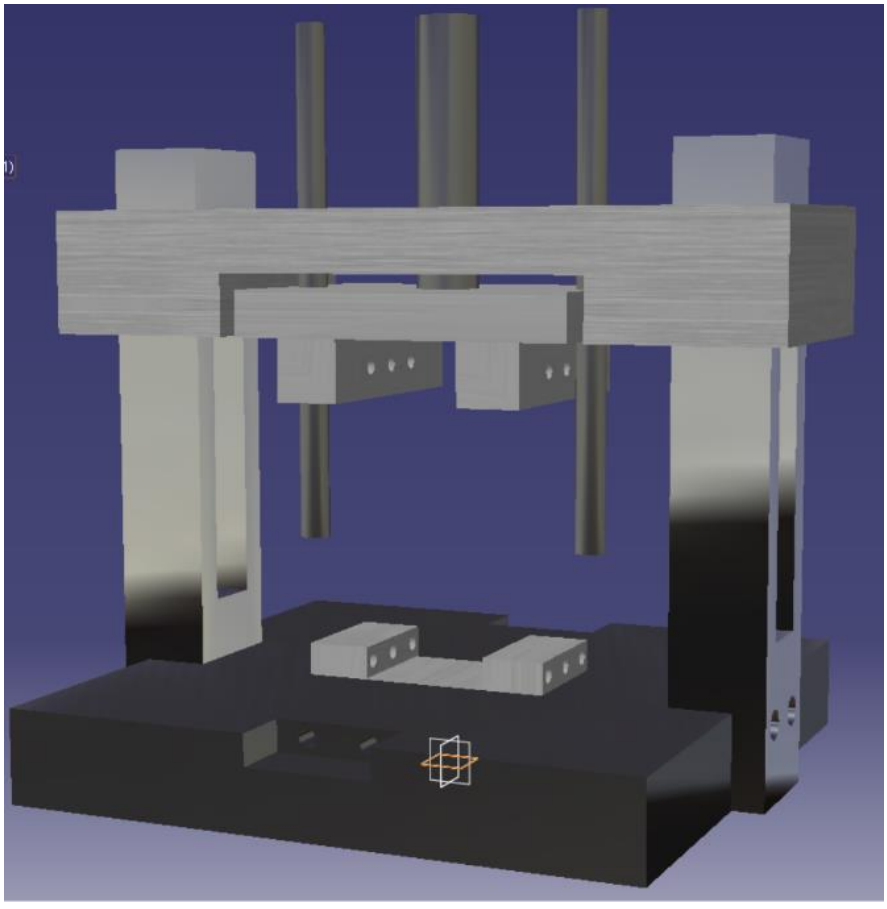

Figure 3.10 - Design of the pre-crack rig CAD model Type B version 2

CAD Model Type C (Figure 3.11) and CAD Model Type D (Figure 3.12) designs are based on applying a pre-crack without using a razor blade and are discussed in the next section. Furthermore, the CAD Model Type C enables specimen positioning, bi-lateral stability and attach to a tensile testing machine creating a pre-crack.

CAD Model B, C, D are faster to load specimens in testing frame and generate the pre-crack in comparison to the CAD Model A which uses a razor blade for generation of pre-crack.

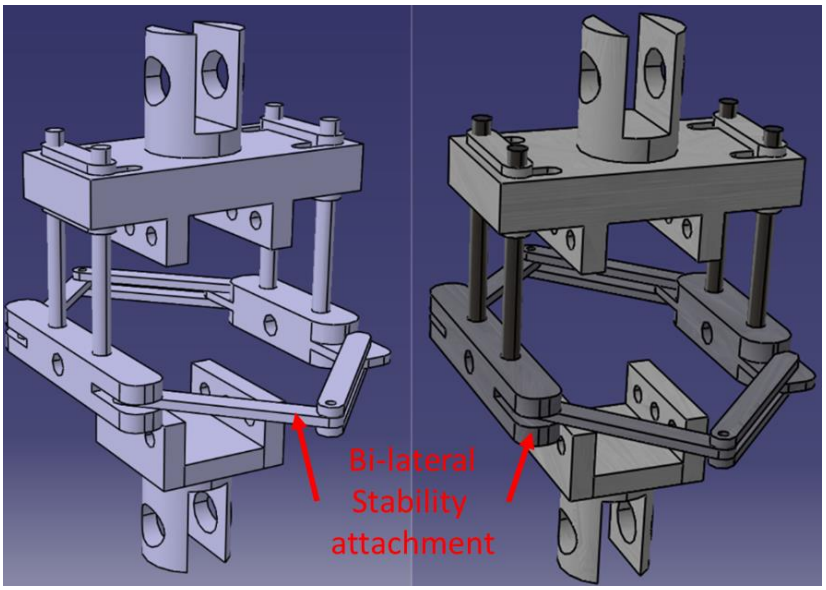

Figure 3.11 - Design of the pre-crack rig CAD model Type C version 3

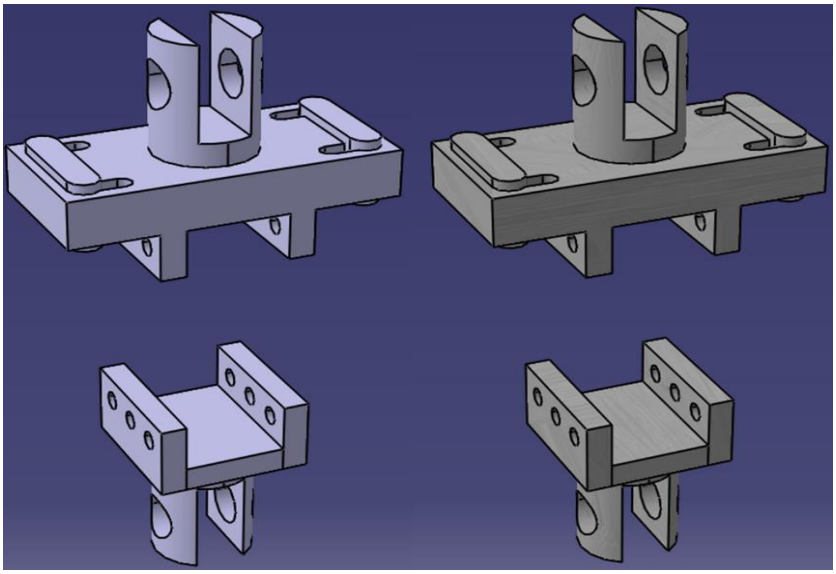

Figure 3.12 - Design of the pre-crack rig CAD model Type D version 4

3.1.4 Development of new pre-crack method

Harris and Tetelman was one of the earliest researchers working on concept of applying compressive load to predict crack arrest for transversely loaded elastic thin plates and evaluate SIF [161, 162]. Pisarenko et al. [163] later investigated the phenomenon of crack arrest in a plate with transverse compression zones to extract SIF in plastic materials. Harris and Tetelman [162] and Pisarenko et al. [163] applied compressive load first to the specimen, then applied a chisel to the specimen notch with a hammer to propagate the crack. The phenomena of crack arrest was investigated found to be in agreement with theoretical and experimental results. However, the effects to residual stress or the type of crack shape was not presented in any of their work.

Another technique for ‘‘growing” a pre-crack in a brittle material was later proposed by Tamura et al. [164]. This general method is illustrated in Figure 3.13 (a), where a pre-crack is generated by applying loading in two directions.

As discussed in chapter 2.3.1, the general relationship between elastic energy release rate G and stress intensity factor K can be obtained as follows [165]:

$$G = -\frac{1}{B}\frac{dU_a}{da} = \frac{\pi\sigma^2 a}{E} = \frac{K^2}{E} \tag{3.1}$$

Then the relation between K_I and G can be obtained by substituting $K_I = \sigma\sqrt{\pi\, a}$ into equation 3.1:

plane stress $$G = \frac{{K_I}^2}{E} \tag{3.2}$$

plane strain $$G = \frac{{K_I}^2}{E}\,(1-\nu^2) \tag{3.3}$$

Under LEFM conditions the prediction of crack growth is the same for both the energy balance and elastic stress field approaches. This equivalence was demonstrated by Irwin, who also indicated that equations 3.2, & 3.3 are geometry independent.

G is indicated in studies as a controlling parameter for fracture in an energy balance approach. We can consider a cracked body is loaded by forces P where a crack length a, the change in the work performed by external forces, F, and the change in elastic energy, Ua as shown in figure 3.13b. the general equation for the energy release rate G, per unit thickness B is:

$$G = \frac{d}{da}(F - U_a) \tag{3.4}$$

or

$$G = \frac{1}{B}\left(P\frac{dv}{da} - \frac{dU_a}{da}\right) = \frac{1}{B}\left(P\frac{dv}{da} - \frac{1}{2}\frac{dPv}{da}\right) \tag{3.5}$$

assuming that the material behaviour is linear elastic, which requires that the relationship force vs displacement to be linear. This is a valid assumption in this case since plasticity is very small for these relatively brittle polymer materials. In a similar way to a linear spring, the potential energy U is a stored member and results in an elastic strain present throughout the volume of the material where v is the displacement ahead of the crack in the vertical direction.

If the crack length a changes by a small amount da, while the displacement v is held constant, the stiffness of the members decreases. This results in the potential energy decreasing by a specific value dU; meaning U decreases due to a release of this specific value of energy. It is understood that the crack length a increases with the rate of change of potential energy and this is defined as the strain energy release rate G as indicated in equation 3.1. The change in crack area is $B(da)$ and the negative sign causes G to turn into a positive value. Therefore, G describes the energy per unit area needed to extend the crack and is anticipated to be one of the key parameters controlling the behaviour of the crack.

In early work by Griffith [35], it was indicated that the potential energy released was believed to be used in the creation of the new free surface on the crack faces. This is roughly true for material that crack with virtually no plastic deformation, as far as the glass material tested by Griffith. However, in material with little plastic deformation, most of the energy may be used for deforming the material in the plastic zone at the crack tip. Irwin applied G to metals and showed that this approach could be used even if the plastic zone was small [166].

Additionally, it should also be noted that the change in F is equal to the external work done Pv where the change in U_a is $\frac{Pv}{2}$. By introducing the compliance factor of the body C, the inverse of its stiffness is achieved that is $C = \frac{v}{P}$ and substitution of C into equation 3.5 transforms into:

$$G = \frac{1}{B}\left(P\frac{dCP}{da} - \frac{1}{2}\frac{dCP^2}{da}\right) \tag{3.6}$$

$$G = \frac{1}{B}\left(PC\frac{dP}{da} + P^2\frac{dC}{da} - \frac{1}{2}P^2\frac{dC}{da} - CP\frac{dP}{da}\right) = \frac{P^2}{2B}\frac{dC}{da} \tag{3.7}$$

From Irwin and Griffith theory and in equation 3.7, it could be understood that by constraining v the displacement ahead of the crack, is equal to zero. Since compliance is proportional to displacement v, then this means that there will be no change in the compliance of the body $\frac{dC}{da}$ and will equal to zero when the compression force is present ahead of the specimen because the flat clamped area is preventing the material from moving in the vertical direction (y axis). This means that the strain energy release rate G must equal to zero, because the material will not have enough energy for the crack to move. Therefore, G must be less that G_{Ic} and the crack cannot grow. This also explains why the clamp must be flat. If a curved clamp is used the area over which the material is constrained in the vertical direction is relatively small and thus the material is not constrained enough to reduce the compliance.

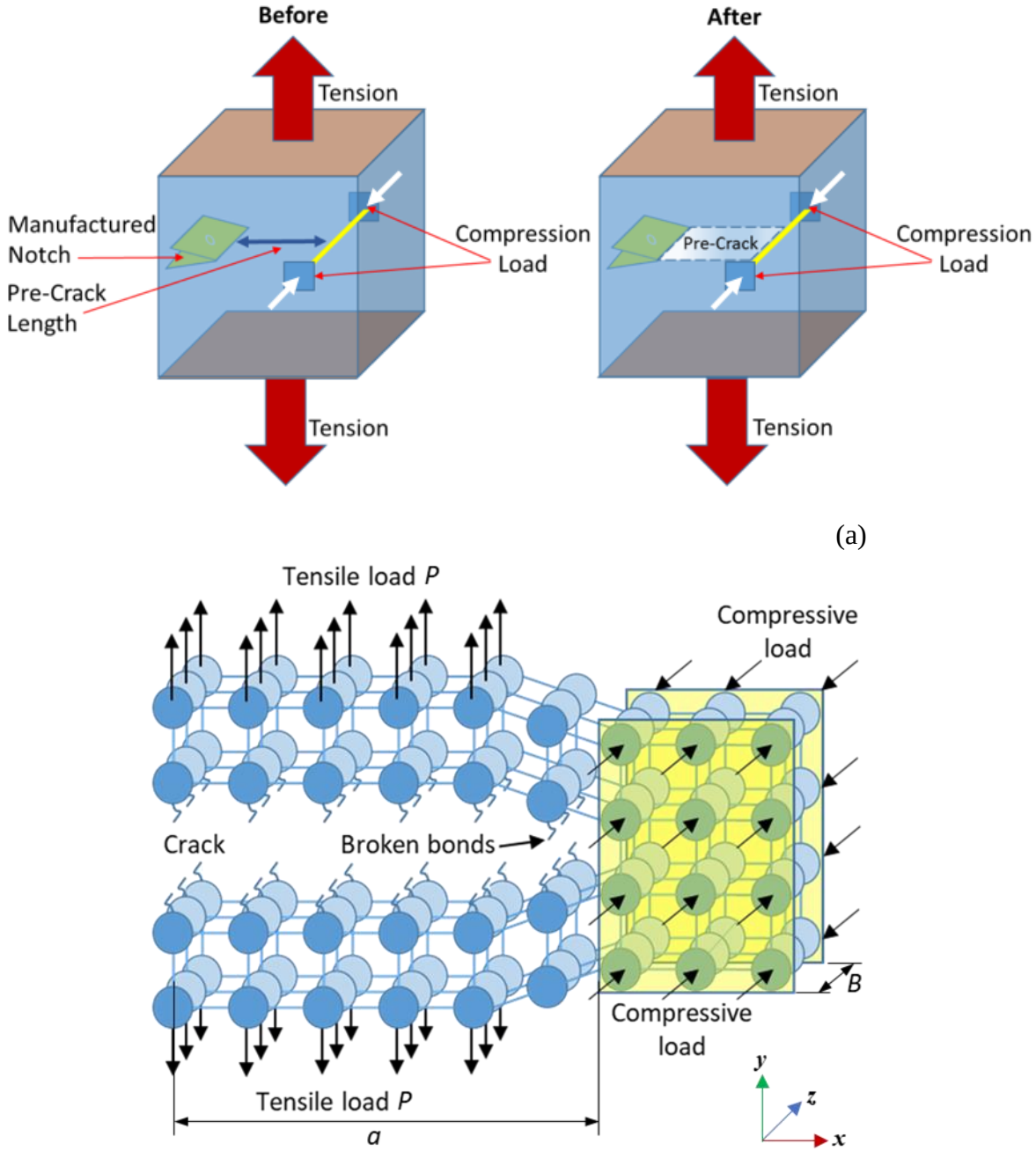

Figure 3.13 - Pre-crack growing principle without using a blade.

An initial compression load is applied in the transverse direction, normal to the surface of the specimen, ahead of the manufactured notch and a secondary tension load is applied with a tensile test frame via loading pins in the direction to open the crack. Tensile loading commences the growth of the pre-crack until the required length is achieved, the compressive load causing

crack arrest. The arrested crack is halted by the compressive load applied to the area ahead of the crack, the molecular bonds are moved closer together which changes the energy required for the crack to propagate further. Due to the molecules being compressed an even greater energy is required for the crack to propagate than the regular required facture energy for the material to propagate a crack towards a path of least resistance if there is no barrier molecules. However, if the applied compressive load is too great and the barrier molecule is small enough, then the propagating crack can travel around the barrier of molecules instead of travelling straight through the barrier of molecules.

Tamura et al. described results in a variety of brittle materials but did not supply enough experimental detail to allow easy replication of the method. They also noted that crack fronts of variable shapes were observed and appeared uncontrollable. This basic theory has been developed into a simple practical method to grow cracks of a repeatable, defined length without the use of a razor blade, thus increasing the safety of the preparation method.

The application of the compressive load was studied using modified Arcan-type specimens made from an untoughened epoxy resin used in aerospace composites. Two clamps, a G-clamp and simple tool-makers clamp (T-clamp) were used to apply the compressive load and these generated very different crack front shapes. The G-clamp produced a curved crack front, whereas the T clamps generated a very straight crack front.

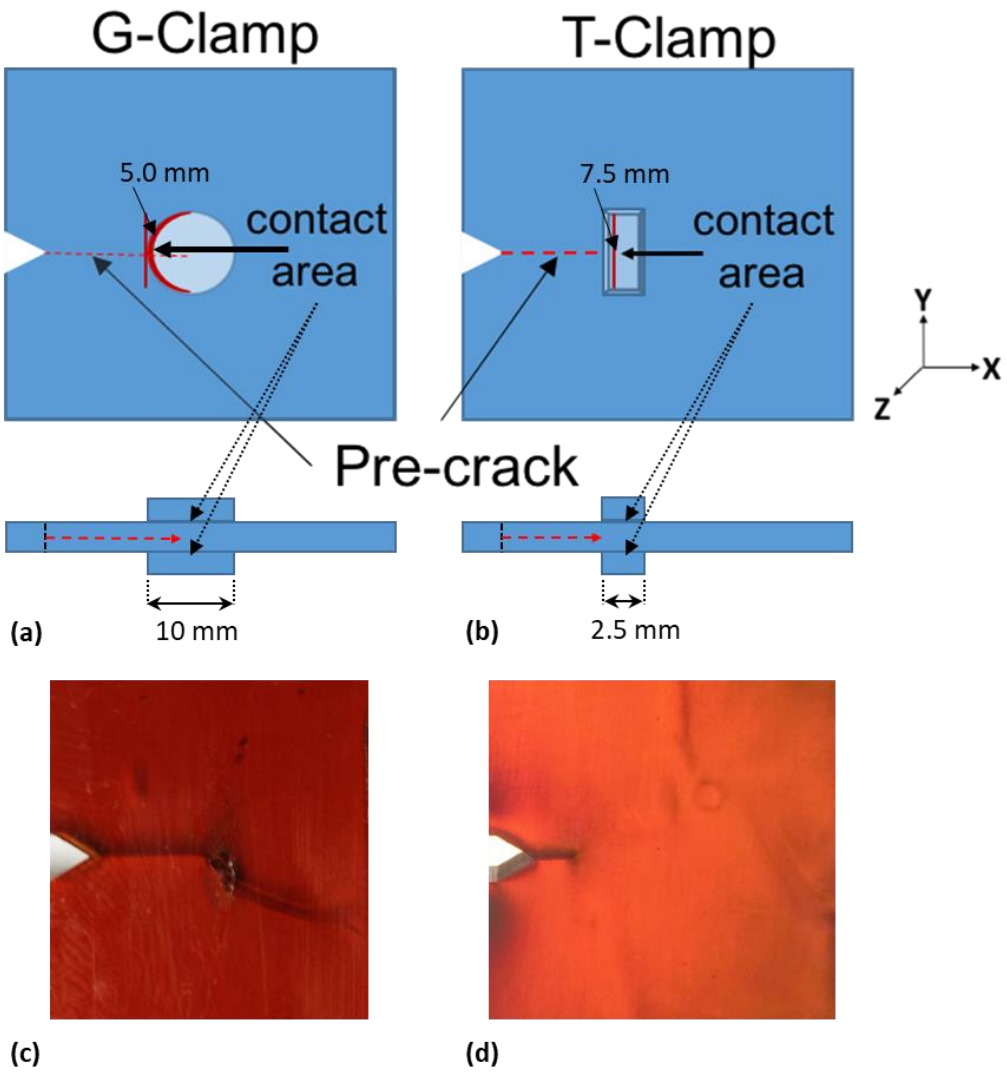

Figure 3.14 - Contact areas of the compressive load of (a) the G-clamp and (b) the T-clamp, (c) G-clamp pre-crack, (d) T-clamp pre-crack.

Figure 3.14 illustrates the key differences between the G-clamp and T-clamp compressive force contact areas. The G-clamp applies a Hertzian-type contact of a ball on a plane, resulting in a small circular contact point; whereas the T-clamp is a larger, flat, rectangular contact area. As the crack meets the area under load, the y-direction dimension of the T-clamp is much larger than that of the G-clamp. In some cases, the contact area of the G-clamp was not sufficiently big to arrest the crack which propagated around the contact area (figure 3.14c). Based on the contact area of the G-clamp, the Hertz analysis shows that, when a sphere of radius R_1 is applied into contact with a loading force F_1, the surrounding region exhibits compression and or

deformation through the surface of the specimen, with the centre displacement by a value of δ in the normal direction, and applying a contact area of radius *a*, given by [167] :

$$a = \left(\frac{3\ F_1\ R_1}{4\ E^*}\right)^{\frac{1}{3}} \tag{3.1a}$$

where F_1 is the applied compressive force onto the surface of the specimen and R_1 is the relative radius of the G-clamp contact area. The effective modulus E^* is defined as

$$E^* = \left[\frac{1 - {\nu_1}^2}{E_1} + \frac{1 - {\nu_2}^2}{E_2}\right]^{-1} \tag{3.1a}$$

where E_1 and E_2 is the modulus for the G-clamp (steel) contact body and the specimen (S-formulation resin). Similarly, ν_1 and ν_2 is the Poisson's ratio of the G-clamp contact body and the specimen respectively. Although the radius of the contact area of the g-clamp is 5mm, the effective contact radius is 0.57 mm (Table 3.2). Furthermore, the contact footprint on the surface of the specimen and the through thickness distribution of the compressive load onto the specimen is not enough to arrest the pre-crack and as a result the pre-crack traversed past arresting point.

E_1 (Mpa)	E_2 (Mpa)	ν_1	ν_2	R_1 (m)	F1 (N)	E*	*a* (mm)
210000	315000	0.30	0.39	0.005	100	0.50	0.57

Table 3.2 - Illustrates the calculated G-Clamp Hertzian contact area.

However, the T-clamp generated a uniform stress through the thickness of the material, hence generating a straight crack front when compared with the crack front from the G-clamp.

Therefore, the T-clamp was chosen to apply clamping load.

The new apparatus uses a tool-makers clamp to apply a compressive load ahead of the notch, and a tensile load of 100N is applied to achieve the desired pre-crack length. (Figure 3.15).

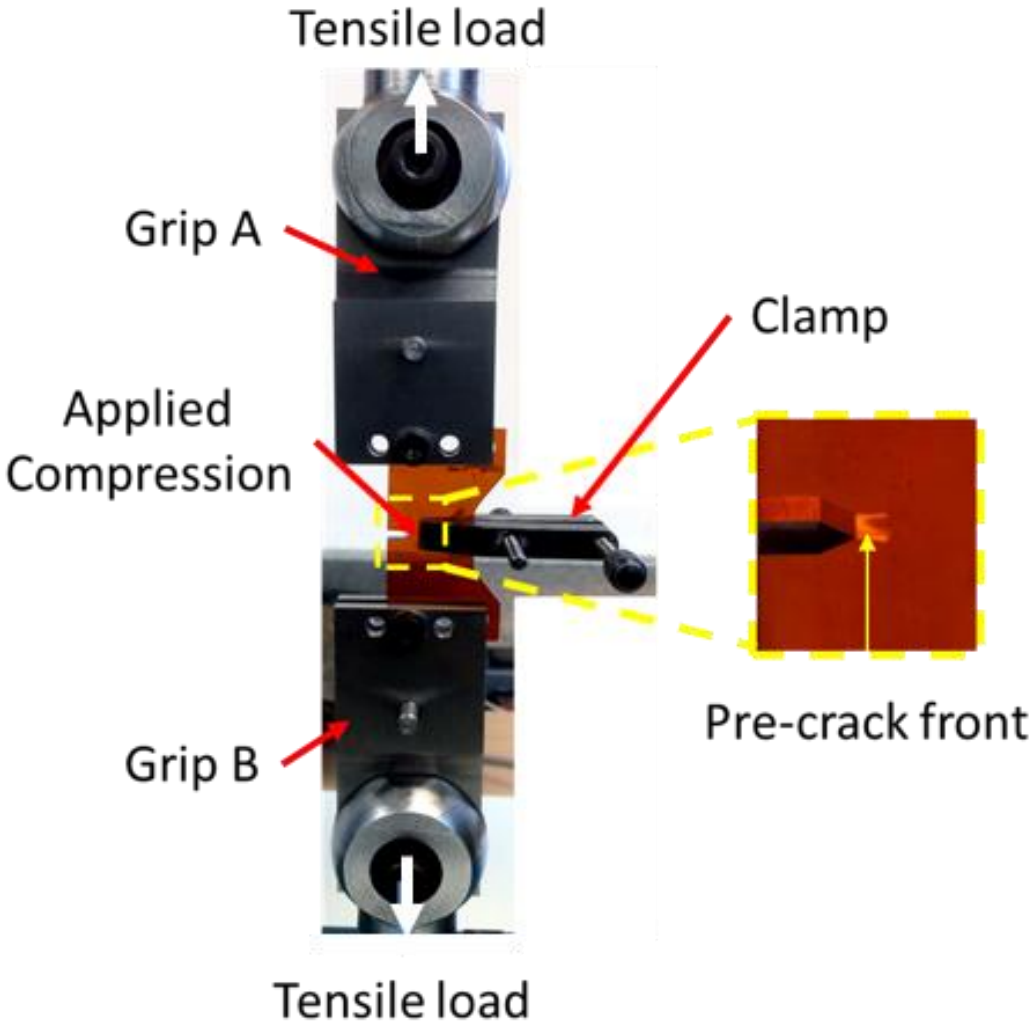

Figure 3.15 - Pre-crack growing principle without using a blade.

3.1.4.1 Determination of optimum compressive load

An experiment was conducted to determine the compressive load required for production of a pre-crack of known length. The compressive load was applied using a 0–5 N m slipper torque wrench on the T-clamp. The compressive load applied to the specimen per unit torque on the clamp was determined by compressing a calibrated load cell with the clamp; 0.5 N m of torque resulted in 100 N of force. A compressive load of 100 N was applied to an untoughened epoxy SJ Arcan specimen used in the apparatus (Figure 3.15). The tensile load was increased slowly until the crack started to propagate and then the load was removed immediately since the crack grew rapidly. The arrest point of the crack was observed. The compressive load was increased

in 100 N steps and the experiment repeated on a new specimen at each step. The desired point of arrest of the crack was the front edge of the clamp. Figure 3.16 illustrates the behaviour of the pre-crack in the modified Arcan specimens with variation of transverse compressive load.

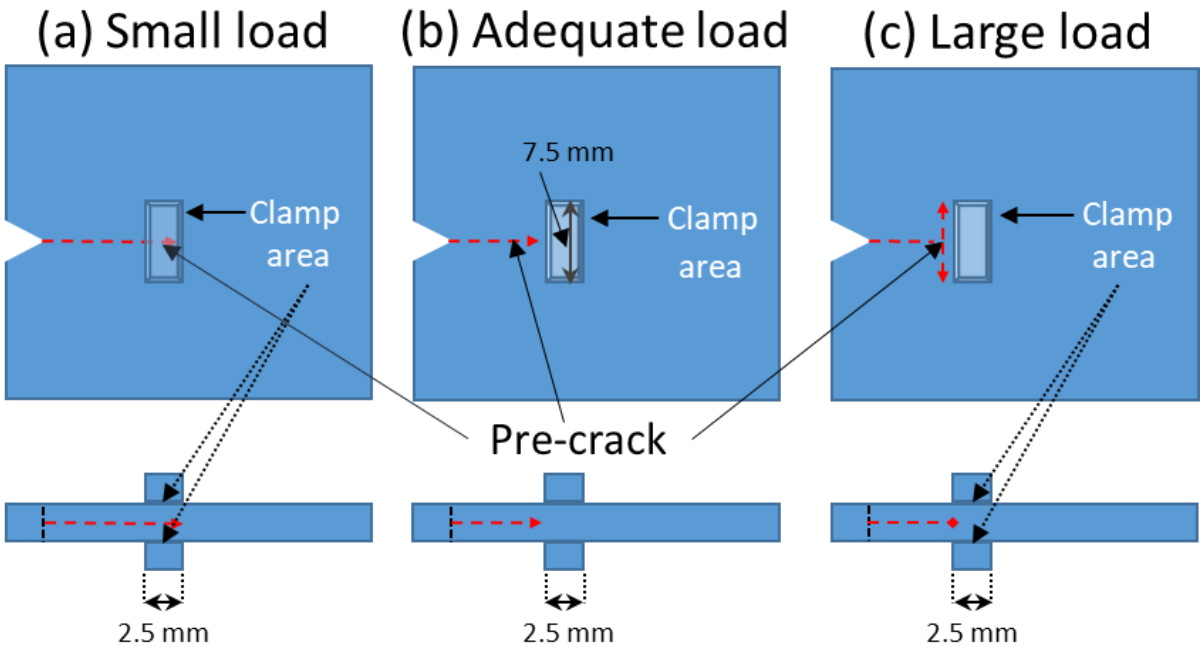

Figure 3.16 - An illustration of pre-crack ‘‘grown” with varying transverse compressive loads on an untoughened epoxy resin.

If the compressive load was insufficient then the pre-crack either propagated fully through the specimen or arrested further than the desired point. If the load was adequate then pre-crack arrested at the desired point. If the compressive load was too large, then the tensile load needed to initiate the crack was also large and the result was that the pre-crack travelled along the axis and then bifurcated and propagated perpendicular to the pre-crack axis (Figure 3.16 c). The optimum compressive load for this material using a 4-mm thick specimen was 300 N and approximately 300 N tensile load was also required to initiate the crack. Following the removal of the compressive load, each specimen was observed in a light field circular polariscope [168] to evaluate the effect of compressive loading. The polariscope allows a visualisation of the residual strains. By observing Figure 3.17, a qualitative comparison of the residual strains can

be made in specimens where cracks have been propagated using the T-clamp method (Figure 3.17 a) and the razor tapping method (Figure 3.17 b). The specimens (Figure 3.17 a and b) were manufactured using a CNC machine; the specimen (Figure 3.17 c) was manufactured using traditional machining techniques. The traditional machining methods clearly introduce large residual strains, whereas the specimen (Figure 3.17 a) shows that the CNC machining eliminates all machining strains.

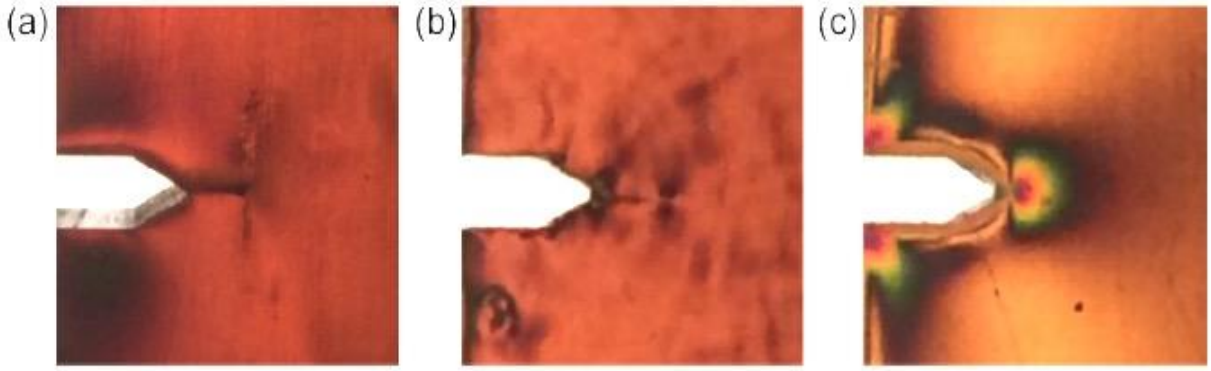

Figure 3.17 - Showing residual strain CNC-machined specimens with a crack introduced (a) using the T-clamp method; (b) using razor tapping; and (c) a specimen machined using traditional machining methods (notch only). The specimens were viewed in a white-light, dark field, circular polariscope.

The razor tapping method introduces a small amount of residual strain at the notch, and also at the crack tip; however, the compressive load in the T-clamp method does not cause any residual strains to remain in the specimen. This is important because if residual strains remained this will have a detrimental effect on the accuracy of the subsequent fracture toughness test.

The current methodology has been developed for use in Digital Image Correlation experiments [10,11]. Microscopic images of one side of the specimen are recorded at increments of load during the fracture test and strain maps determined from these images. The Williams series is then fitted to these strain maps in order to determine the stress intensity factor and fracture toughness. If the crack length is different on the front and rear faces of the specimen, then the stress intensity factor will vary. Tests will also be carried out on many different formulations

of particle-toughened epoxy resins and it is good experimental practise to have identical specimen dimensions and only change the material in order to understand the material behaviour. Hence it is important to have a uniform pre-crack.

A comparative study was conducted to observe the significant difference between razor-tapped pre-crack against the new pre-cracking method. Figure 3.18 indicates the two specimens pre-cracked with both methods, the razor blade tapped (Figure 3.18 a) and the new pre-crack method (Figure 3.18 b). The pre-crack created by the razor blade had a much larger crack front and curvature when compared to the new method. Also, the crack front differs significantly through the thickness of the specimen, resulting in a crack of different lengths on the two faces of the specimen. Effectively the resultant crack length achieved for a given specimen would be difficult to approximate measurement of the pre-crack, without a high degree of error. Thus, it is better to utilise an approach that can give an accurate method to create repeated, controlled pre-cracks. Further investigations were conducted, the findings was presented in recent publication [169] presented in the next section.

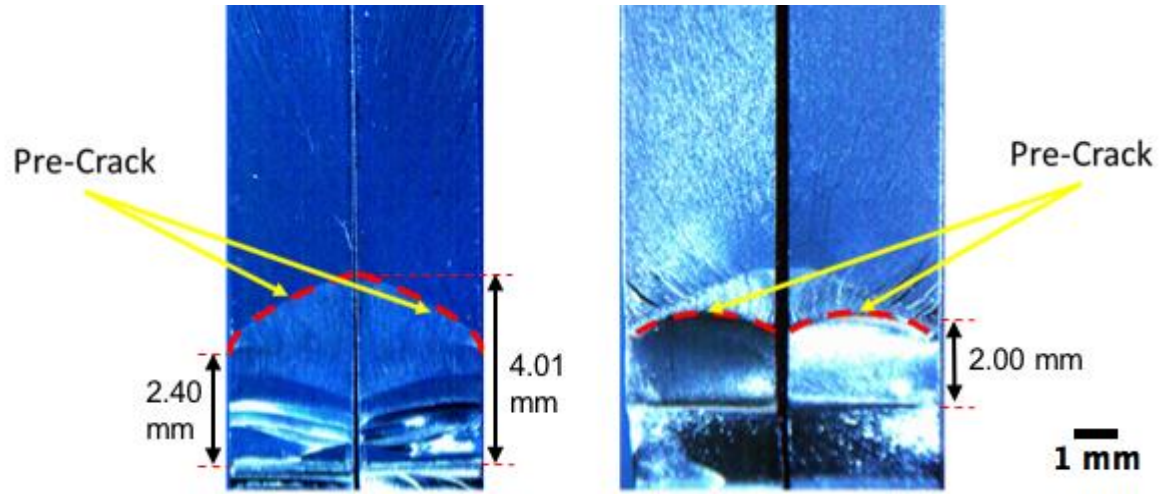

(a) **(b)**

Figure 3.18 - Microscopic image of a specimen pre-crack generated with (a) pre-crack razor blade rig and (b) the new T-clamp method.

3.1.4.2 Repeatability of the method

The pre-crack experiment was repeated on 40 identical untoughened epoxy modified Arcan specimens, with the front edge of the T-clamp positioned at exactly 2 mm from the notch. The T-clamp applied 300 N of compressive force and 300 N tensile force was applied to initiate the crack. The length of both sides (A and B) of the subsequent pre-crack which propagated were measured using a calibrated microscope and the results are shown in Figure 3.19. 35 of the 40 pre-cracks were exactly 2 mm in length to an accuracy of 10 µm. The high repeatability is attributed to the ability of the flat faces of the clamp to apply an appropriately distributed compressive force to arrest the crack at a given distance.

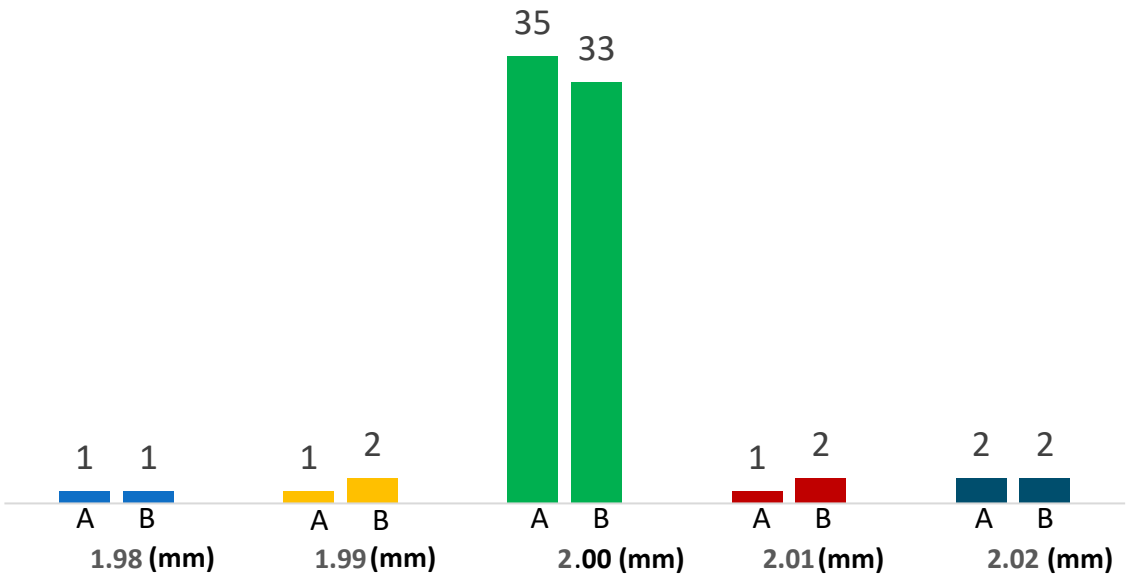

Figure 3.19 - An illustration of the repeatability of the pre-crack with the new methodology with measurements taken from both sides (A and B) of each specimen.

3.1.4.3 Calculation of applied compressive/clamping load

It is important to apply an adequate amount of compressive/clamping load to the specimen before applying the tensile load to propagate an accurate the pre-crack length. Results suggest that the compression load differs with the different materials provided by the sponsor and a single compressive load will not be sufficient for all specimens as shown in Figure 3.20. An investigation was conducted to identify the optimal compressive load for all the formulations, where the torque wrench setting was incrementally applied to each of the t-clamp to generate clamping load on the trial specimens to arrest the pre-crack. The relation between applied torque and clamping force can be calculated by using the equation:

$$T = CdP \tag{3.2}$$

where T is wrench torque (N.m, lbf ft), C is a constant that depends on the bolt material (dry normal bolt 0.2), d is nominal bolt diameter (m, ft) and P is the clamping force (N, lbf). The compressive load values are reported in table 3.3, where different formulations require different clamping force to arrest the pre-crack. The results indicate a linear relationship between the applied torque when compared with K_{Ic} to arrest the pre-crack (Figure 3.20)

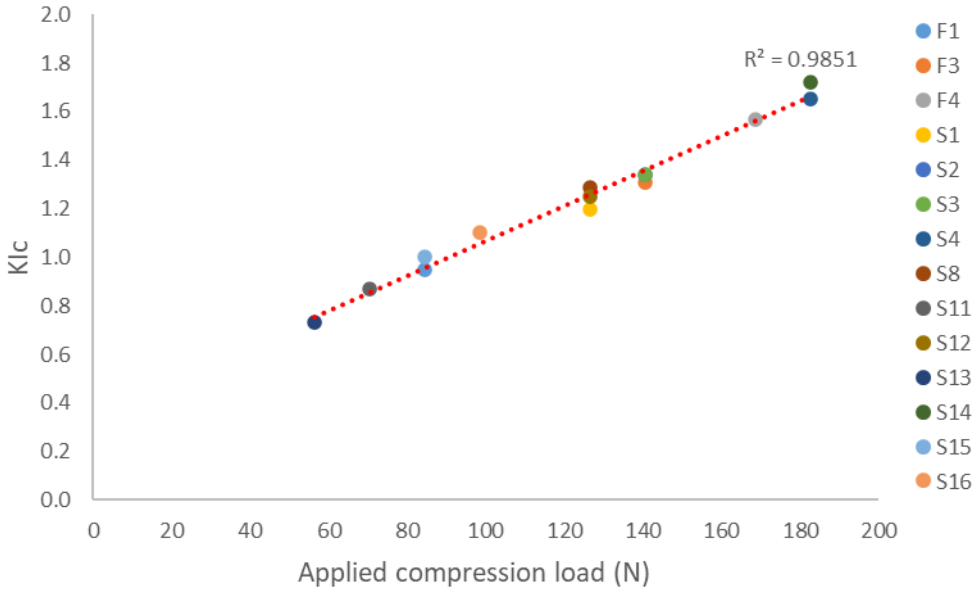

Figure 3.20 - A linear relationship between applied compression load vs K_{Ic}

Specimen	K_{Ic} (MPa.√m)	**Applied Compressive Load**
F1	0.95	84.30
F3	1.31	140.51
F4	1.57	168.61
S1	1.20	126.45
S2	1.34	140.51
S3	1.34	140.51
S4	1.65	182.66
S8	1.29	126.45
S11	0.87	70.25
S12	1.25	126.45
S13	0.73	56.20
S14	1.72	182.66
S15	1.00	84.30
S16	1.10	98.35

Table 3.3 – Illustrates resin formulation requiring different compressive loads

Although the results indicate a linear relationship between different resin formulation, it can be observed several resin systems from different family share similar compressive loading. The novel technique developed in this work provides a simple controllable technique for generating efficient pre-cracking brittle specimens. However, if more time were permitted in this research, further investigation could have been performed deeper into these phenomena and on the applicability of this technique for non-brittle materials and this is recommended in the further work.

3.1.5 Speckle pattern painting

Once the samples are manufactured, a greyscale speckle pattern is applied on to the specimen in a small region 10 mm x 10 mm over the crack tip where the image is analysed. For application of random patterning, area surrounding the specimen is cleaned to remove residual paint. For small-scale deformation, it is important to apply a very fine speckle pattern. However, the unique speckle pattern scale is largely influenced by skilful control over paint size and flow. Specialised airbrush with varying nozzle sizes for controlling the flow and size of paint was used to apply paint onto the specimen surface (Figure 3.21).

The AZTEC A7778 metal body airbrush with variation of nozzles was identified as the ideal airbrush for applying speckle pattern in experiments.

Figure 3.21 - A specialised spray paint gun with different nozzle

A short study was conducted with participation from LaVision for investigating the effects of paint quality, with several different off-the-shelf acrylic water based paints shown in Figure 3.22 and proprietary LaVision spray can paints (Tamiya acrylic, DecoArt and Revell and LaVision custom spray paint). The short study was conducted by applying paints on to specimens with similar dimensions and the change in displacement was recorded and

correlated. Four types of speckle patterns were tested: air-brush developed at the University of Sheffield (ABUS), stickers with transparent background (TSLV) which is identical to (WSLV) without a white background, stickers with white background (WSLV) and aerosol paint (APLV) developed by LaVision were studied. Tensile tests with different ductility on three different materials were studied: a brittle resin, a ductile aluminium alloy and a viscoelastic polymer. The study includes a rigid body, shear and tensile tests. The APLV was found "too shiny" (i.e. may speckles were saturated with minimum light) in the preliminary work and was not fully pursued.

It was observed that the proprietary LaVision spray can paint was shiny and measurements indicated highest level of noise in the image. A high-quality airbrush with variable nozzle was used to apply the other paints, resulting in a high quality and fine speckles with a size of 1-50 μm giving measurable deformation from less than 1 μm. It was observed that Tamiya acrylic matt paint has a small lifespan before turning brittle. Examples of the tested speckle patterns are shown in Appendix 2 the short study report provided to LaVision. Therefore, the Crafter Deco Art acrylic water based paint was selected for future experimental studies.

Figure 3.22 - Paints used in identifying the best paint.

3.2 Discussion

In linear elastic problems, it has been shown that the displacements near the crack tip (or crack front) vary in distance from the crack tip. The stresses and strains are singular at the crack tip and vary dimensionally. The observation of singularity in the strain, the crack faces should be coincident, and the values around the crack tip or crack front should be an accurate representation. Figure 3.7 shows examples 2-D crack front represented as a 3-D model depicting various pre-crack front surface structures.

This chapter illustrates the benefits of the wide range of optimisation developed for improving sensitivity of DIC based experiments. Several optimisation techniques were implemented that emphasise the importance of safety, efficiency, and improvement to the design of experiments (Table 3.4). Therefore, optimising experimental methods will benefit future experiments and enhance not only quantitative but also qualitative results in high throughput mechanical testing.

Type	Optimisation Techniques	Time Taken	Advantages / Disadvantages
Conventional method	Traditional manufacturing specimens	1 Week / Plaque	A traditional manufacturing techniques introduces greater residual stresses, when used with water
New method	CNC machining specimens	1Day / Plaque	A traditional manufacturing techniques introduces some residual stresses
Conventional method	Manually polishing by hand	30 min / Specimen	A time consuming, can hazardous if the user is not wearing a mask.
New method	Utilising a polishing rig	5 min / Specimen	An efficient, accurate, and precise polishing to 0.01 mm
Conventional method	A standard blade utilised to grow a pre-crack manually	5 Min / Specimen	A very difficult to achieve Identical pre-crack length repeatedly
New method	A pre-crack rig utilising a blade	5 Min / Specimen	A difficult to achieve Identical pre-crack length repeatedly
New method	A pre-crack rig without a blade automated	3 Min / Specimen	A possible to achieve specific pre-crack length
Conventional method	Old spray paint gun	10 Min / Specimen	A controllable speckle pattern, more difficult to achieve fine speckles
New method	New spray paint gun	10 Min / Specimen	A controllable speckle pattern, easier to achieve a very fine speckle pattern

Table 3.4 - Optimisation techniques

3.2.1 Specimen Manufacturing

Specimens can be manufactured by Computer Numerical Control (CNC) machine to programme for automation of the entire process. Advantages of this method are a) use of single machine to drill and cut and b) enhanced user safety in a controlled environment.

The isochromatic fringe pattern intensity can be interpreted as an indication of the level of residual stress present. Since, these specimens are observed in a polariscope at rest without applying any load after being subjected to drilling in different environments. Figure 3.1 illustrates the residual stress imparted on to the specimen that can lead to induced weaknesses in the specimen and fracture towards the path of least resistance when subjected fracture testing. The study was conducted using F1 Neat resin, this specimen was selected because of its translucent properties. A common process to both traditional milling and CNC, drilling, was selected to perform this study. The F1 Neat resin was subjected to a repeated drilling; this entailed specimens subjected to a standard drilling, a drilling with water, and finally drilling with coolant. The study concluded with the effect represented in Figure 3.1 visualised through a polariscope and it provided a clear indication of (a) which has the highest impact of residual stress and (b) and (c) are effected far less. Therefore, it is important to consider an accurate specimen manufacturing regime and the CNC manufacturing of specimens is an ideal fabrication method.

3.2.2 Polishing specimens

The introduction of the automated polishing method reduces the time to polish a specimen from 30 minutes to 5 minutes, with the additional advantage of precision in the thickness uniformity.

3.2.3 Development of new pre-crack method

Currently the only suitable and practical pre-crack method for brittle epoxies is to use a razor blade applied to a notch, either by tapping on the razor blade or by slicing side by side. The other prescribed method by standards (ISO 13586:2000, ASTM E399) is to create a pre-crack by subjecting the specimen to fatigue loading until the pre-crack has extended. Creating a pre-crack by fatigue method is disadvantages with brittle materials, as this impart residual stress at the crack tip. Furthermore, fatigue pre-crack will require a lot of time for preparing a batch of specimens for testing and not suitable in an industrial environment. On the other hand, there are several key problems associated with using a razor blade. Firstly, it is difficult to hold the specimen, the razor blade and the small rubber mallet. Secondly positioning the razor blade at the centre of the notch without any bilateral movement accurately is very difficult. Finally, the crucial problem is the control of applied force required to generate the length of the pre-crack.

Pre-Crack Bladed Technique	**Manually Applied by Hand**
Control of bi-lateral movement of blade	Minimal
Risk of safety using a Blade	High
Accurate positioning the blade	Minimal
Risk of removing stuck blade from specimen after pre-cracking	High

Table 3.5 - Illustrates problems associated with old pre-cracking techniques

Table 3.5 illustrates the problems associated with using old pre-cracking method when preparing the specimens. Thus, the conventional manual pre-cracking is not an ideal approach to propagate a natural pre-crack and attention was turned to different methods. In an attempt to solve the initial problem, which is to ensure the bi-lateral stability of the specimen and the razor

blade position before applying a tapping force, an initial rig for pre-cracking was designed and manufactured during the first year of this project [170].

The employment of pre-crack rig addresses the many issues relating to traditional methods of creating pre-cracks. The new method ensures the application of pre-crack in a safe way and increases accuracy of maintaining better degree of control in length variations every time. Prototype models have been designed, developed and manufactured to aid in the manufacturing of pre-cracks.

A simple procedure for generating pre-cracks in brittle polymeric materials has been developed from the technique proposed by Tamura et al. [164]. The new methodology achieves highly repeatable, controllable pre-crack lengths and shapes in specimens for the investigation of fracture parameters, with significantly reduced waste of time and materials.

3.2.4 Speckle pattern painting

The importance of applying appropriate speckle pattern in image based experimental techniques has been widely studied by many researchers [90, 114]. The unique speckle pattern scale, largely depends on requirement such as a) uniformity of speckle size and b) control over paint size and flow. Practically, this is very hard to achieve since it demands a lot of skill and time. The applied speckle pattern enables detection of deformations on a specimen surface when analysed by DIC. Images obtained by DIC are analysed using subsets. It is possible to use the larger subset in green shown in Figure 3.23, but there will be a poor gradient difference in contrast ratio for measuring smaller changes and the range will depend on the number of speckle and size within a subset. The small subset in red shown in Figure 3.23 will not be suitable for correlation, as there will be little or no gradient difference in contrast ratio and will become highly prone to errors. Furthermore, if the speckle pattern is too small, it could be difficult to accurately capture the speckled image on the surface of the specimen.

If the speckle pattern is large and covers the entire subset as red subset shown on Figure 3.23, this will inhibit subset matching. This can be compensated by increase the subsets size but equally undermining the spatial resolution in return. As a rule of thumb the speckle pattern should be random distributed and visible with distinct features that can be tracked.

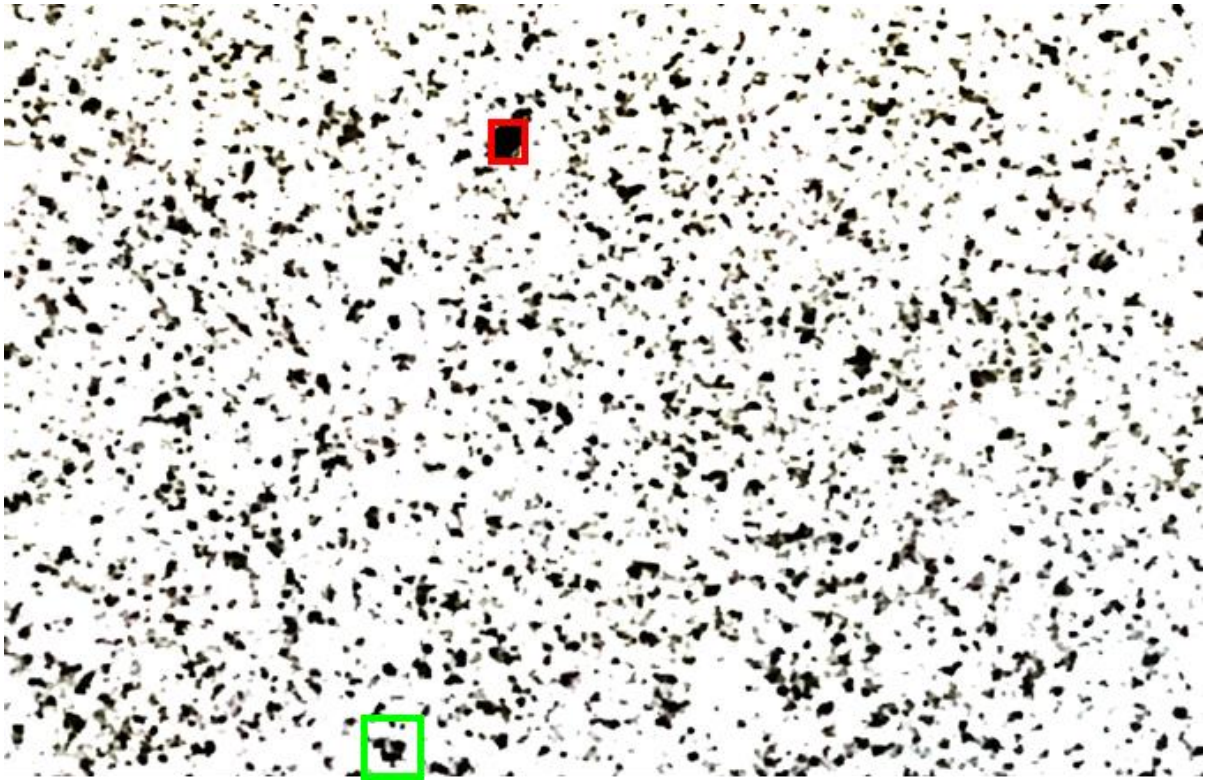

Figure 3.23 - Speckle pattern depicts a large green subset and a small red subset

Images were correlated by tracking the change in the defined subset of the test specimen during changes in movement and/or deformation (Figure 3.24). The pattern in the reference subset is moved until it is matches with the deformed image between the first image to the next image captured. Subsequently the difference is calculated for changes reflected in the x and y direction.

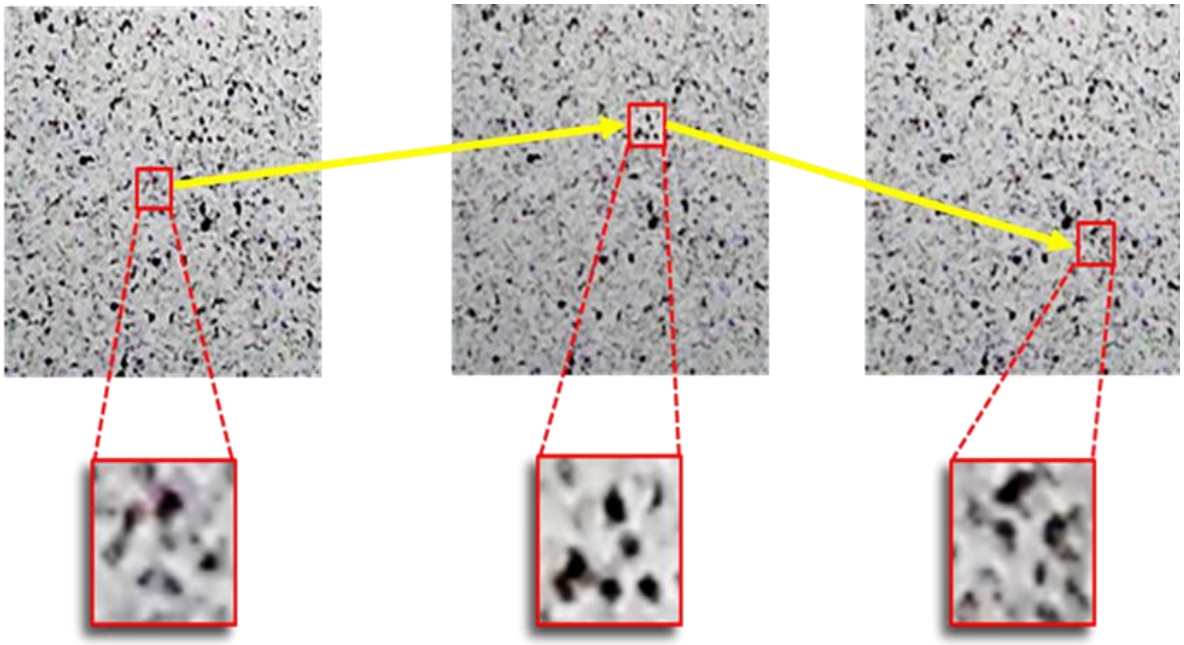

Figure 3.24 - Speckle pattern correlation

It is important to assess the properties of speckle pattern to be applied, researchers have looked into regimes for an ideal speckle pattern [103] and is a highly debated topic in academia and industry. Recent development in application of industrial paint for manufacturing result in custom spray paint manufacturer to pave the way for more control with spray painting. Following investigation into the industrial and domestic uses of spray paint, it was concluded that the Crafter Deco Art acrylic water based paint is most suitable for speckle pattern application in brittle materials.

Selection of an ideal type of paint for application of speckle pattern plays a vital role in determining the nature of the speckles formed. The paint should be a thin layer and matte in colour, as a gloss or satin paints have light reflective properties. The paint reflection can make the correlation to identify the surface area of the specimen as undergoing arbitrary motion inaccurately resulting in erroneous subset changes to be measured, especially under fluctuating high intensity light sources. It is common to paint the surface of the area of the specimen to be measured in a several passes of thin matt white paint, but it is not unusual for experimental specimen to be equally painted in black, especially when the material has a shiny reflective

surface. It is also important to ensure that the paint applied in very thin in coating spread over several passes in a sweeping motion, as a thick coating will lead to some unwanted paint effects, such as dripping and cracking upon drying and thus the measured value will largely consist of paint rather than specimen deformation.

It was observed that Tamiya acrylic matt paint has a small lifespan before turning brittle. Thus, the Tamiya paint will provide a small window between painting the experimentally testing the specimen.

Furthermore, the chemical composition of the paints can cause the specimen or the surface of the specimen to exhibit changes in material properties, resulting in an inaccurate measurement that does not reflect the properties of the material. Therefore, it is very important to optimise the paints with respect to the type of material used and experimental environment.

3.3 Conclusion

Optimisation methods for specimen preparation, manufacturing, polishing, pre-crack application and speckle pattern painting were conducted. Results obtained from these optimisation experiments aided development of accurate and repeatable methodologies which would be used for the specimen preparation in the forthcoming chapters.

CHAPTER 4

Design and development of testing grip and specimen geometry

4.1 Introduction

As introduced in Chapter 2, pure shear (Mode II) deformation in materials can be generated by several complex test configurations and manufacturing processes for repeatable tests along with mode I.

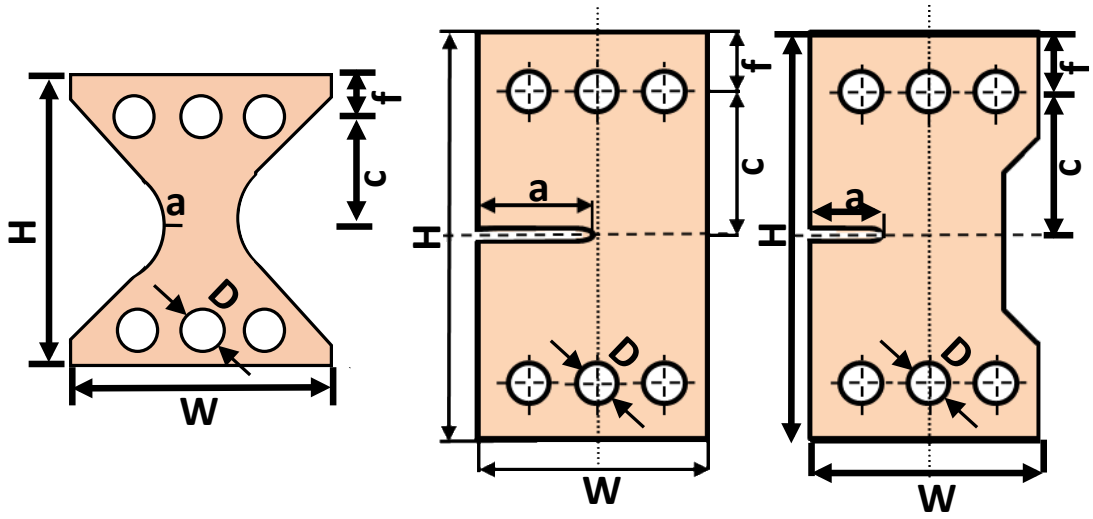

i) Arcan ii) Richard's CTS iii) SJ- Arcan

a) H= height, W=width, a=notch depth, D=hole diameter, c= centred hole spacing to specimen midpoint, f= centred hole spacing to specimen edge

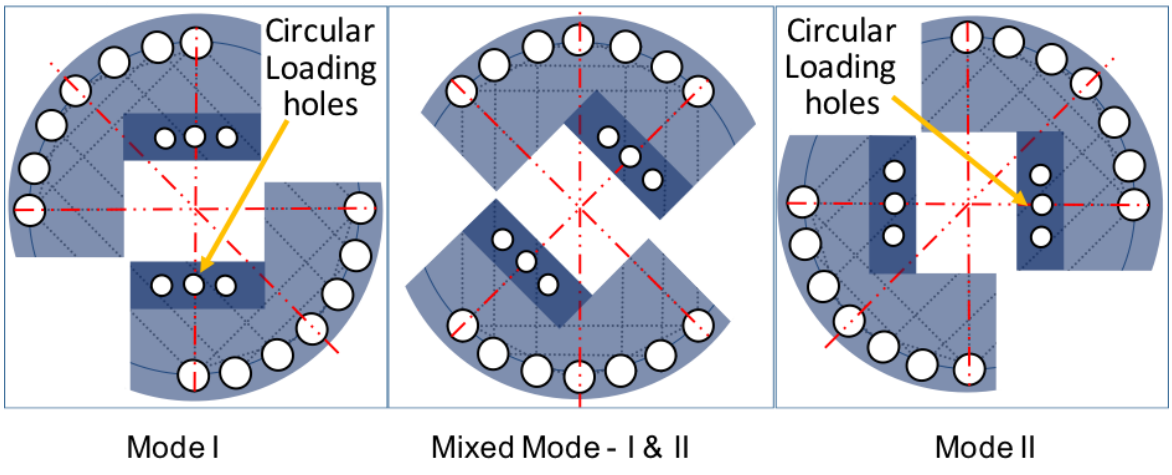

b)

Figure 4.1 - (a) Schematic representation of the Arcan, CTS and SJ Arcan specimens (b) the SJ Arcan mixed mode I & II grip

The Arcan configuration ((Figure 4.1a (i)) was initially created for determining mode II fracture toughness K_{II} [12, 13, 14] and later developed for mixed-mode testing. The key difference between the CTS (Figure 4.1a (ii)) and the Arcan geometry is the narrowing of the Arcan specimen ligand. It has been suggested that the narrowing of the ligand introduces an increase in K_{II}/K_I value for pure mode II loading but involves complicated specifications to manufacture [133]. The SJ Arcan specimen shown in (Figure 4.1a (iii)) was designed by Jones [133] and is different to the CTS and the traditional Arcan shear specimen geometry [171, 172]. It has the reduced ligand length when compared to the CTS but easier to manufacture than the Arcan. The reduced ligand length results in requiring reduced length of the natural crack (pre-crack). Jones indicated [133] that the reduced narrowed ligand length increases K_{II}/K_I value for pure mode II loadings. Hence, current study proposes that using the SJ Arcan geometry with a blunt notch and a pre-crack to conduct experimentation with the SJ Arcan grips would be a suitable experimental approach.

However, experimental observations (Section 5.4.1) indicated that specimen failure occurred at the pins under mixed-mode I&II loading. The failure path was directed towards one of the loading pins which is indicative that failure occurs towards the path of least resistance. It was considered that the grips were over constraining the specimens.

This chapter describes the design and development of specimens and grips to understand the effects of the constraint of the SJ Arcan grips and then to develop a novel testing fixture and specimen that accommodates loading in various modes and enhances high throughput testing for industrial use. The effectiveness of these designs is assessed in Chapter 5 and the best performing methodology used in Chapter 6 for assessment of multiple particle toughened polymers.

4.2 Design and Development of Grips and Specimens

4.2.1 Design of NK Arcan grips

The SJ Arcan grips (Figure 4.1b)) designed by Jones [133] with circular loading holes and 6 6mm loading pins, caused pin loading constraints, eventually resulting in Mode II failure, observed in recent work conducted by S. Jones in section 6.2 [56]. It was also postulated that the constraint influenced the stress intensity factors determined.

The problem of over constraint can be overcome using two different approaches: a) by reducing the size of the loading pins; and b) elongating the three loading holes in different directions as performed Richard [171, 172]. The elongated three-pin loading and the reduced pin size solution were both considered. However, the elongated hole solution may be less sensitive to small variations in specimen dimensions and is a much more effective solution for over-constraint. It is not required to change the SJ Arcan specimen geometry since it is deemed to work well and the new grips were designed to load the existing specimen design.

Figure 4.2 shows a schematic diagram of the modified grip design, named “NK Arcan” with the SJ Arcan specimen. Please refer to Appendix 1 for dimensions of specimen drawings. Figure 4.3 shows annotated photographs comparing the SJ Arcan grips and the NK Arcan grips.

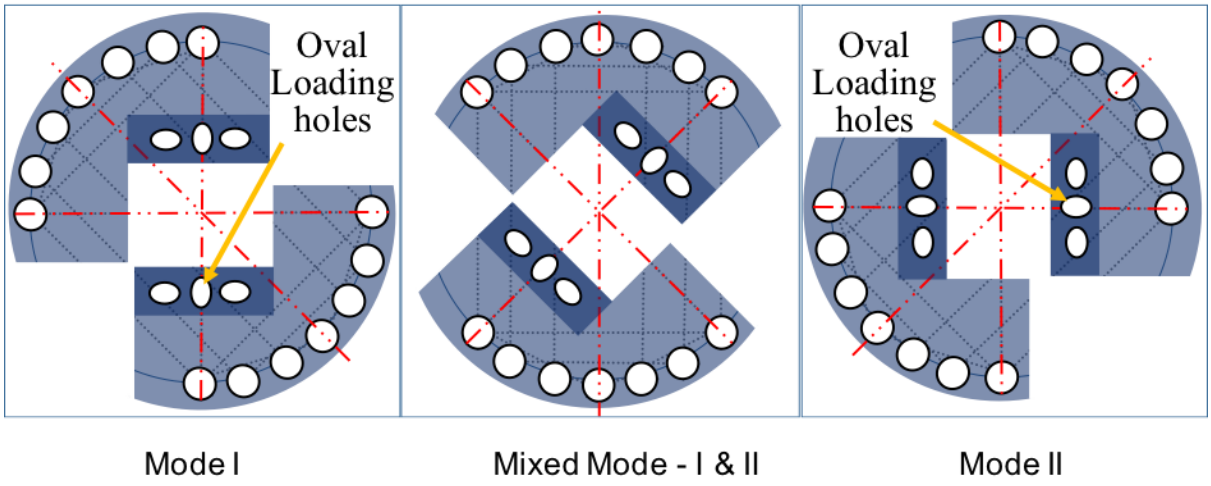

Figure 4.2 - Schematic diagram of NK Arcan mixed mode I & II grip and the loading angles

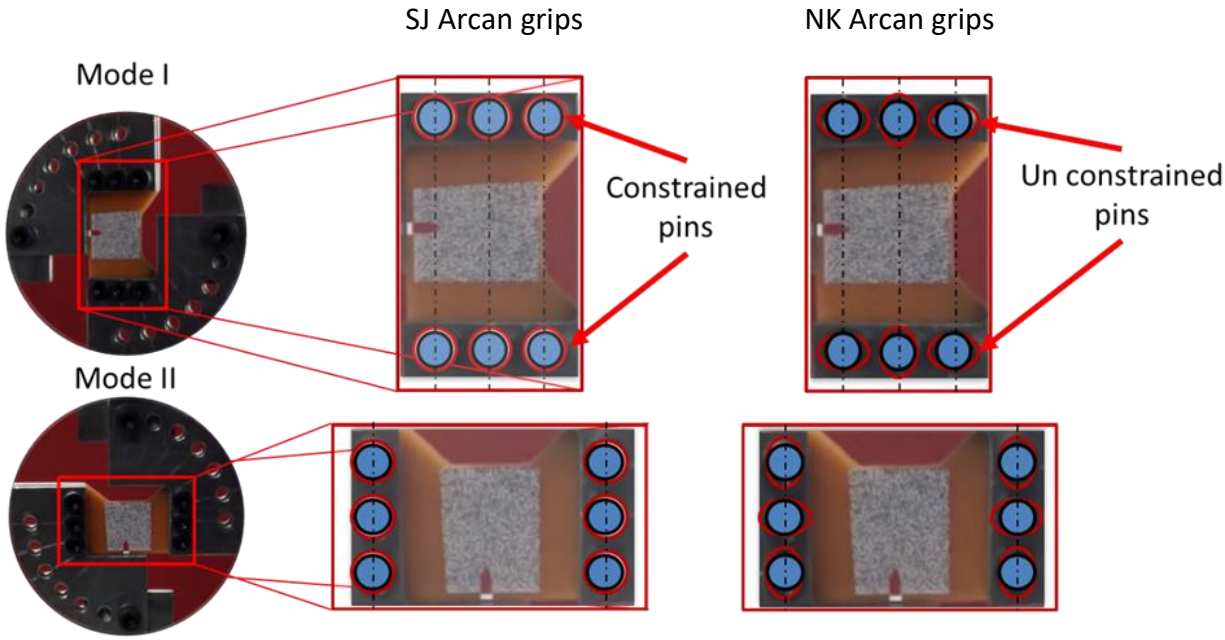

Figure 4.3 - Illustration of the SJ Arcan and modified NK Arcan with elongated hole grips

The oval loading holes remove pin loading constraints which previously resulted in loading angle dependent failure. The NK Arcan grips connect to the SJ Arcan specimen in a similar way to the SJ Arcan grips but using six steel loading pins of reduced diameter of 5 mm. A photoelastic study was conducted to observe the relationship of the stress field distribution through the specimen loaded at 45° (near pure mixed mode). See section 4.2.3 for further details. Experiments were carried out to quantify any differences between these grip designs and these are explained in Chapter 5.

4.2.2 Design of compact tension mixed-mode modified (CTMMM) grips

Although the NK Arcan test fixture resolves the pin loading constraints (explained in Chapter 5), the specimen and grip geometries are still complex to manufacture and require considerable preparation time. The development of a mixed-mode I & II testing regime which is simpler and quicker to manufacture in order to understand the effect of particulate toughening would enable the industry to progress faster and qualify materials effectively. Thus, the Compact Tension- Mixed-mode Modified (CT-MMM) system was developed with a simple specimen geometry and grip loading configuration.

Researchers use different specimen geometries and grips for mode I and mode II testing test respectively. However, the Arcan, SJ Arcan and NK Arcan configurations use only one specimen geometry and one set of grips for multiple modes. Hence it was proposed that the new design must enable mode I, mode II and just one orientation of mixed-mode loading. It was observed that the multiple mode-mixities of the Arcan-type specimens did not necessarily facilitate efficient assessment of material quality.

Thus, the new (CT-MMM) grips were designed to perform mixed-mode material testing with a single modified compact tension (CT) specimen dimension (40mm x 40mm). A typical CT specimen design (Figure 4.4a) alongside the new CT-MMM grip (Figure 4.4b) reveal that the addition of two more holes enable loading in mode II and mixed-mode I&II in addition to mode I. The CT-MMM grips enable testing of materials in tension (pure mode I), shear (near pure mode II), and both combined (mixed-mode I&II) with the same geometry (Figure 4.5).

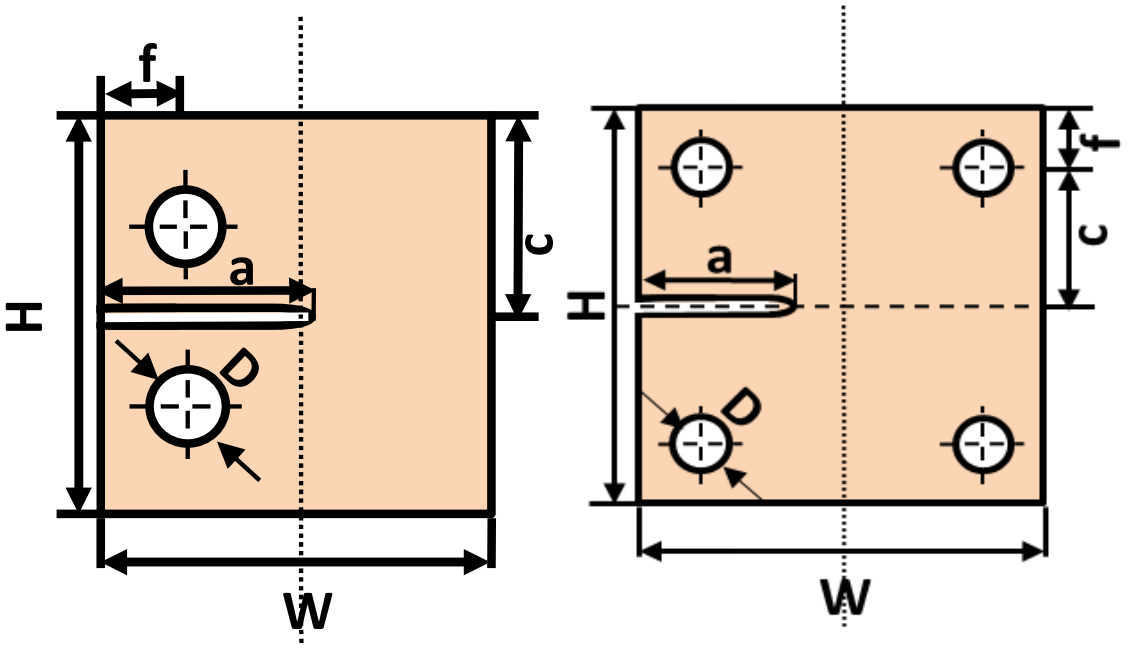

Figure 4.4 - Specimen geometry dimension illustration for a) Compact Tension and b) Compact Tension Mixed Mode Modified.

(a) (b)

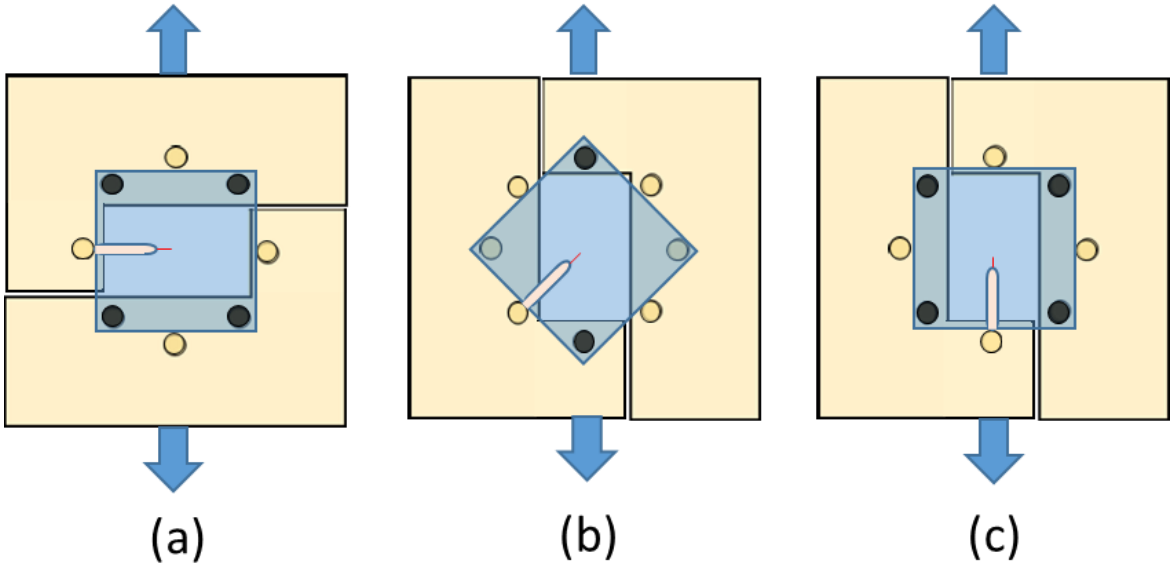

Figure 4.5 - CTMMM grips loading angle illustration in (a) Pure mode I loading, (b) Mixed mode I&I loading and (c) Mode II loading (blue = Specimen, Yellow = Grips)

The CT-MMM grips (Figure 4.6) have eight holes in total through which pins were used to secure the specimen, however not all of these are used for all modes of loading. Figure 4.7 illustrates the holes are used for each loading mode.

For testing these different modes, grip faces were attached together with the help of bolts. Different angles of 45° and 90° were selected and the grips were bolted accordingly to represent the mode I and mode II respectively. The tests are performed on small loads for simulating in larger environments. Both the modes are also performed simultaneously known as mixed mode.

Specimen geometry of the compact tension mixed-mode modified (CTMMM) grips differ from the SJ Arcan and NK Arcan grips since it requires four circular pin loading for mode I, mode II and only two circular pins for mixed-mode I&II loading for even distribution of stress.

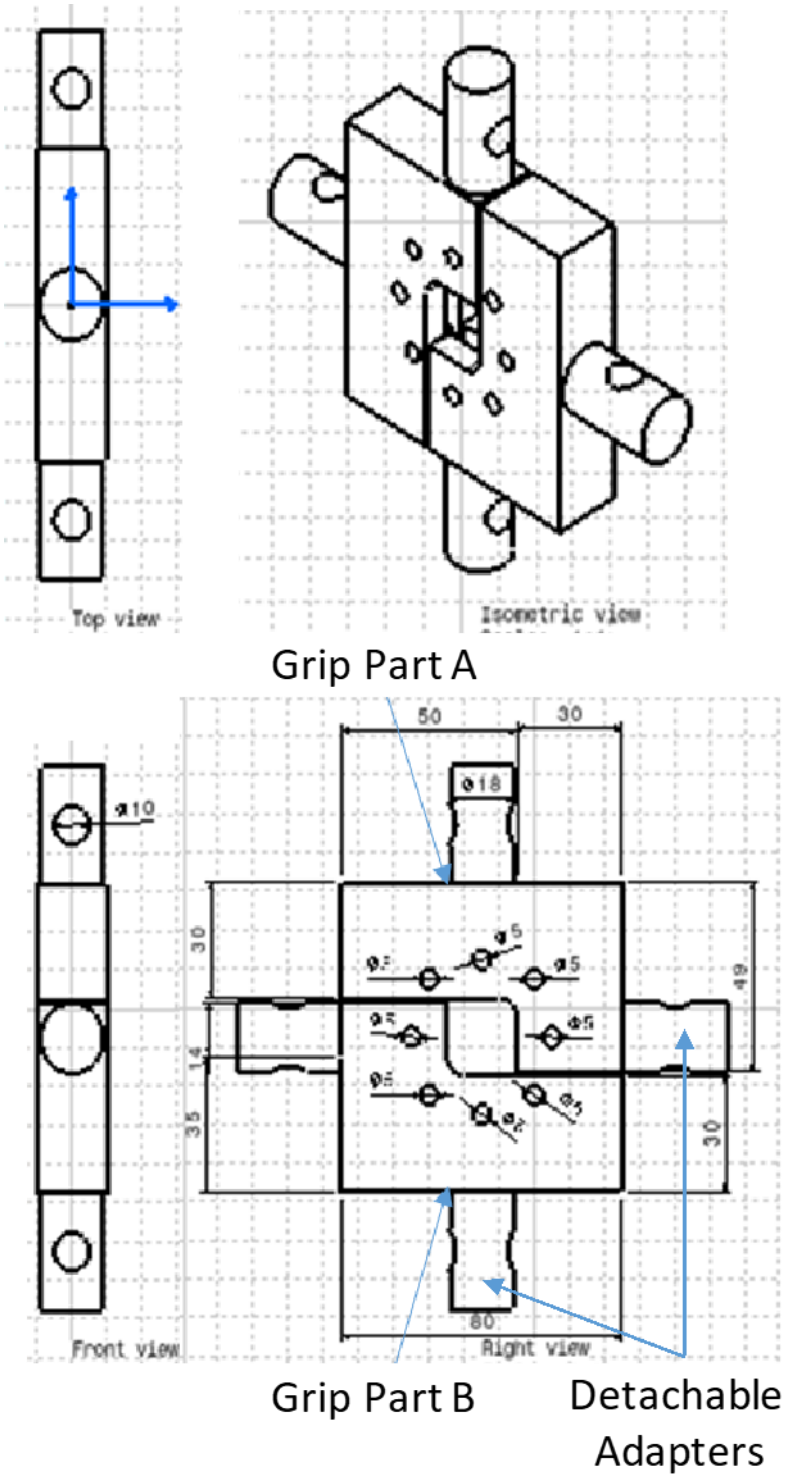

Figure 4.6 - Technical drawing of the CTMMM grips

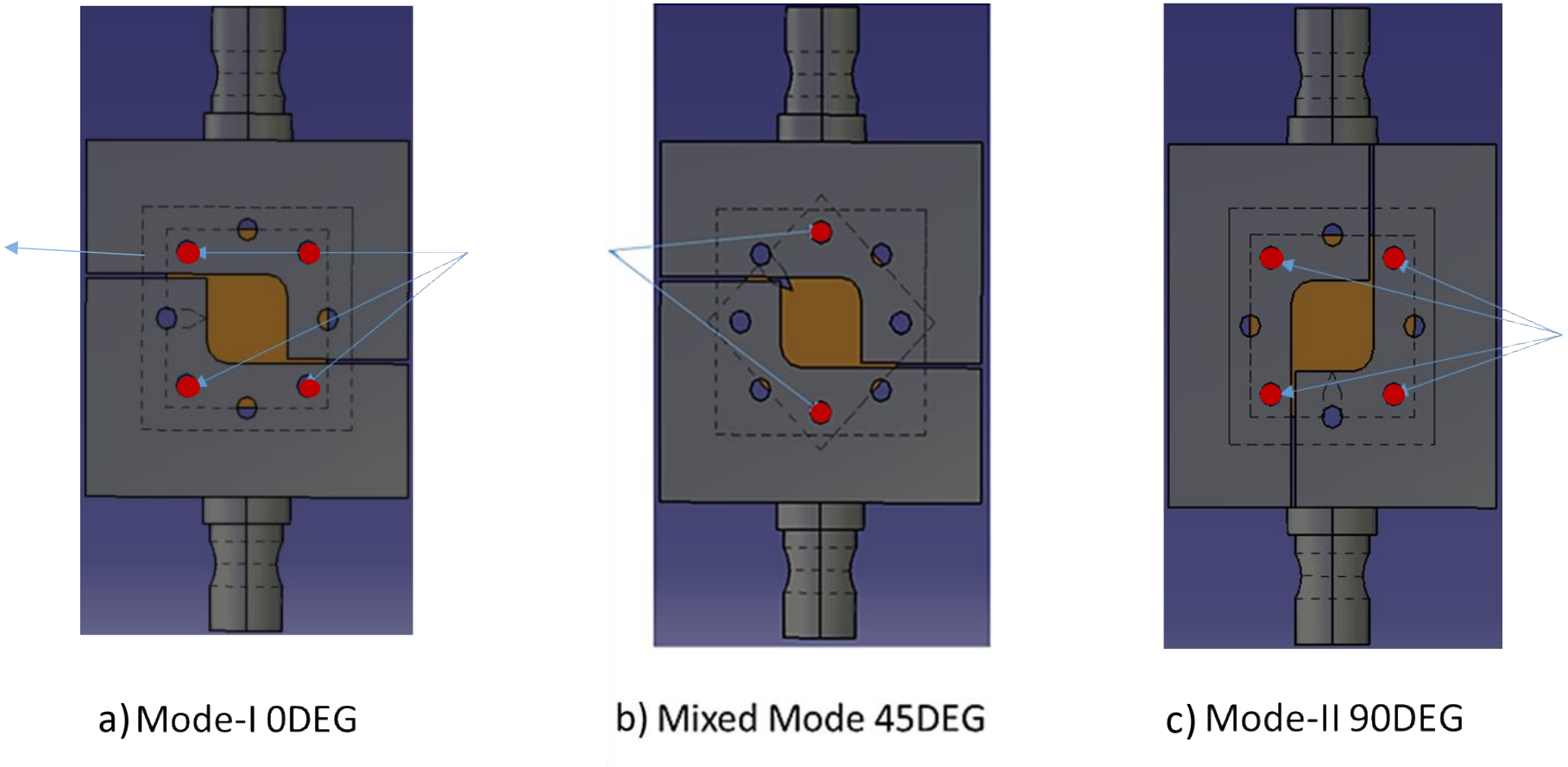

Figure 4.7 - CTMMM grips CATIA model representing a) mode I loading, b) mixed mode I & II loading and c) mode II loading

4.2.3 Photoelasticity based testing of grips

The photoelasticity method explained in section 2.5 was adopted to observe shear-loading behaviour of the different mixed-mode specimens and grips. The SJ Arcan specimen was loaded with the SJ Arcan and NK Arcan grips (Figure 4.1b and Figure 4.2b) and the CTMMM specimen was loaded with the CT-MMM grips (Figure 4.5b). The F1 (neat) resin formulation was used to manufacture the three specimens used in this study. This untoughened resin was chosen because it was transparent and birefringent. Photoelasticity provides a rapid full-field map of contours of maximum shear stress and hence was deemed an efficient method for an initial comparison of the specimen geometries and grip effects.

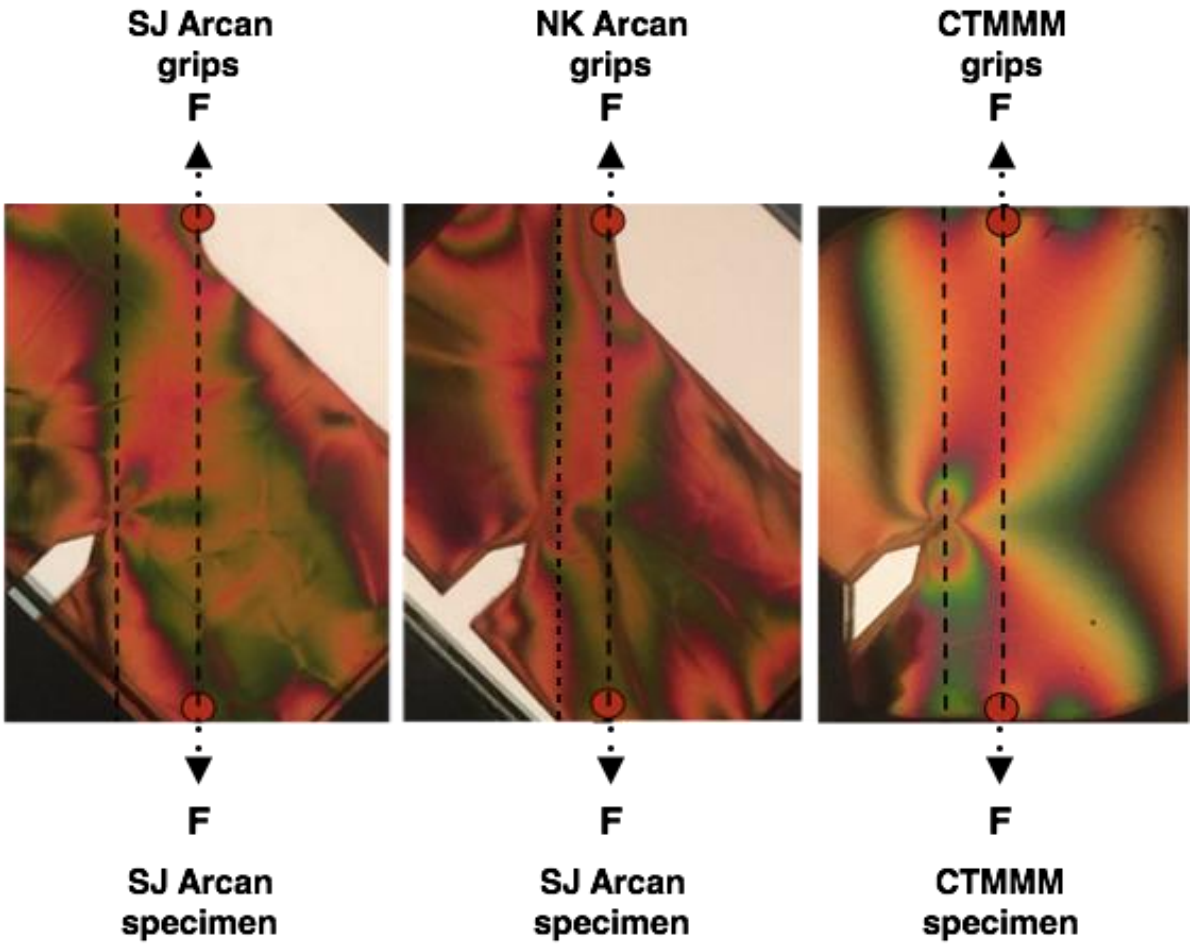

Figure 4.8 - Images of SJ Arcan, NK Arcan and CTMMM in a polariscope loaded 45° mixed mode I&II. The dotted lines show the load line and the crack tip line.

All the specimens were stress free before it each specimen was subjected to a 45° mixed-mode loading and viewed through a circular polariscope. The birefringent images are shown in Figure 4.8. The specimens were placed between the polarisers of the circular polariscope for assessing the levels of stresses. It can be seen from the images that SJ Arcan and NK Arcan specimen do not have uniform stresses, however, in the CTMMM specimen, the distribution is in a more uniform manner even near the edge of the tip.

At low loads, the stress field around the crack tip was observed to be identical and the fringe loops were as expected. The CTMMM gave a more defined fringe with less interference from the grips. The effect of the pin loading constraint was visible when the SJ Arcan grips used and subsequently, un-constrained when the NK Arcan grips were used.

4.2.4 Geometry factor / shape function

The geometry factor *f* or shape function *Y* is necessary to include a dimensional correction factor. The correction factor accounts for the dimension and the geometry configuration of the crack in a test specimen where *f* (a/w) or *Y* (*a/w*) is a function of the crack length *a* and total width *w* of a given test specimen. The term *f* (*a/w*) or Y (*a/w*) represent geometrical correction factor for a given ratio *a/w* can be obtained from the compendium of stress intensity factors [173], however for accuracy this value should be calculated for each specimen. A number of approaches from a number of researchers [174-176] were evaluated to calculate the geometry factor. Researchers Carlsson and Pipes [174] and Tada et al. [176] presented similar geometry factor equations for failure.

Mode I

$$f_I\left(\frac{a}{w}\right) = 1.12 - 0.231\left(\frac{a}{w}\right) + 10.5\left(\frac{a}{w}\right)^2 - 21.27\left(\frac{a}{w}\right)^3 + 30.39\left(\frac{a}{w}\right)^4 \quad (4.1a)$$

Mode II

$$f_{II}\left(\frac{a}{w}\right) = \frac{1.12 - 0.561\left(\frac{a}{w}\right) + 0.085\left(\frac{a}{w}\right)^2 + 0.180\left(\frac{a}{w}\right)^3}{a\left[1 - \left(\frac{a}{w}\right)\right]^{\frac{1}{2}}} \quad (4.1b)$$

Although there are many research studies supporting geometrical correction factors for Mode I, providing a clear and successive approach for standard test specimens, there are limited studies for Mode II. Mode I geometric correction factor equation 4.1a presented by Tada et al. for single edge notch CTS specimen and Carlsson and Pipes for single edge notch Arcan geometry is identical. Where Tada et al. have only evaluated and developed for Mode I, Carlsson and Pipes have developed equations for shape functions f_I and f_{II} for Mode I and Mode II. These are shown in equation 4.1a and 4.1b. Although geometrical correction factor is evaluated for both Mode I and Mode II, there has been very little study on geometrical correction factor for Mixed Mode I and Mode II for single edge notched specimens. The geometric correction factor equation 4.1a and 4.1b have been applied in this work.

4.2.5 Validation of LEFM assumptions

A key part of testing for plane strain fracture toughness is to ensure that the test material undergoes failure predominantly in plane strain. One such material is aerospace epoxy resins which are limited material thickness because the high temperature cured epoxies are difficult to manufacture in thicker sections without incurring an exothermic reaction [177].

In order for plane strain condition to be valid, the process zone size (the area where the occurrence of energy absorption such as shear yielding or plasticity occurs) should be adequately small compared to the ligand length or effective width and test sample thickness.

Tensile testing of a number of materials showed the (0.2% strain) yield stress to be approximately 80 MPa for each formulation. The process zone radius can be estimated by the length r̄ by equation (4.2a).

$$\bar{r} = \frac{(K_Q)^2}{(\sigma_Y)^2} \tag{4.2a}$$

Assuming LEFM behaviour, the sufficient process zone radius distance for the S02 formulation sample test specimen can be shown as:

$$\bar{r} = \frac{(1.34\ x\ 10^6)^2}{(80\ x\ 10^6)^2} = 0.28\ mm \quad (4.2b)$$

(4.2b)

This indicates that the process zone radius distance is sufficiently small for the given, crack length, width and thickness to be significantly greater than 2.5 × $\bar{r}$, for validating LEFM to be considered adequate plane-strain by BS ISO 13586 [38], ensuring K_Q can be regarded as K_{Ic}. For accuracy this value was calculated for each specimen theoretically K_I and K_{II} as mentioned in equation 4.3a and 4.3b. Where K_I and K_{II} is the stress intensity factors for Mode I and Mode II, σ is the applied stress and a is the crack length, t is the specimen thickness and other parameters are previously defined.

$$K_I = f_{\mathrm{I}}\ \sigma \sqrt{\pi\ a}$$

(4.3a)

$$K_{II} = f_{\mathrm{II}}\ \sigma \sqrt{\pi\ a}$$

(4.3b)

The theoretical K_I or K_{Ic} values are calculated from the LEFM validity and can be seen to be consistent with very little deviation and acceptably low for brittle materials of this type between theoretical and experimental values presented in table 4.1.

Specimen	***a*** **(mm)**	***w*** **(mm)**	***a/w***	**t (mm)**	f_{I} **Theory**	f_{II} **Theory**	K_I **Theory**	K_{II} **Theory**	K_I **Exp**	K_{II} **Exp**
S02-T2-0DEG	9.50	40.00	0.24	4.01	1.47	-	1.34	-	1.34	0.05
S03-T3-45DEG	9.50	40.00	0.24	4.00	1.47	1.14	0.89	0.69	0.89	0.64
S01-T2-90DEG	9.50	40.00	0.24	4.00	-	1.14	-	0.78	0.00	0.79

Table 4.1 - Analytical approach for three specimens

The experimental K_I & K_{II} values presented in table 4.1 were calculated using DICITAC approach. The approach is explained in section 2.5. Furthermore, all the specimen comparisons use the same thickness, crack length and geometry throughout the thesis and as such the fracture toughness can be directly compared and no consideration need be given to plane strain condition.

4.3 Conclusion

Current testing procedures for evaluating tension and shear properties that affect the fracture of novel toughened material is labour intensive with longer experimental time and complex specimen preparation technique resulting in a knock-on effect in many industries such as the aerospace and automotive manufacturing sector.

In conventional testing, different specimen geometries and grips for each test with mode I and mode II testing. Most industries prefer a fast and efficient solution for high through put testing of material and it is here where the new NK Arcan test fixture and SJ Arcan specimen show that such improvements are plausible. The CTMMM grip designed to employ a modified compact tension geometry for testing of mode I (tension), mode II (shear) and mixed-mode I and II (shear/tension), incorporated the mixed-mode I&II test grip design to ensure accurate high throughput testing methodology which can be easily adopted by the industry for determining and evaluating fracture toughness of novel chemistry.

Furthermore, data is presented in this chapter for stress intensity factors obtained using novel experimental setups and formulations. For values K_I and K_{II} calculated using the DICITAC code ($K_I Exp$) are comparable with theoretical K_I and K_{II} for the new specimen geometry setup.

CHAPTER 5

Mixed mode testing of toughened unmodified resin (F-Formulation)

5.1 Introduction

This chapter aims to investigate fracture behaviour of unmodified toughened epoxies in mode I, mode II, mixed mode I and mode II.

The chapter is separated into four sections and begins with a summary of the characteristics of thermoplastic and thermoset resins systems followed by a review of literature in mixed-mode toughened epoxy studies, and the direction of experimental study. Toughened epoxies were investigated with 3D DIC in (near) pure shear, to measure the effect of out-of-plane strain measurement and evaluated to identify an ideal experimental setting. Digital Image Correlation (DIC) reads surface patterns that occur naturally or have been applied on the surface at the time of the experimentation. It then tracks the movement of these patterns. The displacement of the patterns are analysed within the discrete subsets of the image. The maximum correlation in each window corresponds to the displacement where the length and direction is provided for each window. This technique was developed recently by Mike Sutton[89] for calculating the displacement field by processing multiple recorded images of a specimen. In two dimensional DIC systems, multiple grey scale images are constantly recorded using a single camera. Additionally, other analogue data such as LVDT signals can also be recorded simultaneously. In this project LaVision DIC hardware equipment and Davis 8.1 Strain Master software configuration was used to capture successive images with simultaneous analogue device data input. A series of experiments were conducted in mode I, mode II, mixed mode I and mode II with different unmodified toughened epoxy and the grip loading configurations described in chapter 4.1 and 4.2. The Young's Modulus (E) and Poisson's ratio (ν) was provided by the sponsoring organisation (table 5.1) used to study and obtain stress intensity factors K_I and K_{II}.

Formulation	*E*	*v*
F1	3.15	0.39
F3	3.18	0.39
F4	3.11	0.39

Table 5.1 – F-formulation data table provided by sponsoring organisation

5.1.1 Background

Predominantly, the failure mode of components takes place in mode I. Therefore, mode I has more research in the literature, when compared to mode II and mixed mode I & II. There are various tests and standards that are available for mode I fracture and material properties. However, other techniques to determine mode II and mixed mode I & II fracture are problematic. There has been much work that has been conducted to study the fracture of interfaces like adhesive joints or composite layers for shear loading. Mainly there are two types of loading bulk materials in pure mode I and both of this are described in the British and International standards [38]. In composite materials the materials are usually tested with mode I loading for interlaminar and intralaminar orientations. The former usually involves creating a composite panel with a strip of release film at the centre for initiating stress concentration, whereas the latter tests the toughness in the regions that are rich in fiber [178].

Different methods have been practised by different researchers to assess composite fracture toughness of resins as a part of a composite, in this chapter efforts have been made to assess fracture toughness of resin materials using Digital Image Correlation (DIC) and DICITAC, a software that was developed in-house (Mechanical Engineering Department, University of Sheffield).

The Digital Image Correlation (DIC) algorithms require the selection of subset size and overlap, which is the key selection criteria that affects the quality of the result. Displacement calculations are determined across the entire region of the subset. Therefore, the smaller the subset selected, the higher the displacement field resolution and the larger the subset, the

greater the grayscale data is available for the algorithm to determine displacements fields accurately. The selection of subset size must be based on the type of speckled pattern used and the type of continuous displacement. Advancement in technology with time advance improvement in the development of DIC technology. In particular, the time taken to correlate displacements is improved in the order of minutes instead of hours, it is common for many expert users in the field to perform a number of different subset sizes with algorithm options for accurate processing of results. Full field displacement measurements at every data point in each subset within processing field of view. In general displacement field data points are not linked to the specific pixel, instead it is linked to averaged displacement field region surrounding the data point. The assessment of DIC displacement field assessment utilises iterative least square method (ILS) [179], available in LaVision Davis 8.1 Strain Master Code. LaVision DaVis 8.1 Strain Master is used as straight out of a box tool and aim to address variables required for the ILS calculation such as subset size and step size or percentage of overlap by subset evaluation. Different subset sizes were used to check the sensitivity of the subset size for determining the strain fields in the y-coordinate (ε_{yy}) as shown in figure 5.1. In Each figure in Figure 5.1 displays the full field of view with the crack position from left to right. The sub figures also show the grey areas shows strains higher than 1%.

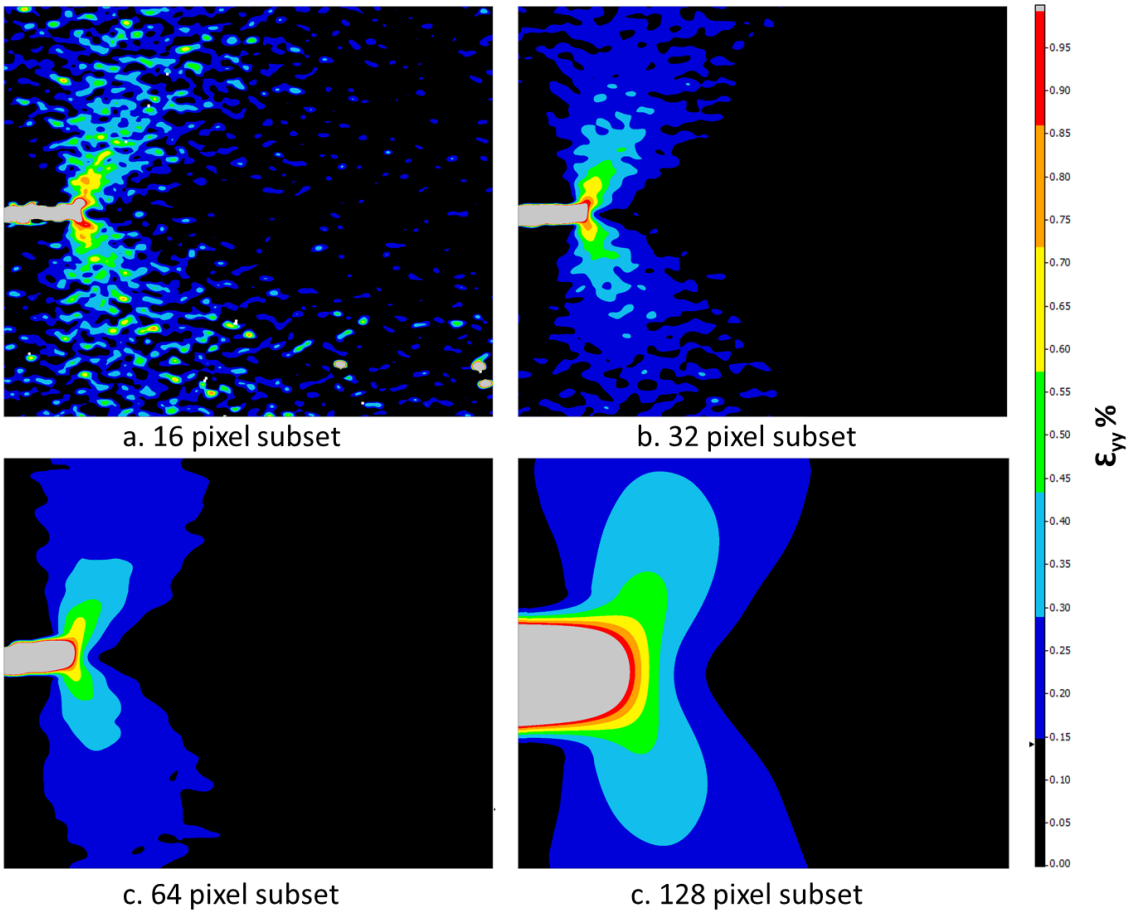

Figure 5.1 - ε_{yy} (interpolated) strain fields around a crack tip in a CT-MMM specimen determined using different subset sizes.

Figure 5.1 indicates that the strain field around the crack tip can be seen to reduce as subset size increases. Also, the Airbrush speckle pattern noise levels can be seen at the lowest subset size. The level of noise is evident in the 5.1 figure but there is a substantially more noise in the 32-pixel subset correlations than in the larger 64-pixel correlations. After further assessment, it can be determined that LSM algorithm with 64-pixel subset with 25 % overlap generates the best compromise between accuracy and resolution. An ε_{yy} strain field determined using different subset size shown in figure 5.2.

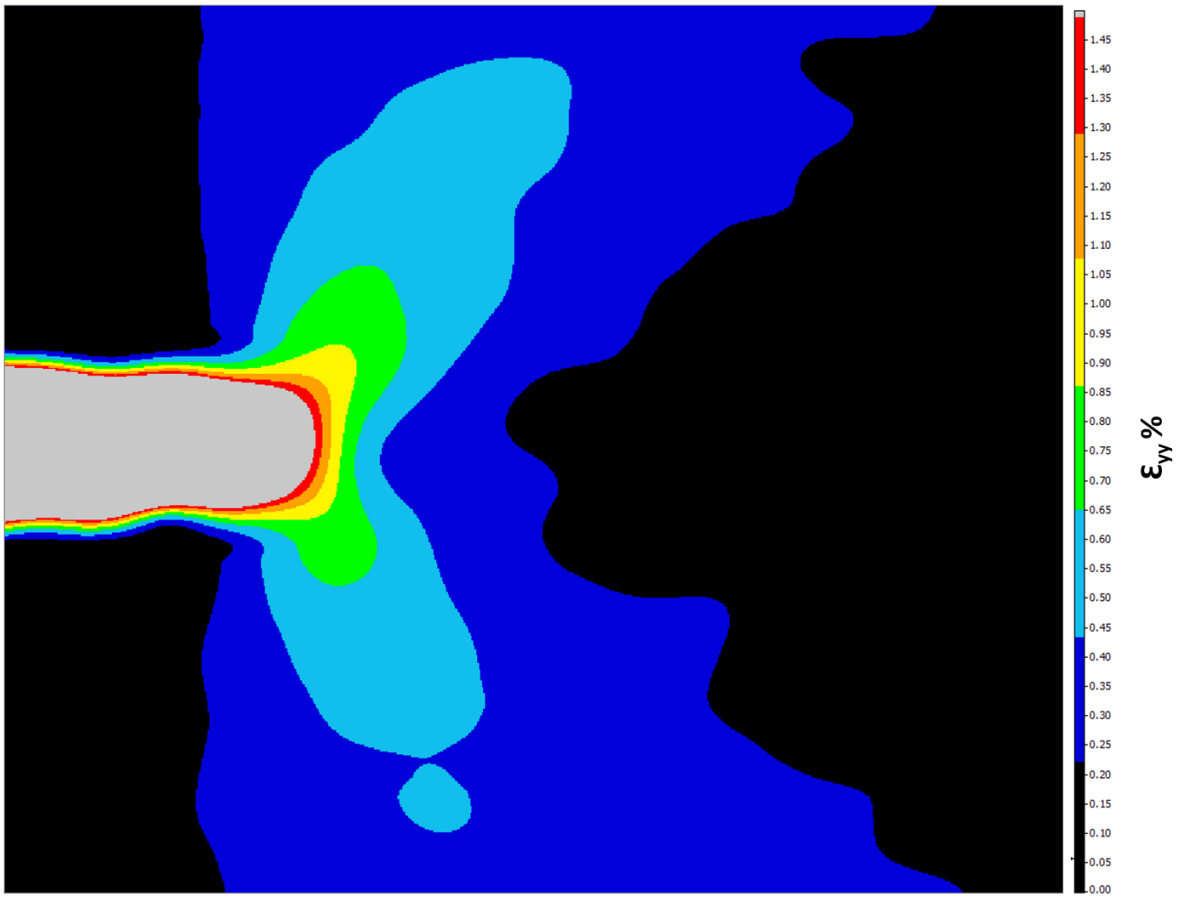

Figure 5.2 - ε_{yy} strain fields around a crack tip in a CT-MMM specimen determined using multi-pass 64x64 pixel subset size with a 25% overlap.

The following DIC configuration algorithms, algorithm options and variables were chosen:

Correlation mode	Relative to initial frame
Integration window	Square
Subset size	64 pixels, 25% overlap
Post processing	Default LaVision - Least Square Method

Table 5.2 - Selected DIC algorithms

The DICITAC software provides stress intensity values in mode I (K_I), mode II (K_{II}) and T-Stress using Williams series solution.

Mode I

$$\sigma_{xx} = \frac{K_I}{\sqrt{2\pi r}}\cos\frac{\theta}{2}\left(1 - \sin\frac{\theta}{2}\sin\frac{3\theta}{2}\right) + T + A\sqrt{\boldsymbol{r}}\cos\frac{\theta}{2}\left(1 + \sin^2\frac{\theta}{2}\right) + O(r)$$

$$\sigma_{yy} = \frac{K_I}{\sqrt{2\pi r}}cos\frac{\theta}{2}\left(1 + sin\frac{\theta}{2}sin\frac{3\theta}{2}\right) + A\sqrt{r}cos\frac{\theta}{2}\left(1 - sin^2\frac{\theta}{2}\right) + O\left(r^{3/2}\right)$$

$$\tau_{xy} = \frac{K_I}{\sqrt{2\pi r}}cos\frac{\theta}{2}sin\frac{\theta}{2}cos\frac{3\theta}{2} - A\sqrt{r}sin\frac{\theta}{2}cos^2\frac{\theta}{2} + O(r)$$

(5.1a)

Mode II

$$\sigma_{xx} = \frac{-K_{II}}{\sqrt{2\pi r}}sin\frac{\theta}{2}\left(2 + cos\frac{\theta}{2}cos\frac{3\theta}{2}\right) + B\sqrt{\boldsymbol{r}}sin\frac{\theta}{2}\left(2 + cos^2\frac{\theta}{2}\right) + O(r)$$

$$\sigma_{yy} = \frac{K_{II}}{\sqrt{2\pi r}}sin\frac{\theta}{2}cos\frac{\theta}{2}cos\frac{3\theta}{2} - B\sqrt{r}sin\frac{\theta}{2}cos^2\frac{\theta}{2} + O\left(r^{3/2}\right)$$

$$\tau_{xy} = \frac{K_{II}}{\sqrt{2\pi r}}cos\frac{\theta}{2}\left(1 - sin\frac{\theta}{2}sin\frac{3\,\theta}{2}\right) + B\sqrt{r}cos\frac{\theta}{2}\left(1 + sin\frac{\theta}{2}sin\frac{3\theta}{2}\right) + O\left(r^{3/2}\right)$$

(5.1b)

The advantage of using the parameter extraction method is that it does not require measurement of crack lengths or loading angles since the stress intensity factor values are measured directly from the DIC vector displacement field. The DICITAC method has been validated for modes I and II [180]. DICITAC (Digital Image Correlation Intensity factor and T-stress Code) [52, 54, 55], is a program that used MATLAB simulation created by Dr. Mohammad Zanganeh at the University of Sheffield as part of his PhD research. It was developed for extracting the fracture parameters from unique displacement fields obtained by the DIC calculations. DICITAC gives multiple options to the user, including extraction of fracture parameters using Williams [10] crack tip stress solution techniques. This allows the use of the

Williams method for extracting the T-stress. This framework uses the equations of Williams stress solution in a Cartesian displacement form to find the unknown constants for the displacement fields. The compact tension specimen is presented for both mode I and mode II and compared with the formulations by comparing the measured DIC values with the derived DICITAC values for identifying the accuracy.

5.1.2 Data Point Region

Until date a limited number of studies investigate the effect of the region of data points collected on the extracted fracture parameters. A wide range of regions was used to extract fracture parameters for assessing the effect of window of data collection. The influence of the data window of inclusion or exclusion of displacement vectors behind or ahead of the crack tip was investigated for Mode I specimen, S13-T3-0DEG.

Figure 5.3 shows images captured from different regions of displacement vectors. The displacement vectors are presented in xy-grid location with separate options to visualise u and v vectors (representative x and y displacement directions). Colour scales have been used to indicate the magnitude of vector represented by the z axis dimension. However, the scales have been removed from the images in the Figure 5.3 for clarity and the crack tip has been identified with a plus symbol “+” with in a circle (crosshair).

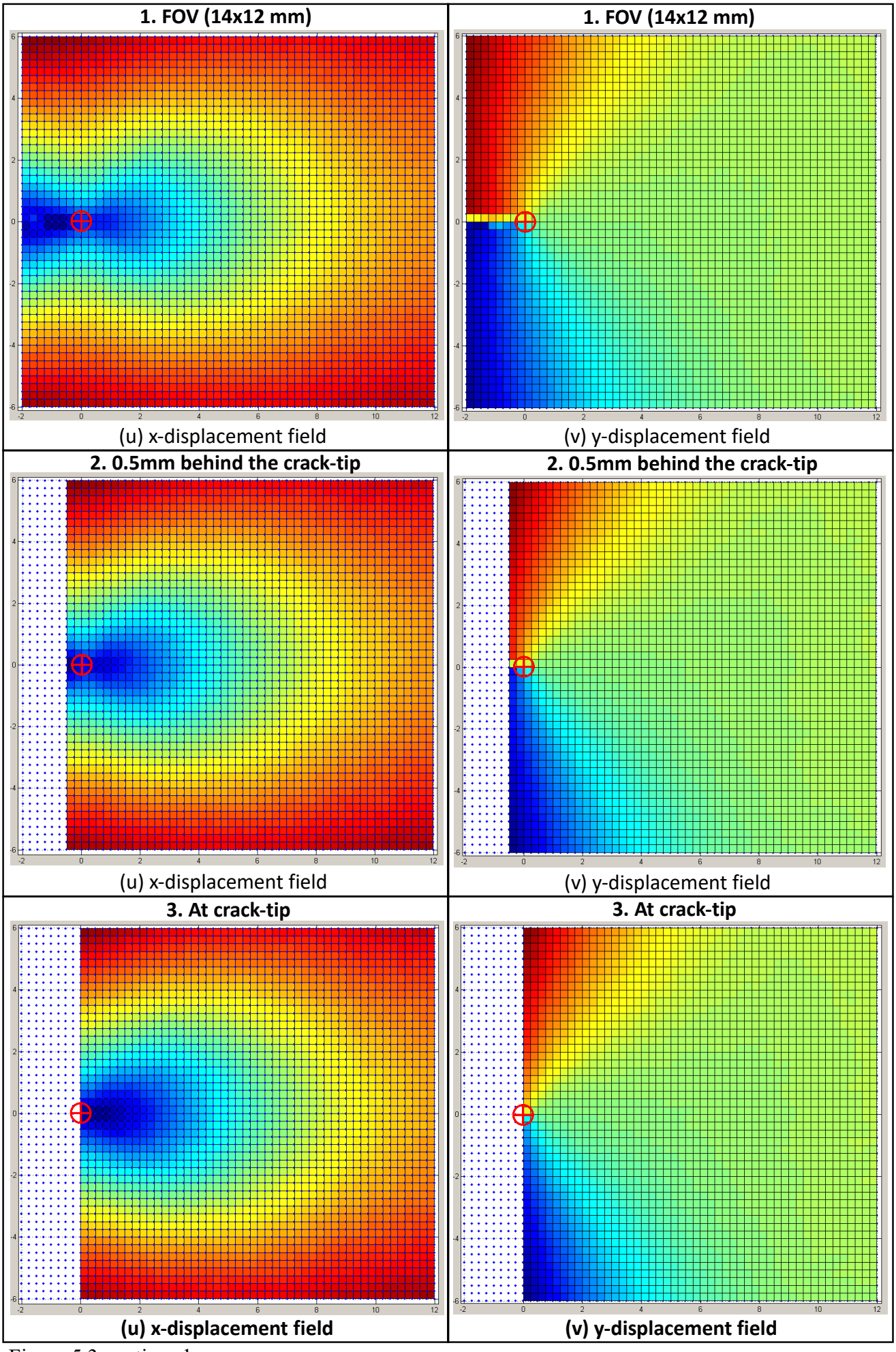

Figure 5.3 continued

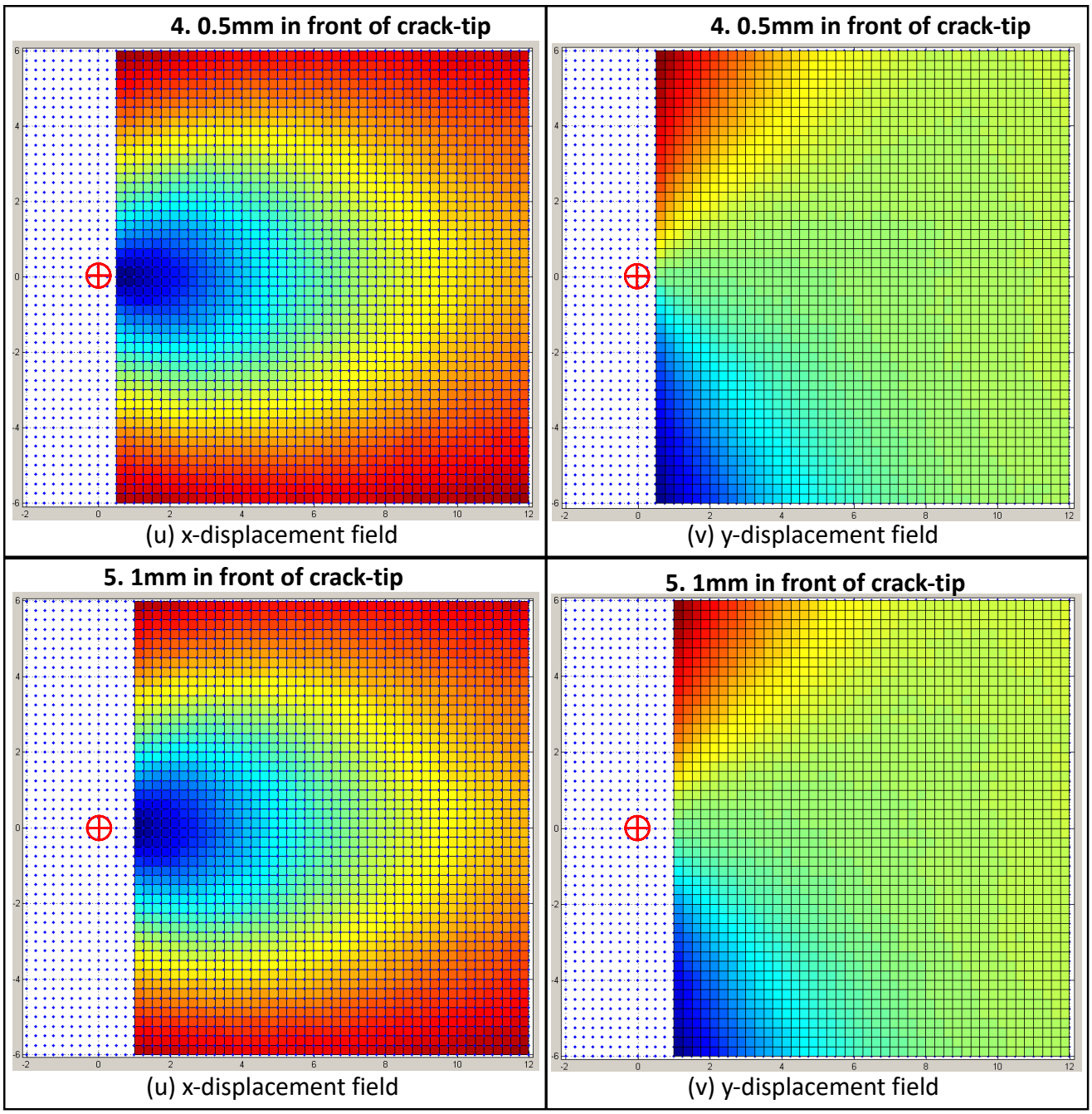

Figure 5.3 - Figure table showing different data point region in pure mode I specimens indicating crack-tip with crosshairs.

Numerical values calculated for K_I are 1.18 MPa$\sqrt{}$m and K_{II} should be zero. The values computed by DICITAC tool have an accuracy limit of ±0.02 MPa/m as a rough comparison of displacement field accuracy of deviations.

Although the DICITAC Matlab code is able to evaluate and extrapolate SIF for Fracture toughness K_c very well using the Williams series solution, it is not possible to determine the T -stress using Muskhelishvili's approach and only using two terms of Williams' solution is not enough to determine the T-stress and a minimum of three or more terms is needed. Mohammed Zangeneh's research indicates, when using Williams' approach to determine the T-stress and stress intensity factors; the results obtained from displacements were more robust and a convergent trend was observed for the T-stress and the stress intensity factors when the number of terms of Williams solution was increased, than results obtained using stress fields.

5.2 Investigating Unmodified Toughened Epoxy

Of the few experimental studies conducted on mixed mode fracture of toughened epoxies, most of them focus on determining stress intensity factors from load data, crack length and geometry factors by fitting the fourth order polynomial to finite element analysis. A study conducted by Nurse and Patterson in 1993 determined mode II stress intensity factor using photoelasticity applied to the four point bending testing suggested that the technique used evaluates Mode II and Mode I problems accurately and prompts further studies to include high order terms effect [141]. Tomlinson, Nurse and Patterson in 1997 studied stress intensity factors (SIF) for mixed mode I & II cracks with thermoelastic data applied on a centre angle cracked aluminium tensile test panel and developed a reliable thermoelastic method [53].

A novel approach is taken to study stress intensity factors that were extracted from digital image correlation (DIC) displacement data using the Williams series solution. Until recently, experiments were focussed towards identifying mode I, a common mode of failure. This is because mode I (tensile) fracture studies are well studied than modes II (shear) and mixed mode I & II.

Preliminary objective of this project was to validate previous work conducted by Jones [133], and studies were focussed towards characterising material properties of neat and particulate

toughened epoxy. Further to optimisation of experimental procedures (described in chapter 3 and 4), experiments were conducted to improve the methodology of material characterisation. This chapter describes the mixed mode I and II experiments and are divided into four main sections - a) Section 5.3.2 - investigation of out-of-plane effects of brittle epoxies, b) Section 5.4 - assessing the modified Arcan grips and specimens (SJ Arcan), c) Section 5.4.3 - investigation of the original Arcan grips (SJ-Arcan) captured with the modified Arcan specimen (NK-Arcan) and d) Section 5.4.4 & 5.4.5 - testing the new developed high-through-put CT-MMM grip and specimen. Experiments were conducted with three different grip geometries and specimen materials provided by Cytec. The three F-Formulation (F1, F3 and F4) materials provided were strategically selected by Cytec with different formulations of material. These materials were subjected to loading until failure, the F-Formulation were used with three grip configurations.

Failure of different materials were analysed with respect to resistance of fracture and crack path stability by extracting K_I and K_{II} values. The DIC displacement field data was fed into DICITAC software to extract stress intensity factors (K_{IQ} and K_{IIQ}) (i.e. K_I and K_{II} at point of specimen failure). These values were graphically plotted along with loading angle. Linear regression were displayed on the graphs. The DICITAC software fits the Williams series crack tip field solution to extract key fracture parameters SIF values (K_I and K_{II}).

5.3 Mixed mode I and mode II experimental methods

Samples from toughened unmodified epoxies (F1, F3 & F4) were subjected to failure by Mode I, Mode II and Mixed Mode I&II testing in the configurations as described in section 4.2.1. Since the epoxies (F1, F3 & F4) were characterised previously in the SJ Arcan grips by researchers in the University of Sheffield [181], fracture toughness was studied only in pure Mode I, pure Mode II and pure Mixed Mode I&II testing in 0°, 45° and 90° loading angles using different grips. K_I and K_{II} at fracture was determined by DICITAC software. All experiments were conducted four times to ensure repeatability. Statistical analysis was performed by Student's T-Test and inter class correlation (ICCC) reliability tests. Surface strain maps were generated by DIC using methods described in next section.

5.3.1 Experimental setup for both 2D and 3D DIC

Unlike 2D DIC (Figure 5.4) that generates in-plane strain along the *x* and *y* axis, 3D DIC (Figure 5.6) generates both in-plane and out-of-plane deformation along the *x, y* and *z*-axis respectively. Analysis of out-of-plane deformation is of paramount importance to ensure accuracy in strain measurements obtained.

Features of the La-Vision 2013 DIC imaging system (Figure 5.4) used in 2D DIC the system include a 5MP CCD sensor camera, synchronised dual LED lighting, a TOKINA (TOKINA AT-X M100 PRO D F2.8 Macro) 100 mm macro lens and a Tinius Olsen 25kN frame with 5kN resolution based load cell.

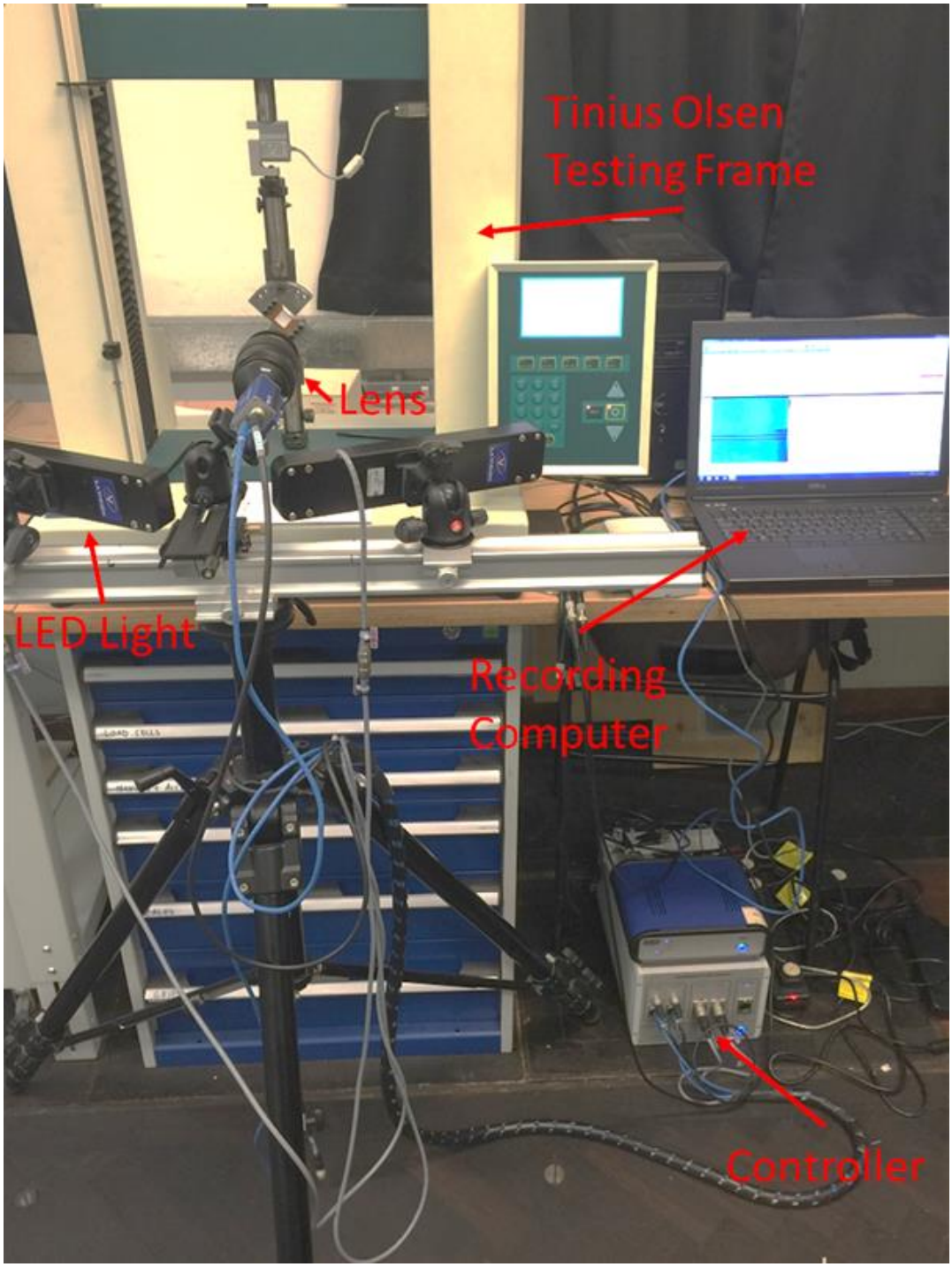

Figure 5.4 - La Vision DIC equipment set up 2D DIC

Rotation of the camera was aligned with the specimen crack tip direction to ensure the acquired displacement vector field is parallel to the *x*-axis. A Manfrotto 454 micro positioning plate (micro positioning plate) as shown in 3D DIC (Figure 5.6) was adapted to the camera mounting and tripod for enabling simple angular rotation of the camera that matches with mixed mode specimen loading angles. A specimen is placed in the loading position and the two-high

magnification macro lenses are focused onto the specimen surface by ensuring the image covers the entire field of view. Please refer to Appendix 1 for specimen dimensions.

Two Imager E-Lite 5M (12-bit colour, 5-megapixel resolution CCD camera) were used to 3D capture successive images and record on the computer. The Imager E-Lite 5M camera can capture up to 14 frames per second per camera and is often configured manually based on experimental needs. Configuration set for the current experiment was 2 frames per second.

The experiment was illuminated with two LED lights that were automatically synchronised with the recording frame rate. The illumination intensity could be adjusted to avoid flooding the field of view with too much light. Care must be taken to perform the experiment in a controlled environment since the light effect can exhibit a strobing light condition. Alternatively, other LED lighting sources could be used. Problems associated with optimum lighting are discusses in section 2.4.1.2 Davis 8.1.6 software (LaVision) was used with the DIC testing equipment and successive images were captured. Davis 8.1.6 has 256 colours palette was used for observing the intensity maps on the screen. Spirit levels were used to achieve accurate angular alignment on the camera and successive images were captured and checked.

Control of Tinius Olsen test frame is independent of Davis 8.1.6 software. The start sequence for recording and loading was initiated at the same time individually. Although the specimen loading and image capture was independently executed, successive images were captured in tandem with the load and displacement per image. The load and displacement from the test frame is directly connected via the National Instrument analogue to digital (AD) converter, which was connected to the DIC system allowing the image, load value and test frame extension to be captured simultaneously.

Following configuration of the 3D DIC equipment, the specimen was also calibrated. The specimen is removed from the grip holder and the calibration plate is placed in the same

position as the specimen surface. The calibration is conducted by capturing 0.25mm images of the glass calibration substrate (figure 5.5) and correlating the distance per pixel in the image. Furthermore, the calibrated image was used for image correlation during post processing.

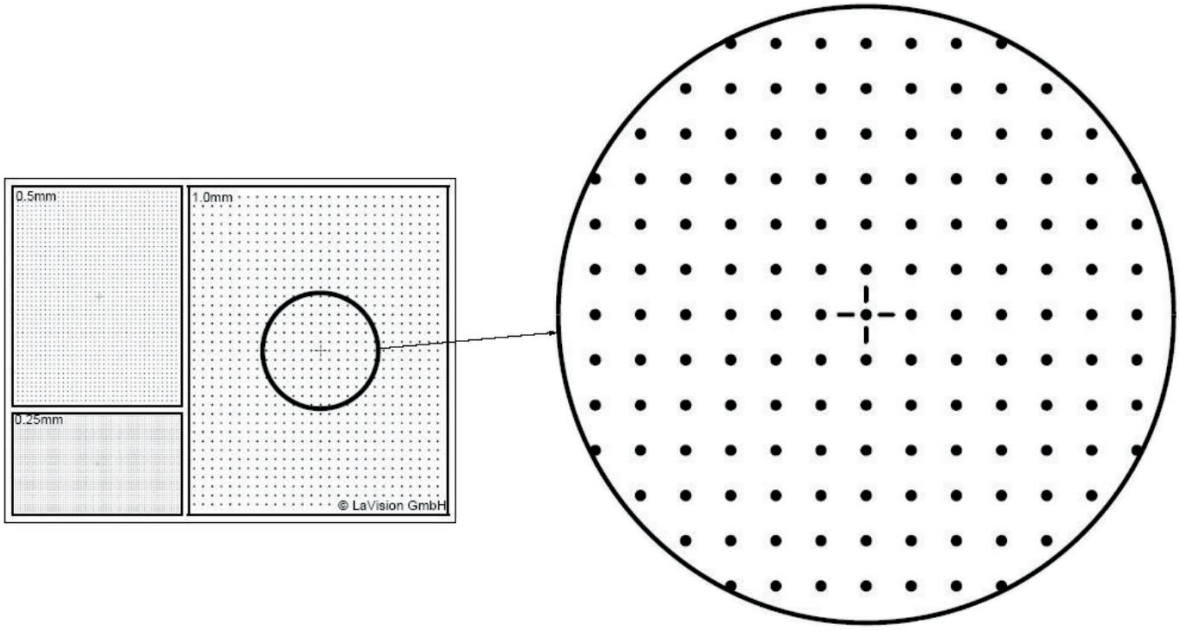

Figure 5.5 - La Vision DIC calibration substrate

Any more than 400 images contribute very little towards accuracy of strain map and occupy storage space. Therefore, the test specimens were loaded to failure at 2 frames per second and set to capture an average of 400 images per experiment. Finally, the series of captured images were processed by least squared processing function and results were observed in a strain map. The experimental setup configuration for 2D DIC involves a single camera being configured and calibrated by positioning directly ahead of the test sample in the equipment whereas in the case of 3D DIC, two cameras are positioned in different angles pointing towards the specimen. To analyse the out-of-plane effects, specimen geometry design of SJ modified Arcan specimens (Figure 4.1a) were studied in NK Arcan grips (Figure 4.2) in the 3D-DIC arrangement. Specimens were loaded to failure at 90° loading angle that is referred as (near) pure shear. The test specimens were loaded with 0.5 mm/min displacement rate in a dual column 25kN Tinius Olsen testing frame as shown in 2D DIC equipment (Figure 5.4). The images were recorded at 0.5Hz with failure loads occurring between 300-1000 N for test specimens. 5kN load cell was

used to measure load and test specimens in mode I (Figure 5.6a), mode II (Figure 5.6c) and mixed mode I and mode II (Figure 5.6b). Experiments were performed three times with specimens for the F3 material being loaded to failure in loading angles 90°.

Displacement around the tip of the crack of the three F3 toughened test specimens were measured by analysis of images captured by 3D DIC system. In-plane vector fields (x and y-axis) and out-of-plane (z-axis) were analysed by Matlab to extract Crack Tip Opening Displacement (CTOD) values. A Matlab code was created to aid in the processing of the displacement of vectors (Vx, Vy, Vz) ahead of the crack tip and analyse the effects of out-of-plane deformation. The results are discussed in section 5.3.2.

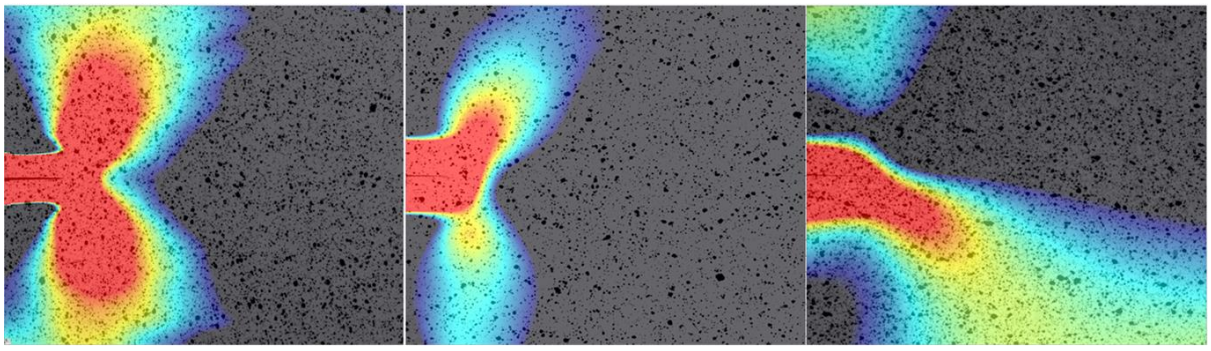

(a) (b) (c)

Figure 5.6 - DIC image with Strain field overlayed on specimen, (a) mode I, (b) mode I&II and (c) mode II

For fracture testing (Section 5.4), specimens were loaded to failure at 0°, 45°, and 90° loading angles, where 0° is (pure) tension, 45° is (pure) mixed mode I and mode II and 90° is (near) pure shear. The test specimens were loaded with 0.5 mm/min displacement rate in a dual column 25kN Tinius Olsen testing frame and images were captured using the 2D DIC system at 0.5Hz with failure loads occurring between 300-1000 N for the different test specimen. 5kN load cell was used to measure load and test specimens in Mode I, Mode II and Mixed mode I and mode II. Experiments were performed four times with specimens for each material being

loaded to destruction in loading angles 0°, 45° and 90°. Fracture parameters were determined using the DICITAC software.

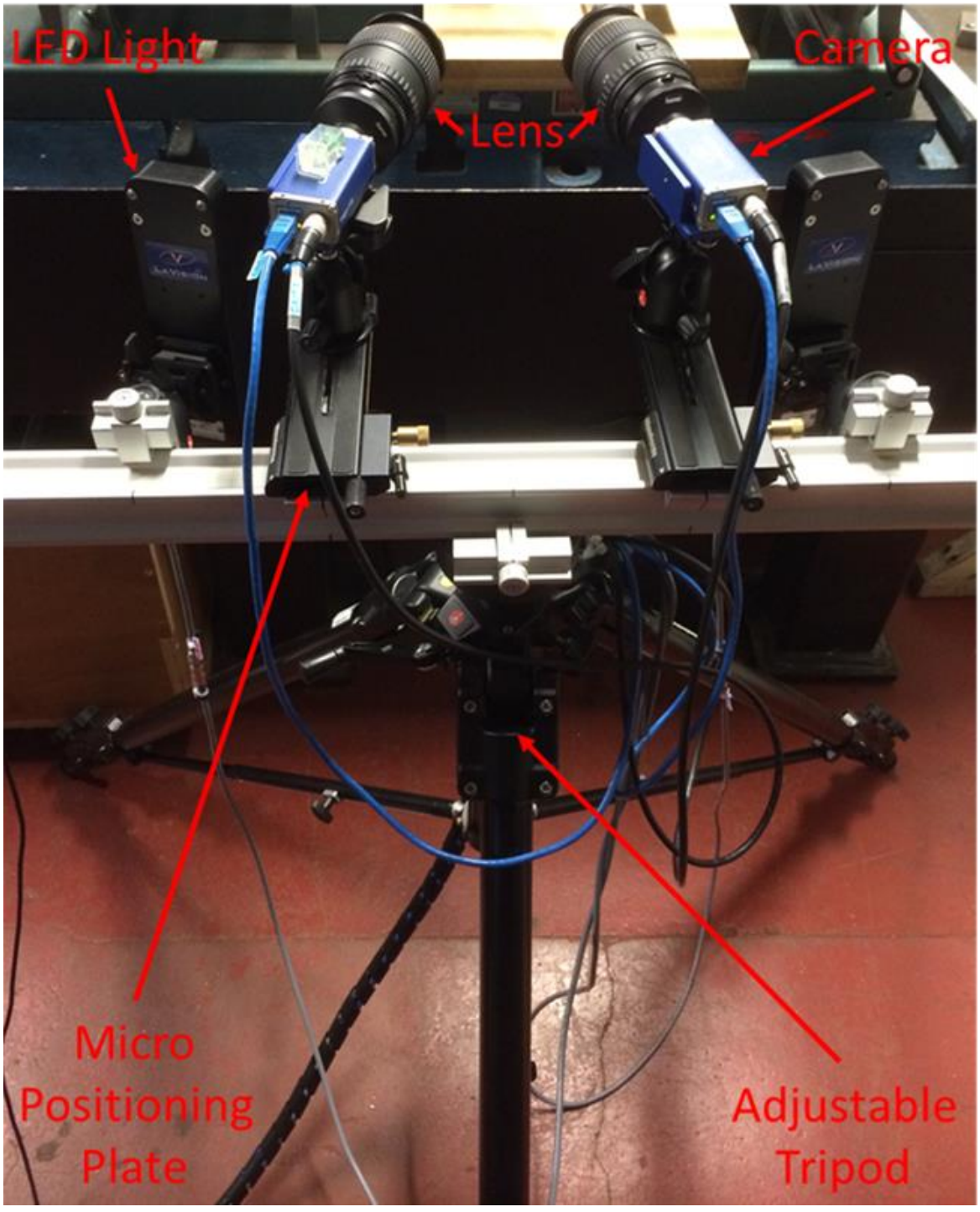

Figure 5.7 - La Vision DIC equipment set up 3D DIC

5.3.2 Investigation of out of plane effects of brittle epoxies using 3D DIC

A 3D experimental investigation was conducted as described in section 5.3.1 in order to assess the magnitude of out of plane deformation for brittle specimens and optimise the DIC system for future experimentation. F-formulation samples (F3) were tested using 3D DIC to assess the out-of-plane measurements. The vector field nomenclature (Figure 5.8) and the Crack Tip Opening Displacement vector magnitudes in the x, y and z directions are shown in Table 5.3. While a single camera is sufficient for the 2D DIC, more cameras are needed for the 3D DIC. Two cameras have been used in this work to record the digital images from two different viewpoints.

In this method, the user obtains a sequence of images that is taken while testing the material. The first image is usually taken without any load. The sequence of images are analysed by search for any changes in the pattern. These changes in the pattern are reduced for the individual subsets and this correlates to the changes that describe the direction and the length of the vector. In a two-dimensional DIC, a standard single camera is fixed for achieving the plane deformation whereas for the three-dimensional DIC, a dual camera setup is fixed for the surface measurements. From this, the strains are calculated for the whole surface by using local derivative calculations. When CT-MMM tests are carried out for the mixed mode, the problem is eliminated. When the lens is adjusted, the focal length also gets adjusted; hence the focal length must be kept constant. This ensures that the distance between the camera and lens are maintained within the optimum levels. By maintaining the distance, the quality of the calibration will not be affected even when there is change in the location of the specimen. Results (Table 5.3) revealed that out-of-plane deformation observed in toughened unmodified F-formulation sample (F3) was negligible, suggesting that out of plane deformation was not

influenced when loaded to failure in the NK Arcan grips. It is likely that modifications in pin loading constraints confers protection against out of plane displacement due to shear.

Images of F3 sample subjected to loading using NK Arcan grips and processes using 3D DIC revealed that surface strain could be detected along x, y and z axis (Figure 5.8). Findings show that in-plane displacement (Vy) effects in the y-axis (shear) is greater than the in-plane displacement (Vx) in x-axis (tension) (Table 5.3) in F3 formulation specimens. Notably, out-of-plane displacement (Vz) in the z direction (through thickness) is even less for the out-of-plane vector in the z-axis (Figure 5.9).

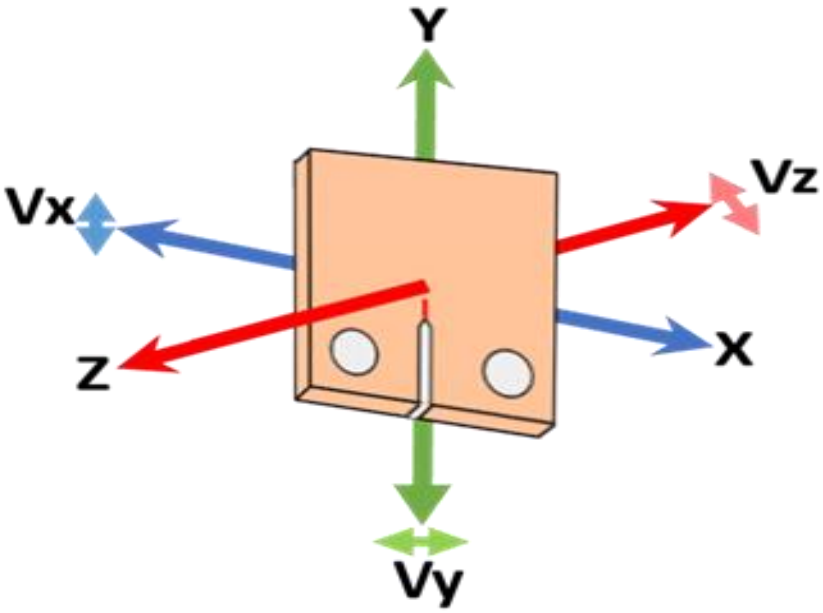

Figure 5.8 - 3D Digital Image Correlation Vector Field

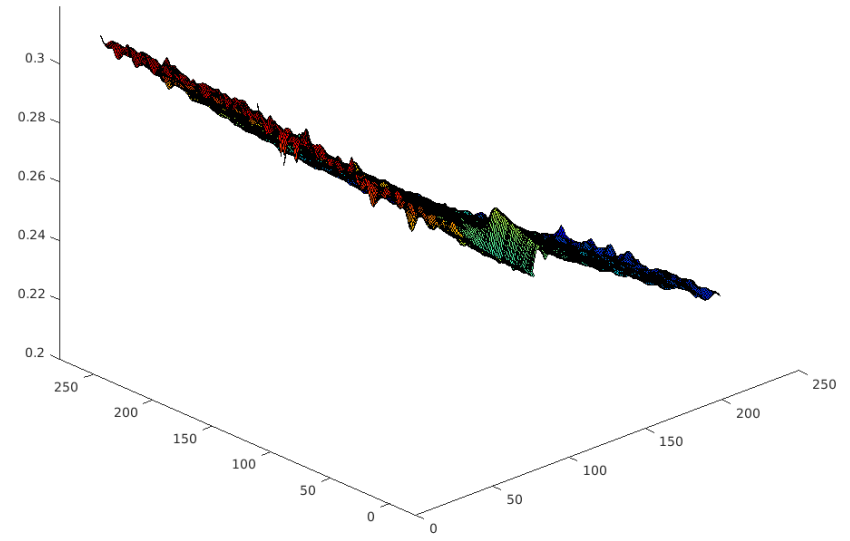

Vx

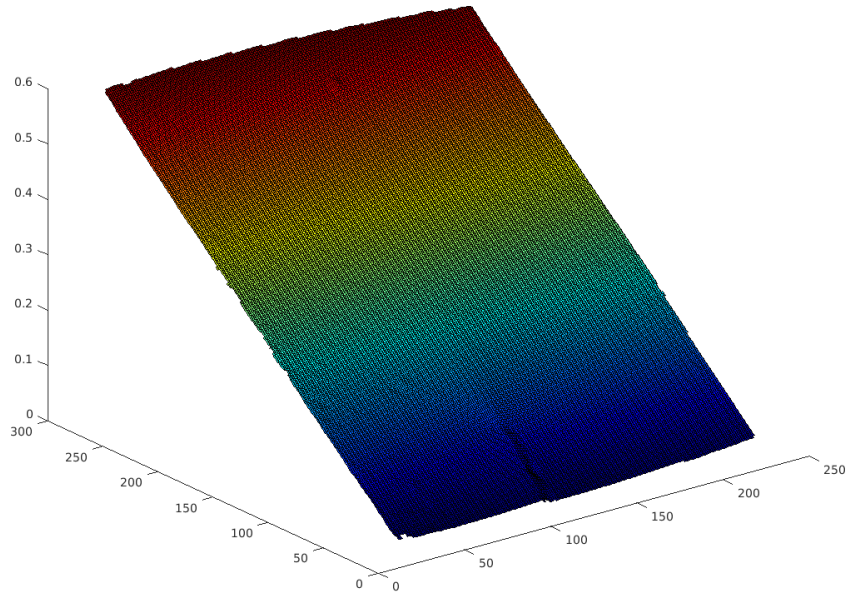

Vy

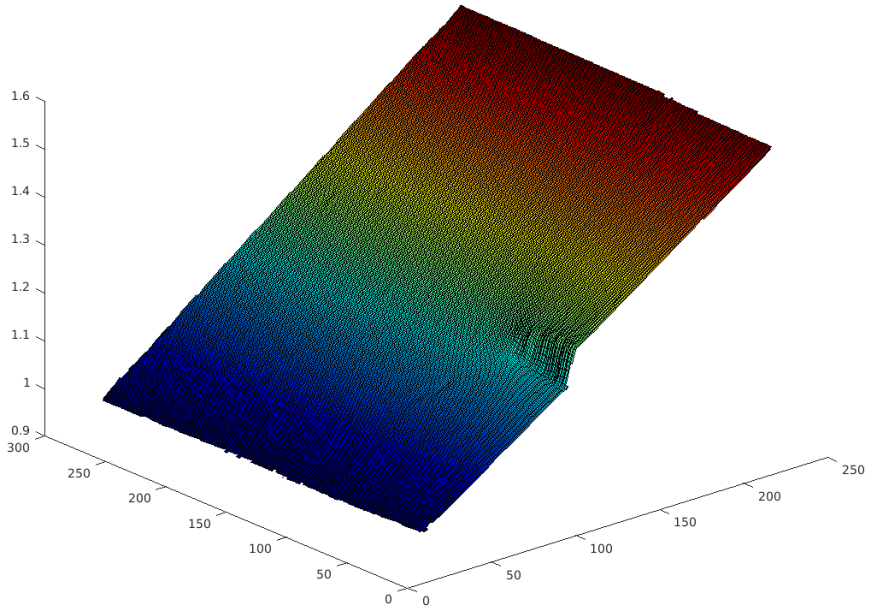

Vz

Figure 5.9 - Vx, Vy and Vz Matlab plots for F3-T1-90DEG Specimen

Specimen	(Vy) (micron)	(Vz) (micron)	(Vx) (micron)
F33D-T1	**7.3**	**8.5**	**81**
F33D-T2	**4.68**	**0.31**	**37**
F33D-T3	**17.5**	**0.35**	**75**
Average	**9.82667**	**3.05333**	**64.33333**

Table 5.3 - F3 formulation out-of-plane effect results, Vy (in the y-axis), Vx (in the x-axis) and Vz (in the x-axis).

The data indicates that there is little or no significant difference in the out of plane vectors for 3D DIC experiments for the family of resin specimens. Therefore, it was concluded that 2D DIC could be used for experimental investigations in future.

5.4 Mixed mode testing of unmodified epoxies loaded to failure

Quantification of fracture behaviour and characterisation of fracture parameters plays a role of paramount importance in defining the behaviour of a fracture in resin when to loaded to failure. Nature of a crack tip stress fields cannot be described with accuracy particularly where plasticity is significant [182]. Multiple parameters such as *K* (Stress Intensity Factor), T-stress, crack tip opening displacement (CTOD), crack tip opening angle (CTOA) and *J* (the energy contour integral), could be measured using novel experimental stress analysis techniques and these parameters are further explained in [7, 9, 183-185].

Numerous studies have been conducted to identify failure modes of the mode I (tension) and mode II (shear), in this chapter studies were focussed on the effect of loading specimens to failure in both modes (Mixed mode I & II). Whilst materials being studied in this chapter are all toughened polymers without particle modifications, it is noteworthy to observe that the fracture behaviour of these samples differ when loaded to failure in different grips at different loading angles.

Loading angles play a vital role in the crack tip displacement behaviour when samples are loaded to failure [186]. Previous studies conducted by researchers in University of Sheffield have shown that the Arcan/Banks Sills type specimens was the most suitable for testing bulk modified specimens [181]. The Arcan type specimens were tested in various loading angles in the Arcan grips initially modified and used by S. Jones [181], NK Arcan grip and the CT-MMM grip developed in this study. The specimens were loaded in different angles (0°, 45°, 90°) in different grip orientations as described in Chapter 4 in different grip configurations; the SJ Arcan, NK Arcan, and CT-MMM grips. Geometry of modified Arcan specimens were used to test specimens in both SJ Arcan and NK Arcan grips whereas specimen geometry of those tested in CTMMM were based on compact tension geometry.

Digital image correlation functions as an experimental tool to determine displacement fields around crack tips [94]. The displacement data was extracted by using Williams series stress solution to obtain SIF mode I (K_I), SIF mode II (K_{II}) and mixed mode I and mode II (K_{II}/K_I). The neat resin is used as a control in this study is chemically an untoughened resin that lacks particles and toughening polymers, vis-a-vis study samples that are chemically toughened and devoid of particles. The two toughened formulations supplied by Cytec Engineering Ltd were subjected to consistent testing procedures. Based on the simple rule of mixtures, it is implied that the toughened polymers and their interfaces would be similar. However, findings show differences in resistance to shear and stress intensity values in mixed mode I and model II failure.

5.4.1 SIF at Fracture of F1, F3 and F4 formulation samples; loaded with SJ Arcan and NK Arcan in three loading angles (0°, 45° and 90°) using 2D DIC.

SJ specimens were analysed using both SJ grips and NK grips using the methodology as described in section 5.3.1 to assess if the SJ specimen was overly constraining and whether the NK design could nullify pin loading constraints. A 2-mm pre-crack was generated in each specimen using the method described in Section 3.1.

Figure 5.10-5.12 shows the SIF at failure of formulation F1 (Neat) (Figure 5.10), F3 (Figure 5.11) and F4 (Figure 5.12) at increasing loading angles 0º is pure Mode I, 90º is pure Mode II and 45º is Mixed Mode I and Mode I. The blue diamond markers are K_I and the red squares, K_{II}. The open markers are the SJ Arcan specimens using SJ Arcan grips, the closed markers are SJ Arcan specimens using NK Arcan grips.

The F1 formulation (neat) (Figure 5.10) displays significant resistance to shear when loaded at 90° in SJ Arcan grips. In mode I (0°) K_I and K_{II} for SJ grips is significantly lower than NK Arcan grips. Although, in mode II (90°) K_I is significantly lower for the SJ grips than NK grips and K_{II} is much higher for the SJ grips than the NK grips. The SJ K_I linear regression intersects with K_{II} at slightly above 30 degrees, whereas the NK intersects above 40 degrees. The toughened resin F3 and F4 was tested with NK and the SIF K_I and K_{II} is different between the two grips. It is evident that SJ loading condition in mixed mode I and II is greatly influenced by the constrained pins. Resistance to shear between two grips for F3 (Figure 5.11) and F4 (Figure 5.12) samples were 0.2 MPa.√m.

It was hypothesised that the effect of over-constrained pin loading would affect the stress intensity factor values K_I and K_{II} for testing when testing with the SJ grips. Furthermore, the SJ grips were expected to contribute to an increase in shear when in mode I, decreased K_I and K_{II} values in Mode II. The NK grip design is an improvement on the SJ grips, as issues related

to loading in pin constraints were overcome by modifying the circular pin loading configuration to an elliptical hole as discussed in section 4.2.1. This modification resulted in constraint free loading. The SJ Arcan grip data were obtained from previous work conducted at the University of Sheffield [56, 181]. The average, Standard Deviation (SD), Standard Error of the Mean (SEM) and the Coefficient of Variance (CV) is calculated for both K_I and K_{II} with different test angles. This is performed for F1, F3 and F4 of NK Arcan samples. The analysis for NK Arcan for F1 sample is shown in Table 5.4. It can be seen that for K_I, the average is highest at 0°, whereas the CV is highest for 90°. In the case of K_{II}, both the average and the CV is the highest for 45°.

Test Angle	F1 K_I NK	AVERAGE	SD	SEM	CV K_I	F1 K_{II} NK	AVERAGE	SD	SEM	CV K_{II}
0	0.70	0.81	0.10	0.05	0.12	0.04	0.05	0.01	0.01	0.21
0	0.94					0.04				
0	0.82					0.06				
0	0.79					0.06				
45	0.38	0.42	0.10	0.06	0.24	0.72	0.59	0.22	0.13	0.37
45	0.53					0.34				
45	0.34					0.70				
90	0.19	0.13	0.08	0.04	0.67	0.94	1.02	0.21	0.10	0.21
90	0.15					0.89				
90	0.16					0.91				
90	0.00					1.33				

Table 5.4 - Analysis of NK ARCAN F1 sample for different angles

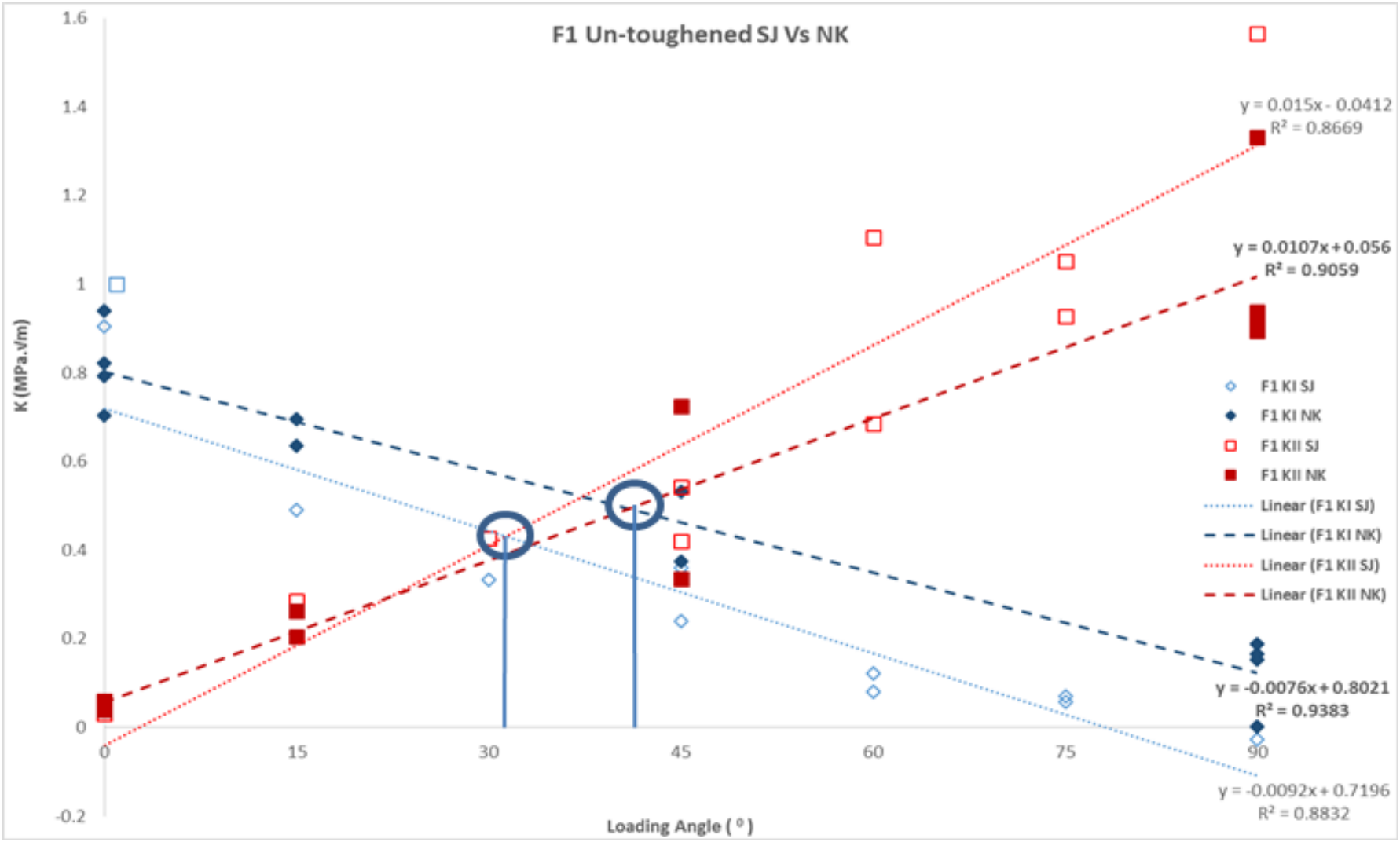

Figure 5.10 - SIF at Fracture K_I & K_{II} for F1 untoughened resin samples (n=4).

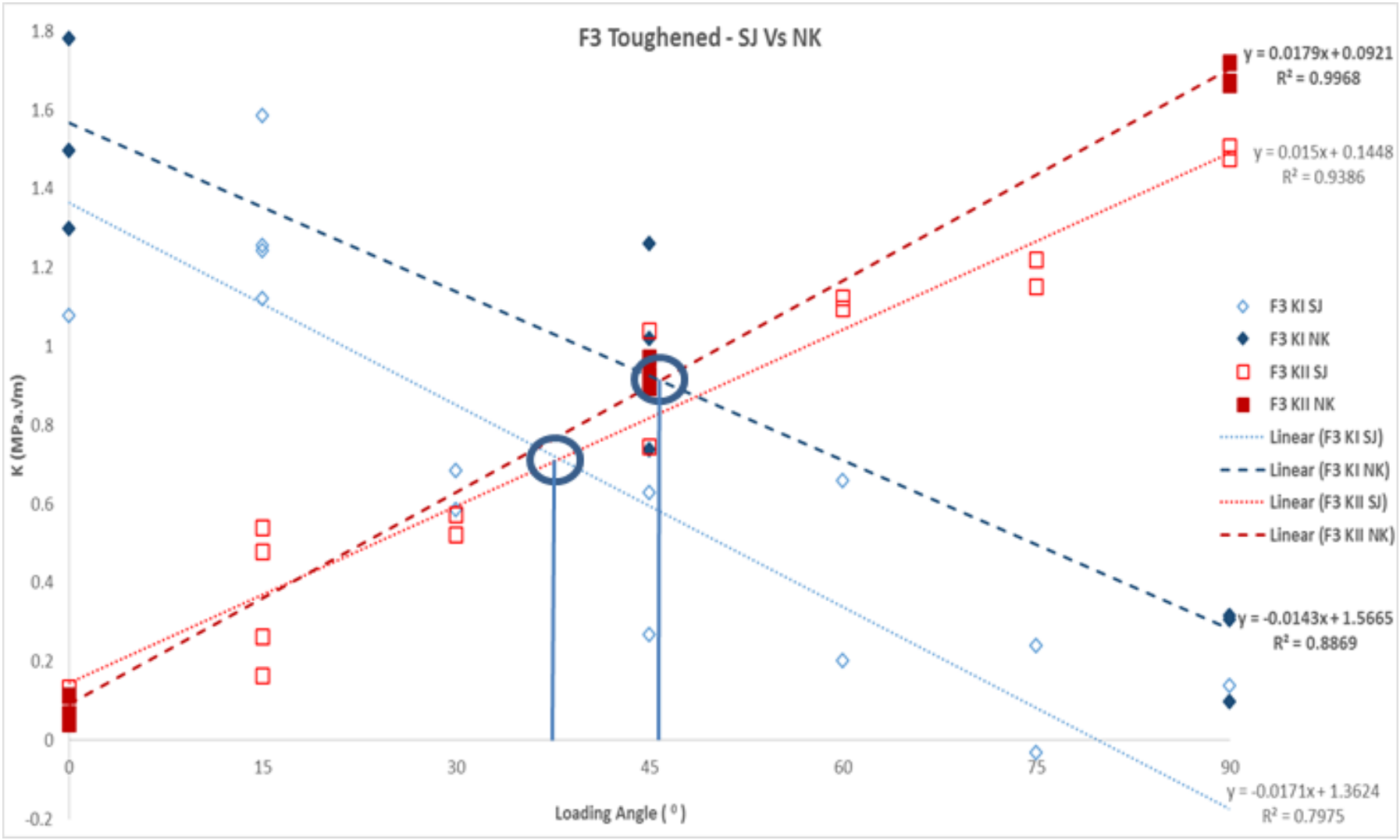

Figure 5.11 - SIF at Fracture K_I and K_{II} for F3 modified resin samples (n=4).

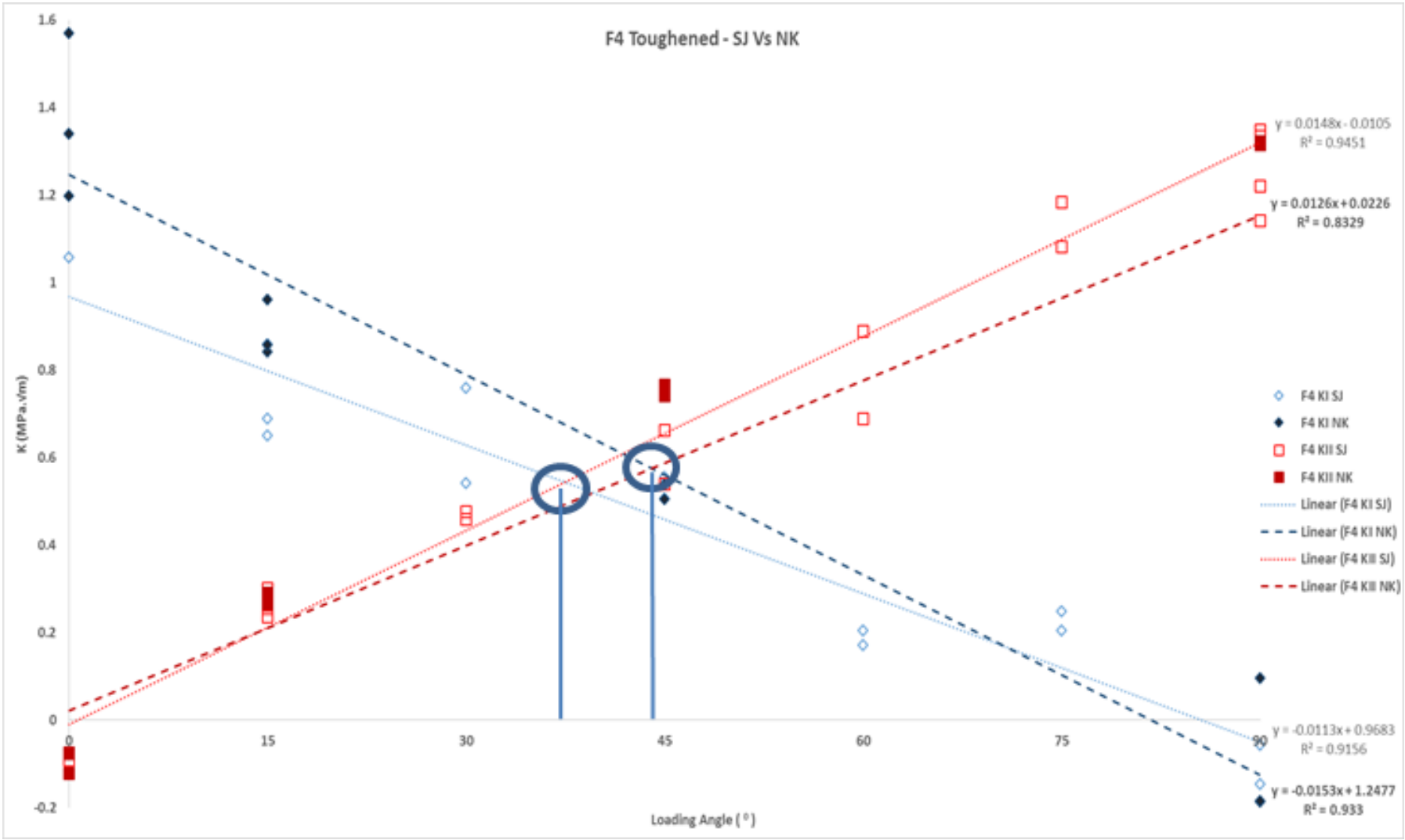

Figure 5.12 - SIF at Fracture K_I & K_{II} for F4 toughened resin samples (n=4).

5.4.2 SIF at Fracture of F3 and F4 formulation samples; loaded with SJ Arcan and SJ Arcan Repeat in three loading angles (0˚, 45˚ and 90˚) using 2D DIC.

SJ specimen were studied using SJ grips as described in section 5.3.1 in order to assess whether the differences in the experiment in section 5.5.1 were real or were influenced by scatter. New SJ Arcan specimens were manufactured and tested using SJ Arcan grips and compared to the results obtained previously [56, 181] with SJ specimen and grips.

Figure 5.13-5.14 shows the SIF at failure of formulation F1 (Neat), F3 and F4 at increasing loading angles 0º is pure Mode I and 90º is pure Mode II and 45º is Mixed Mode I and Mode I. The blue diamond markers are K_I and the red squares, K_{II}. The open markers are the SJ Arcan specimens using SJ Arcan grips, the closed circular blue and red markers are SJ Arcan repeat specimens with SJ Arcan grips for K_I and K_{II} respectively.

The SJ Arcan repeat was conducted with F3 and F4 particulate toughened material. (referred as Sheff-F3 and Sheff-F4 in previous work conducted by S Jones, University of Sheffield). The experimental repeats using SJ Arcan specimens displayed differences compared to the SJ Arcan repeat in the K_I and K_{II} values of the samples F3 (Figure 5.13) and F4 (Figure 5.14). The SJ Arcan repeat has a very close resemblance to the SJ Arcan data with very little scatter between the two sets of results shown in Figure 5.13 -5.14. Linear regression between the two grips SJ Arcan and SJ Arcan repeat were similar in all loading conditions. Resistance to shear displayed by specimens loaded in both grips SJ Arcan and SJ Arcan repeat were similar with negligible difference of 0.1 MPa.√m.

Preliminary studies on SJ grips conducted at University of Sheffield using toughened resin F3 and F4 suggested that the SJ test repeats conducted using the samples from same material composition (F3 & F4) would yield similar K_I and K_{II} as values observed in the previous SJ data set.

The SJ-Arcan (SJ) with modified Arcan specimen (SJ grips) were tested with F3 and F4 to evaluate SJ grip configuration. Although it was expected that the K_I and K_{II} values of SJ and SJ repeat were similar, the SJ Arcan repeat showed very little scatter present between the two sets of results suggesting that the difference between the two sets of result could be due to the differences in batches of the material manufactured.

Findings obtained by testing specimens in two different grip configurations suggest that the pin loading constraints inhibit pure mode II failure during mixed mode I & II loading. Further, it suggests that changes observed in the F-Formulation are a direct result of pin loading constraints that influence dominance of mode I during mixed mode I and II.

Although a counter measure for mode I dominance was proposed by H. A. Richard's grips design originally in 1983 [172], it was not explored further. Banks-Sills also observed issues arising due to pin loading constraints [97, 187-189]. However, they could not identify causes for Mode I dominance and hence were unable to achieve pure shear. The issue of pin loading constraints has been taken into consideration when designing modified NK grips which led to obtaining "pure" mode II and mixed mode I and II failure.

Although the NK grips produced "near pure" mode II and mixed mode I and II, it was still complex to manufacture the modified Arcan specimens and a time-consuming experiment to conduct. Hence, it was proposed that there could be an alternate method for conducting mode I, mode II and mixed mode I and II experiments using the CT-MMM grip as an alternative to achieve a high through-put in-plane fracture testing of mode I, mixed mode I & II and pure mode II.

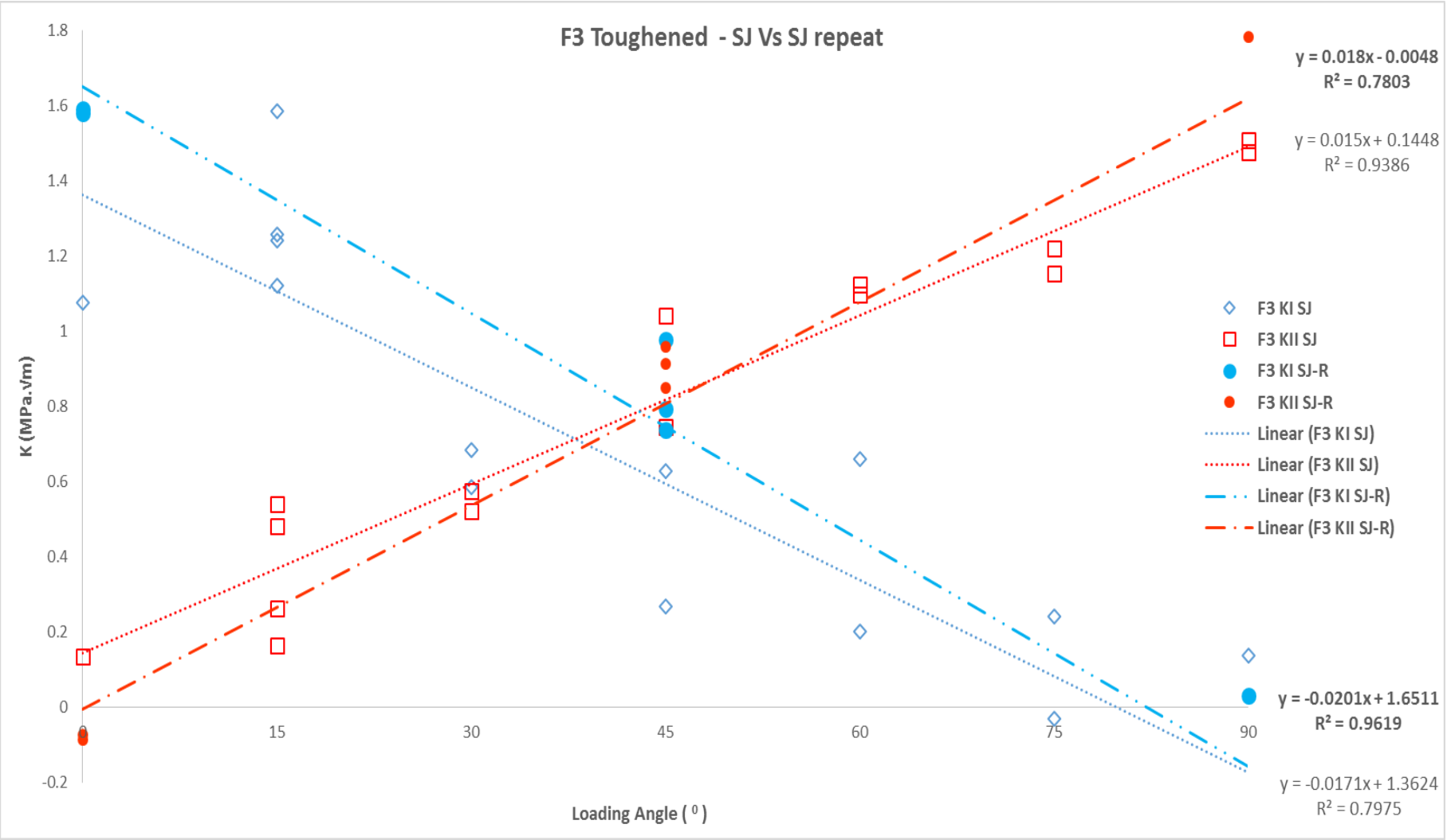

Figure 5.13 - SIF at Fracture K_I and K_{II} for F3 toughened resin samples (n=4) for SJ Arcan and SJ Arcan Repeat.

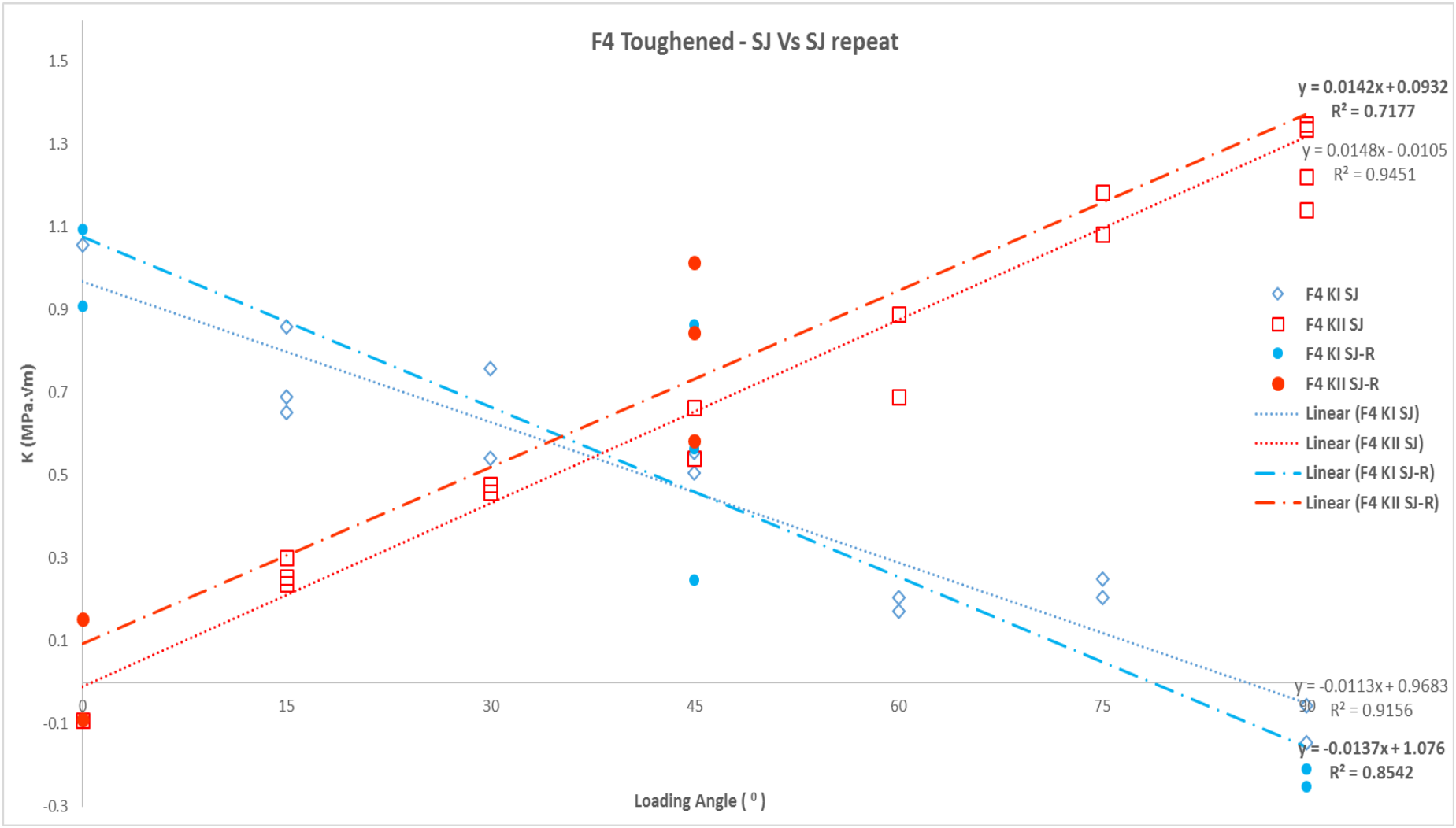

Figure 5.14 - SIF at Fracture K_I and K_{II} for F4 toughened resin samples (n=4) for SJ Arcan and SJ Arcan Repeat.

5.4.3 SIF at Fracture of F1 and F3 formulation samples; loaded with SJ Arcan and CT-MMM in three loading angles (0˚, 45˚ and 90˚) using 2D DIC.

F1 and F3 formulation samples were loaded with SJ Arcan and CT-MMM grips as described in section 5.3.1 to assess if the K_I and K_{II} values influenced by pin loading constraints.

Figure 5.15-5.16 shows the SIF at failure of formulation F1 (Neat), F3 and F4 at increasing loading angles 0º is pure Mode I and 90º is pure Mode II and 45º is Mixed Mode I and Mode I. The blue diamond markers are K_I and the red squares, K_{II}. The open markers are the SJ Arcan specimens using SJ Arcan grips, the closed circular blue and red markers are CT-MMM grips with CT-MMM specimen for K_I and K_{II} respectively.

The F1 formulation (neat) (Figure 5.15) displays significant resistance to shear when loaded at 90º in SJ Arcan. In mode I (0°) K_I and K_{II} for SJ grips is significantly lower than CT-MMM grips. Although, in mode II (90°) K_I is significantly lower for the SJ Arcan grips than CT-MMM grips and K_{II} is much higher for the SJ Arcan grips than the CT-MMM grips. The SJ K_I linear regression intersects with K_{II} at 30 degrees, whereas the CT-MMM intersects slightly above 45 degrees. The toughened resin F3 (Figure 5.16) was tested with CT-MMM and the SIF K_I and K_{II} is different between the two grips. It is evident that SJ Arcan loading condition in mixed mode I and II is greatly influenced by the constrained pins. Resistance to shear between two grips for F3 samples were 0.4 MPa.√m.

The average, Standard Deviation (SD), Standard Error of the Mean (SEM) and the Coefficient of Variance (CV) is calculated for both K_I and K_{II} with different test angles. This is performed for F1, F3 and F4 of CT MMM samples.

Test Angle	F1 K_I CT-MMM	AVERAGE	SD	SEM	CV K_I	F1 K_{II} CT-MMM	AVERAGE	SD	SEM	CV K_{II}
0	1.00	0.95	0.21	0.09	0.22	0.03	0.08	0.03	0.01	0.44
0	1.10					0.08				
0	1.06					0.06				
0	1.09					0.09				
0	0.54					0.07				
0	0.90					0.13				
45	0.76	0.74	0.06	0.03	0.08	0.36	0.31	0.03	0.02	0.11
45	0.65					0.30				
45	0.79					0.31				
45	0.75					0.28				
90	0.17	0.25	0.07	0.03	0.26	1.29	1.03	0.21	0.10	0.20
90	0.33					1.11				
90	0.28					0.87				
90	0.22					0.86				

Table 5.5 - Analysis of CTMMM F1 sample for different angles

In the proposed CTMMM F1 sample, the average value is the highest for the test angle of 0° for K_I, whereas the highest CV value is for 90°. Both the SD and SEM peaks at 0°. In the case of K_{II}, the average value, SD and the SEM is the highest for 90°, whereas the CV is the highest got 0°.

Test Angle	F3 K_I CT-MMM	AVERAGE	SD	SEM	CV K_I	F3 K_{II} CT-MMM	AVERAGE	SD	SEM	CV K_{II}
0	1.35	1.31	0.05	0.03	0.04	0.12	0.04	0.07	0.04	1.51
0	1.25					0.01				
0	1.32					0.01				
45	0.80	0.95	0.16	0.08	0.17	0.63	0.57	0.06	0.03	0.11
45	0.91					0.60				
45	0.91					0.57				
45	1.18					0.48				
90	0.04	0.14	0.09	0.04	0.64	1.26	1.30	0.05	0.03	0.04
90	0.26					1.24				
90	0.13					1.34				
90	0.13					1.34				

Table 5.6 - Analysis of CTMMM F3 sample for different angles

In the proposed CTMMM F3 sample, the average K_I value is the highest for the test angle of 0° for K_I, whereas the highest CV value is for 90°. Both the SD and SEM peaks at 45°. In the case of K_{II}, the average value is the highest for 90°, whereas the CV is the highest got 0°. The values of SD and SEM are comparatively low with the highest being 0°.

Test Angle	F4 K_I CT-MMM	AVERAGE	SD	SEM	CV K_I	F4 K_{II} CT-MMM	AVERAGE	SD	SEM	CV K_{II}
0	1.34	1.57	0.22	0.10	0.14	0.06	0.08	0.05	0.02	0.55
0	1.87					0.03				
0	1.53					0.12				
0	1.71					0.14				
0	1.41					0.07				
45	1.27	1.04	0.16	0.08	0.15	0.52	0.45	0.06	0.03	0.14
45	0.93					0.37				
45	0.97					0.47				
45	0.99					0.44				
90	0.32	0.24	0.15	0.09	0.63	1.36	1.24	0.21	0.12	0.17
90	0.07					1.36				
90	0.33					1.00				

Table 5.7 - Analysis of CTMMM F4 sample for different angles

In the proposed CTMMM F4 sample, the average value is the highest for the test angle of 0° for K_I, whereas the highest CV value is for 90°. Both the SD and SEM peaks at 0°. In the case of K_{II}, the average value, SD and the SEM is the highest for 90°, whereas the CV is the highest for 0°. While this analysis was performed for all the available samples, the FI, F3 and F4 samples for the CTMMM are shown in Table 5.5, 5.6 and 5.7 respectively. Findings obtained from DIC revealed that in mode I (0°) K_I and K_{II} for SJ grips is significantly lower than NK grips. Although, in mode II (90°) K_I is significantly lower for the SJ grips than NK grips and K_{II} is much higher for the SJ grips than the NK grips. The SJ K_I linear regression intersects with K_{II} at slightly above 30 degrees, whereas the NK intersects above 40 degrees. The toughened resin F3 and F4 was tested with NK and the SIF K_I and K_{II} is different between the two grips. Thus, it was evident that SJ loading condition in mixed mode I and II was greatly influenced by the constrained pins.

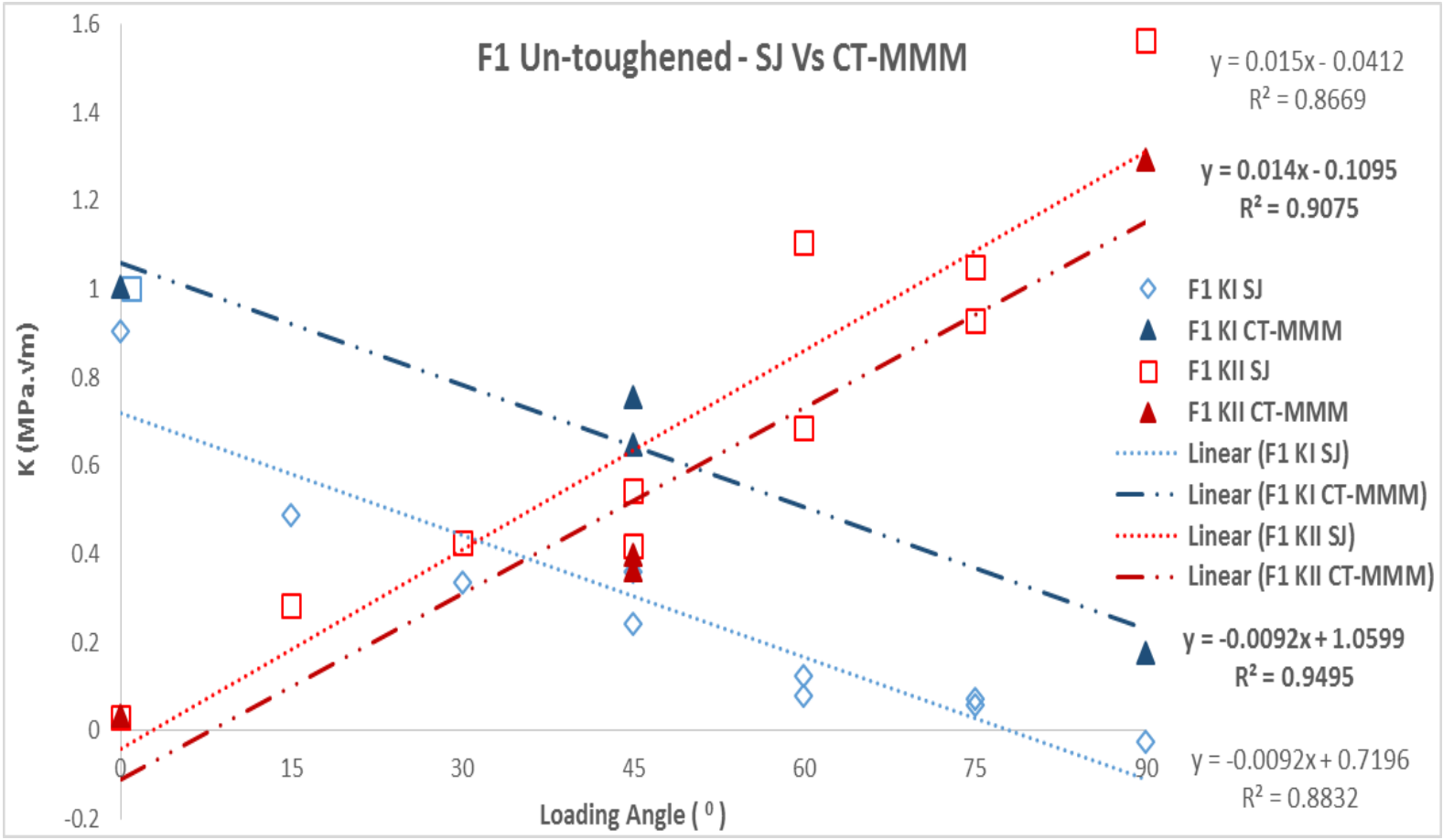

Figure 5.15 - SIF at Fracture SIF K_I and K_{II} for F1 untoughened resin samples (n=4) for CTMMM and SJ Arcan.

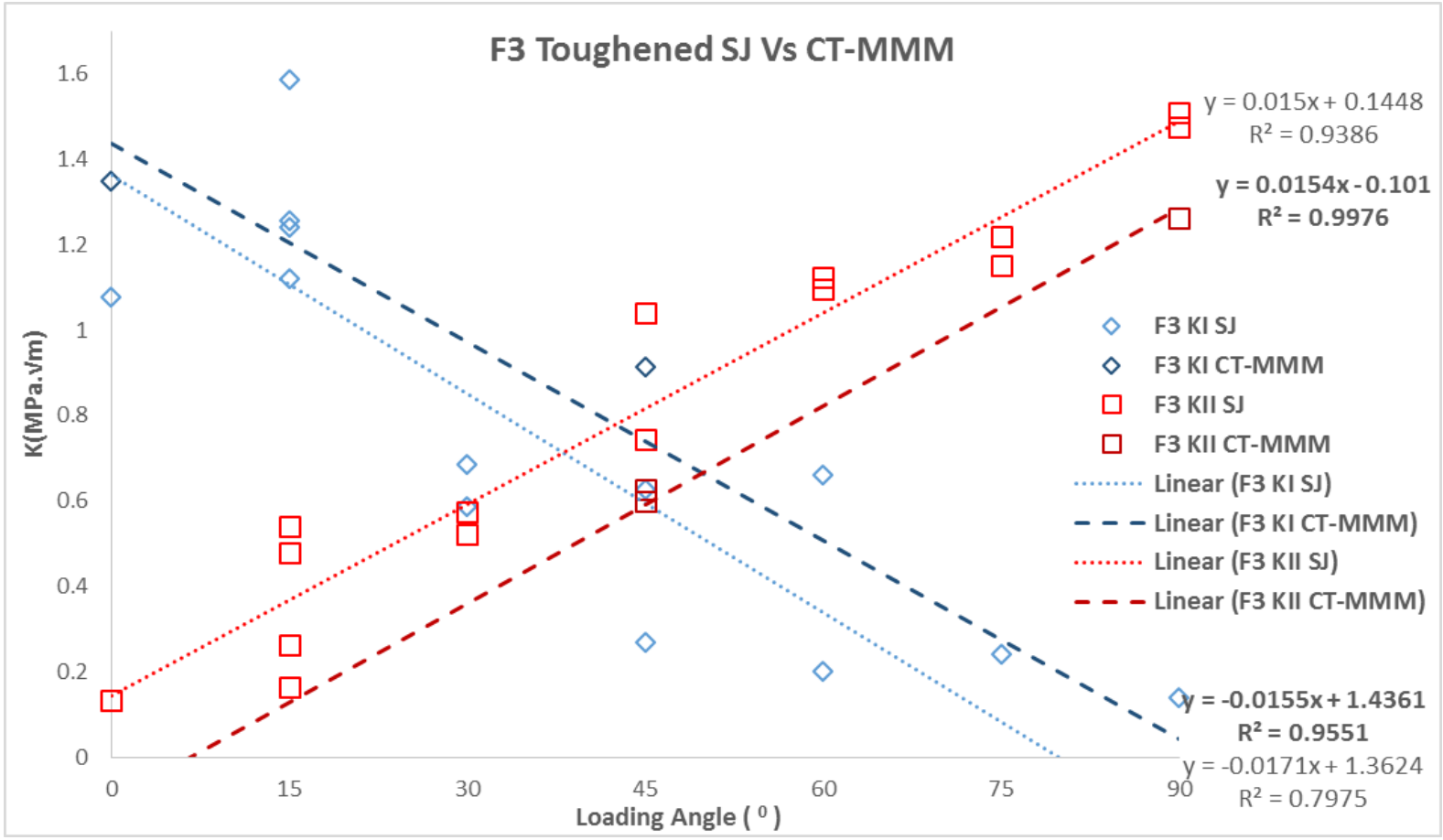

Figure 5.16 - SIF at Fracture K_I and K_{II} for F3 toughened resin samples (n=4) for CTMMM and SJ Arcan.

5.4.4 SIF at Fracture of F1 and F3 formulation samples; loaded with NK Arcan and CT-MMM in three loading angles (0˚, 45˚ and 90˚) using 2D DIC.

SJ specimen were studied using NK grips and CT-MMM specimen with CT-MMM grips as described in section 5.3.1 in order to assess whether if both loading configuration in the experiment were similar. We hypothesize that the NK grips and CTMMM are the same loading in mode I, mode II and mixed mode I&II.

Figure 5.17-5.18 shows the SIF at failure of formulation F1 (Neat), F3 at increasing loading angles 0º is pure Mode I and 90º is pure Mode II and 45º is Mixed Mode I and Mode I. The closed blue diamond and red square markers are the SJ Arcan specimens using NK Arcan grips for K_I and K_{II}. The closed red and blue triangle markers are the, CT-MMM with CT-MMM specimen for K_I and K_{II} respectively.

The F1 and F3 formulation samples were loaded with NK Arcan and CT-MMM grips to assess if the K_I and K_{II} values are influenced by pin loading constraints. The F1 formulation (neat) (Figure 5.17) displays marginal resistance to shear when loaded at 90º in NK Arcan. In mode I (0°) K_I and K_{II} for NK Arcan grips is marginally lower than CT-MMM grips. Although, in mode II (90°) K_I is marginally lower for the NK Arcan grips than CT-MMM grips and K_{II} is marginally small for the SJ Arcan grips than the CT-MMM grips. The NK Arcan K_I linear regression intersects with K_{II} at marginally less to 45 degrees, whereas the CTMMM intersects slightly above 45 degrees. The toughened resin F3 (Figure 5.18) was tested with CT-MMM and the SIF K_I and K_{II} is similar between the two grips. It is evident that NK Arcan loading condition in mixed mode I and II is under similar loading constraints. Resistance to shear between two grips for F3 samples were marginally small at 0.1 MPa.√m.

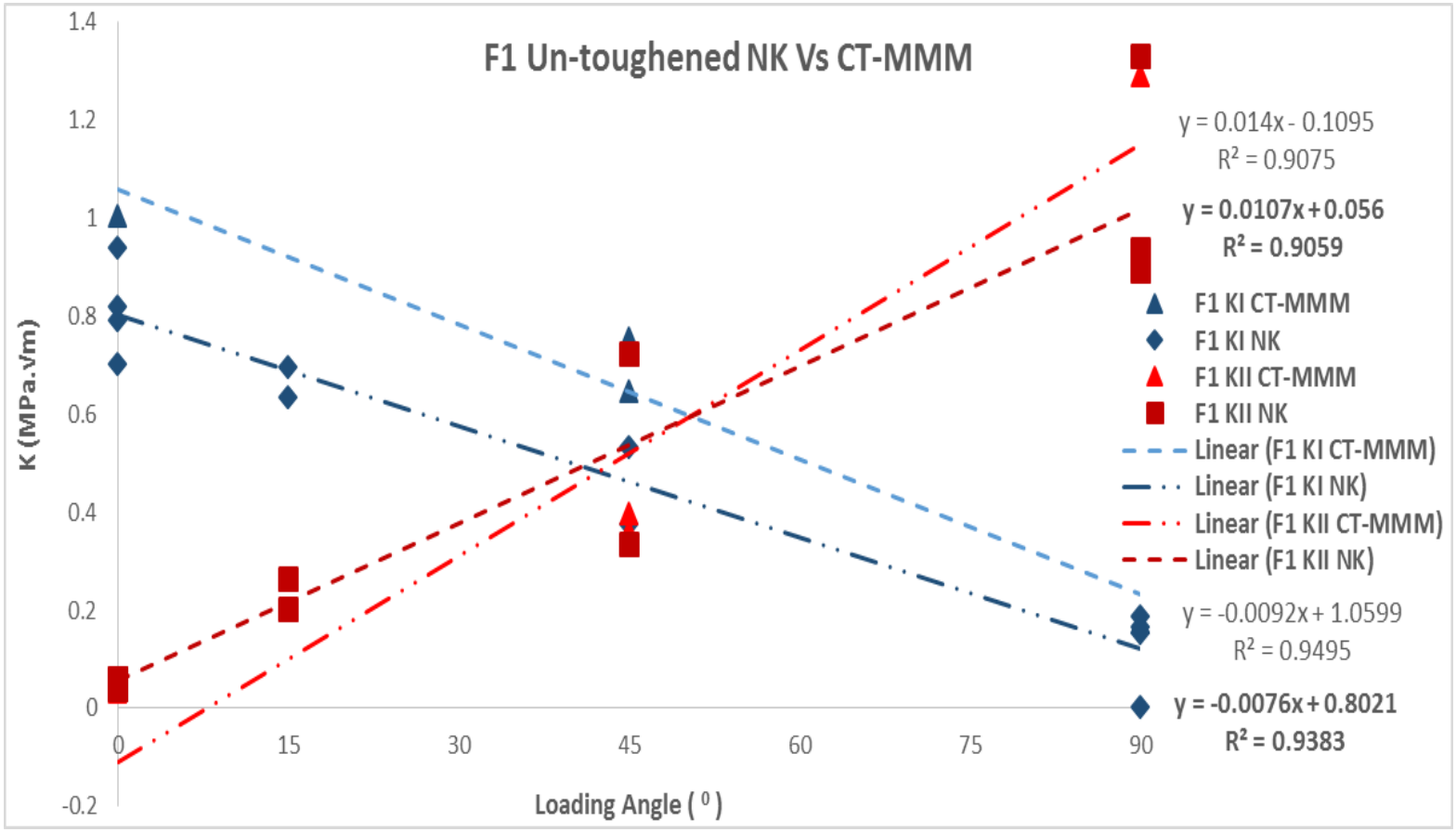

Figure 5.17 - SIF at Fracture K_I and K_{II} for F1 untoughened resin samples (n=4) for CTMMM and NK Arcan

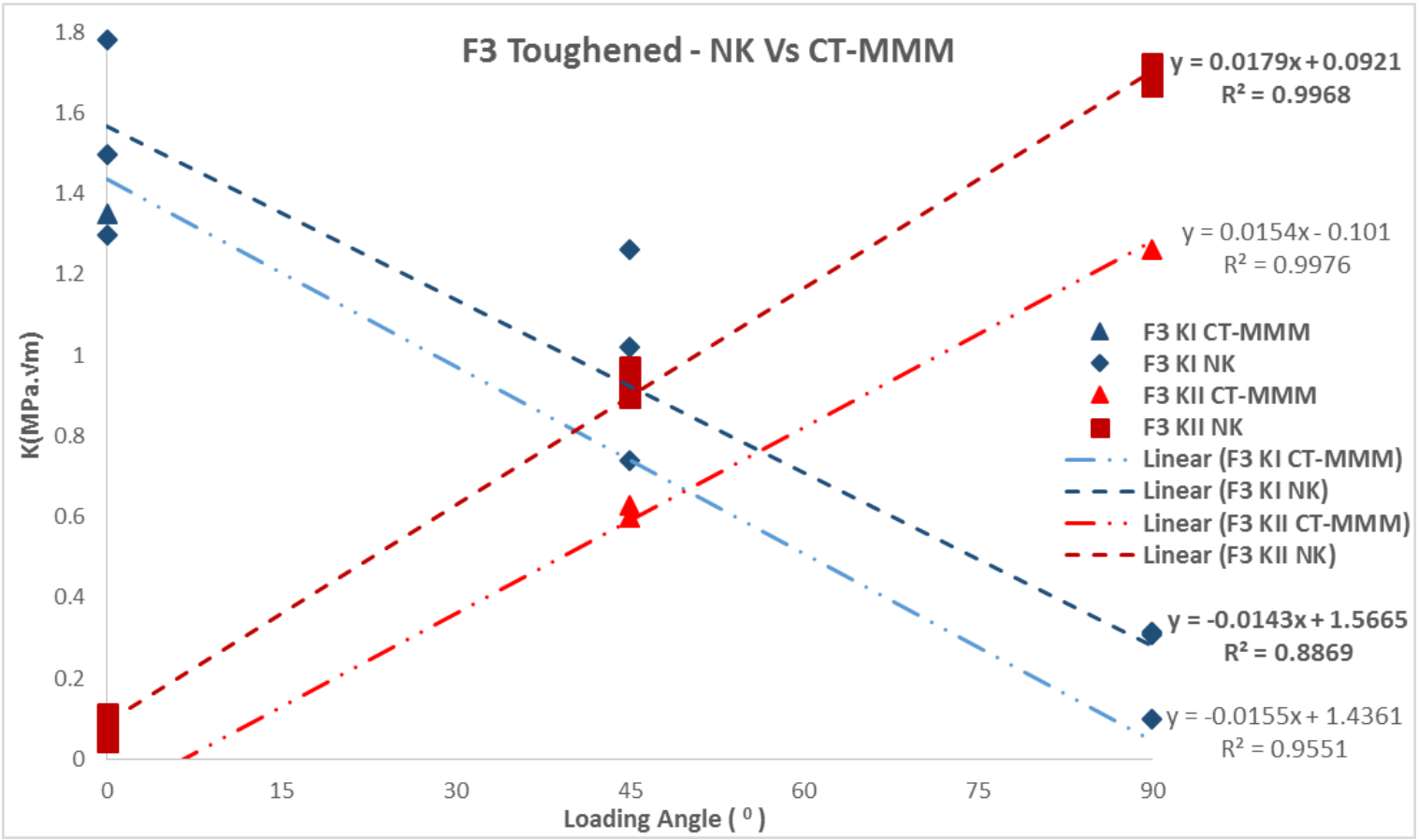

Figure 5.18 - SIF at Fracture K_I and K_{II} for F3 toughened resin samples (n=4) for CTMMM and NK Arcan.

CT-MMM grips were developed to facilitate material testing in mode I, mode II, mixed mode I&II. The design of the grip benefits from no pin loading constraints, simple specimen geometry to manufacture, preparation and loading of test specimens with ease. It is hypothesised that the CT-MMM would yield similar K_I and K_{II} values to the NK Arcan since the NK Arcan is not influenced by pin loading constraints. Therefore, results obtained by loading of F-formulation samples in CT-MMM grips were compared with results from SJ and NK Arcan grips. It was expected that the stress intensity factors K_I and K_{II} obtained in the CT-MMM grips would be markedly different to SJ Arcan grip results and similar to NK Arcan grip results. In lines with the hypothesis, specimens tested in both CT-MMM and NK Arcan grips displayed similar fracture toughness values (K_I and K_{II}) in mode I, mode II and mixed mode I and II failure in all loading angles.

The pin loading constraint of SJ Arcan was more apparent when SIF values are compared with the CT-MMM. In both NK and CT-MMM, the SJ (SJ-Arcan) grips appears to be influenced by tension albeit CT-MMM appeared to be greatly influenced by shear under mixed mode I & II.

5.4.5 Statistical Analysis – Student's T-test Results

The fracture toughness parameters obtained show subtle variations amidst data sets. A statistical analysis was conducted to compare the significance of different populations of data sets using Student's t-test [190] (Table 5.8) on the assumption of a difference between sample means. Intraclass correlation coefficient (ICCC) was assessed using SPSS software [191]. Findings indicate that the SIF values obtained by using SJ Arcan grip significantly differs from NK Arcan grip.

In a Student's t-test, the first ICCC analysis value indicate the reliability and the second p-value indicate the significance of the ICCC value suggesting that the CT-MMM grip result is the same as the NK Arcan. This support the confidence in CT-MMM experimental investigation of fracture toughness of toughened polymers in mode I, mode II and mixed mode I&II testing. Table 5.9 shows the Intra K_I values of F3 and F4 testing of SJ-grips were 0.90 (p-value = 0.03) and 0.99 (p-value=0.00) respectively whereas intra K_{II} values were observed as 0.99 (p-value = 0.00) and 0.98 (p-value=0.01) for F3 and F4 samples. When the specimen samples were tested in NK Arcan and CTMMM grips, Intra K_I values were noted as 0.99 (p-value = 0.00) and 0.93 (p-value=0.01) respectively. Notably intra K_{II} values were observed as 0.95 (p-value = 0.01) and 0.96 (p-value=0.05) for F3 and F4 samples tested in NK Arcan and CTMMM grips. Findings show that the intra class correlation values for K_I and K_{II} display statistically significant differences between specimens loaded in the grips subjected to testing; Test 1 (section 5.4.2) is similar, Test 2 (section 5.4.1) is different, and Test 3 (section 5.4.4) is similar.

Test 1		
F3 SJ Arcan	F3 SJ Repeat	0.17
F4 SJ Arcan	F4 SJ Repeat	0.29
Test 2		
F3 SJ Arcan	F3 NK Arcan	0.04
F4 SJ Arcan	F4 NK Arcan	0.03
Test 3		
F3 NK Arcan	F3 CTMMM	0.15
F4 NK Arcan	F4 CTMMM	0.16

Test 1
SJ Arcan Vs SJ Arcan Repeat – expected to be similar.

Test 2
SJ Arcan Vs NK Arcan – expected to be different.

Test 3
NK Arcan Vs CTMMM – expected to be similar.

P-Value significance criteria
below T=< 0.05 is statistically different populations
above T= > 0.05 it is not statistically different
above T= > 0.95 is statistically similar in populations

Table 5.8 – Student t-test analysis of relationship between different loading grips

The Intra class correlation measures the reliability of measurements for data that has been collected as groups, the K_I and K_{II} values for different grip configurations as shown in table 5.9.

Data obtained from IBM SPSS v22 Statistics				
F3 Average Measures Intra-class Correlation Coefficient				
Test	Intra-KI	P-value	Intra-KII	P-value
SJ Arcan Vs SJ Arcan Repeat	0.90	0.03	0.99	0.00
NK Arcan Vs CTMMM	0.99	0.00	0.95	0.01

Data obtained from IBM SPSS v22 Statistics				
F4 Average Measures Intra-class Correlation Coefficient				
Test	Intra-KI	P-value	Intra-KII	P-value
SJ Arcan Vs SJ Arcan Repeat	0.99	0.00	0.98	0.01
NK Arcan Vs CTMMM	0.93	0.01	0.96	0.05

Intra-class coefficient value above 0.7 is highly significant and repeatable
The P-Value for the Intra-class Correlation Coefficient <0.05 = High Significance
High Significance means similar population

Table 5.9 - Intra-class correlation coefficient analysis of relationship between different grips

The intra K_I values and intra K_{II} values and the corresponding P-values are given in the table 5.9 for both F3 and F4 Inter class correlation coefficient. The value of the Intra K_I and Intra K_{II} is tabulated for F3 and F4 are given in figure 5.19 and 5.20 respectively. For F3, it can be seen that the correlation coefficient for intra K_{II} is higher than intra K_I in the case of SJ Arcan Vs SJ

Arcan Repeat. On the contrary, in the case of NK Arcan Vs CTMMM, the correlation coefficient for intra K_{II} is less than that of intra K_I. For F4 average measures, it is the opposite. it can be seen that the correlation coefficient for intra K_{II} is lower than intra K_I in the case of SJ Arcan Vs SJ Arcan Repeat. On the contrary, in the case of NK Arcan Vs CTMMM, the correlation coefficient for intra K_{II} is higher than that of intra K_I. These results are discussed in the next section.

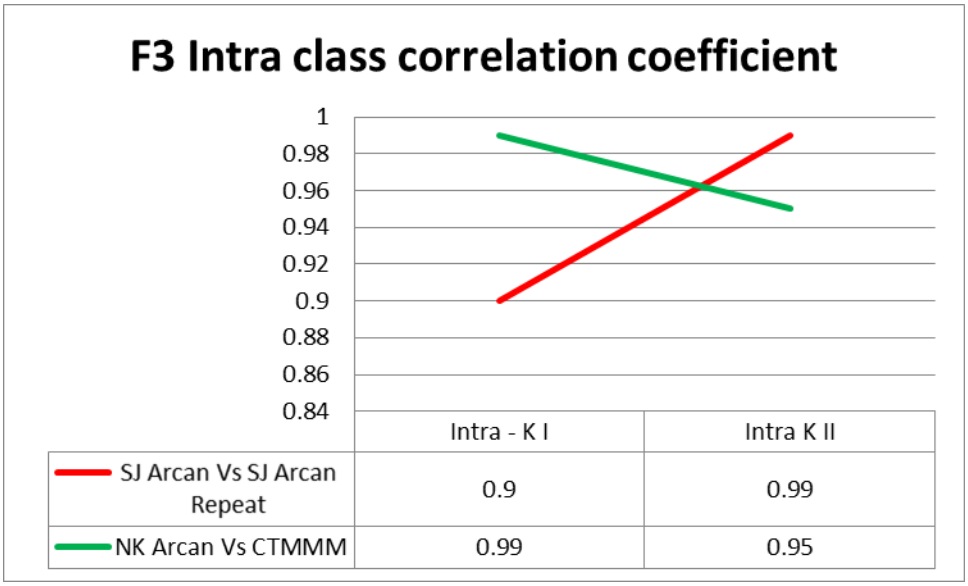

Figure 5.19 - F3 Inter-class correlation coefficient

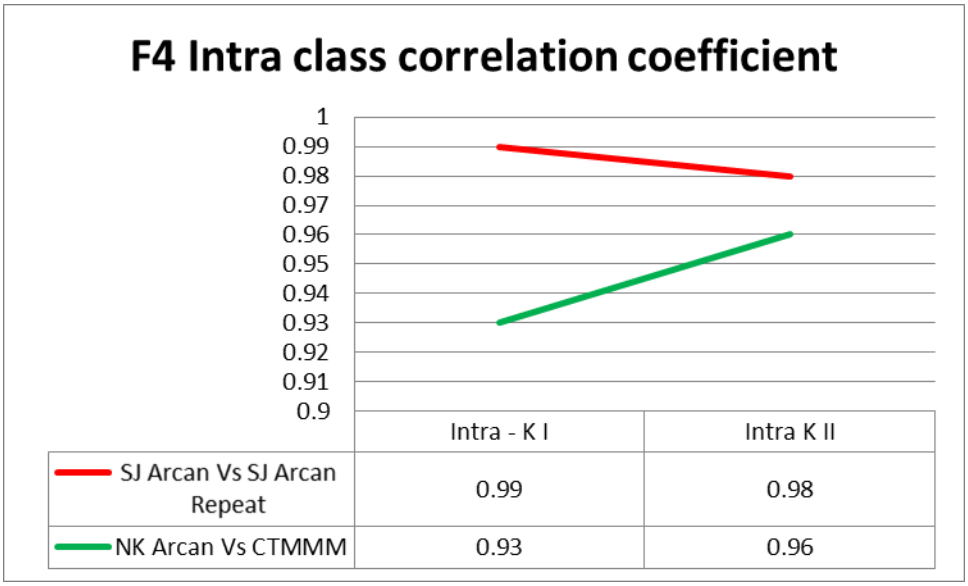

Figure 5.20 - F4 Inter-class correlation coefficient

5.5 Discussion

Researchers have been working on resin modifying mechanisms such as infusion of particles in interlaminar layers of both untoughened and toughened resins as is explained in section 2.10. Toughened polymers with such modifications find a wide range of applications in the composite industry and find applications in enhancing composite performance. These toughened polymers are subjected to extensive testing to ensure that that fracture toughness is not compromised in large production.

This chapter aims to study the influence of mixed mode testing in modifying resin properties such as resistance to shear and tension, in different loading configurations using digital image correlation techniques.

The fracture toughness parameters were subjected to statistical analysis to determine significance of variations observed in the findings (Table 5.8 - 5.9). Analysis was performed to compare the significance of different populations using Student's t-test to test hypothesis on the assumption of a difference between sample means based on defined p-value significance criteria. Intraclass correlation coefficient was assessed using SPSS software.

Based on pre-defined set of p-value significance criteria used extensively (Table 5.8), SJ Arcan significantly differs from NK Arcan and this verifies the difference between the two grip arrangements discussed in section 5.4.1 where the pin loading constraints contribute to the variations in the results. However, since it was hypothesized that the two groups (SJ and NK) would be similar in population we concluded that Student’s t-Test is not an accurate measure of assessing probability of variations between SJ Arcan vs S SJ Arcan repeat and NK Vs CT-MMM.

Hence, the inter-class correlation coefficient (ICCC) reliability measurement was used in future experimentation to determine the significance and repeatability of data sets. The Intra Class Correlation Coefficient (ICCC) is a measure of the reliability of measurements or ratings.

The ICCC reliability and significance functions in two parts; one the ICCC value for the compared set of data, must be greater than 0.7 and the second p-value for the ICCC should be less than 0.05. The first ICCC analysis value indicated reliability of data and the second p-value indicated significance of the ICCC value (Table 5.9). The two statistical analysis (Student's t-Test and ICC) suggest that the SJ Arcan and NK Arcan are different and NK Arcan and CTMMM are similar. This means that CT MMM can be used to evaluate SIF of the material.

5.6 Conclusion

This chapter provides an understanding of the influence of pin loading constraints on stress intensity when toughened polymers were loaded to failure in tension (K_I) and shear (K_{II}) in different loading angles. Results section 5.4.1 indicate that pin loading constraints influence resistance to shear in mode I failure [189]. Contrary to previous work, findings reveal that testing of toughened unmodified specimens in 'pure' mode I, 'pure' mode II and 'pure' mixed mode I&II could be achieved by loading in 0º, 90º and 45º angles respectively. Findings imply that when unmodified toughened polymers are loaded at 45º angle in the CTMMM grip that is devoid of pin loading constraints, facture toughness values for both tension (K_I) and shear (K_{II}) could be achieved for mixed mode I&II. The CTMMM grips facilitate minimising human efforts to test samples in various loading angles, thus reducing overall experimental time for industrial applications. Therefore, this design will be used in the final set of results on a range of toughened modified (particle) resins in chapter 6 to evaluate SIF of the material.

CHAPTER 6

Mixed mode testing of toughened modified resin (S-Formulation)

6.1 Introduction

Epoxy polymers belong to a group of thermosetting polymers and exhibit high performance as a part of fibre reinforced composite materials and as binding agents. They serve as excellent materials for engineering due to inherent properties such as high modulus, strength and stable thermodynamics. However, they are inherently less tough and therefore their cross-linked structure influences resistance to shear. Hence, they are brittle in structure and display poor resistance to crack initiation and propagation [192]. Toughness of brittle epoxy polymers could be improved by incorporation of dispersed particles [24, 193-197] or thermoelastic polymers [198-201]. Although it is difficult to characterise or control particle size, properties of the epoxy polymer could be altered by incorporation of these particles. However, particle type and number can influence the absorption of energy or redirection of energy in a resin system. Studies by Nakamura et al. [200, 201] and Cho et al. [198] focus research on the effect of particle size and its influence in fracture toughness. The combined effect of particle type, number and size could be critical in determining the material performance.

Very few studies have been focussed on exploring toughening mechanisms that control the behaviour of epoxy materials modified by particle incorporation. However, the relationship between molecular characteristics and mechanical properties of polymers have been a subject of discussion between academics and industrial researchers. Studies have been focussed either on the molecular level or on a microscale level to determine guidelines for construction of tailored and toughened materials. Their objective was to address if the polymers intrinsic deformation behaviour is modified by a known toughening system.

There have been a limited number of studies on the influence of particle formulations on fracture toughness under mode I, mode II and mixed mode loading. The development of the CTMMM specimen and grips described in Chapter 4 and the efficient specimen preparation methodology (Chapter 3) facilitates the efficient testing of many specimens of different

formulations. Therefore, investigation of the fracture behaviour of toughened and modified epoxies was carried out with aim of discriminating potential methods of failure for different formulations. Efforts in this chapter were made to study the influence of particle toughening on material fracture toughness stress intensity values when loaded in tension (mode I), shear (mode II) and c) combination of tension and shear (mixed mode I & II) using the compact tension mixed mode modified (CTMMM) specimen and grips with data capture using 2D DIC.

6.2 Methods

Samples from toughened particle modified epoxies (S-Formulation) Samples (S1, S2, S3, S4, S5, S6, S7, S8, S10, S11, S12, S13 & S14) were manufactured with 14% weight loading (wl) with different particles. Particle concentration in the S4 family of epoxy were further modified by 5% weight loading and 10% weight loading and named S15 and S16 respectively. All particle modifications in specimens were unknown to the author and Youngs Modulus (E) and Poisson's ratio (v) for all S formulation (Table 6.1) were measured and provided by Cytec Engineering Ltd. Theis experiments found that the E and v did not change with different particles.

Formulation	E	v
S	3.4	0.35

Table 6.1 - S-formulation data table provided by sponsoring organisation

The modified toughened epoxies were subjected to Mode I, Mode II and Mixed Mode I&II testing as described in Section 5.3.1. Fracture toughness was assessed by studying stress intensity factor SIF at failure and increasing load (K_I and K_{II}) of 15 resins in 0°, 45° and 90° loading angles using CTMMM grips and compared to the behaviour of neat resin specimens (S1). Surface strain maps were generated by DIC using methods described in section 5.2 and stress intensity values K_I and K_{II} were determined using the DICITAC software. Strain energy (G_{Ic} and G_{IIc}) of both resins and composites was studied and changes relative to neat were analysed.

The differences in K_I and K_{II} values of the samples (S2, S3, S4, S5, S6, S7, S8, S10, S11, S12, S13, S14, S15 & S16) in comparison to Neat (S1) were plotted graphically as fold change in Figure 6.7 for K_I and 6.10 for K_{II}. All experiments were conducted four times to ensure repeatability.

6.3 Kinked Cracks

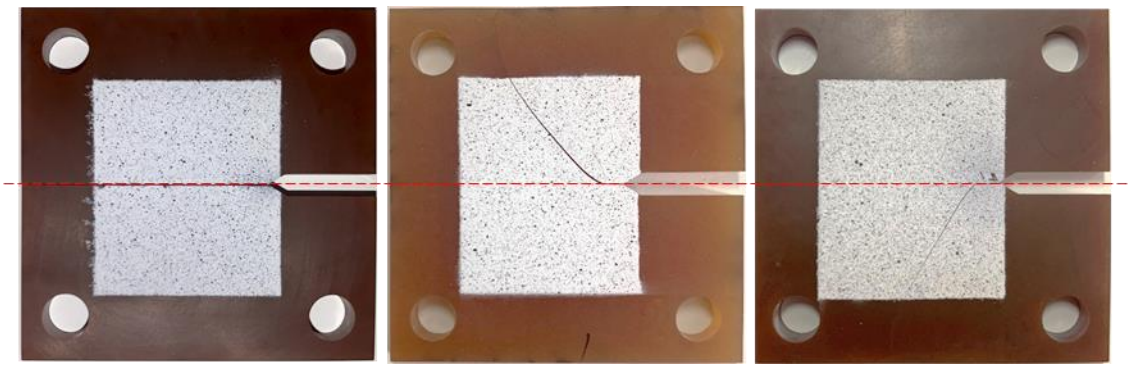

Figure 6.1 -Test samples exhibiting straight crack and kinked cracks, first (S13-0DEG), middle (S3-45DEG) and last (S13-90DEG)

All test samples except pure mode I specimens exhibit kinked cracks as shown in figure 6.1. The kinked crack curvature angle is measured at the initial crack kink as indicated in figure 6.1. Cracks exhibiting curvature is measured at the initial kink of the crack, as illustrated in figure 6.1. The Kink angle is measured digitally using an imaging tool (ImageJ) [202], the ImageJ tool has an estimated accuracy of around ±1°. The method is shown in figure 6.2; in this figure the angle is measured and subtracted from 180° to obtain the kinked crack angle. All the measured kinked angles are presented for all the test samples against loading angle in figure 6.3 and for baseline/neat materials are presented separately in figures 6.4 and 6.5.

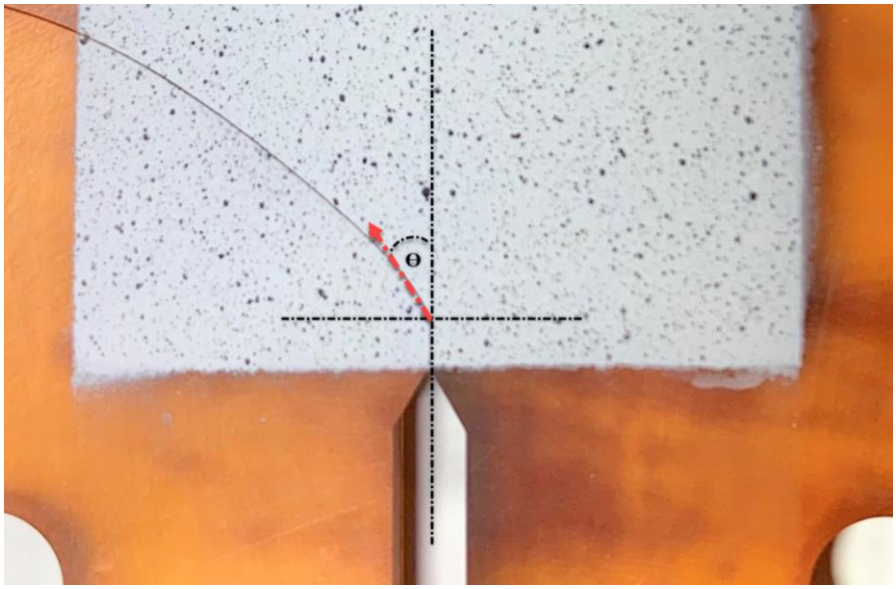

Figure 6.2 - Measuring kinked cracks angle Θ in a specimen

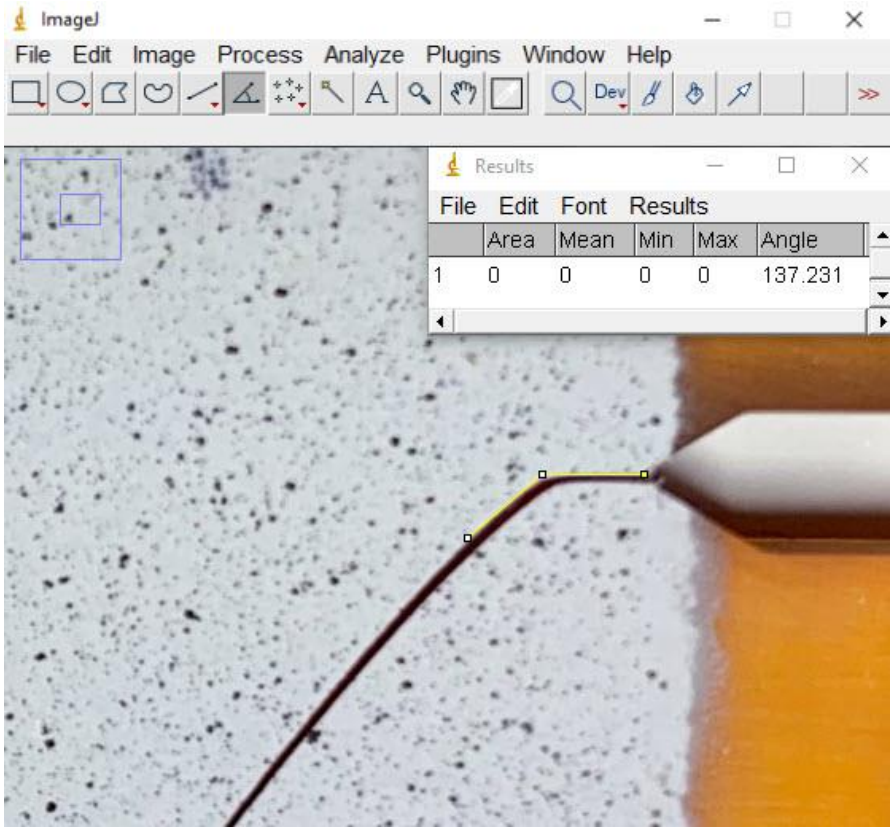

Figure 6.3 - Measuring kinked cracks angle Θ using ImageJ

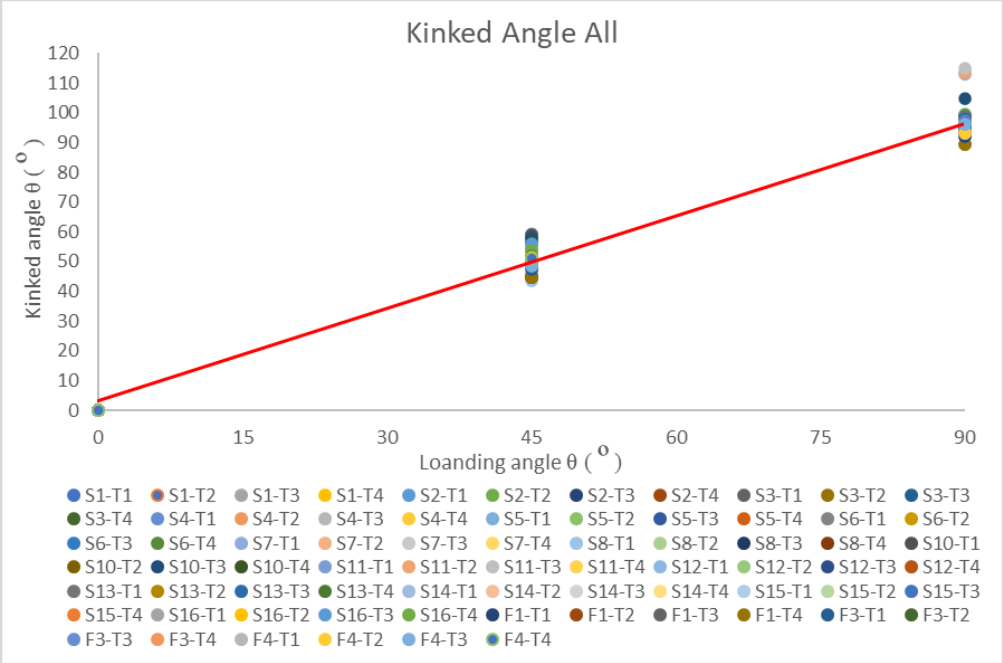

Figure 6.4 - Cracked kink angle vs loading angle for all test F & S Formulation specimens

Figure 6.4 shows the variation of cracked kink angles for all test F & S formulation materials in 0°, 45° and 90° loading angles. There is a significant amount of scatter in the cracked kink angles observed in specimens loaded at 45° and 90° loading angles. Figure 6.5 and 6.6 show the baseline/neat F1 and S1 test specimens cracked kink angles with very little or no noteworthy scatter.

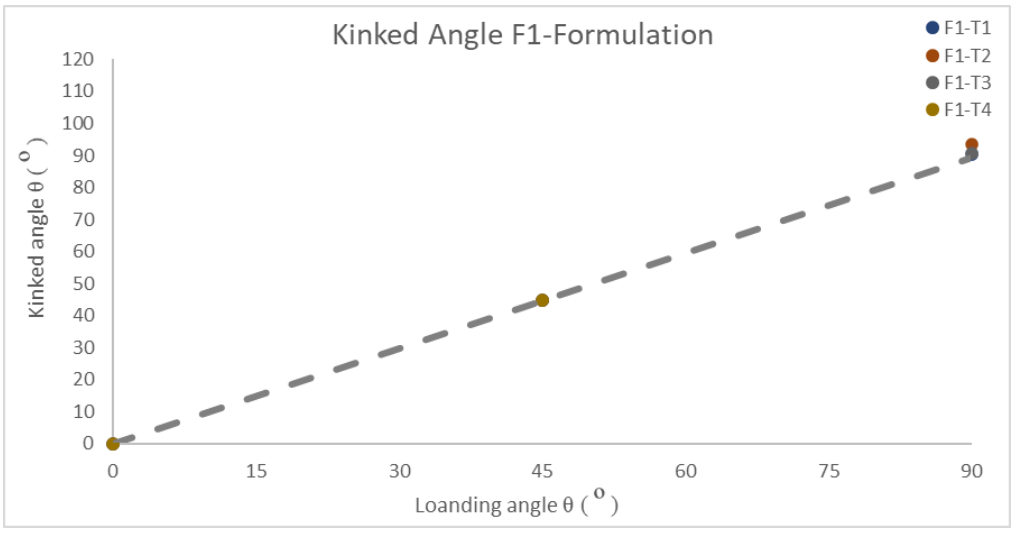

Figure 6.5 - Baseline/Neat F-Formulation (F1) crack kink angles

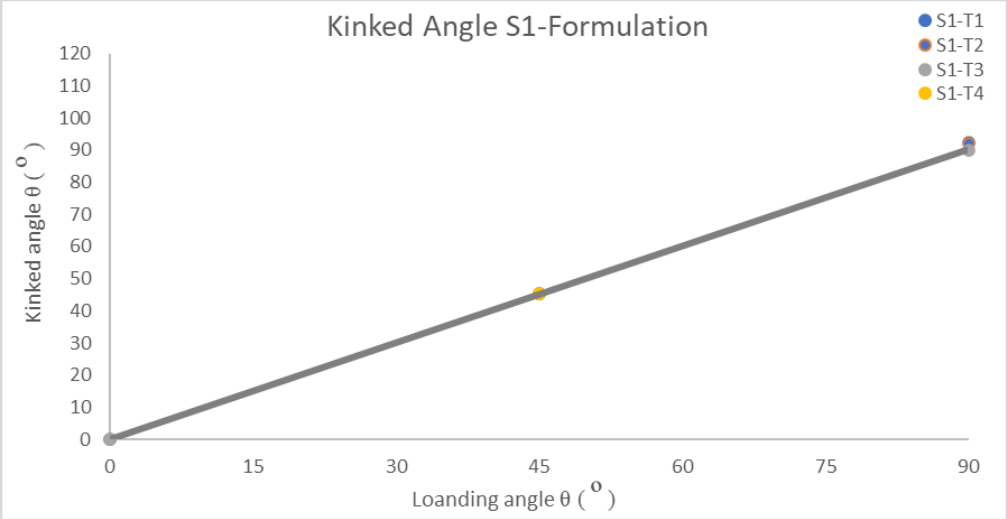

Figure 6.6 - Baseline/Neat F-Formulation (F1) crack kink angles

Figures 6.5 and 6.6 show no significant differences between kink angles at given loading angles for both baseline/neat F and S formulations specimens tested. Figure 6.5 and 6.6 indicate good correlation between loading angle and cracked kink angle. Comparing figure 6.4 with figure 6.5 and figure 6.6, it can be seen that only particle toughened epoxy materials exhibit a change in cracked kink angle, and it is suggested that the deduction could be made from the particle toughening influences kinked crack angle differently for different loading angles.

6.4 Results

6.4.1 Stress intensity factor and behaviour up to failure in Mode I (K_I) in modified specimens

The results presented in this section refers to mode I experiments during loading up to failure under mode I and mode II for all s-formulation specimen. Figure 6.8-6.9 shows the K_I values obtained for samples (S2, S3, S4, S5, S6, S7, S8, S10, S11, S12, S13, S14, S15 & S16) from start of loading up to failure at 0º (grey colour), 90º (orange colour), and 45º (blue colour) loading angles and plotted graphically. The negative values observed in the plotted graph is due to the scatter in the load cell data observed during the start of the experiment. The differences in K_I and K_{II} values in comparison to the neat specimen (S1) were plotted graphically as fold change as described in Figure 6.7.

Mode I failure of S-formulation specimens were characterised by extracting K_I values up to failure. Fold changes in K_I values for different specimens relative to the neat specimen (S1) (Table 6.2) displayed that samples exhibited improved fracture toughness (Figure 6.7).

At 0° loading angle (Mode I failure) specimens S2, S3, S4, S5, S6, S7, S8, S10, S12 and S14 (Figure 6.8-6.9) display increased SIF at failure with specimen S10 displaying highest SIF (K_I) and S12 displaying lowest SIF (K_I).

At 90° loading angle (Mode II failure) all specimens display improved fracture toughness with specimen S8 displaying highest SIF (K_I) and S2 displaying lowest SIF (K_I).

At 45° loading angle (Mode I &II failure) almost all specimens display improved fracture toughness with specimen S13 exceptionally displaying no change. Specimen S14 displayed highest SIF (K_I) and S15 displayed lowest SIF (K_I).

Graphical representation of fracture behaviour up to failure (Table 6.3) showed that at 0° loading angle Mode I failure was observed in all samples except S14 (Figure 6.9c) and S16 (Figure 6.9e) which exhibited particle induced resistance. At 90° loading angle mode I influenced particle resistance was observed in S12 (Figure 6.9a), S13 (Figure 6.9b), S14

(Figure 6.9c), S15 (Figure 6.9d) and S16 (Figure 6.9e) specimens. Marginal mode I dominance was observed in S2 (Figure 6.8b), S3 (Figure 6.8c) and S4 (Figure 6.8d). At 45° loading angle, mixed mode I & II induced failure was observed in all samples except S14 (Figure 6.9c) which displayed particle induced resistance.

It is interesting to observe (figure 6.8-6.9) that the increase in loading provides a lot of information on how the behaviour of the material changes non-linearly in some specimens when the load is increased to failure. Furthermore, observations in the failure of mode I, mode II and mixed mode I&II suggest that S4 (Figure 6.8d), S10 and S14 (Figure 6.9c) have the most resistance to Mode II. However, S10 has the best overall material performance.

It can be seen (Table 6.3) that when the weight loading increases, the fracture energy and damage resistance in mode II loading of the resin system, increases almost all formulation except S11 and S13, with improvement in the SIF K_I at fracture. The reason for the difference in mode I K_I values for all resin system S11 and S13 could be a result of crack front bridging (figure 2.2). This could be due to the obstructions to the propagation of the crack front by the particulates which causes the primary cracks energy to increase as the particulates absorb, which forms a secondary crack and provide an increase in the toughness. It is believed that the particulates alone could be undergoing an inelastic deformation at a micro scale level.

Samples	0° (K_I) MPa.√m	Fold change at 0° loading	45° (K_I) MPa.√m$^{1/2}$	Fold change at 45° loading	90° (K_I) MPa.√m	Fold change at 90° loading
S1	**1.2**	**0**	**0.63**	**0**	**0**	**0**
S2	1.34	0.14	0.77	0.14	0.17	0.17
S3	1.34	0.14	0.89	0.26	0.25	0.25
S4	1.65	0.45	1	0.37	0.27	0.27
S5	1.48	0.28	1	0.37	0.32	0.32
S6	1.54	0.34	0.99	0.36	0.33	0.33
S7	1.5	0.3	1.01	0.38	0.41	0.41
S8	1.29	0.09	0.94	0.31	0.61	0.61
S10	1.75	0.55	1.05	0.42	0.23	0.23
S11	0.87	0	0.72	0.09	0.45	0.45
S12	1.25	0.05	0.84	0.21	0.25	0.25
S13	0.73	0	0.62	0	0.46	0.46
S14	1.72	0.52	1.08	0.45	0.44	0.44
S15	1	0	0.64	0.01	0.28	0.28
S16	1.1	0	0.85	0.22	0.43	0.43

Table 6.2 - Fold changes (yellow colour) relative to neat (S1) associated with fracture toughness (K_I) of toughened modified S-Formulation specimens with 14%, 5% (S15) and 10% (S16) particle weight loading.

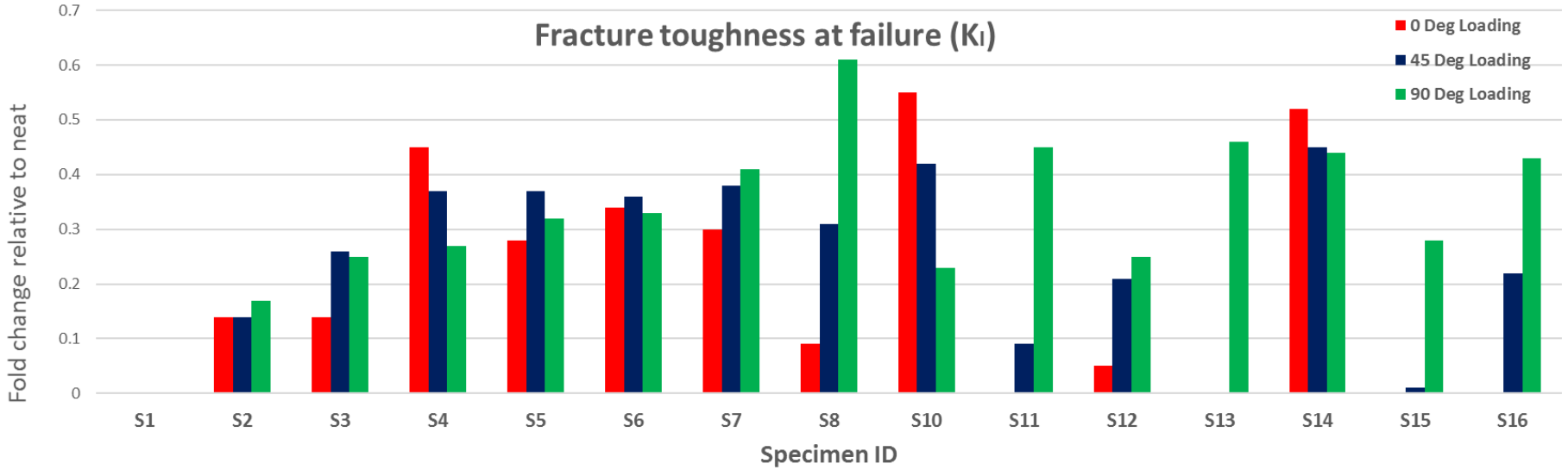

Figure 6.7 - Fold changes in K_I values at fracture (K_{IMAT}) for different specimens relative to the neat specimen (S1)

Samples	0 DEG (KI)	45 DEG (KI)	90 DEG (KI)	Fig no
S1	Mode I failure	Mode I failure	No change	Figure 6.8 a
S2	Particle influence	Particle influence	Particle influence	Figure 6.8 b
S3	Particle influence	Particle influence	Particle influence	Figure 6.8 c
S4	Increased particle influence	Increased particle influence	Increased particle influence	Figure 6.8 d
S8	Marginal particle influence	Particle influence	Increased particle influence	Figure 6.8 e
S11	Particle resistance	Marginal particle influence	Increased particle influence	Figure 6.8 f
S12	Marginal particle influence	Particle influence	Particle influence	Figure 6.9 a
S13	Particle resistance	Particle resistance	Increased particle influence	Figure 6.9 b
S14	Increased particle influence	Increased particle influence	Increased particle influence	Figure 6.9 c
S15	Particle resistance	Particle resistance	Particle influence	Figure 6.9 d
S16	Particle resistance	Increased particle influence	Increased particle influence	Figure 6.9 e

Table 6.3 - Fracture behaviour in K_I up to failure in particle modified s-formulation resin samples subjected to loading

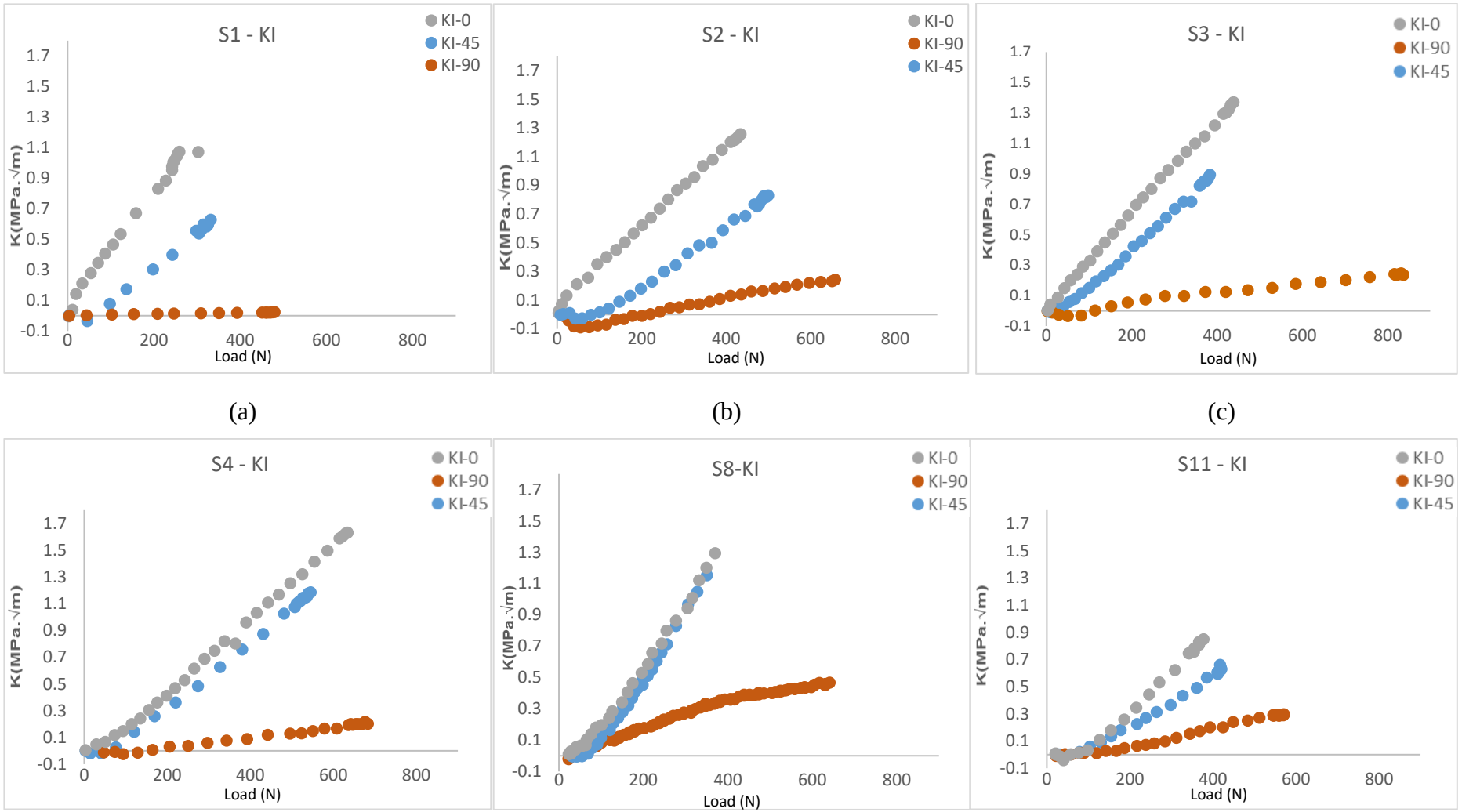

Figure 6.8 - K_I values of specimens a) S1, b) S2, c) S3, d) S4, e) S8 and f) S11 subjected to loading in three loading angles (0°,45° & 90°).

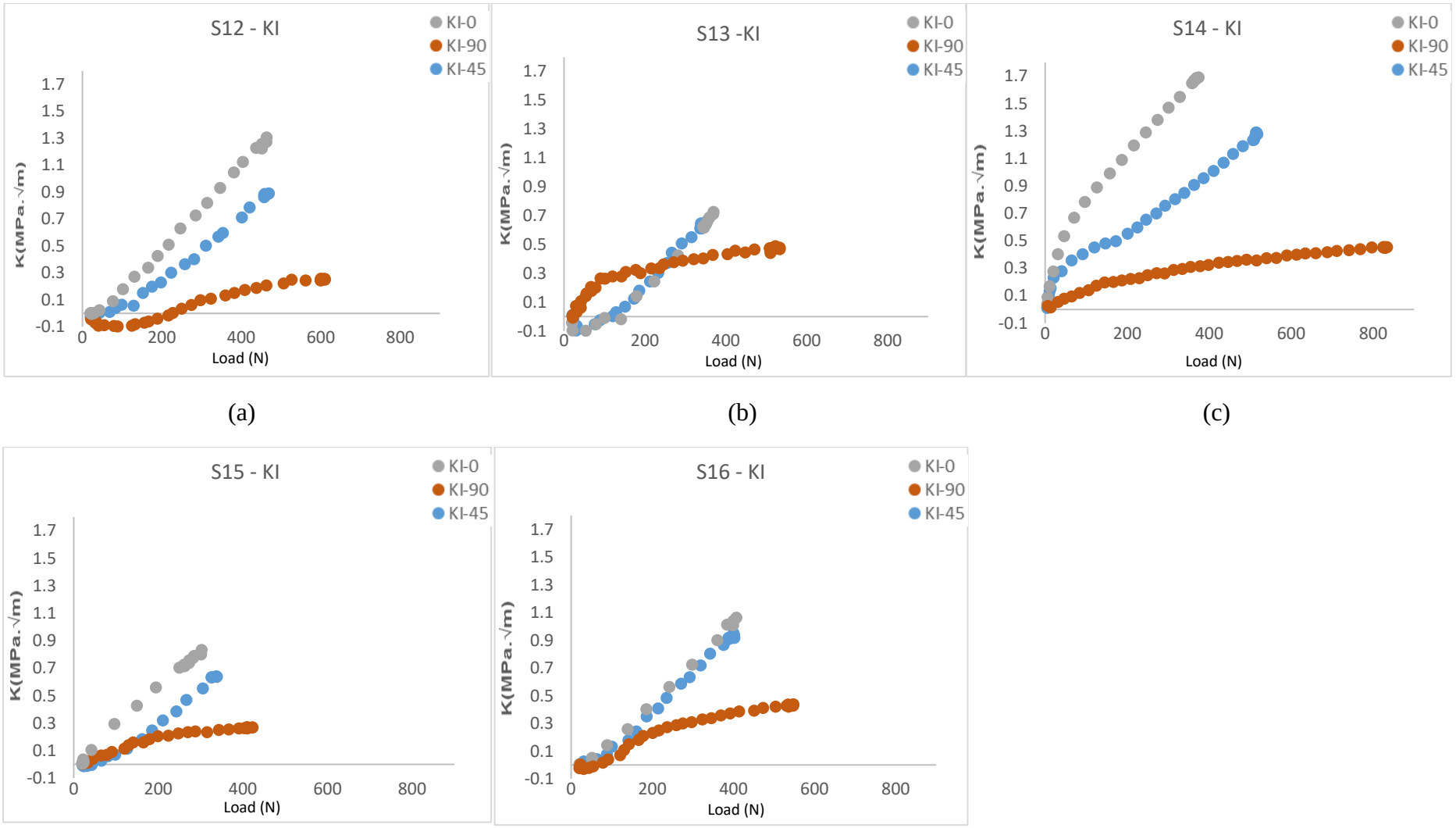

Figure 6.9 - K_I values of specimens a) S12, b) S13, c) S14, d) S15 and e) S16 subjected to loading in three loading angles (0°,45° & 90°).

6.4.2 Stress intensity factor and behaviour up to failure in Mode II (K_{II}) in modified specimens

The results presented in this section refers to mode II experiments during loading up to failure under mode I and mode II for all s-formulation specimen. Figure 6.11-6.12 shows the K_{II} values obtained for samples (S2, S3, S4, S5, S6, S7, S8, S10, S11, S12, S13, S14, S15 & S16) from start up to failure were assessed at 0º (grey colour), 90º (orange colour), and 45º (blue colour) loading angles and plotted graphically. The negative values observed in the plotted graph is due to the scatter in the load cell data due observed during the start of the experiment. The differences in K_I and K_{II} values in comparison to the neat specimen (S1) were plotted graphically as fold change as described in Figure 6.10.

Mode I failure of s-formulation specimens were characterised by extracting K_I values up to failure. Fold changes in K_I values for different specimen's relative to the neat specimen (S1) (Table 6.4) displayed that samples exhibited improved fracture toughness (Figure 6.11).

At 0° loading angle (Mode I failure) all specimens displayed marginal improvement in fracture toughness with specimens S3, S10 and S14 displaying no changes in resistance. S8 displayed the highest SIF (K_I) and S13 displaying lowest SIF (K_I).

At both 90° loading angle (Mode II failure) and at 45° loading angle (mode I &II failure), all specimens display improved fracture toughness with specimen S8 displaying highest SIF (K_I). Graphical representation of fracture behaviour up to failure (Table 6.5) showed that at 0° loading angle, linear Mode II failure was observed in all samples. At 90° loading angle, all specimens exhibited Mode II failure. However, particle resistance was observed in S2, S12, S13, S14 and S16. At 45° loading angle, linear Mode II failure was observed in all samples.

It is interesting to observe (figure 6.11-6.12) that the increase in loading provides a lot of information on how the behaviour of the material changes non-linearly in some specimens when the load is increased to failure as is observed in specimen S13 (Figure 6.12b), S14 (Figure

6.12c), S16 (Figure 6.12e). Furthermore, observations in the failure of mode I, mode II and mixed-mode suggest that S3, S5, S8 and S4 have the most resistance to Mode II. However, S8 has the best overall material performance.

It can be seen (Table 6.5) that when the weight loading increases the fracture energy and damage resistance in mode II loading of the resin system, increases in almost all formulations except S15 and S16. The reason for the difference in mode II K_{II} values for S15 and S16 could be a result of not enough particulate dispersion for fracture resistance to occur.

Samples	0° (K_{II}) MPa.√m	Fold change at 0° Loading	45° (K_{II}) MPa.√m	Fold change at 45° Loading	90° (K_{II}) MPa.√m	Fold change at 90° Loading
S1	0	0	0.36	0	0.81	0
S2	0.11	0.11	0.46	0.1	0.85	0.04
S3	-0.06	0	0.64	0.28	1.43	0.62
S4	0.03	0.03	0.62	0.26	1.23	0.42
S5	0.07	0.07	0.76	0.4	1.5	0.69
S6	0.05	0.05	0.65	0.29	1.08	0.27
S7	0.08	0.08	0.64	0.28	1.34	0.53
S8	0.12	0.12	0.82	0.46	1.65	0.84
S10	0	0	0.71	0.35	1.36	0.55
S11	0.07	0.07	0.53	0.17	1.02	0.21
S12	0.05	0.05	0.52	0.16	0.98	0.17
S13	0.01	0.01	0.48	0.12	0.94	0.13
S14	0	0	0.69	0.33	1.43	0.62
S15	0.02	0.02	0.42	0.06	0.84	0.03
S16	0.04	0.04	0.57	0.36	1.13	0.32

Table 6.4 - Fold changes (yellow colour) relative to neat (S1) associated with fracture toughness (K_{II}) of toughened modified s-formulation specimens with 14%, 5% (S15) and 10% (S16) particle weight loading.

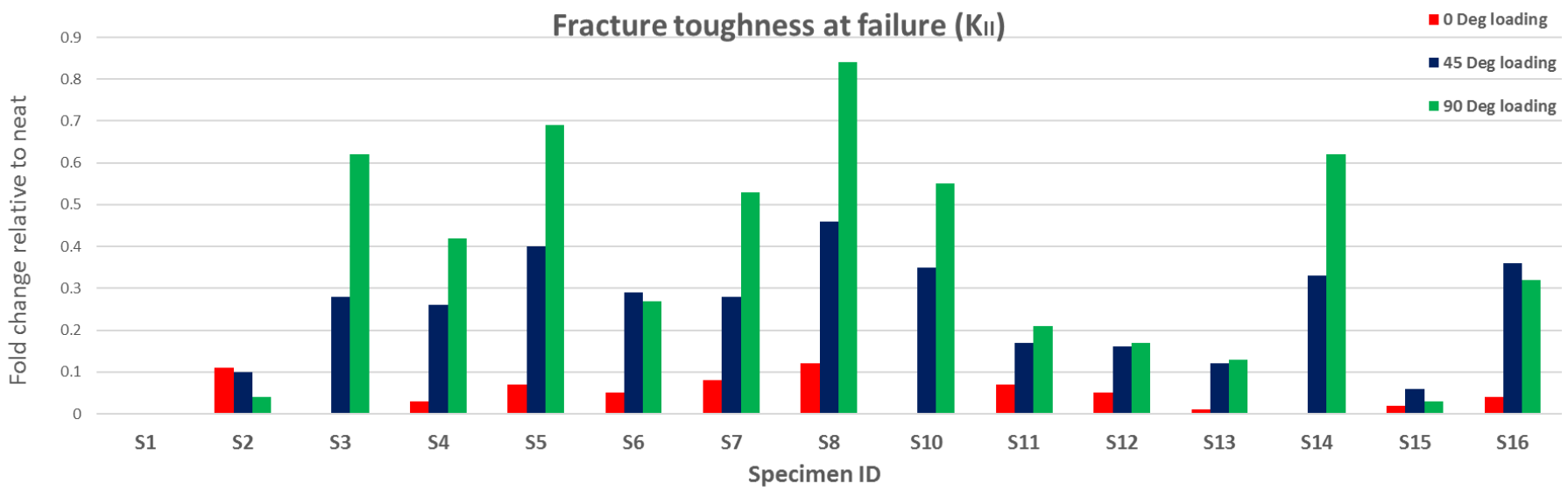

Figure 6.10 - Fold changes in K_{II} values at fracture (K_{IIMAT}) for different specimens relative to the neat specimen (S1)

Samples	0 DEG (KII)	45 DEG (KII)	90 DEG (KII)	Fig no
S1	No change	Mode II Failure	Mode II failure	Figure 6.11 a
S2	Marginal particle influence	Marginal particle influence	Marginal particle influence	Figure 6.11 b
S3	Particle resistance	Increased particle influence	Increased particle influence	Figure 6.11 c
S4	Marginal particle influence	Increased particle influence	Increased particle influence	Figure 6.11 d
S8	Marginal particle influence	Increased particle influence	Increased particle influence	Figure 6.11 e
S11	Particle resistance	Increased particle influence	Increased particle influence	Figure 6.11 f
S12	Marginal particle influence	Marginal particle influence	Increased particle influence	Figure 6.12 a
S13	Marginal particle influence	Marginal particle influence	Marginal particle influence	Figure 6.12 b
S14	Particle resistance	Increased particle influence	Increased particle influence	Figure 6.12 c
S15	Marginal particle influence	Marginal particle influence	Marginal particle influence	Figure 6.12 d
S16	Marginal particle influence	Increased particle influence	Increased particle influence	Figure 6.12 e

Table 6.5 - Fracture behaviour in K_{II} up to failure in particle modified s-formulation resin samples subjected to loading.

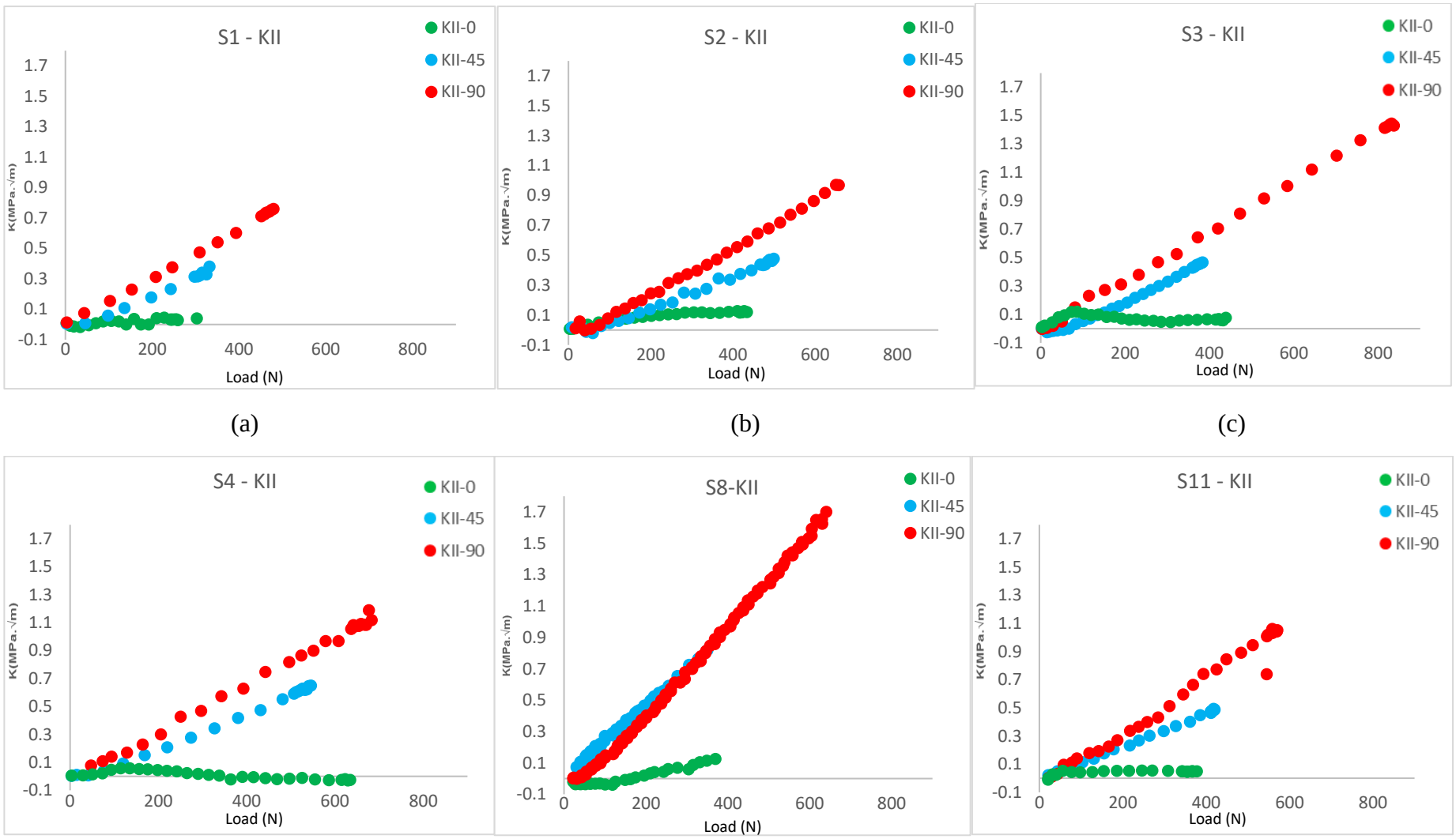

Figure 6.11 - K_{II} values of specimens a) S1, b) S2, c) S3, d) S4, e) S8 and f) S11 subjected to loading in three loading angles (0°,45° & 90°).

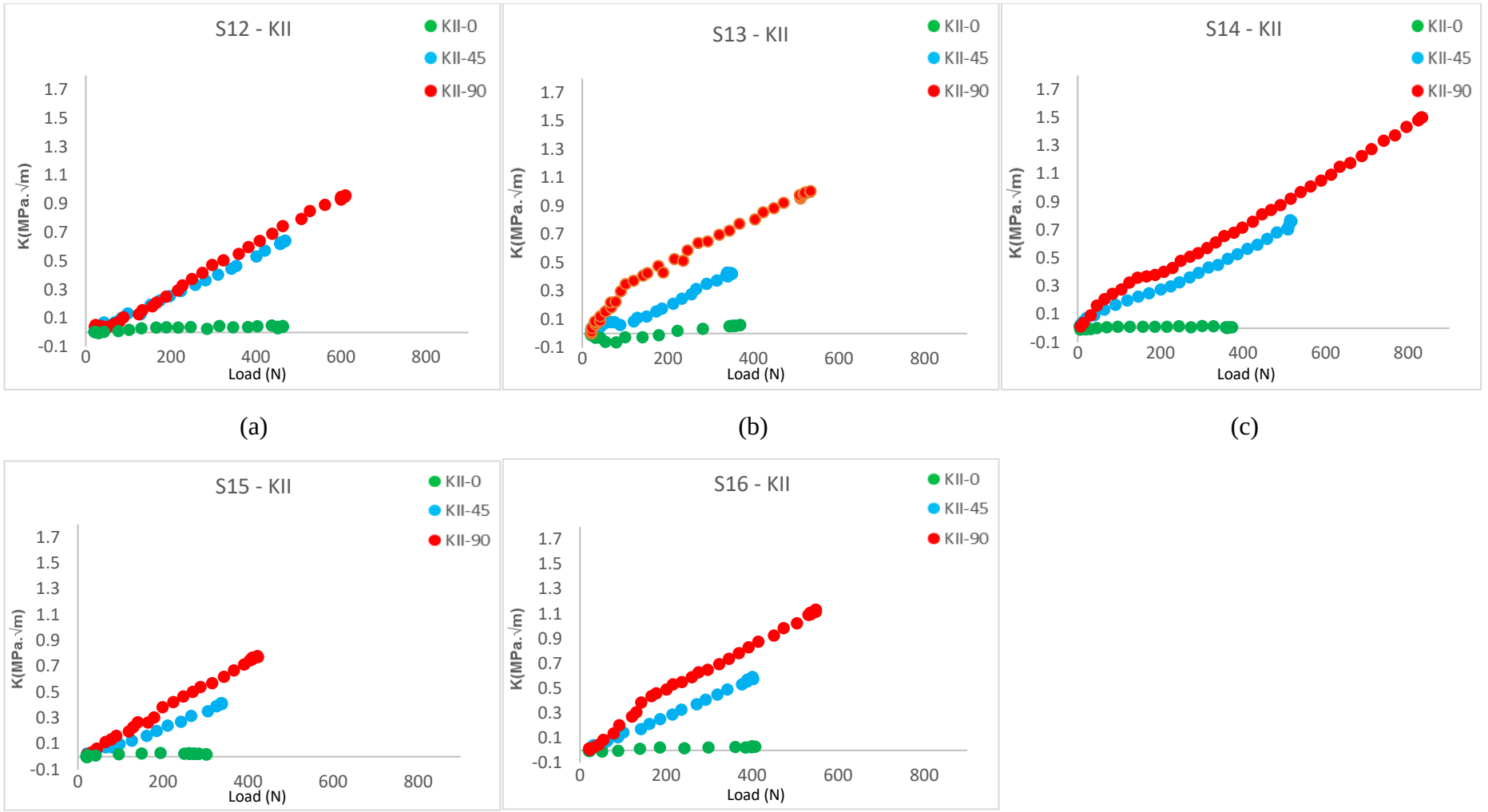

Figure 6.12 - K_{II} values of specimens a) S12, b) S13, c) S14, d) S15 and e) S16 subjected to loading in three loading angles (0°,45° & 90°)

6.4.3 SIF with increased loading (K_I and K_{II}) of resin modified specimens

The results presented in this section refers to mode I, mode II and mixed mode I&II experiments at failure under mode I and mode II for all s-formulation specimens.

Figures 6.13-6.16 shows K_I (orange colour) and K_{II} (blue colour) values obtained for samples (S2, S3, S4, S5, S6, S7, S8, S10, S11, S12, S13, S14, S15 & S16) plotted graphically at the point of failure.

Toughened epoxies modified with 14% particle weight loading (Cytec Engineering Ltd) when subjected to fracture testing by Mode I, Mode II and Mixed mode I & II testing in CTMMM grips displayed differences in stress intensity values (K_I and K_{II}) (Table 6.6)

For K_{II} value of the neat resin (S1) (Figure 6.13a) subjected to Mode I loading (0° loading) we would expect the values to be 0 MPa.√m and as predicted the experimental value was 0.00 MPa.√m .

The samples that displayed K_{II} values in 0° loading that is close to the neat resin are S3 (-0.06 MPa.√m) (Figure 6.13c), S4 (0.04 MPa.√m) (Figure 6.13d), S10 (0.00 MPa.√m) (Figure 6.15a), S13 (0.01 MPa.√m) (Figure 6.15d) and S14 (0.00 MPa.√m) (Figure 6.16a). The samples that displayed K_{II} values at failure in 0° loading that is different to the neat resin are S2 (0.11 MPa.√m) (Figure 6.13b), S5 (0.07 MPa.√m) (Figure 6.14a), S6 (0.05 MPa.√m) (Figure 6.14b), S7 (0.08 MPa.√m) (Figure 6.14c), S8 (0.12 MPa.√m) (Figure 6.14d), S11 (0.07 MPa.√m) (Figure 6.15b) and S8 (0.05 MPa.√m) (Figure 6.14d). Notably, K_I values in 0° loading of S-formulation samples (S2-S8 & S10-S14) display differences in comparison to the neat resin (S1) (Figure 6.13a). The reason all other specimens exhibiting shearing, it is due to particles influence towards mode II.

K_{II} value at failure of the neat resin (S1) (Figure 6.13a) subjected to mode II loading (90°) was 0.81 MPa.√m. Notably, in 90° loading s-formulation specimen S2 (0.85 MPa.√m.) (Figure

6.13b) displayed similarities with the neat resin (S1) (Figure 6.13a) whereas none of the s-formulation samples displayed K_I values at failure is similar to the neat resin (-0.02 MPa.√m). K_{II} value at failure of the neat resin (S1) (Figure 6.13a) subjected to mixed mode I & II loading (45°) was 0.36 MPa.√m. Notably, the K_I values in 45° loading none of the S-formulation samples (S2-S8 & S10-S14) displayed similarities with the neat resin (S1) (Figure 6.13a). Only s-formulation samples S13 (0.62 MPa.√m) (Figure 6.15d) displayed K_I values that are similar to the neat resin (0.63 MPa.√m).

Notably, for K_{II} values in 45° loading none of the s-formulation samples (S2-S8 & S10-S14) displayed similarities with the neat resin (S1). Only formulation sample S13 (0.62 MPa.√m) (Figure 6.9b) displayed K_I values that are similar to the neat resin (0.63 MPa.√m).

	0°		45°		90°	
Samples	K_I MPa.√m	K_{II} MPa.√m	K_I MPa.√m	K_{II} MPa.√m	K_I MPa.√m	K_{II} MPa.√m
S1	1.2	0	0.63	0.36	-0.02	0.81
S2	1.34	0.11	0.77	0.46	0.17	0.85
S3	1.34	-0.06	0.89	0.64	0.25	1.43
S4	1.65	0.03	1	0.62	0.27	1.23
S5	1.48	0.07	1	0.76	0.32	1.5
S6	1.54	0.05	0.99	0.65	0.33	1.08
S7	1.5	0.08	1.01	0.64	0.41	1.34
S8	1.29	0.12	0.94	0.82	0.61	1.65
S10	1.75	0	1.05	0.71	0.23	1.36
S11	0.87	0.07	0.72	0.53	0.45	1.02
S12	1.25	0.05	0.84	0.52	0.25	0.98
S13	0.73	0.01	0.62	0.48	0.46	0.94
S14	1.72	0	1.08	0.69	0.44	1.43

Table 6.6 - SIF values K_I and K_{II} at failure for all unmodified and particle modified S-formulation resin samples.

Figures 6.17-6.21 demonstrates in a different way the deviation of the crack tip behaviour from the expected loading behaviour due to the particles as observed in section 6.4.1 and 6.4.2. The analysis of results in Figures 6.17-6.20 compares SIF K_I Vs K_{II} with increase loading between S1 neat resin against all other formulations. It can be seen in Figure 6.17 that the S1 specimen is failing in pure mode I without the influence from mode II, in mixed mode I&II influenced by mode I and mode II and in pure mode II without the influence from mode I. This indicates that the specimen loaded in the new CTMMM grips in mode I and mixed mode I&II and mode II are failing in respective modes accurately. Although, the other formulations are loaded the same as S1, they are failing in different modes to what they have been loaded. Hence, this phenomenon can only be due the particles changing the crack propagation mode.

It can also be seen clearly in Figure 6.18-6.20 that there are only small or insignificant deviations in mode I performance influenced by mode II in all particulate toughened specimens; in mixed mode I&II S8, S11, S12, S13 exhibit deviation influenced by mode II; and in mode II all formulation indicates deviations influenced by mode I. Figure 6.19 for S11 and S12 and Figure 6.20 for S13 and S14 exhibit a small deviation in mode I performance where difference is attributed to the influence of mode II. S2 in Figure 6.17, S3 and S8 in Figure 6.18 were observed to have the greatest deviation in mode I performance attributed to the influence of mode II.

A similar pattern of mode II influence was observed in mixed mode I & II performance, where in S8 (Figure 6.18), S11 and S12 (Figure 6.19), and S13 (Figure 6.20) were observed to have the greatest difference. However, in mixed mode I & II performance S14 (Figure 6.20) was observed to be influenced in mode I instead of mode II like all the other formulations.

In mode II performance, S3 (Figure 6.18) and S11 (Figure 6.19) has a linear mode I influence. However, the mode II performance of S8 (Figure 6.18), S13 and S14 (Figure 6.20) observed to have resistance to mode I influence. Notably, for mode II performance S12 (Figure 6.19) has

the greatest resistance to mode I influence starting at a K_{II} value of 0.4 (MPa.√m) when compared to the other formulations.

The variation in the deviation between the specimens can be attributed to the differing particles present in the individual formulation. Additionally, the mode II deviation is a very interesting insight, in general a resin system's function is to provide composites with support from shear failure and the difference in performance can be observed. It is evident in the results that the performance can be clearly observed and differentiated between different particles and % weight loading.

Figure 6.21 compares the SIF K_I Vs K_{II} of all the formulations. Figure 6.21 clearly demonstrates the relative capability of different materials where the area under the curve indicates the maximum material fracture toughness that each formulation with particle differing in performance. Most interestingly it can be observed when comparing S1to S2, both K_I and K_{II} are proportionally enhanced for S2 performance. Whereas both S13 and S8 are observed to be proportionally more enhanced in mode II performance with S8 having the highest K_{II} value and S13 having the lowest K_I value at fracture. This analysis approach is a very good way to compare resin formulation capability in a high through put testing environment and compliments the CTMMM testing strategy.

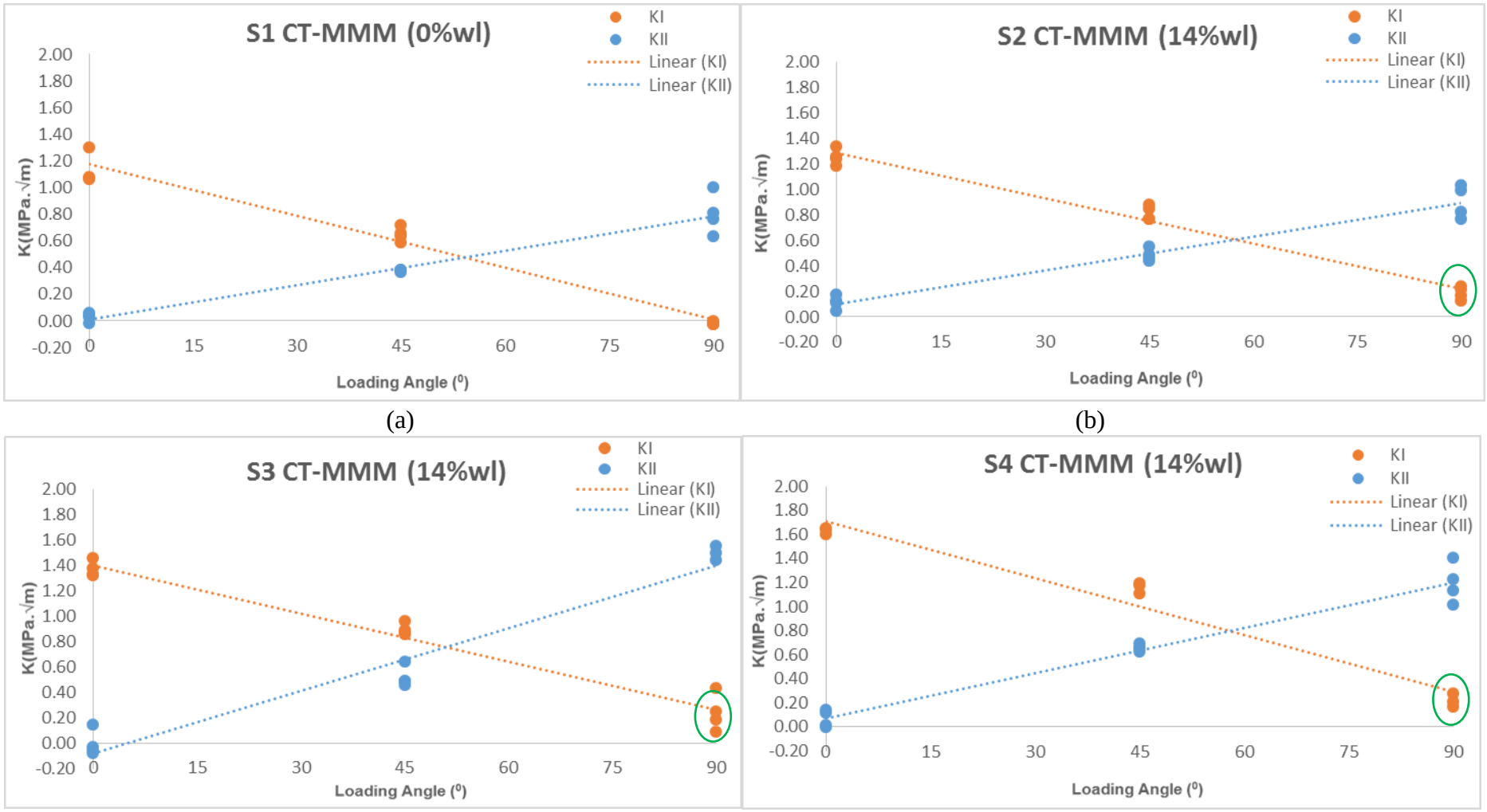

Figure 6.13 - SIF at Fracture K_I and K_{II} for unmodified S1 and particle modified resin samples S2, S3 and S4 (n=4) subjected to loading in three loading angles (0°,45° & 90°).

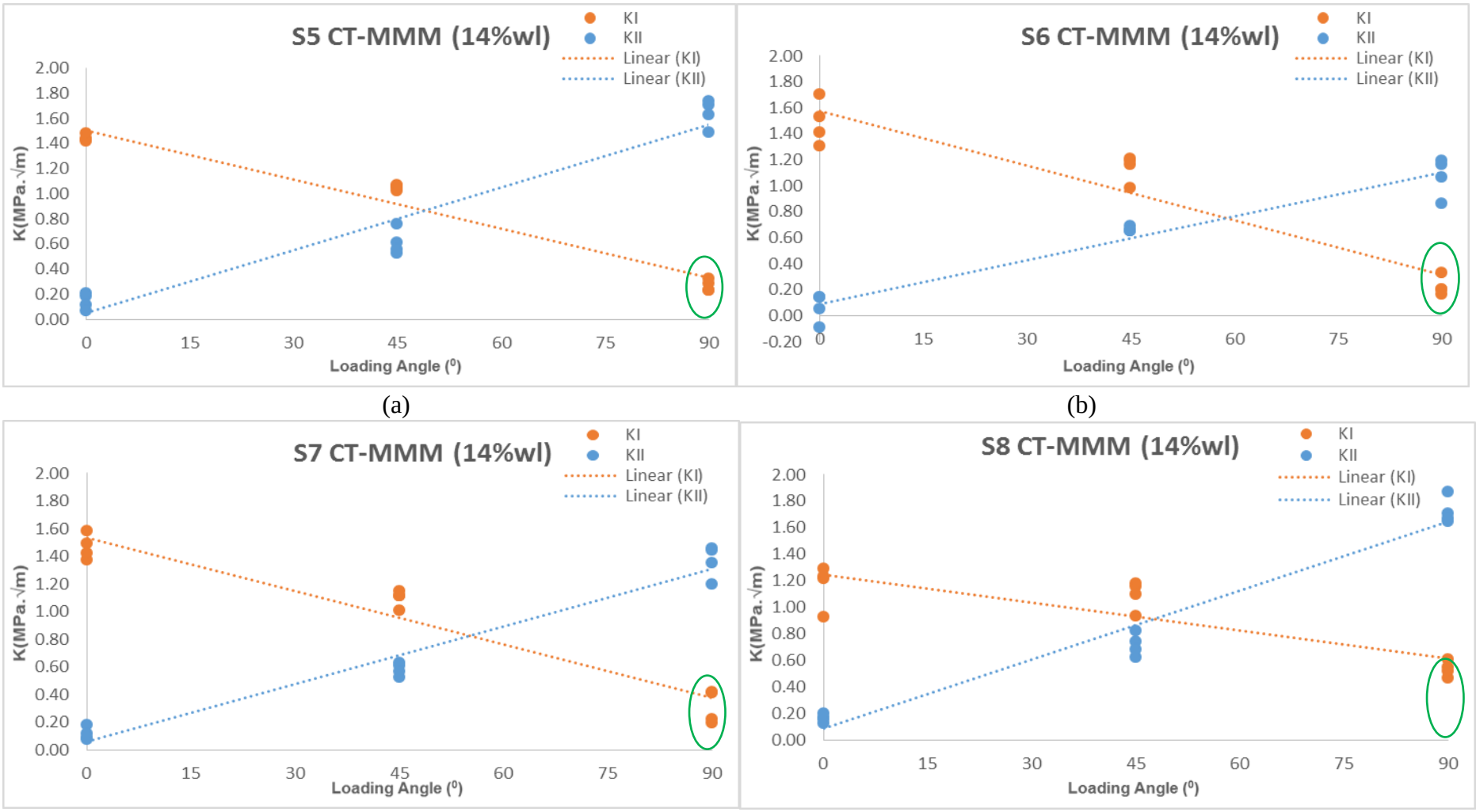

Figure 6.14 - SIF at Fracture K_I and K_{II} for particle modified resins S5, S6, S7 and S8 samples (n=4) subjected to loading in three loading angles (0°,45° & 90°).

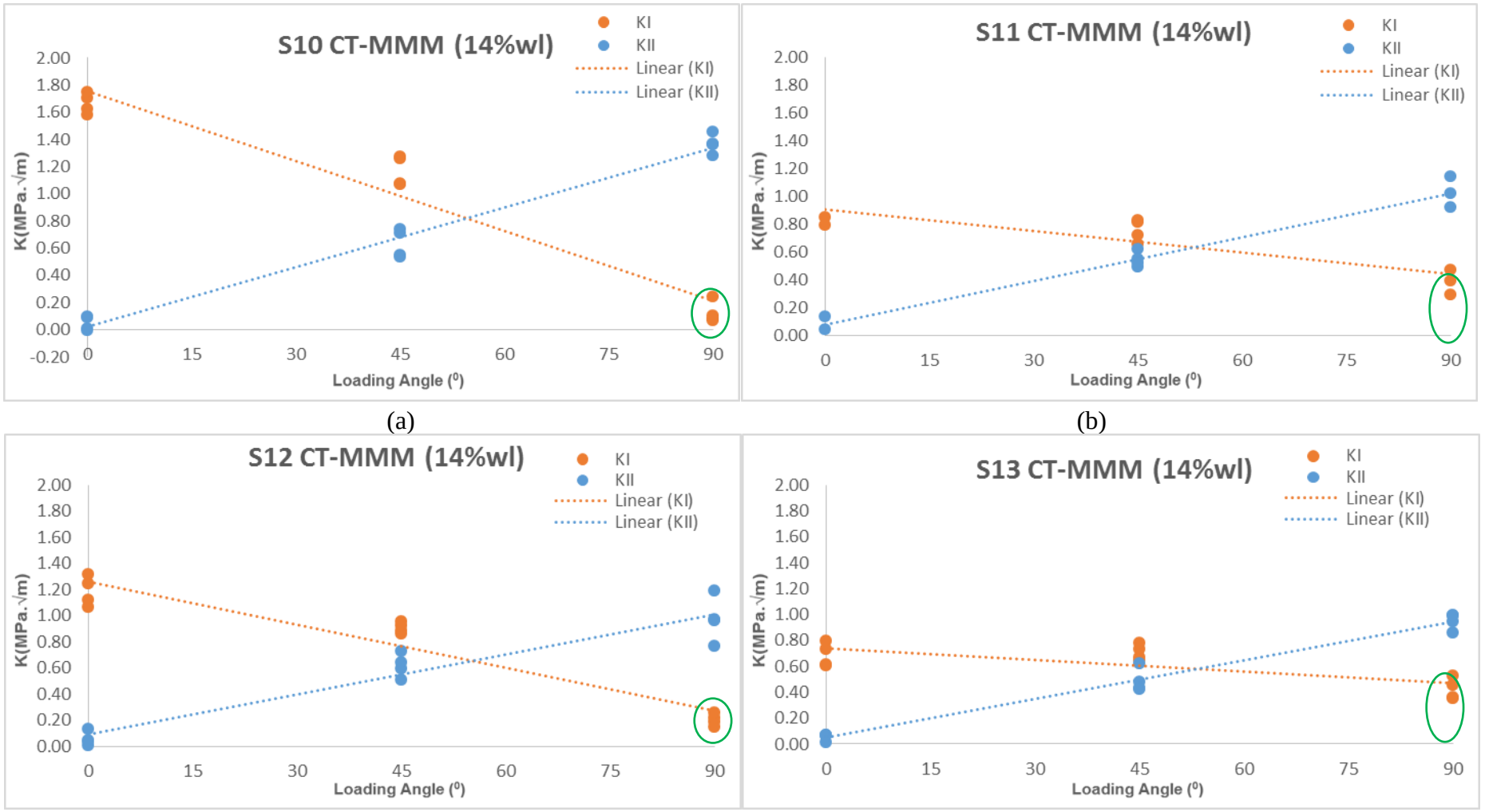

Figure 6.15 - SIF at Fracture K_I and K_{II} for particle modified resins S10, S11, S12 and S13 samples (n=4) subjected to loading in three loading angles (0°,45° & 90°).

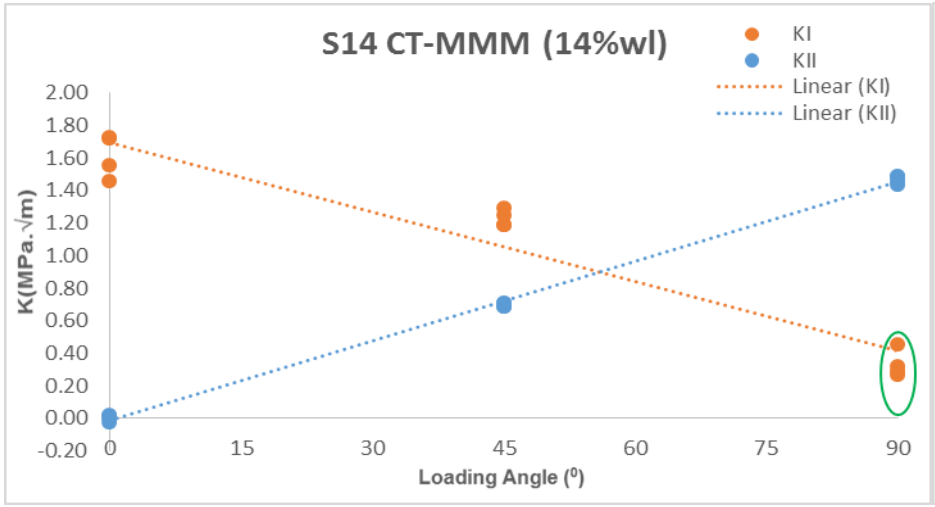

(a)

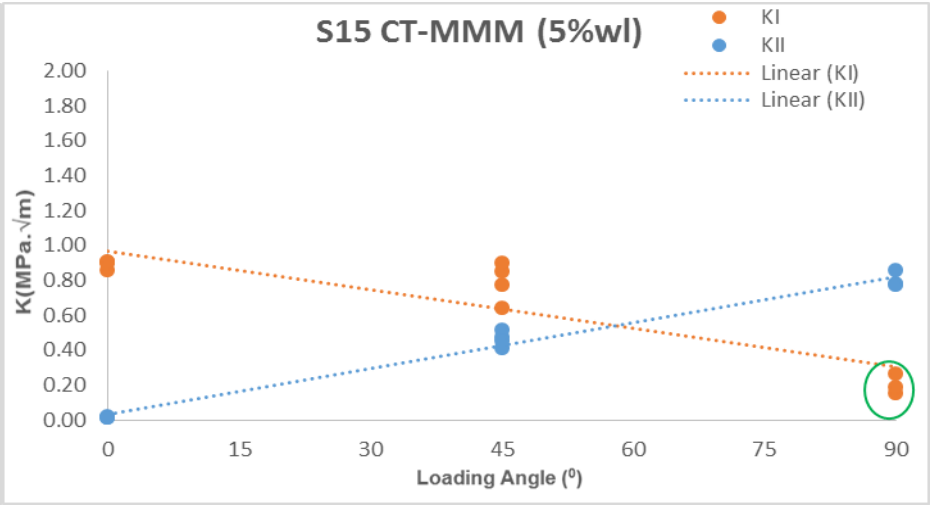

(b)

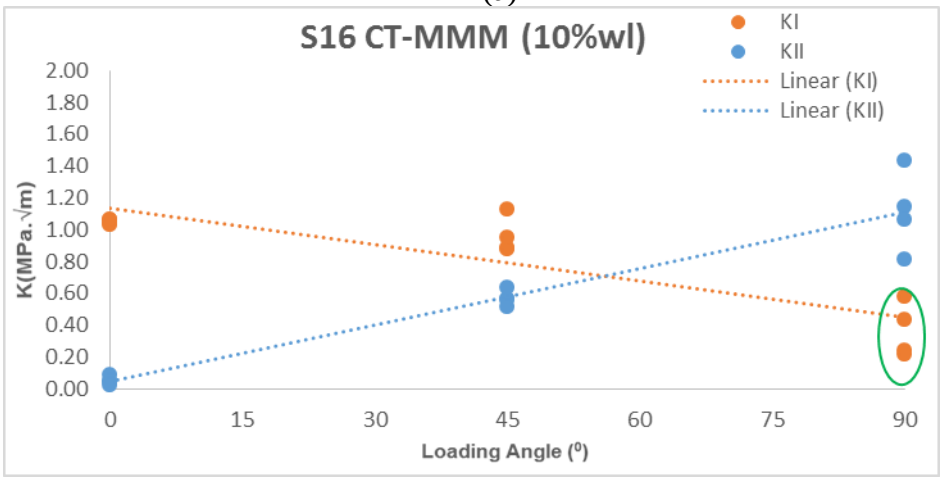

(c)

Figure 6.16 - SIF at Fracture K_I and K_{II} for particle modified resins S14, S15 and S16 samples (n=4) subjected to loading in three loading angles (0°,45° & 90°).

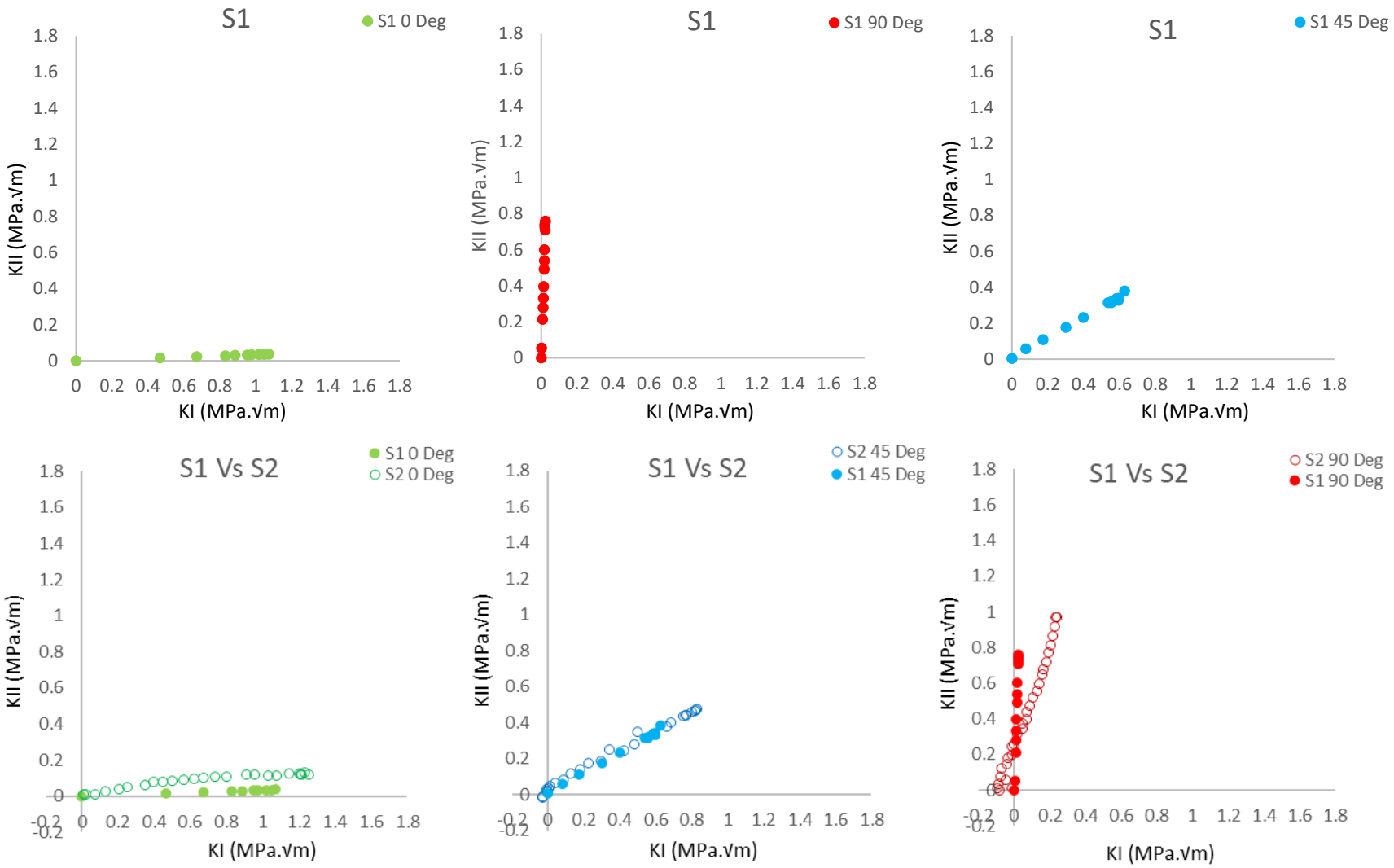

Figure 6.17 - SIF up to Fracture K_I Vs K_{II} for unmodified S1 and particle modified resin samples S2 subjected to loading in three loading angles (0°, 45° & 90°)

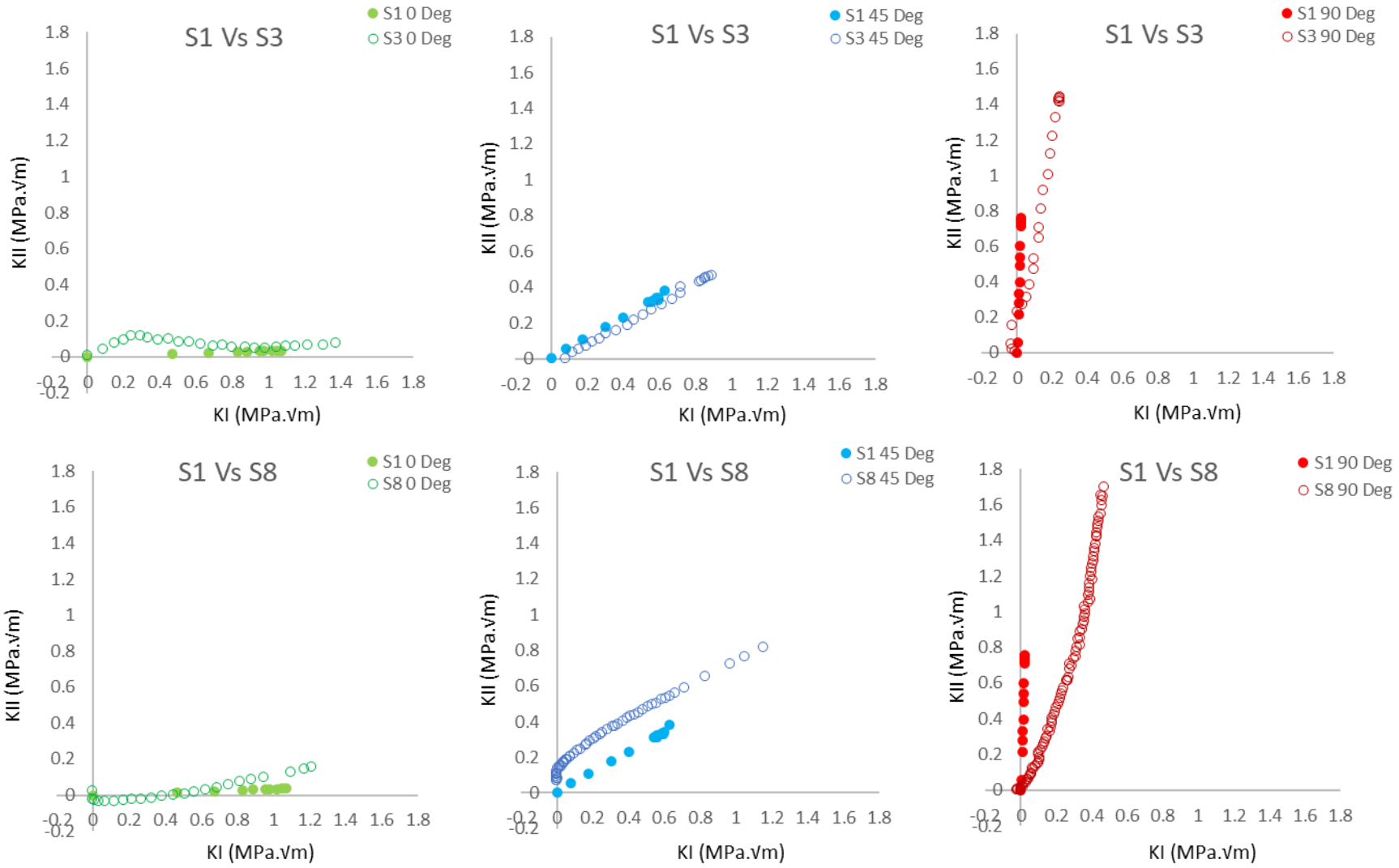

Figure 6.18 - SIF up to Fracture K_I Vs K_{II} for unmodified S1 and particle modified resin samples S3 & S8 subjected to loading in three loading angles (0°, 45° & 90°)

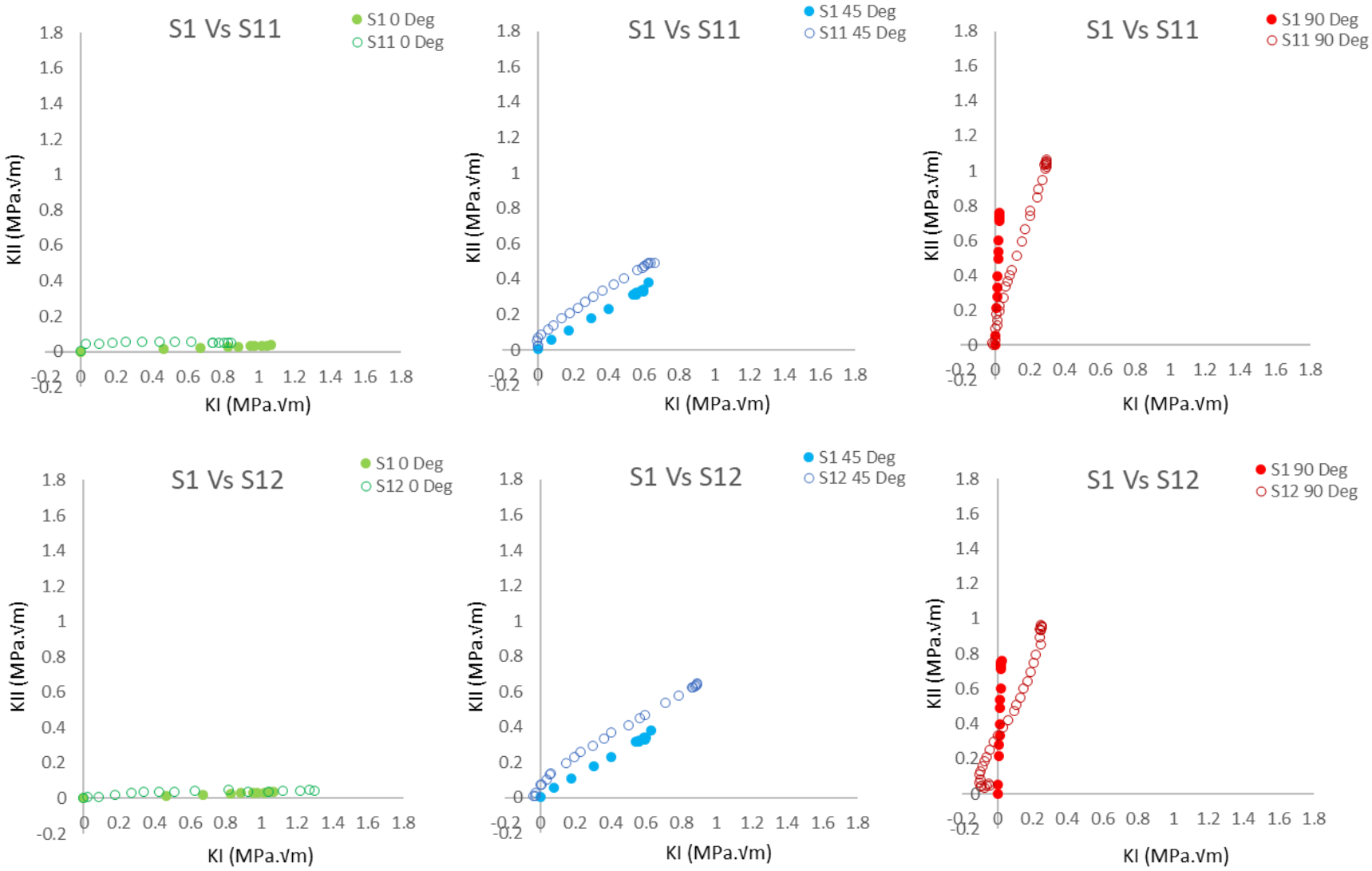

Figure 6.19 - SIF up to Fracture K_I Vs K_{II} for unmodified S1 and particle modified resin samples S11 & S12 subjected to loading in three loading angles (0°, 45° & 90°)

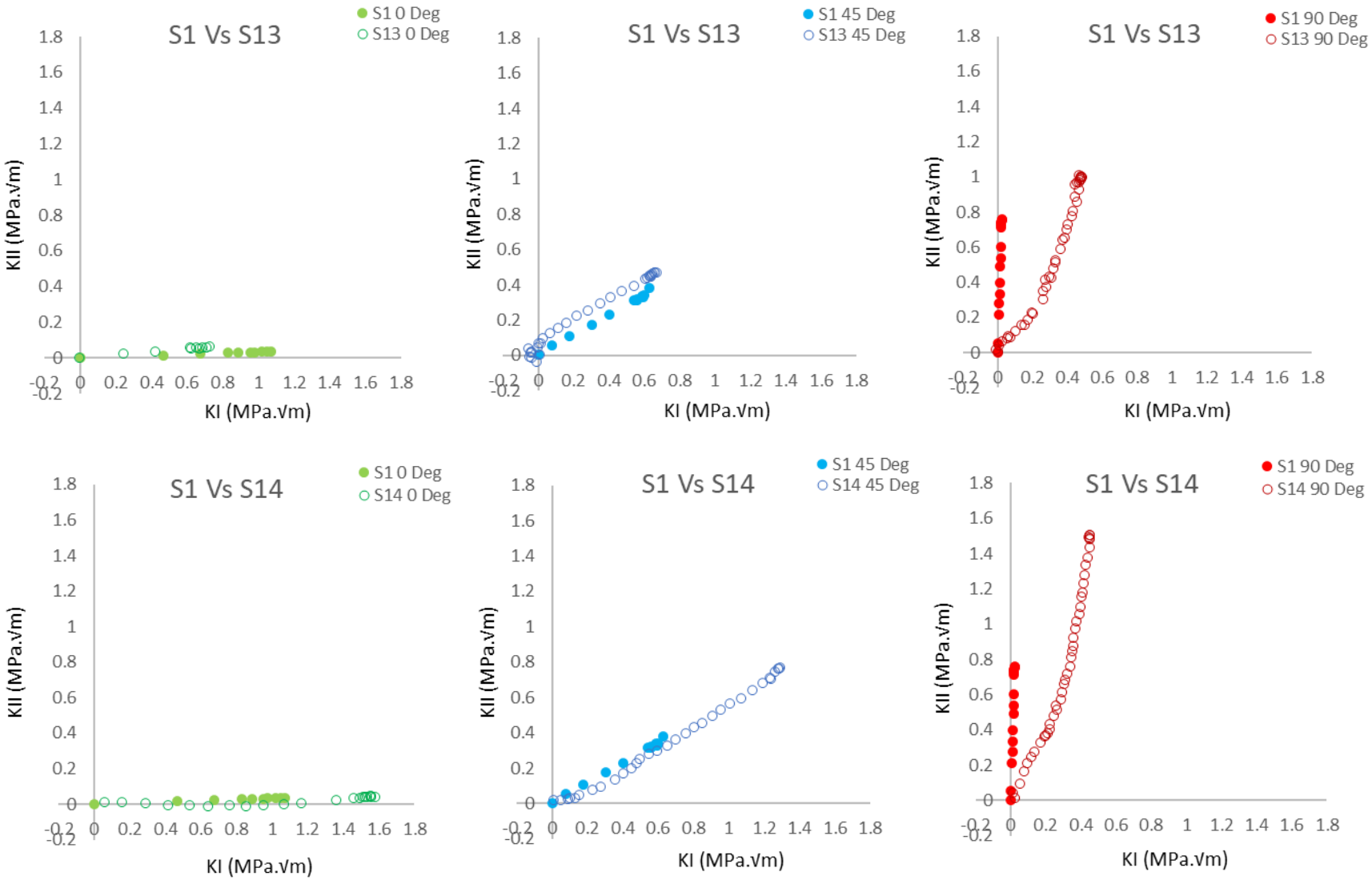

Figure 6.20 - SIF up to Fracture K_I Vs K_{II} for unmodified S1 and particle modified resin samples S13 & S14 subjected to loading in three loading angles (0°, 45° & 90°)

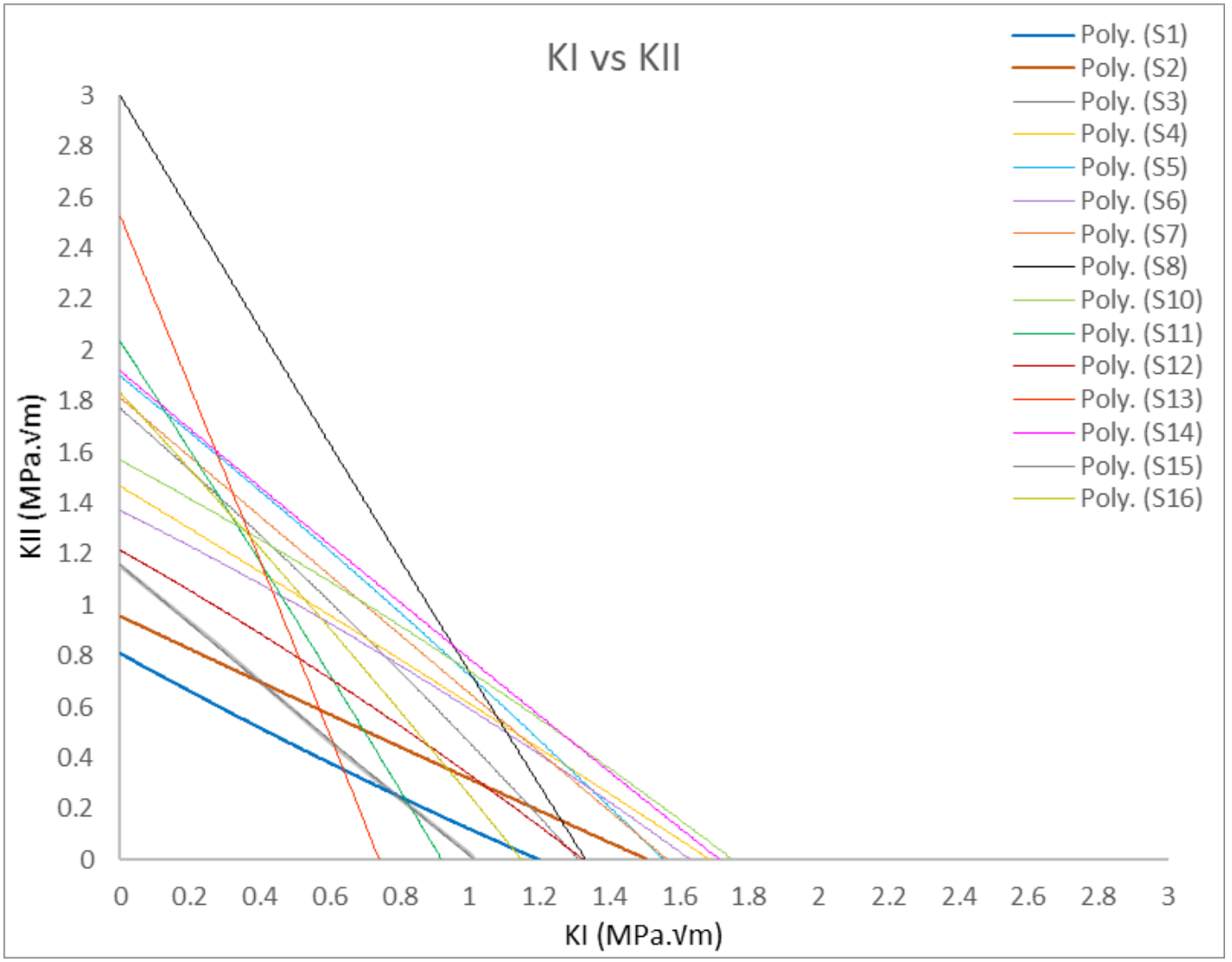

Figure 6.21 - SIF polynomial fit of K_I Vs K_{II} plot for S1, S2, S3, S4, S5, S8, S10, S11, S12, S13, S14, S15 & S16

6.4.4 SIF at fracture (K_I and K_{II}) of resin modified specimens in different weight loading configurations with materials from the same family

The results presented in this section refers to mode I, mode II and mixed mode I&II experiments at failure under mode I and mode II for specimens from the same s-formulation "family". A summary of all the different weight loading configurations with toughened epoxies from the same family is shown in Figure 6.22.

Toughened epoxies S15 (Figure 6.23c) and S16 (Figure 6.23d) modified with 5% and 10% particle weight loading (Cytec Engineering Ltd) respectively, when subjected to fracture testing by Mode I, Mode II and Mixed mode I & II testing in CTMMM grips displayed differences in stress intensity values for K_I and K_{II}.

K_{II} value of the neat resin (S1) subjected to Mode I loading (0°) was 0.00 MPa.√m. The samples that displayed K_{II} values similar to the neat resin are S15 (0.02 MPa.√m) (Figure 6.23c) and S16 (0.04 MPa.√m) (Figure 6.23d). Notably, K_I values of S-formulation samples S15 (1.0 MPa.√m) (Figure 6.23c) & S16 (1.1 MPa.√m) (Figure 6.23d) differ in comparison to the neat resin (1.2 MPa.√m) .

K_{II} value of the neat resin (S1) subjected to mixed mode I & II loading (45°) was 0.36 MPa.√m. The samples that displayed K_{II} values different to the neat resin are S15 (0.42 MPa.√m) (Figure 6.23c) and S16 (0.57 MPa.√m) (Figure 6.23d).

Notably, K_I values of S-formulation samples S16 (0.85 MPa.√m) (Figure 6.23d) display differences in comparison to the neat resin (0.63 MPa.√m). Formulation samples S15 (0.64 MPa.√m) (Figure 6.23c) displayed K_I values that are similar to the neat resin (0.63 MPa.√m).

K_{II} value of the neat resin (S1) (Figure 6.23a) subjected to mode II loading (90º) was 0.81 MPa.√m. Notably, S-formulation specimen S15 (0.84 MPa.√m.) (Figure 6.23c) displayed

similarities with the neat resin (S1) (Figure 6.23a) whereas none of the S-Formulation samples displayed K_I values similar to the neat resin (-0.02 MPa.√m).

Toughened epoxies of the S4 family, named as S15 (Figure 6.23c) and S16 (Figure 6.23d) were further modified with 5% and 10% particle weight loading (Cytec Engineering Ltd) respectively. When S15 and S16 were subjected to fracture testing by Mode I, Mode II and Mixed mode I&II testing, differences in stress intensity values (K_I and K_{II}) in 5% (S15) (Figure 6.23c), 10% (S16) (Figure 6.23d) and 14% (S4) (Figure 6.23b) particle loading modifications were observed.

Mode I failure of s-formulation specimens were characterised by extracting K_I values up to failure. Fold changes in K_I values for different specimen's relative to the neat specimen (S1) (Table 6.7) displayed that samples exhibited improved fracture toughness (Figure 6.22).

At 0° loading angle (Mode I failure) all specimens displayed marginal improvement in fracture toughness with specimens S15 and S16 displaying no changes in resistance. S4 displayed the highest SIF (K_I) and S15 displaying lowest SIF (K_I).

K_{II} value of the particle toughened resin (S4) (Figure 6.23b) subjected to Mode I loading (0°) was 0.03 MPa.√m. The samples that displayed K_{II} values similar to the S4 are S15 (0.02 MPa.√m) (Figure 6.23c) and S16 (0.04 MPa.√m) (Figure 6.23d). Notably, K_I values of S-formulation samples S15 (1.0 MPa.√m) (Figure 6.23c) & S16 (1.1 MPa.√m) (Figure 6.23d) differ in comparison to the S4 particle toughened resin (1.65 MPa.√m) (Figure 6.23b).

K_{II} value of the particle toughened resin (S4) subjected to mixed mode I&II loading (45°) was 0.62 MPa.√m. K_{II} values displayed by S15 (0.42 MPa.√m) (Figure 6.23c) and S16 (0.57 MPa.√m) (Figure 6.23d) differ with the S4 (Figure 6.23b). Notably, K_I values of S-formulation samples S15 (0.64 MPa.√m) (Figure 6.23c) and S16 (0.85 MPa.√m) (Figure 6.23d) display differences in K_I values to the S4 particle toughened resin (1.0 MPa.√m) (Figure 6.23b).

Mode II failure of s-formulation specimens were characterised by extracting K_{II} values up to failure. Fold changes in K_{II} values for different specimen's relative to the neat specimen (S1) (Table 6.8) displayed that samples exhibited improved fracture toughness (Figure 6.22).

At 0° loading angle (Mode II failure) all specimens displayed marginal improvement in fracture toughness with specimens S4, S15 and S16 displaying small changes in resistance. S16 displayed the highest SIF (K_{II}) and S4 displaying lowest SIF (K_{II}).

K_I value of the particle toughened resin (S4) subjected to mode II loading (90°) was 0.27 MPa.√m (Figure 6.23b). The samples that displayed similar K_I values S4 particulate toughened resin are S15 (0.28 MPa.√m) (Figure 6.23c). Notably, K_{II} values of S-formulation samples S15 (0.84 MPa.√m) and S16 (1.13 MPa.√m) (Figure 6.23d) display differences in K_{II} values to the S4 particle toughened resin (1.23 MPa.√m).

Similarly, as observed in section 6.4.3 for different particles, in this section Figure 6.24-6.25 demonstrates in a different way the deviation of the crack tip behaviour from the expected loading behaviour due to the same particle and only differing in weight loading. The analysis of results in Figure 6.24-6.25 compares SIF K_I Vs K_{II} with increase loading between S1 neat resin against S4, S15 and S16 formulations. It has been established that in the previous section S1 specimen is fails in pure mode I without the influence from mode II, in mixed mode I&II influenced by mode I and mode II and in pure mode II without the influence from mode I indicates that the CTMMM induces specimen to fail in respective modes accurately. Although, the S4, S15 and S16 are loaded the same as S1, they are failing in different modes to what they have been loaded. Hence, this phenomenon can only be due the particles and weight loading changing the crack propagation mode. In Figures 6.24 and 6.25, S4, S15, and S16 exhibit deviation in mode I performance, where the greatest difference in deviation is observed in S4. Similarly, in mixed mode I&II S4, S15, S16 exhibit deviation influenced by mode II performance, where the greatest difference in deviation is observed in S4. Whereas, in mode II

S4, S15 and S16 exhibit deviation influenced by mode I performance, where both S4 and S16 have greatest difference in deviation.

Notably, S4 has the highest wl concentration of 14% and in second place S16 which has 10% wl and in last place S15 with 10% wl. The variation in the deviation between the specimens can be attributed to the weight loading percentage with marginal difference between 14% wl (S4) and 10% wl (S16).

Samples	0° (K_I) MPa.√m	Fold change at 0° loading	45° (K_I) MPa.√m$^{1/2}$	Fold change at 45° loading	90° (K_I) MPa.√m	Fold change at 90° loading
S1	**1.2**	**0**	**0.63**	**0**	**0**	**0**
S4	1.65	0.45	1	0.37	0.27	0.27
S15	1	0	0.64	0.01	0.28	0.28
S16	1.1	0	0.85	0.22	0.43	0.43

Table 6.7 - Fold changes (yellow colour) relative to neat (S1) associated with fracture toughness (K_I) of toughened modified s-formulation specimens with 14%, 5% (S15) and 10% (S16) particle weight loading.

Samples	0° (K_{II}) MPa.√m	Fold change at 0° Loading	45° (K_{II}) MPa.√m	Fold change at 45° Loading	90° (K_{II}) MPa.√m	Fold change at 90° Loading
S1	**0**	**0**	**0.36**	**0**	**0.81**	**0**
S4	0.03	0.03	0.62	0.26	1.23	0.42
S15	0.02	0.02	0.42	0.06	0.84	0.03
S16	0.04	0.04	0.57	0.36	1.13	0.32

Table 6.8 - Fold changes (yellow colour) relative to neat (S1) associated with fracture toughness (K_{II}) of toughened modified s-formulation specimens with 14%, 5% (S15) and 10% (S16) particle weight loading.

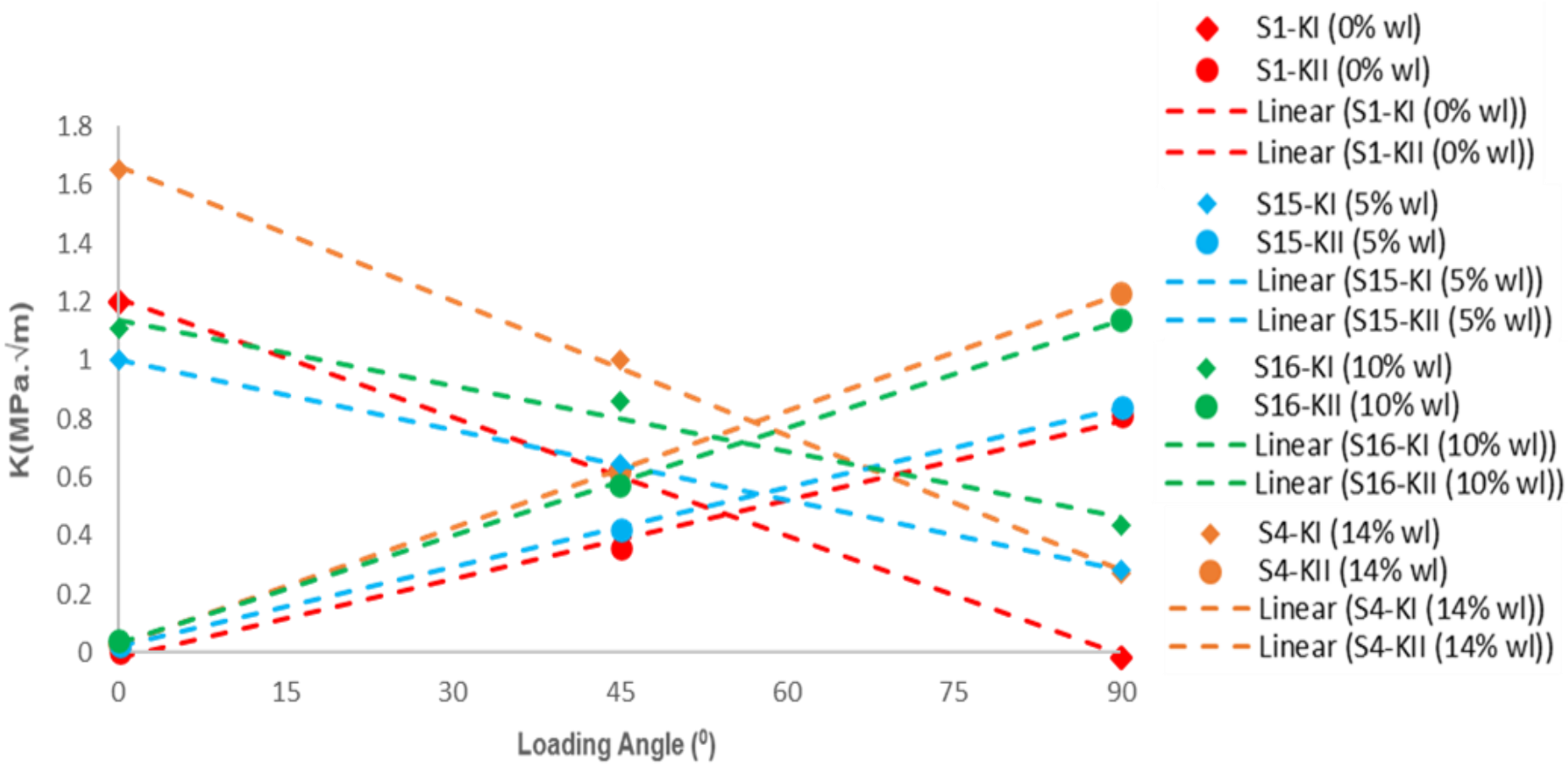

Figure 6.22 - SIF at Fracture K_I and K_{II} for particle modified resins S1, S4, S15 and S16 subjected to loading in three loading angles (0°,45° & 90°).

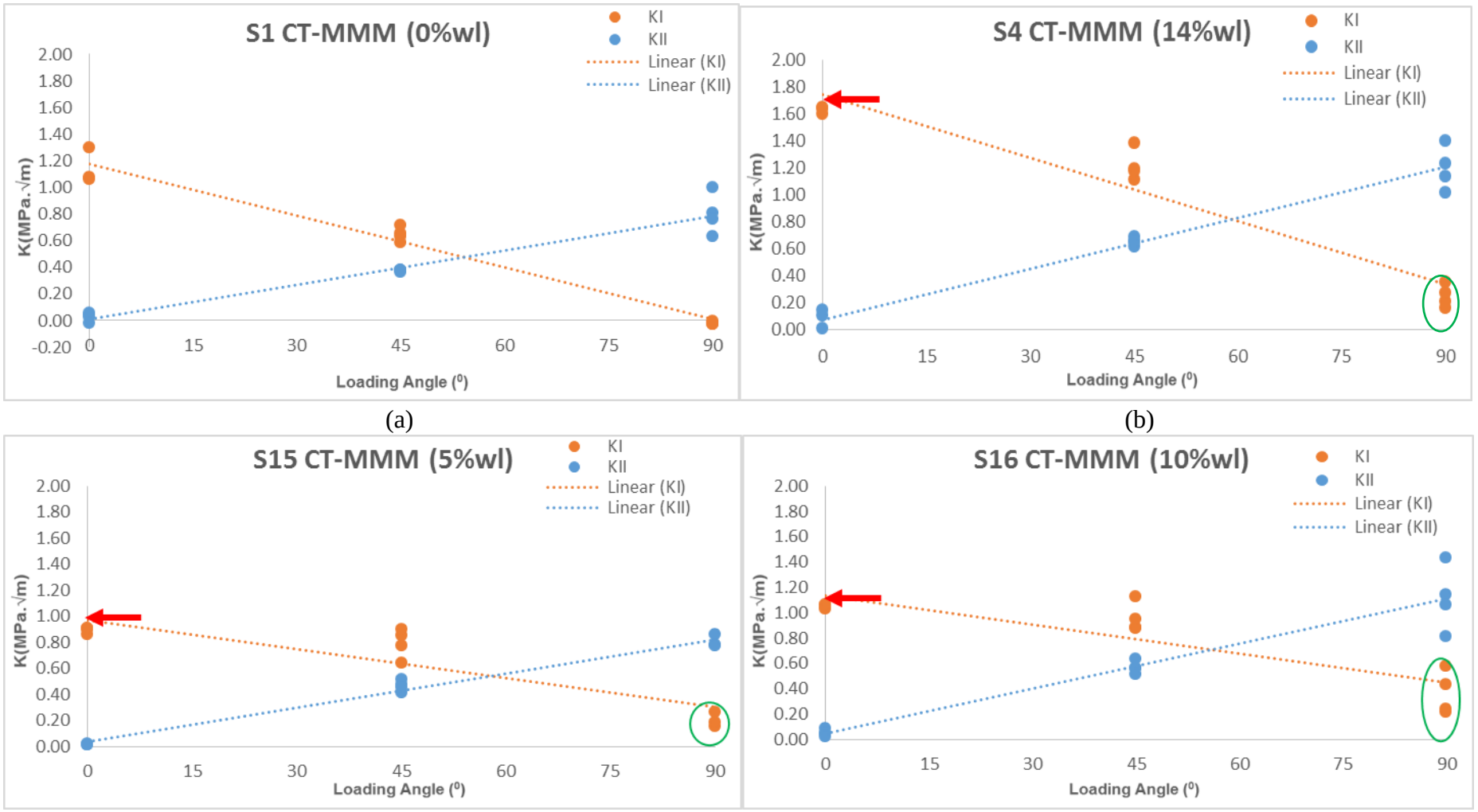

Figure 6.23 - SIF at Fracture K_I and K_{II} for unmodified S1 and particle modified resin samples S4, S15 and S16 samples (n=4) respectively subjected to loading in three loading angles (0°, 45° & 90°)

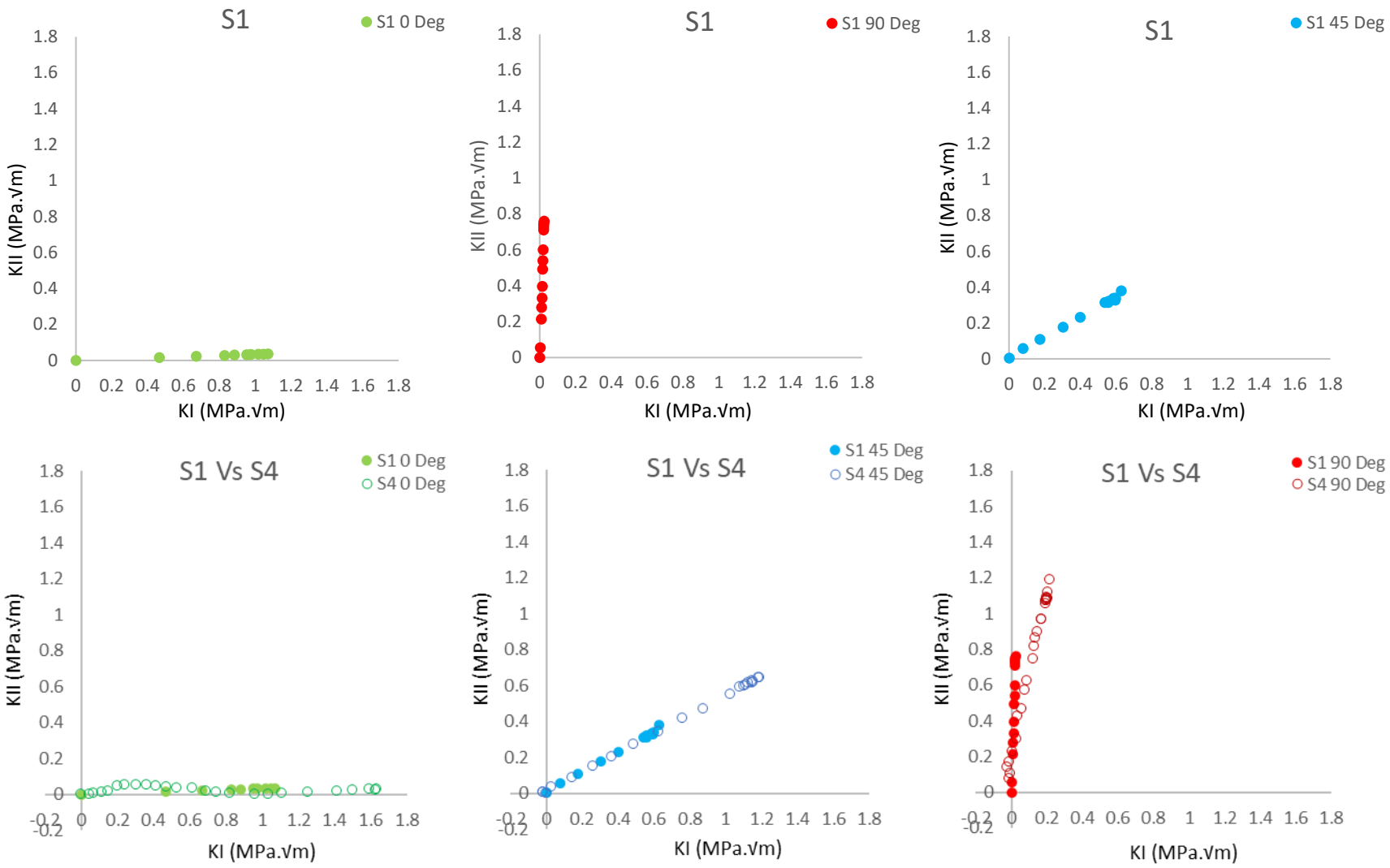

Figure 6.24 - SIF up to Fracture K_I Vs K_{II} for unmodified S1 and particle modified resin samples S1 & S4 subjected to loading in three loading angles (0°, 45° & 90°)

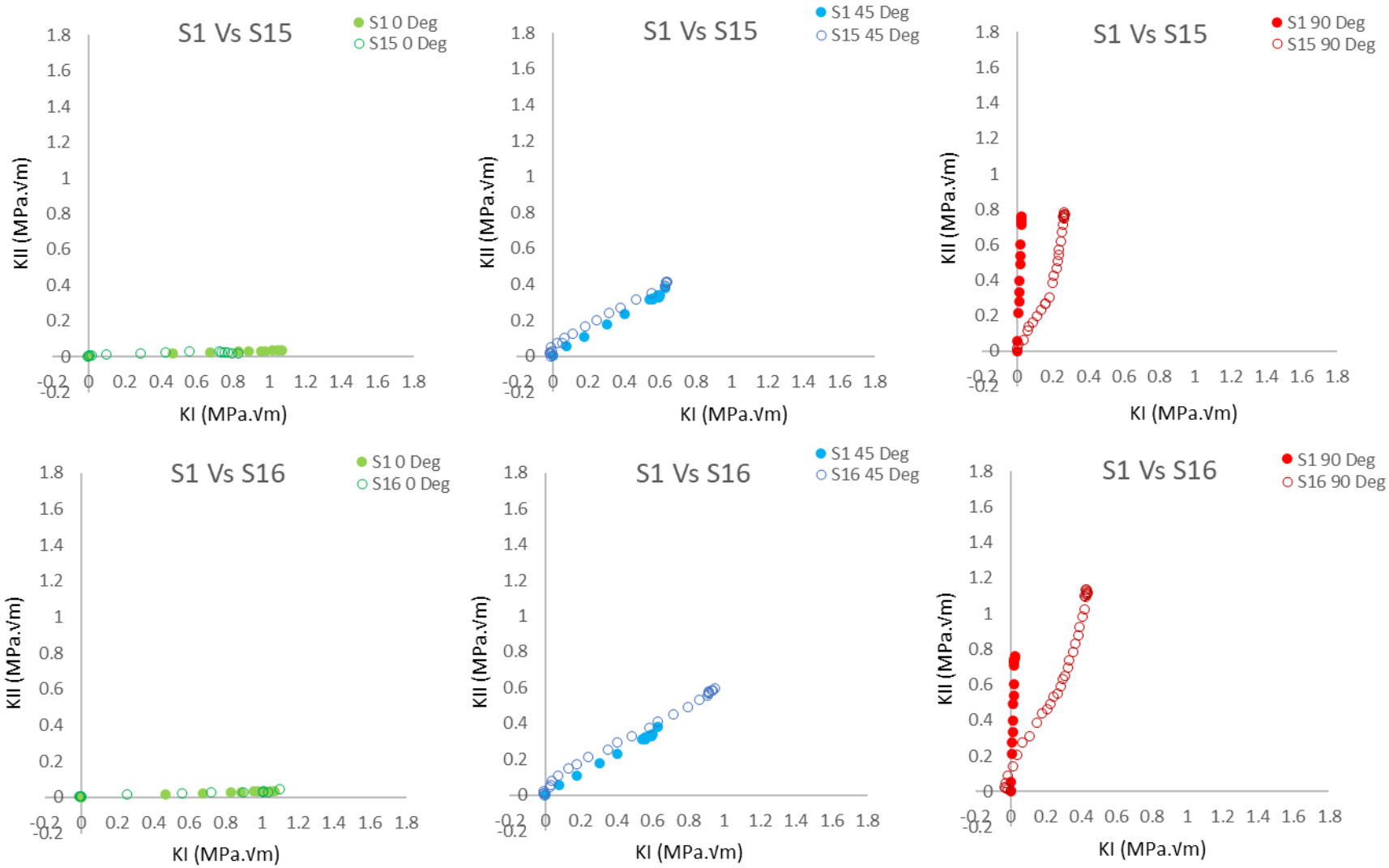

Figure 6.25 - SIF up to Fracture K_I Vs K_{II} for unmodified S1 and particle modified resin samples S15 & S16 subjected to loading in three loading angles (0°, 45° & 90°)

6.4.5 Strain energy (G_C) of resin and composite subjected to failure

The Failure of S- formulation specimens were characterised by extracting strain energy values in mode I (G_{Ic}) and mode II (G_{IIc}) of resins and resin modified composites subjected to failure. The differences in G_{Ic} and G_{IIc} values of the samples (S2, S3, S4, S5, S6, S7, S8, S10, S11, S12, S13, S14, S15 & S16) in comparison to Neat (S1) were plotted graphically as fold change. Fold changes in both G_{Ic} and G_{IIc} relative to the neat specimen (S1) (Table 6.9) displayed that fracture toughness was altered in resin modified composites (Figure 6.26). Resin modified composites displayed changes in strain energy values in mode I (G_{Ic}) and mode II (G_{IIc}) in comparison to their respective resin samples. Notably, specimens S8, S10, S11 and S12 showed marked decrease of mode I strain energy in (G_{Ic}) of -53, -158, -158 and -298 J/m^2 respectively. Specimens S10, S11, S12 and S13 showed marked decrease of mode II strain energy in (G_{IIc}). All the strain energy experimental values G_{Ic} and G_{IIc} presented in this section was provided by Cytec Industries Ltd to compare between composite and resin

	Resin G_{IIc}	Fold Change G_{IIc} Resin	G_{II} Composite	Fold Change G_{IIc} Composite	Resin G_{Ic}	Fold Change G_{Ic} Resin	G_{I} Composite	Fold Change G_{Ic} Composite
S1	193	0	928	0	349	0	280.2016	0
S2	243	50	1033	105	462	113	367.7646	88
S3	574	382	2417	1489	553	203	350.252	70
S4	426	233	2154	1226	689	339	612.941	333
S5	794	602	2294	1366	612	263	718.0166	438
S6	343	150	1944	1016	655	306	332.7394	53
S7	550	357	1891	963	636	286	595.4284	315
S8	874	681	876	-53	458	109	297.7142	18
S10	550	357	771	-158	816	466	245.1764	-35
S11	410	217	771	-158	199	-150	245.1764	-35
S12	285	92	630	-298	444	95	192.6386	-88
S13	264	72	1086	158	141	-208	262.689	-18
S14	632	439	1291	363	769	420	350.252	70
S15	256	63			240	-109		
S16	380	188			324	-25		

Table 6.9 - Strain energy in mode I (G_{Ic}) and in mode II (G_{IIc}) in resin and resin containing composite.

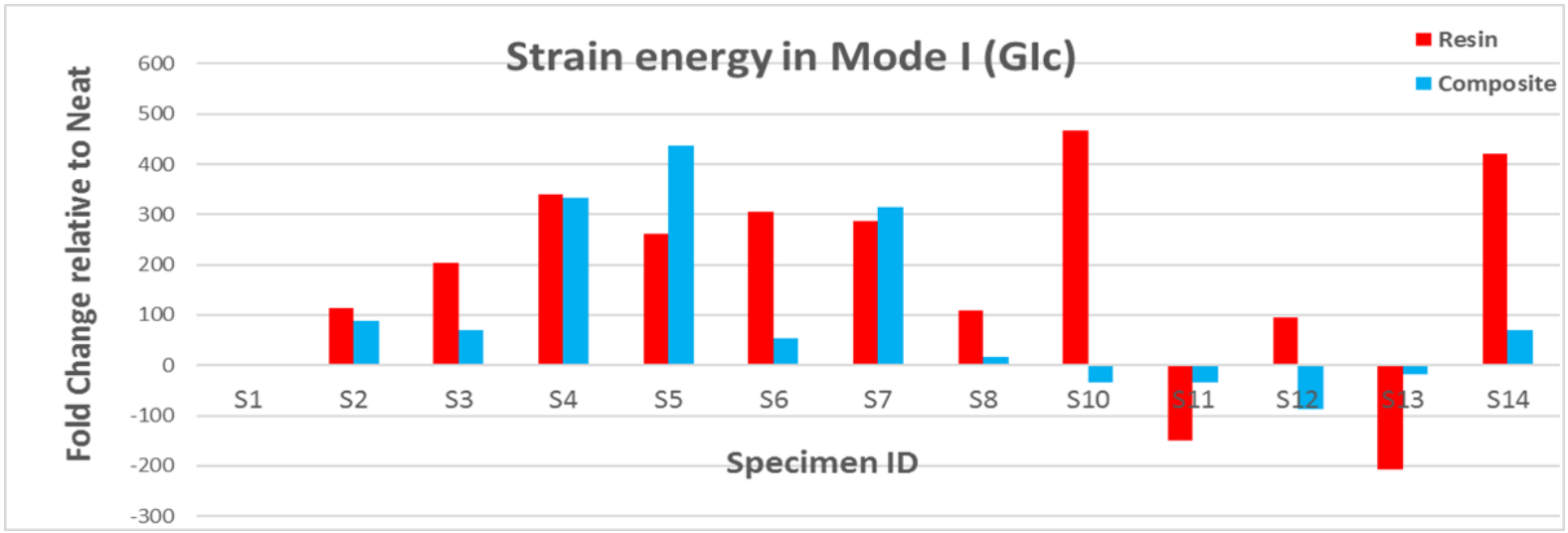

(a)

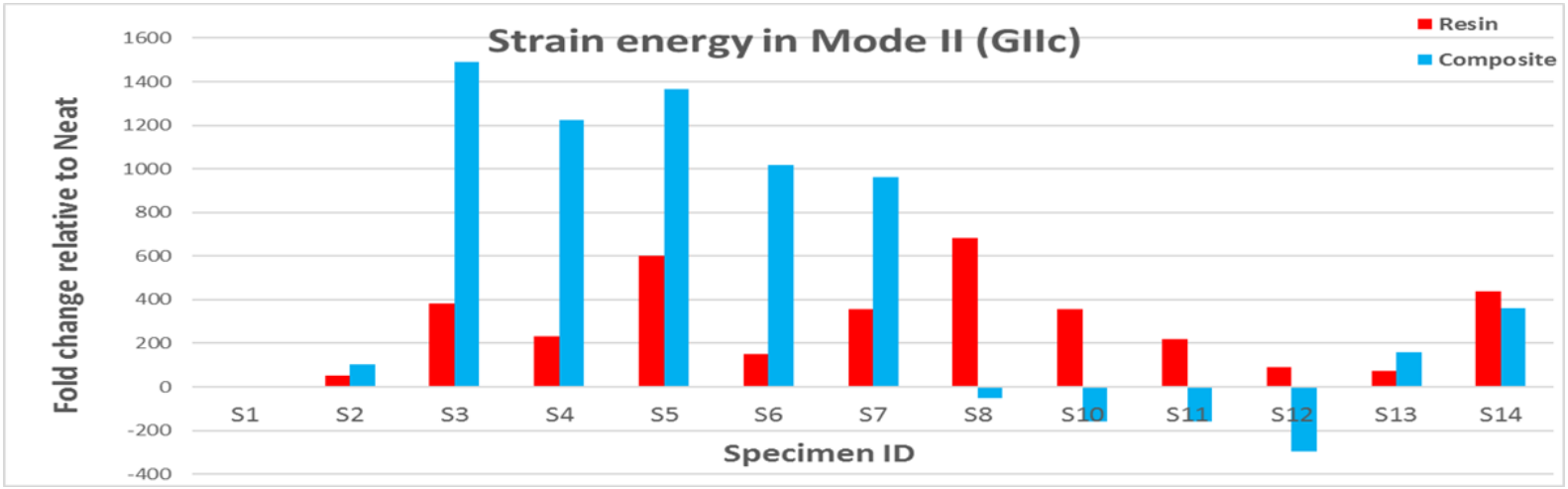

(b)

Figure 6.26 - Strain energy in mode I (G_{Ic}) (a) and in mode II (G_{IIc}) (b) in resin and resin containing composites.

6.5 Discussion

Results obtained in Chapter 5, by studying the fracture behaviour of toughened unmodified F-Formulation samples showed that the toughened epoxies behave very differently in mode I, mode II and mixed mode I & II. These findings suggest that variations in fracture behaviour are influenced by pin loading constraints and may be altered by particle introduction in the toughened resin system. Findings revealed that the CT-MMM grips facilitated fracture testing in 'pure' mode I, 'pure' mode II and 'pure' mixed mode I&II by loading in 0º, 90º and 45º loading angles respectively; this is demonstrated by the results of testing the "neat" resin, S1. Therefore, a high throughput characterisation of fracture behaviour of 15 materials shown in Figure 6.27 provided by Cytec Engineering Ltd was conducted. Specimens were grouped as those belonging to materials made of different particle types with 14% weight loading, S4 family of specimens from materials made with same particle type but 5% and 10% weight loading for S15 and S16 specimen respectively. These specimens were labelled as S-Formulation samples and for proprietary purposes particle type and concentration were not included in the study.

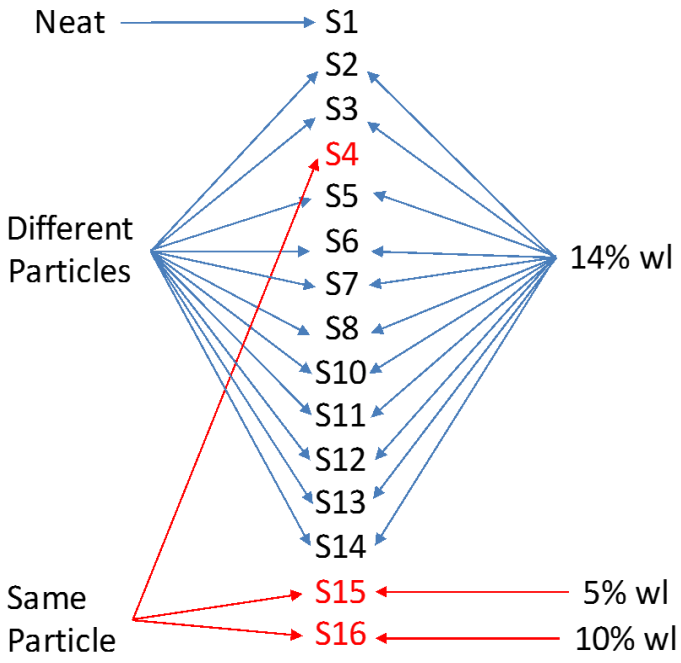

Figure 6.27 - Grouping of toughened and modified specimens tested in the CT-MMM grips.

6.5.1 SIF at fracture in loading and behaviour up to failure in K_I & K_{II} in modified resins

To assess the behaviour of crack propagation in toughened modified resins, K values up to failure were extracted and fold changes in K_I and K_{II} values relative to the neat were calculated for all specimens.

All of the 14% wl s-formulation specimens display an increase in K_I values in comparison to the neat (S1) for all loading configurations suggesting that particle toughening confers resistance to Mode I loading (Figure 6.8-6.9), Mode II loading (Figure 6.11-6.12) and Mixed mode I and II loading in most specimens exhibit improved fracture toughness. However, samples S11, S13, S15 and S16 do not show resistance to Mode I dominated failure. Interestingly, S13 did not show any change compared to S1 (neat) in K_I at 45º loading angle compared to S1 (neat) and 0º loading angle suggesting that particle toughening confers resistance only in Mode II failure.

Whilst S4 showed an increase compared to S1 (neat) in K_I at 0º, 45º and 90º loading angles, specimens belonging to the same family of resins (S15 and S16) did not show any change in K_I at 0º loading angle compared to neat. This feature is notable since it suggests that despite that all the three specimens belong to resins infused with same particle type, differential fracture behaviour is not dominated by particle type, instead dominated by weight loading. The weight loading is important. Specimens S4, S15 and S16 were modified by 14%, 5% and 10% weight loading with same type particle. Therefore, it is likely that varied behaviour of resins belonging to the same family of particles is influenced more by weight loading of particles. In other terms, these findings seem to suggest that the concentration of particles determine and reflect material's resistance to fracture and loading more than particle type. One could conclude that since the specimen S4 displays maximum weight loading with 14% particle concentration, the material is able to show increased fracture toughness (K_{Imat}) at all loading angles. However,

at lesser concentrations 5% and 10% as in S15 and S16 shows no fracture toughness change due to Mode I failure.

Fracture toughness to shear (K_{IImat}) was observed to be increased in 90º loading angles for all specimens suggesting that particle toughening confers particle induced resistance to Mode II induced failure. All specimens display increase in K_{II} values in comparison to the neat (S1) suggesting that particle toughening confers marginal resistance to Mode I failure, high resistance to Mode II failure and resistance to Mixed mode I and II failure.

Strikingly, S15 and S16 belonging to the S4 family display fracture toughness profile which improves upon increasing particle weight loading concentration. S15 specimen shows very little improvement to fracture toughness at all loading angles due to 5% weight loading suggesting that particle concentration contributes to enhancing fracture toughness in toughened modified resins.

Interestingly, specimen S8 shows an increased K_I and K_{II} in all three loading angles suggesting that particle toughening improves fracture toughness to great extent in Mode II and in Mixed Mode I and II. However, particle modification could confer very little toughness increase to the dominant Mode I failure.

To study the influence of increasing load values on particle induced fracture toughness, load values that induced failure in different specimens were noted. Surprisingly, the analysis showed that S15 specimen with 5% particle loading displayed lowest resistance to load at all three loading angles.

All these evidences strongly suggest that particle concentration directly influences fracture toughness of modified resin systems.

6.5.2 SIF at fracture of resins - Stress intensity factors (K_I and K_{II}) in resin modified specimens

Well-dispersed microscopic particles have been shown to improve toughness and stiffness in resin material. When a material undergoes particle induced transformation and experiences crack propagation, stress/strain relationship is altered. Materials are normally characterised for improving tension or shear properties by either Mode I tests or Mode II tests. Strain induced stress modifications at the crack tip is assessed by extracting the SIF value (K_I) and (K_{II}) generated in Mode I, Mode II, and Mixed Mode I & II loading.

Findings in this study revealed that when toughened epoxies modified with 14% particle weight loading (Cytec Engineering Ltd) were subjected to fracture testing by Mode I, Mode II and Mixed mode I&II loading in CTMMM grips, varied stress profile was detected at crack tip of all specimens. This is quantified through the SIF. When the stress intensity factor value of the S-Formulation toughened modified resins were compared with the SIF value of neat resin at all loading angles, the SIF values (K_I &K_{II}) either reflected each other or acted independent of each other, depending on the different particles.

At 0º loading angle an increase in K_I and a decreased K_{II} value suggests fracture occurs in Mode I. However, an increased K_{II} and a decreased K_I suggests fracture in shear even though the loading is in Mode I tension. Increased K_{II} values and decreased K_I value at 90º loading angle, suggests fracture is in Mode II. Thus, this method of testing discriminates the different material behaviours well. It is interesting to note that at 45º loading angle, pure mixed mode values of K_I and K_{II} vary depending on mode dominated failure.

Focusing on the shear loading 90º for some of the particulate toughened resin it be seen that there are some unexpected behaviours in mode II performance. Taking figure 6.20 as an example, the toughened material S13 is behaving as expected in mode I and mixed mode I & II loading. However, in pure shear loading the toughened resin is behaving in mixed mode manner where there is a clear step change in SIF. It can be observed from Figure 6.20 that S13 increasing SIF in K_{II} but not in K_I. The fracture is returning to what the geometry wants to do rather than what the material is designed to do. Additionally, the increase in SIF magnitude for S13 when compared to S1, indicates that S13 is increasing in toughness. The gradient step change in S13 is the point of which the particles stop dominating in shear and specimen geometry dominates the failure mode. Therefore, S13 toughening system is not only is increasing in toughness, it is also controlling the failure of the specimen. The exact reasons for this phenomenon are unknown, since we do not know what type particles are employed. Although the step change may indicate a possible non-linear behaviour, this behaviour would most likely not show in a standardised test and at present there are no standardised test for K_{II} approaches to verify. What we do know is that we can differentiate between the material with different particles with this test method through CTMMM. The advantage in the advancement of testing with CTMMM is that we can see the effect of the particles in a high throughput rapid manner compared to other testing strategies.

6.5.3 Material performance by shear strain energy (G_{II} and K_{II}) of modified resins and composite

Shear strain energy G_{IIc} is defined as rate of energy release at the point of shear in a material loaded to fracture. Shear fracture originates in the laminar region when composites are subjected to shear loading. This is a common phenomenon in composites because they are produced in a panel form, thus making them vulnerable to shear loading such as bending.

Measurement of G_{IIc} has been used as a method to characterise crack propagation and fracture toughness in composite materials. In the current study efforts were focused to assess the differences in strain energy of toughened modified resins and composites infused with these modified resins.

Shear strain energy values obtained from S-formulation specimens subjected to failure were characterised by extracting mode I (G_{Ic}) and mode II (G_{IIc}) of resins and also resin modified composites subjected to failure. Fold changes in both G_{Ic} and G_{IIc} (Table 6.9) relative to the neat specimen (S1) show that G_{Ic} values (Figure 6.26a) were marginally altered in most composites in comparison to the resins. Surprisingly in sample S10, S11 and S13 showed a regression in strain energy pattern. Interestingly, G_{IIc} values (Figure 6.19b26b) were higher for sample S2-S7 suggesting that particle modification in resins improve the fracture resistance to failure in mode II. In lines with previous observations for G_{Ic} samples S11 and S12 showed a regression of strain energy suggesting that particle modification does not improve performance of a composite in fracture.

Notably, the S8 sample shows marginal increase of G_{Ic} value and a regression of G_{IIc} value suggesting that particle modification improves composite performance to a marginal degree only in mode I. These findings suggest that the testing methodology developed in this study is an efficient method for differentiation of fracture behaviour of different particulate formulations and could be used for efficient screening in future.

6.6 Conclusion

This chapter investigates the fracture behaviour of toughened and modified epoxies with the aim of discriminating potential methods of failure for different s-formulations. Efforts were made in studying the influence of particle toughening on material fracture toughness values loaded in mode I, mode II and mixed mode I&II using CTMMM grips.

From the results in section 6.4.1 (Figure 6.8-6.9) for specimens loaded mode I and section 6.4.2 for specimens loaded in mode II (Figure 6.11 -6.12), it was possible to observe materials with different particles behave differently. When specimens are loaded to failure in pure mode I, it is expected there will be no mode II effects. However, all specimen except the neat (S1) exhibited mode II behaviour when loaded in mode I. This can be seen numerically in the mode I fold change analysis relatively to neat resin (S1) in table 6.2. Equally when specimens are loaded to failure in pure mode II it is expected that there will be no mode I effects. However, all specimen except S10, S14 and S1 (neat) exhibited mode I when loaded in pure mode II. This can be seen in the numerically in the mode II fold change analysis relatively to neat resin (S1) in table 6.4.

Additionally, from the results evaluated in section 6.4.3 it was possible to understand that the % wl effect in the particle toughened material played a major contributary role in dominance in mode I and mode II. Furthermore, the results in section 6.4.4 identifies that it possible to observe the difference in effects of % wl loading with different material families.

In conclusion, chapter 6 indicates that it is possible to successfully evaluate material fracture toughness of toughened and modified epoxies and discriminate potential methods of failure in different s-formulations.

CHAPTER 7

Discussion of findings

Linear elastic fracture mechanics is a widely adopted method used in quantification and characterisation of resin and composites. Improving the toughness of composites gathers a lot of commercial interest, particularly for large scale production of composites that find applications in several industries such as aerospace, defence, marine, etc. Most industries use testing methodologies such as ASTM E399, BS ISO 13586:2000 and testing involves crack tip opening displacement (CTOD), single edge notch tension (SENT), R-Curves and other standard mechanical tests such as tensile testing. Most of these tests are conducted at mode I (Tension) testing where the specimens are loaded to tension and fracture behaviour was studied. Often data acquired from these experiments do not fully accurately represent changes experienced by the material and its performance in failure in actual service, resulting in losses during large scale production. Thus, it is necessary to perform advanced analysis of fracture testing of specimens in mode II (Shear) and in mode mixity to ensure that the material is subjected to quantitatively and qualitative characterization at different loading modes.

Improving fracture toughness, especially by particulate toughening mechanisms, finds a lot of commercial interest since a few reports have established that infusion of particles in the inter-laminar and intra-laminar region improves material performance by several orders of magnitude [203-205]. However, understanding the chemical and physical changes associated with particle induced toughening mechanisms in mixed mode remains incomplete. This study provides an effective approach to differentiate particle toughened resins with experimentally with SIF, the CTMMM developed in this study provides a novel experimental in pure mode I, pure mode II and pure mixed mode I&II.

Material toughness can be considered to originate from the residual strain fields that develop during loading to failure. The crack tip stress intensity induces transformation of a volume of material near the crack tip and eventually results in enhanced fracture toughness. It has been observed (Figure 5.5) that the initial process zone, prior to crack growth remains in resting state

and hence shows no variations in stress intensity. Once generated, the crack develops to the zone of transformed strain, thus inducing variations in stress intensity.

Studies performed in the current EPSRC funded CASE project were aimed to achieve a) a high through-put testing methodology to characterize fracture behaviour, b) study the influence of Mode I (Tension), Mode II (Shear) and Mixed Mode I and II in specimens loaded in 0°, 90° and 45° loading angle and c) influence of Mixed Mode I and II testing in modified and unmodified epoxies. Since literature shows that material behaviour is influenced by various factors such as grips used for testing, pin loading constraints, loading angles, shear, and tension, these variables were considered in designing experiments. In plane surface displacement of stress was studied by 2D digital image correlation and photoelasticity.

The study commenced with experiments that optimised the preparation techniques to design a novel standardised approach for fracture testing [106]. These optimisation experiments led to the development of a novel pre-crack generation rig that ensures growth of pre-crack in a consistent and a safer method, thus significantly reducing time involved in generating cracks in a specimen.

In conventional testing, different specimen geometries need testing with different grips for testing of specimen in different modes. However, the CT-MMM grip developed during this work enables specimen with different geometries to be loaded for testing in mode I, mode II and mixed mode I &II. When toughened unmodified epoxies were loaded to failure in tension (K_I) and shear (K_{II}) in different loading angles in the CT MMM grips, facture toughness values for both tension (K_I) and shear (K_{II}) could be achieved for mixed mode I&II. Thus, the CTMMM grips, that are devoid of pin loading constraints, significantly facilitate reduction of human efforts to test samples in various loading angles, thus reducing overall experimental time for industrial applications.

Toughened modified epoxies subjected to failure in CTMMM grips displayed increased toughness comparison to the neat (S1) suggesting that particle toughening confers resistance to Mode I failure, Mode II failure and Mixed mode I and II failure in most specimens subjected to tension (K_I). Increased K_{II} values in comparison to the neat (S1) suggests that particle toughening confers marginal resistance to Mode I failure, high resistance to Mode II failure and resistance to Mixed mode I and II failure.

Interestingly, specimens from the same family of resins, display varied response to fracture toughness and that increasing particle concentration proportionally increases resistance to failure and fracture toughness. Notably, the S15 specimen with 5% particle loading displayed lowest resistance to load at all three loading angles.

Differences in strain energy of toughened modified resins and composites infused with modified resins suggests that fold changes in both G_{Ic} and G_{IIc} relative to the neat specimen (S1) suggest that particle modification in resins could modify fracture resistance to failure.

Additionally, it should be noted that due to strategic importance of material chemistry relationship and its performance, the research was advised against reverse engineering and not to take any microscopic images for investigation and that the sponsoring organisation will provide material parameters required for calculation (modulus and Poisson's ratio).

As discussed in literature review, behaviour of T-stress was observed to be non-correlative between specimen tested with same material type and loading configuration and as a result was it not considered to be a part of this research investigation. Jones [56] observed that the differences in behaviour when a Mode II component was subject to a (mode I) crack growth and indicates that the toughening mechanisms present in pure mode I crack has differing efficacies between Mode I and mixed-mode I&II loading.

It is thought that the T-stress could be dominated by mode I and geometrical constraints such as material thickness and longer pre-crack length and influenced by constrained experimental

loading configuration and presents opportunity for future work in a standardised approach for T-stress evaluation of resins systems.

However, based on the multitude of experimental SIF preformed in this study, the results indicate that it is inadequate to depend only on mode I fracture toughness testing to predict mode II and mixed mode I&II performance in materials such as particulate toughened epoxies. It is believed that this is the first time the effects contributed by particle toughening has been directly attributed to its physical behaviour in mode I, mode II and mixed mode I&II that is correlated with bulk material performance.

15 different modified toughened resin formulation with different weight loading (wl) of undisclosed particles type and size and an unmodified neat resin system were found to exhibit differing fracture behaviour and fracture toughness properties. Notably, a novel accurate measuring mode I, mode II and mixed mode I&II material toughness found to clearly identify the performance enhancement and diminution as direct result of toughening mechanism for each formulation between composite and resin.

Exploring experimental mechanics techniques in this way, the long-running unresolved challenge has been made possible to move forward significantly in the field of study. The impact of translating resin to bulk material (composites) relationship provides an endless future benefit in accelerating the development and use of novel material that will benefit to society and enable rapid reduction in carbon emissions. The benefits of being able to identify comparable resin and composite performance will greatly enhance the ability to optimally select appropriate material for use without the need for including a high build safety factor during manufacturing of a composite and provide the ability to accelerate development of composite research.

It is anticipated that the findings in this study will guide and enhance understanding into toughened materials and support future resin to bulk material characterisation methodology and provide the ability to enhance material performance in advanced structures.

It is believed that the array of novel metrological methods developed in this study, and the observed behaviour of the formulated materials, can help drive further development of even tougher and more advanced material chemistry.

CHAPTER 8

Conclusions and future work

The SIF to failure was successfully measured in 15 different resin formulated specimens by parameter extraction with using DIC displacement fields combined with the Williams approach. Implemented for the first in performing a comprehensive a high throughput experimental study to accurately assess the effect of the crack tip location definition, data collected. It is expected that these studies will support industries and researchers to employ the use of experimental technique in combination with the DICITAC tool more effectively and efficiently in the future without the need to perform a multitude of experimental investigations. The findings in this study have been of great commercial importance for the sponsoring organization Cytec industries and other commercial industries due to following reasons:

- A novel pre-crack initiation tool has been developed to generate pre cracks for specimen preparation in a consistent and safe manner [169].
- An efficient methodology has been established for all aspects of specimen preparation.
- The out-of-plane effects using specimens and grips developed here have been proved to be insignificant and therefore the simpler 2D-DIC system is sufficient.
- The CTMMM grip and specimen developed and tested in this research is devoid of pin loading constraints and hence produces ‘PURE’ Mode I, ‘PURE’ Mode II and ‘PURE’ Mixed Mode I&II testing of resin systems and composites.
- Findings provide strong evidence to suggest that particle concentration influences fracture toughness of a material and hence should be considered as a vital parameter in fracture testing.
- The combined preparation and testing methodology using 2D DIC and the fracture parameter extraction methods have been demonstrated to be an efficient and effective way to screen different resin formulations.

- An array of novel metrological methods developed in this study will help discriminate fracture behaviour of the formulated materials and help drive further development of even tougher and more advanced material chemistry.

Recommendations for future work

The convincing findings in this study strongly suggest that particle concentration directly influences fracture toughness of modified resin systems. However, it is not very clear if reduced fracture toughness in specimen with 5% particle loading reflects influence of particle distribution in a resin system. It is likely that reduced particle concentration leads to uneven distribution and orientation of particles within the resin system and hence future studies should be focussed on understanding and developing methodologies to characterise effects of particle distribution.

Additionally, the newly developed novel standardised CTMMM testing for mode I, mode II and mixed mode I&II have only been studied in brittle material with LEFM conditions. The CTMMM can be modified further to employ for testing in mode I, mode III, mixed mode I&III and mixed mode I&II and with differing material.

The pre-crack technique developed for this study is sufficient for use as a tool to generate accurate pre-crack length that arrests ahead of the clamping load. However, there is much scope in understanding the relationship between material thickness and compressive load for arresting the pre-crack and tensile load require to propagate the pre-crack and would be a valuable addition to the academic field.

REFERENCES

References

1. Günay, K.A., P. Theato, and H.-A. Klok, *Standing on the shoulders of Hermann Staudinger: Post-polymerization modification from past to present.* Journal of Polymer Science Part A: Polymer Chemistry, 2013. **51**(1): p. 1-28.
2. Boeing. *787 Dreamliner Visionary Design - Composite and Advanced Composite Use*. [Boeing Internet Source] 2013 [cited 2013 01/03/2013]; 787 Dreamliner Visionary Design - Composite and Advanced Composite Use]. Available from: http://www.boeing.com/newairplane/787/design_highlights/#/visionary-design/composites/advanced-composite-use.
3. Airbus. *A350 XWB Shaping Efficiency*. Introduction to the latest technology - Airbus [Website] 2013 2013 [cited 2013 03/03/2013]; New Airbus A350 WXB]. Available from: http://www.a350xwb.com/.
4. Marks, P. *Aviation – The shape of wings to come*. Technology [The New Scientist - Aviation] 2005 29 June 2005 [cited 2013 01/03/13]; 29 June 2005:[Aviation – The shape of wings to come]. Available from: http://www.newscientist.com/article/dn7552-aviation--the-shape-of-wings-to-come.html?full=true.
5. Smith, F., *Advanced Lightweight Structures*, in *Materials Technology: Advanced Performance Materials*. 2006. p. 102-104.
6. Hayes, B.S. and L.M. Gammon, *Optical Microscopy of Fiber-Reinforced Composites*. 2010, ASM International.
7. Anderson, T.L. and T.L. Anderson, *Fracture mechanics : fundamentals and applications*. 2005, Boca Raton, Fla. ; London: Boca Raton, Fla. ; London : Taylor & Francis, 2005.
8. Gdoutos, E.E. and E.E. Gdoutos, *Fracture mechanics [electronic resource] : an introduction*, ed. I. NetLibrary. 2005, Dordrecht : Norwell, MA: Dordrecht : Springer ; Norwell, MA : Distributed in North, Central and South America by Springer, 2005.
9. Janssen, M. and M. Janssen, *Fracture mechanics [electronic resource]*, ed. J. Zuidema, et al. 2002, Delft: Delft : VSSD, 2002.
10. Amacher, R., et al., *Thin ply composites: Experimental characterization and modeling of size-effects.* Composites Science and Technology, 2014. **101**: p. 121-132.
11. Sihn, S., et al., *Experimental studies of thin-ply laminated composites.* Composites Science and Technology, 2007. **67**(6): p. 996-1008.
12. Hsieh, T.H., et al., *The toughness of epoxy polymers and fibre composites modified with rubber microparticles and silica nanoparticles.* Journal of Materials Science, 2010. **45**(5): p. 1193-1210.
13. Kim, J., et al., *Fracture toughness of CFRP with modified epoxy resin matrices.* Composites Science and Technology, 1992. **43**(3): p. 283-297.
14. Pearson, R.A. and A.F. Yee, *Toughening mechanisms in thermoplastic-modified epoxies: 1. Modification using poly(phenylene oxide).* Polymer, 1993. **34**(17): p. 3658-3670.
15. Withers, P.J., *Mechanical failure: Imaging cracks in hostile regimes.* Nat Mater, 2013. **12**(1): p. 7-9.
16. Singh, S. and I.K. Partridge, *Mixed-mode fracture in an interleaved carbon-fibre/epoxy composite.* Composites Science and Technology, 1995. **55**(4): p. 319-327.
17. Drakonakis, V.M., et al., *Matrix hybridization in the interlayer for carbon fiber reinforced composites.* Polymer Composites, 2010. **31**(11): p. 1965-1976.
18. Stevanovic, D., et al., *Effect of starting defect for interlaminar fracture testing of interlayer-toughened fiber reinforced composites.* Journal of Materials Science Letters, 2001. **20**(7): p. 629-632.
19. Bagheri, R. and R.A. Pearson, *Role of particle cavitation in rubber-toughened epoxies: 1. Microvoid toughening.* Polymer, 1996. **37**(20): p. 4529-4538.

20. Bagheri, R. and R.A. Pearson, *Role of particle cavitation in rubber-toughened epoxies: II. Inter-particle distance.* Polymer, 2000. **41**(1): p. 269-276.
21. Yahyaie, H., et al., *Toughening mechanisms of rubber modified thin film epoxy resins.* Progress in Organic Coatings, 2013. **76**(1): p. 286-292.
22. Giannakopoulos, G., K. Masania, and A.C. Taylor, *Toughening of epoxy using core–shell particles.* Journal of Materials Science, 2011. **46**(2): p. 327-338.
23. Zamanian, M., et al., *Fracture toughness of epoxy polymer modified with nanosilica particles: Particle size effect.* Engineering Fracture Mechanics, 2013. **97**(0): p. 193-206.
24. Di Pasquale, G., et al., *New high-performance thermoplastic toughened epoxy thermosets.* Polymer, 1997. **38**(17): p. 4345-4348.
25. Hayes, B.S. and J.C. Seferis, *Modification of thermosetting resins and composites through preformed polymer particles: A review.* Polymer Composites, 2001. **22**(4): p. 451-467.
26. Hsieh, T.H., et al., *The toughness of epoxy polymers and fibre composites modified with rubber microparticles and silica nanoparticles.* Journal of Materials Science, 2009. **45**(5): p. 1193-1210.
27. Pearson, R.A. and A.F. Yee, *Influence of particle size and particle size distribution on toughening mechanisms in rubber-modified epoxies.* Journal of Materials Science, 1991. **26**(14): p. 3828-3844.
28. Mao, D. *Functionalized carbon nanotubes CNTs expand epoxy applications*. [Web Article] 2011 28/02/2011 [cited 2013 01/03/2013]; Carbon Nano Tube Advancements]. Available from: http://www.electroiq.com/articles/stm/2011/02/functionalized-carbon-nanotubes-cnts-expand-epoxy-applications.html.
29. Dowling, N.E., *Mechanical behavior of materials : engineering methods for deformation, fracture, and fatigue*. 2013, Boston: Pearson.
30. Hertzberg, R.W., R.P. Vinci, and J.L. Hertzberg, *Deformation and fracture mechanics of engineering materials.* 2013.
31. Anderson, T.L., *Fracture mechanics : fundamentals and applications.* 2005.
32. Anderson, T.L. and T.L. Anderson, *Solutions manual for Fracture mechanics : fundamentals and applications*. 1991, Boca Raton: CRC Press.
33. Sun, C. and Z.H. Jin, *Fracture Mechanics*. 2012.
34. Irwin, G.R., *Analysis of stresses and strains near the end of a crack transversing a plate.* Trans. ASME, Ser. E, J. Appl. Mech., 1957. **24**: p. 361-364.
35. Griffith, A.A., *The Phenomena of Rupture and Flow in Solids.* Philosophical Transactions of the Royal Society of London. Series A, Containing Papers of a Mathematical or Physical Character, 1921. **221**(582-593): p. 163-198.
36. Rice, J.D. *Mathematical analysis in the mechanics of fracture*. 1968.
37. Kinloch, A.J., *Fracture behaviour of polymers / A.J. Kinloch and R.J. Young*, ed. R.J. Young. 1983, London: Applied Science.
38. Standard, B., *Plastic - Determination of Fracture Toughness (G_{IC} and K_{IC}) - Linear Elastic Fracture Mechanics (LEFM) Approach*. 2000, British Standard International Standard Organisation: International Standard Organisation.
39. Sih, G.C., *Strain-energy-density factor applied to mixed mode crack problems.* International Journal of Fracture, 1974. **10**(3): p. 305-321.
40. Di Leonardo, G., *Fracture toughness characterization of materials under multiaxial loading.* International Journal of Fracture, 1979. **15**(6): p. 537-552.
41. Reeder, J.R., *3D mixed-mode delamination fracture criteria - An experimentalist's perspective.* Damage Compos, 2006. **1**.
42. Scibetta, M., *Mixed Mode Brittle Fracture and Fatigue in Support to Structural Integrity Assessment of Laminar Flaws.* Procedia Materials Science, 2014. **3**: p. 847-854.
43. Krueger, R., *Virtual crack closure technique: History, approach, and applications.* Applied Mechanics Reviews, 2004. **57**(2): p. 109-143.

44. Williams, M.L., *On the stress distribution at the base of a stationary crack.* Journal of Applied Mechanics, 1957. **24**: p. 109-114.
45. Westergaard, H.M., *Bearing Pressure and Cracks.* Journal of Applied Mechanics, 1939. **61**.
46. Cotterell, B., *Notes on the paths and stability of cracks.* International Journal of Fracture Mechanics, 1966. **2**(3): p. 526-533.
47. Cotterell, B. and J.R. Rice, *Slightly curved or kinked cracks.* International Journal of Fracture, 1980. **16**(2): p. 155-169.
48. Maccagno, T.M. and J.F. Knott, *The fracture behaviour of PMMA in mixed modes I and II.* Engineering Fracture Mechanics, 1989. **34**(1): p. 65-86.
49. Gunnars, J., P. Ståhle, and T.C. Wang, *On crack path stability in a layered material.* Computational Mechanics, 1997. **19**(6): p. 545-552.
50. Fleck, N., *Crack path selection in a brittle adhesive layer.* International Journal of Solids and Structures, 1991. **27**(13): p. 1683-1703.
51. Yates, J.R., et al., *Crack paths under mixed mode loading.* Engineering Fracture Mechanics, 2008. **75**(3–4): p. 319-330.
52. DÍAz, F.A., et al., *Measuring stress intensity factors during fatigue crack growth using thermoelasticity.* Fatigue & Fracture of Engineering Materials & Structures, 2004. **27**(7): p. 571-583.
53. Tomlinson, R.A., A.D. Nurse, and E.A. Patterson, *ON DETERMINING STRESS INTENSITY FACTORS FOR MIXED MODE CRACKS FROM THERMOELASTIC DATA.* Fatigue & Fracture of Engineering Materials & Structures, 1997. **20**(2): p. 217-226.
54. Tomlinson, R.A. and E.J. Olden, *Thermoelasticity for the analysis of crack tip stress fields — a review.* Strain, 1999. **35**(2): p. 49-55.
55. Zanganeh, M., et al., *T-stress determination using thermoelastic stress analysis.* 2008.
56. A, J.S., *An experimental investigation of the fracture behaviour of particulate toughened epoxies*. 2013, University of Sheffield. p. 224.
57. Zanganeh, M., *Experimental investigation of crack paths.*, in *Mechanical Engineering*. 2009, University of Sheffield.
58. Chen, B., et al., *Crack Path Selection in Adhesively-Bonded Joints: The Role of Material Properties.* The Journal of Adhesion, 2001. **75**(4): p. 405-434.
59. Fleck, N.A., J.W. Hutchinson, and S. Zhigang, *Crack path selection in a brittle adhesive layer.* International Journal of Solids and Structures, 1991. **27**(13): p. 1683-1703.
60. Abanto-Bueno, J. and J. Lambros, *An Experimental Study of Mixed Mode Crack Initiation and Growth in Functionally Graded Materials.* Experimental Mechanics, 2006. **46**(2): p. 179-196.
61. Geubelle, P.H. and W.G. Knauss, *Crack Propagation at and Near Bimaterial Interfaces: Linear Analysis.* Journal of Applied Mechanics, 1994. **61**(3): p. 560-566.
62. Erdogan, F. and G.C. Sih, *On the Crack Extension in Plates Under Plane Loading and Transverse Shear.* Journal of Basic Engineering, 1963. **85**(4): p. 519-525.
63. Palaniswamy, K. and W.G. Knauss, *II - On the Problem of Crack Extension in Brittle Solids Under General Loading A2 - NEMAT-NASSER, S*, in *Mechanics Today*. 1978, Pergamon. p. 87-148.
64. Aliha, M.R.M., M.R. Ayatollahi, and B. Kharazi, *Mode II Brittle Fracture Assessment Using ASFPB Specimen.* International Journal of Fracture, 2009. **159**(2): p. 241-246.
65. Gol'dstein, R.V. and R.L. Salganik, *Brittle fracture of solids with arbitrary cracks.* International Journal of Fracture, 1974. **10**(4): p. 507-523.
66. Sih, G.C., *Mechanics of Fracture Initiation and Propagation: Surface and Volume Energy Density Applied as Failure Criterion*. 1991: Springer Netherlands.
67. Sih, G.C. and J.W. Ho, *Sharp notch fracture strength characterized by critical energy density.* Theoretical and Applied Fracture Mechanics, 1991. **16**(3): p. 179-214.

68. Smith, D.J., M.R. Ayatollahi, and M.J. Pavier, *The role of T-stress in brittle fracture for linear elastic materials under mixed-mode loading.* Fatigue & Fracture of Engineering Materials & Structures, 2001. **24**(2): p. 137-150.
69. Aliha, M.R.M. and M.R. Ayatollahi, *Analysis of fracture initiation angle in some cracked ceramics using the generalized maximum tangential stress criterion.* International Journal of Solids and Structures, 2012. **49**(13): p. 1877-1883.
70. Ayatollahi, M.R. and M.R.M. Aliha, *Cracked Brazilian disc specimen subjected to mode II deformation.* Engineering Fracture Mechanics, 2005. **72**(4): p. 493-503.
71. Ayatollahi, M.R., M.R.M. Aliha, and H. Saghafi, *An improved semi-circular bend specimen for investigating mixed mode brittle fracture.* Engineering Fracture Mechanics, 2011. **78**(1): p. 110-123.
72. Ayatollahi, M.R. and A.R. Torabi, *Tensile fracture in notched polycrystalline graphite specimens.* Carbon, 2010. **48**(8): p. 2255-2265.
73. Ayatollahi, M.R. and A.R. Torabi, *Failure assessment of notched polycrystalline graphite under tensile-shear loading.* Materials Science and Engineering: A, 2011. **528**(18): p. 5685-5695.
74. Ayatollahi, M.R., M.R.M. Aliha, and M.M. Hassani, *Mixed mode brittle fracture in PMMA—An experimental study using SCB specimens.* Materials Science and Engineering: A, 2006. **417**(1): p. 348-356.
75. Mai, Y.-W. and B. Cotterell, *On the essential work of ductile fracture in polymers.* International Journal of Fracture, 1986. **32**(2): p. 105-125.
76. Chao, Y.J., S. Liu, and B.J. Broviak, *Brittle fracture: Variation of fracture toughness with constraint and crack curving under mode I conditions.* Experimental Mechanics, 2001. **41**(3): p. 232-241.
77. Chao, Y.J. and S. Yang, *Higher order crack tip fields and its implication for fracture of solids under mode II conditions.* Engineering Fracture Mechanics, 1996. **55**(5): p. 777-794.
78. Chen, B. and D.A. Dillard, *The effect of the T-stress on crack path selection in adhesively bonded joints.* International Journal of Adhesion and Adhesives, 2001. **21**(5): p. 357-368.
79. ASTM, *ASTM D5045-99, Standard Test Methods for Plane-Strain Fracture Toughness and Strain Energy Release Rate of Plastic Materials*, in *ASTM D5045-99*. 1999, ASTM International, West Conshohocken, PA: www.astm.org.
80. Suresh, S., et al., *Mixed-Mode Fracture Toughness of Ceramic Materials.* Journal of the American Ceramic Society, 1990. **73**(5): p. 1257-1267.
81. Kinloch, A.J., et al., *The mixed-mode delamination of fibre composite materials.* Composites Science and Technology, 1993. **47**(3): p. 225-237.
82. Tay, T.E., J.F. Williams, and R. Jones, *Characterisation of pure and mixed mode fracture in composite laminates.* Theoretical and Applied Fracture Mechanics, 1987. **7**(2): p. 115-123.
83. Pawliska, P., H.A. Richard, and P. Diekmann, *The behaviour of cracks in elastic-plastic materials under plane normal and shear loadings.* International Journal of Fracture, 1993. **62**(1): p. 43-54.
84. Brown, E.N., P.J. Rae, and C. Liu, *Mixed-mode-I/II fracture of polytetrafluoroethylene.* Materials Science and Engineering: A, 2007. **468–470**(0): p. 253-258.
85. Choupani, N., *Experimental and numerical investigation of the mixed-mode delamination in Arcan laminated specimens.* Materials Science and Engineering: A, 2008. **478**(1–2): p. 229-242.
86. Greer Jr, J.M., S.E. Galyon Dorman, and M.J. Hammond, *Some comments on the Arcan mixed-mode (I/II) test specimen.* Engineering Fracture Mechanics, 2011. **78**(9): p. 2088-2094.
87. Biner, S.B., *Fatigue crack growth studies under mixed-mode loading.* International Journal of Fatigue, 2001. **23, Supplement 1**(0): p. 259-263.
88. Cloud, G.L., *Optical methods of engineering analysis*. 1998, Cambridge [u.a.: Cambridge Univ. Press.

89. Sutton, M.A., et al., *Determination of displacements using an improved digital correlation method.* Image and Vision Computing, 1983. **1**(3): p. 133-139.
90. Michael A. Sutton, J.-J.O., Hubert W. Schreier, *Image Correlation for Shape, Motion and Deformation Measurements - Basic Concepts, Theory and Applications*. 1 ed. 2009: Springer. 321.
91. Sutton, M.A., et al., *Three-dimensional digital image correlation to quantify deformation and crack-opening displacement in ductile aluminum under mixed-mode I/III loading.* Optical Engineering, 2007. **46**(5).
92. Tiwari, V., M.A. Sutton, and S.R. McNeill, *Assessment of High Speed Imaging Systems for 2D and 3D Deformation Measurements: Methodology Development and Validation.* Experimental Mechanics, 2007. **47**(4): p. 561-579.
93. Reu, P., *Introduction to Digital Image Correlation: Best Practices and Applications.* Experimental Techniques, 2012. **36**(1): p. 3-4.
94. Sutton, M.A., et al., *The effect of out-of-plane motion on 2D and 3D digital image correlation measurements.* Optics and Lasers in Engineering, 2008. **46**(10): p. 746-757.
95. Adams, D.F. and D.E. Walrath, *Current Status of the Iosipescu Shear Test Method.* Journal of Composite Materials, 1987. **21**(6): p. 494-507.
96. d'Almeida, J.R.M. and S.N. Monteiro, *The Iosipescu test method as a method to evaluate the tensile strength of brittle materials.* Polymer Testing, 1999. **18**(6): p. 407-414.
97. Banks-Sills, L., M. Arcan, and H. Gabay, *A mode II fracture specimen—finite element analysis.* Engineering Fracture Mechanics, 1984. **19**(4): p. 739-750.
98. Haddadi, H. and S. Belhabib, *Use of rigid-body motion for the investigation and estimation of the measurement errors related to digital image correlation technique.* Optics and Lasers in Engineering, 2008. **46**(2): p. 185-196.
99. Hoult, N.A., et al., *Experimental accuracy of two dimensional strain measurements using Digital Image Correlation.* Engineering Structures, 2013. **46**: p. 718-726.
100. Pan, B., D. Wu, and J. Gao, *High-temperature strain measurement using active imaging digital image correlation and infrared radiation heating.* The Journal of Strain Analysis for Engineering Design, 2014. **49**(4): p. 224-232.
101. Pan, B., Z. Lu, and H. Xie, *Mean intensity gradient: An effective global parameter for quality assessment of the speckle patterns used in digital image correlation.* Optics and Lasers in Engineering, 2010. **48**(4): p. 469-477.
102. Hua, T., et al., *Evaluation of the quality of a speckle pattern in the digital image correlation method by mean subset fluctuation.* Optics & Laser Technology, 2011. **43**(1): p. 9-13.
103. Lecompte, D., et al., *Quality assessment of speckle patterns for digital image correlation.* Optics and Lasers in Engineering, 2006. **44**(11): p. 1132-1145.
104. Reu, P., *Speckles and their relationship to the digital camera.* Experimental Techniques, 2014. **38**(4): p. 1-2.
105. Reu, P., *All about Speckles: Speckle Density.* Experimental Techniques, 2015. **39**(3): p. 1-2.
106. Reu, P., *Calibration: Stereo Calibration.* Experimental Techniques, 2014. **38**(1): p. 1-2.
107. Reu, P., *All about speckles: Speckle Size Measurement.* Experimental Techniques, 2014. **38**(6): p. 1-2.
108. Reu, P., *All about Speckles: Contrast.* Experimental Techniques, 2015. **39**(1): p. 1-2.
109. Lava, P., et al., *Impact of lens distortions on strain measurements obtained with 2D digital image correlation.* Optics and Lasers in Engineering, 2013. **51**(5): p. 576-584.
110. Bornert, M., et al., *Assessment of Digital Image Correlation Measurement Errors: Methodology and Results.* Experimental Mechanics, 2009. **49**(3): p. 353-370.
111. Reu, P., *Hidden Components of 3D-DIC: Interpolation and Matching – Part 2.* Experimental Techniques, 2012. **36**(3): p. 3-4.
112. Reu, P., *Hidden Components of DIC: Calibration and Shape Function – Part 1.* Experimental Techniques, 2012. **36**(2): p. 3-5.

113. Pan, B., et al., *Systematic errors in two-dimensional digital image correlation due to lens distortion.* Optics and Lasers in Engineering, 2013. **51**(2): p. 140-147.
114. Reu, P., *Hidden Components of DIC: Calibration and Shape Function—Part 1.*
115. Reu, P., *Hidden Components of 3D-DIC: Triangulation and Post-processing – Part 3.* Experimental Techniques, 2012. **36**(4): p. 3-5.
116. Reu, P., *Stereo-Rig Design: Creating the Stereo-Rig Layout – Part 1.* Experimental Techniques, 2012. **36**(5): p. 3-4.
117. Cloud, G., *Optical Methods in Experimental Mechanics.* Experimental Techniques, 2007. **31**(6): p. 27-29.
118. Cloud, G., *Optical Methods in Experimental Mechanics.* Experimental Techniques, 2008. **32**(1): p. 13-16.
119. Cloud, G., *Optical Methods in Experimental Mechanics.* Experimental Techniques, 2008. **32**(3): p. 15-17.
120. Cloud, G., *Optical Methods in Experimental Mechanics.* Experimental Techniques, 2008. **32**(5): p. 13-16.
121. Cloud, G., *Optical Methods in Experimental Mechanics.* Experimental Techniques, 2008. **32**(6): p. 21-23.
122. Cloud, G., *Optical Methods in Experimental Mechanics.* Experimental Techniques, 2008. **32**(2): p. 11-15.
123. Cloud, G., *Optical Methods in Experimental Mechanics.* Experimental Techniques, 2009. **33**(2): p. 13-17.
124. Cloud, G., *Optical Methods in Experimental Mechanics.* Experimental Techniques, 2009. **33**(4): p. 11-14.
125. Cloud, G., *Optical Methods in Experimental Mechanics.* Experimental Techniques, 2009. **33**(1): p. 13-16.
126. Cloud, G., *Optical Methods in Experimental Mechanics.* Experimental Techniques, 2009. **33**(5): p. 13-17.
127. Cloud, G., *Optical Methods in Experimental Mechanics.* Experimental Techniques, 2010. **34**(2): p. 15-18.
128. Cloud, G., *Optical Methods in Experimental Mechanics.* Experimental Techniques, 2010. **34**(3): p. 13-17.
129. Cloud, G., *Optical Methods in Experimental Mechanics.* Experimental Techniques, 2010. **34**(4): p. 15-19.
130. Cloud, G., *Optical Methods in Experimental Mechanics.* Experimental Techniques, 2010. **34**(5): p. 11-15.
131. Cloud, G., *Optical Methods in Experimental Mechanics.* Experimental Techniques, 2010. **34**(6): p. 11-14.
132. James, M.N., et al., *Guest editorial: Special issue on characterisation of crack tip stress fields.* Fatigue and Fracture of Engineering Materials and Structures, 2012.
133. Jones, S. *An experimental investigation of the fracture behaviour of particulate toughened epoxies*. [Thesis] 2013; 224].
134. Zanganeh, M., R.A. Tomlinson, and J.R. Yates. *T-stress determination using digital image correlation*. 2008.
135. Zanganeh, M., R.A. Tomlinson, and J.R. Yates. *T-stress determination using TSA and DIC*. 2008.
136. Hild, F. and S. Roux, *Digital Image Correlation: from Displacement Measurement to Identification of Elastic Properties – a Review.* Strain, 2006. **42**(2): p. 69-80.
137. Roux, S., J. Réthoré, and F. Hild, *Digital image correlation and fracture: an advanced technique for estimating stress intensity factors of 2D and 3D cracks.* Journal of Physics D: Applied Physics, 2009. **42**(21): p. 214004.

138. Roux, S. and F. Hild, *Stress intensity factor measurements from digital image correlation: post-processing and integrated approaches.* International Journal of Fracture, 2006. **140**(1): p. 141-157.
139. Kirugulige, M.S. and H.V. Tippur, *Measurement of Fracture Parameters for a Mixed-Mode Crack Driven by Stress Waves using Image Correlation Technique and High-Speed Digital Photography.* Strain, 2009. **45**(2): p. 108-122.
140. Du, Y., et al., *Evaluation Using Digital Image Correlation of Stress Intensity Factors in an Aerospace Panel.* Experimental Mechanics, 2011. **51**(1): p. 45-57.
141. Nurse, A.D. and E.A. Patterson, *DETERMINATION OF PREDOMINANTLY MODE II STRESS INTENSITY FACTORS FROM ISOCHROMATIC DATA.* Fatigue & Fracture of Engineering Materials & Structures, 1993. **16**(12): p. 1339-1354.
142. Lopez-Crespo, P., et al., *The stress intensity of mixed mode cracks determined by digital image correlation.* The Journal of Strain Analysis for Engineering Design, 2008. **43**(8): p. 769-780.
143. McNeill, S.R., W.H. Peters, and M.A. Sutton, *Estimation of stress intensity factor by digital image correlation.* Engineering Fracture Mechanics, 1987. **28**(1): p. 101-112.
144. Nurse, A.D. and E.A. Patterson, *EXPERIMENTAL DETERMINATION OF STRESS INTENSITY FACTORS FOR CRACKS IN TURBINE DISCS.* Fatigue & Fracture of Engineering Materials & Structures, 1993. **16**(3): p. 315-325.
145. Muskhelishvili, N.I., *Some basic problems of the mathematical theory of elasticity; fundamental equations, plane theory of elasticity, torsion, and bending*. 1963, Groningen: P. Noordhoff.
146. Cotterell, B., *On fracture path stability in the compact tension test.* International Journal of Fracture Mechanics, 1970. **6**: p. 189-192.
147. Tong, J., *T-stress and its implications for crack growth.* Engineering Fracture Mechanics, 2002. **69**(12): p. 1325-1337.
148. Zakeri, M., M.R. Ayatollahi, and M. Guagliano, *A Photoelastic Study of T-stress in Centrally Cracked Brazilian Disc Specimen Under Mode II Loading.* Strain, 2011. **47**(3): p. 268-274.
149. Roux, S. and F. Hild, *Toughness measurement in brittle materials from digital image correlation.* 11th International Conference on Fracture 2005, ICF11, 2005. **7**.
150. Besnard, G., F. Hild, and S. Roux, *"Finite-Element" Displacement Fields Analysis from Digital Images: Application to Portevin–Le Châtelier Bands.* Experimental Mechanics, 2006. **46**(6): p. 789-803.
151. Yates, J.R., M. Zanganeh, and Y.H. Tai, *Quantifying crack tip displacement fields with DIC.* Engineering Fracture Mechanics, 2010. **77**(11): p. 2063-2076.
152. Zanganeh, M., *Digital Image Correlation Intensity factor and T-stress Analyser Code (DICITAC)*. 2010, University of Sheffield: University of Sheffield.
153. Materials, A.S.f.T.a., *Standard Test Method for Mode I Interlaminar Fracture Toughness of Unidirectional Fiber-Reinforced Polymer Matrix Composites*. 2007, ASTM: ASTM International.
154. Williams, J.G., J.M. Hodgkinson, and A. Gray, *The determination of residual stresses in plastic pipe and their role in fracture.* Polymer Engineering & Science, 1981. **21**(13): p. 822-828.
155. Kristof, S. and N. James, *A review on the effect of mechanical drilling on polymer nanocomposites.* IOP Conference Series: Materials Science and Engineering, 2014. **64**(1): p. 012031.
156. Savabi, G., et al., *Effect of the processing cycle on dimensional changes of heat-polymerized denture base resins.* Dental Research Journal, 2015. **12**(4): p. 301-306.
157. Cunha, L.G., et al., *INFLUENCE OF THE CURING METHOD ON THE POSTPOLYMERIZATION SHRINKAGE STRESS OF A COMPOSITE RESIN.* Journal of Applied Oral Science, 2008. **16**(4): p. 266-270.

158. ASTM, *Standard Test Method for Determining J-R Curves of Plastic Materials, ASTM International*, in *ASTM D6068-10*. 2010, www.astm.org: ASTM International, West Conshohocken, PA.
159. ASTM, *Standard Test Method for Linear-Elastic Plane-Strain Fracture Toughness KIc of Metallic Materials*, in *ASTM E399-12e3*. 2012, www.astm.org: ASTM International, West Conshohocken, PA.
160. ASTM, *Standard Test Method for Measurement of Fracture Toughness*, in *ASTM E1820-16*. 2016, www.astm.org: ASTM International, West Conshohocken, PA.
161. Harris, D.O., *Stress intensity factors for transversely loaded elastic plates and their application to predictions of crack arrest.* Engineering Fracture Mechanics, 1972. **4**(2): p. 277-294.
162. Harris, D.O. and A.S. Tetelman, *Crack arrest in transversely loaded elastic plates.* Engineering Fracture Mechanics, 1972. **4**(1): p. 93-106.
163. Pisarenko, G.S., V.P. Naumenko, and V.I. Koval, *Phenomenon of crack arrest in a plate with transverse compression zones.* Strength of Materials, 1978. **10**(1): p. 6-11.
164. Tamura, K., Tamura S, Hasjimoto, *A Precrack introducing method in CT-Specimens for measuring KIC values of brittle materials*, in *15th International Conference of Experimental Mechanics*, T. K, Editor. 2011, ICEM15: Portugal. p. 7.
165. Ewalds, H.L. and R.J.H. Wanhill, *Fracture mechanics*. 1989, London: Edward Arnold.
166. Irwin, G.R., et al., *BASIC ASPECTS OF CRACK GROWTH AND FRACTURE*. 1967, ; Naval Research Lab., Washington, D. C. p. Medium: X; Size: Pages: 82.
167. Johnson, K.L., *Contact Mechanics*. 1985, Cambridge: Cambridge University Press.
168. Tomlinson, R.A. and Z.A. Taylor, *Photoelastic materials and methods for tissue biomechanics applications.* Optical Engineering, 2015. **54**(8): p. 081208-081208.
169. Kuppusamy, N. and R.A. Tomlinson, *Repeatable pre-cracking preparation for fracture testing of polymeric materials.* Engineering Fracture Mechanics, 2016. **152**: p. 81-87.
170. N.Kuppusamy, *The effect of particulate toughening on crack path stability in resin and composite, MPhil-PhD transfer report*. 2013, University of Sheffield: Unpublished report.
171. Richard, H.A., *A new compact shear specimen.* International Journal of Fracture, 1981. **17**(5): p. R105-R107.
172. Richard, H.A. and K. Benitz, *A loading device for the creation of mixed mode in fracture mechanics.* International Journal of Fracture, 1983. **22**(2): p. R55-R58.
173. Rooke, D.P., *Compendium of stress intensity factors*. 1976, London :: H.M.S.O.
174. Carlsson, L.A., D.F. Adams, and R.B. Pipes, *Experimental Characterization of Advanced Composite Materials, Fourth Edition*. 2014: Taylor & Francis.
175. Chao, Y.J. and S. Liu, *On the failure of cracks under mixed-mode loads.* International Journal of Fracture, 1997. **87**(3): p. 201-223.
176. Tada, H., et al., *Stress Analysis Results for Common Test Specimen Configurations*, in *The Stress Analysis of Cracks Handbook, Third Edition*. 2000, ASME Press. p. 0.
177. Reboredo, M.M. and A. Vazquez, *Curing of thermosetting polymers by an external fluid.* Polymer Engineering & Science, 1995. **35**(19): p. 1521-1526.
178. Standard, B., *Fibre Reinforced Plastic Composites - Determination of Mode I Interlaminar Fracture Toughness, GIc, for Unidirectional Reinforced Materials*. 2001: International Standard Organisation.
179. Pan, B., et al., *Digital image correlation using iterative least squares and pointwise least squares for displacement field and strain field measurements.* Optics and Lasers in Engineering, 2009. **47**(7): p. 865-874.
180. Mohammad, Z.G., *Experimental investigation of crack paths*, in *Mechanical Engineering*. 2008, Univeristy of Sheffield: Univeristy of Sheffield.

181. Jones, S.A. and R.A. Tomlinson, *Investigating mixed-mode (I/II) fracture in epoxies using digital image correlation: Composite GIIc performance from resin measurements.* Engineering Fracture Mechanics, 2015. **149**: p. 368-374.
182. Hufnagel, T.C., U.K. Vempati, and J.D. Almer, *Crack-Tip Strain Field Mapping and the Toughness of Metallic Glasses.* PLOS ONE, 2013. **8**(12): p. e83289.
183. Broek, D., *Mechanisms of fracture and crack growth*, in *Elementary engineering fracture mechanics*. 1982, Springer Netherlands: Dordrecht. p. 24-66.
184. Knott, J.F., *The Science and Engineering of Fracture*, in *Advances in Fracture Resistance and Structural Integrity*, V.V. Panasyuk, et al., Editors. 1994, Pergamon: Oxford. p. 13-49.
185. Zhu, X.-K. and J.A. Joyce, *Review of fracture toughness (G, K, J, CTOD, CTOA) testing and standardization.* Engineering Fracture Mechanics, 2012. **85**(0): p. 1-46.
186. Sutton, M.A., et al., *Development and application of a crack tip opening displacement-based mixed mode fracture criterion.* International Journal of Solids and Structures, 2000. **37**(26): p. 3591-3618.
187. Banks-Sills, L., M. Arcan, and Y. Bortman, *A mixed mode fracture specimen for mode II dominant deformation.* Engineering Fracture Mechanics, 1984. **20**(1): p. 145-157.
188. Banks-Sills, L. and J. Schwartz, *Crack Paths in Adhesive Bonds*, in *Recent Advances in Experimental Mechanics: In Honor of Isaac M. Daniel*, E.E. Gdoutos, Editor. 2002, Springer Netherlands: Dordrecht. p. 225-234.
189. Banks-Sills, L. and D. Sherman, *J II fracture testing of a plastically deforming material.* International Journal of Fracture, 1991. **50**(1): p. 15-26.
190. Walker, I., *Research Methods and Statistics*. 2010: Palgrave Macmillan.
191. Field, A., *Discovering Statistics Using IBM SPSS Statistics*. 2013: SAGE Publications.
192. Quaresimin, M., et al., *Toughening mechanisms in polymer nanocomposites: From experiments to modelling.* Composites Science and Technology, 2016. **123**: p. 187-204.
193. Gojny, F.H., et al., *Influence of different carbon nanotubes on the mechanical properties of epoxy matrix composites – A comparative study.* Composites Science and Technology, 2005. **65**(15): p. 2300-2313.
194. Jansen, B.J.P., et al., *Rubber-Modified Glassy Amorphous Polymers Prepared via Chemically Induced Phase Separation. 3. Influence of the Strain Rate on the Microscopic Deformation Mechanism.* Macromolecules, 1999. **32**(19): p. 6283-6289.
195. McGrail, P.T. and S.D. Jenkins, *Some aspects of interlaminar toughening: reactively terminated thermoplastic particles in thermoset composites.* Polymer, 1993. **34**(4): p. 677-683.
196. Meijer, H.E.H. and L.E. Govaert, *Mechanical performance of polymer systems: The relation between structure and properties.* Progress in Polymer Science, 2005. **30**(8): p. 915-938.
197. Miller, K.J., *THE BEHAVIOUR OF SHORT FATIGUE CRACKS AND THEIR INITIATION PART I—A REVIEW OF TWO RECENT BOOKS.* Fatigue & Fracture of Engineering Materials & Structures, 1987. **10**(1): p. 75-91.
198. Cho, J., M.S. Joshi, and C.T. Sun, *Effect of inclusion size on mechanical properties of polymeric composites with micro and nano particles.* Composites Science and Technology, 2006. **66**(13): p. 1941-1952.
199. Fu, S.-Y., et al., *Effects of particle size, particle/matrix interface adhesion and particle loading on mechanical properties of particulate–polymer composites.* Composites Part B: Engineering, 2008. **39**(6): p. 933-961.
200. Nakamura, Y., et al., *Effect of particle size on fracture toughness of epoxy resin filled with angular-shaped silica.* Polymer, 1991. **32**(12): p. 2221-2229.
201. Nakamura, Y., et al., *Effect of particle size on the fracture toughness of epoxy resin filled with spherical silica.* Polymer, 1992. **33**(16): p. 3415-3426.
202. Schneider, C.A., W.S. Rasband, and K.W. Eliceiri, *NIH Image to ImageJ: 25 years of image analysis.* Nature Methods, 2012. **9**(7): p. 671-675.

203. Pomázi, Á. and A. Toldy, *Particle Distribution of Solid Flame Retardants in Infusion Moulded Composites.* Polymers, 2017. **9**(7): p. 250.
204. Panse, P., et al., *Mechanical properties of hybrid structural composites reinforced with nanosilica.* Polymer Composites, 2016. **37**(4): p. 1216-1222.
205. Domun, N., et al., *Improving the fracture toughness and the strength of epoxy using nanomaterials - a review of the current status.* Nanoscale, 2015. **7**(23): p. 10294-10329.

Appendix

Appendix 1

Test specimen dimensions

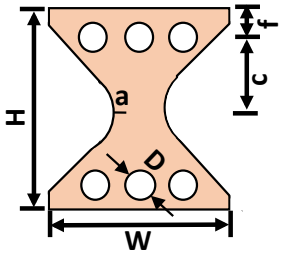

a = 15 mm
c = 37 mm
D = 8 mm
f = 24 mm
H = 98 mm
W = 84 mm

1a) Banks-Sills Arcan specimen dimensions

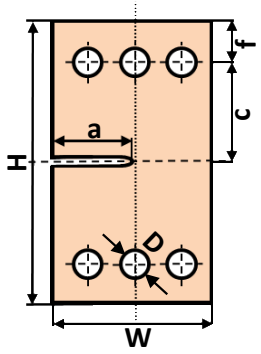

a = 54 mm
c = 27 mm
D = 17 mm
f = 37 mm
H =145 mm
W = 90 mm
Thickness = 10 mm

1b) H.A Richard CTS specimen dimensions

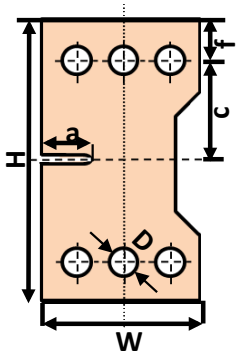

a = 8 mm
c = 23 mm
D = 6 mm
f = 5 mm
H = 56 mm
W = 30 mm
Thickness = 4 mm

1c) SJ-Arcan Mixed-Mode specimen dimensions

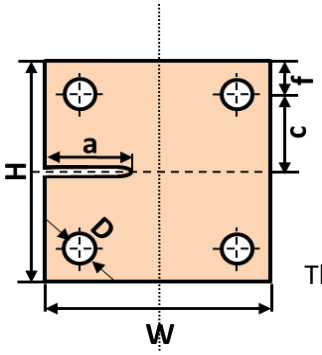

a = 18 mm
c = 10 mm
D = 6 mm
f = 5 mm
H = 40 mm
W = 40 mm
Thickness = 4 mm

1d) CTMMM Mixed-Mode specimen dimensions

Appendix 2

Pre cracking methodology paper

Engineering Fracture Mechanics 152 (2016) 81–87

Contents lists available at ScienceDirect

Engineering Fracture Mechanics

journal homepage: www.elsevier.com/locate/engfracmech

Technical Note

Repeatable pre-cracking preparation for fracture testing of polymeric materials

Nithiananthan Kuppusamy, Rachel A. Tomlinson *

Department of Mechanical Engineering, The University of Sheffield, Mappin Street, Sheffield S1 3JD, UK

ARTICLE INFO

Article history:
Received 7 December 2015
Accepted 9 December 2015
Available online 17 December 2015

Keywords:
Fracture parameter
Linear elastic fracture mechanics (LEFM)
Natural crack
Notch
Pre-crack

ABSTRACT

Currently, in order to create a sharp pre-crack in a polymeric material for fracture toughness testing, a hand-held razor blade is used. This technique produces cracks of varying angle, length, and crack-front shape. Additionally, there are considerable safety concerns regarding the handling of sharp razor blades. A repeatable, safe method of producing a consistent, sharp pre-crack of a specified length, orientation and crack front is presented here, by use of a simple custom fixture. The specimen preparation procedure has wide applicability for fracture analysis of many brittle materials.

1. Introduction

Composite materials are substituting more conventional materials in load-bearing applications in many industries in order to reduce the weight of a component and provide bespoke material properties. As a result, composite materials are being used in applications in which structural integrity of the component is critical. Therefore, the accurate determination of fracture toughness parameters is becoming increasingly important in the characterisation of the mechanical properties of a composite material in the development process. Several standards exist to assist in this testing process, for example, ASTM E399 [1], for the determination of plane strain fracture toughness of metals which was first issued in 1970. A similar procedure for testing plastic materials, ASTM D5045 [2] was issued in 1990; followed by a *Standard Test Method for Determining J–R Curves of Plastic Materials* (ASTM 6068), issued in 1996. BS ISO 13586:2000, *Plastic – Determination of Fracture Toughness (G_{IC} and K_{IC}) – Linear Elastic Fracture Mechanics (LEFM) Approach* was issued in 2000.

This long history of standards could lead a person to naively assume that performing a plane strain fracture toughness test for a polymeric material would be straightforward. A fracture toughness test requires a number of notched specimens all containing a pre-crack, of known length, which is introduced to simulate a natural crack into the material. Both the British International Standard (BS ISO) 13586:2000 [3] and American Standard Test Method (ASTM) D5045 [2], which guide testing for the plane strain fracture toughness of polymers, indicate that the pre-crack should be created naturally by tapping at the centre of the notch with a new razor blade. The standards alternatively suggest creating a pre-crack by sliding a new razor blade in either a sawing motion (side-to-side) or slicing repeatedly in a single direction. If it is not possible to create a pre-crack using the above methods, the standards warn not to apply pressure to the new razor blade on to the centre of the notch, since this could introduce residual stresses at the tip of the natural crack and effectively alter the measured K_{Ic} values [2,3]. It is suggested in the ASTM D6068 [4], that pre-cracking may be performed by induced fatigue cycles, however this is

* Corresponding author.
E-mail addresses: n.kuppusamy@sheffield.ac.uk (N. Kuppusamy), r.a.tomlinson@sheffield.ac.uk (R.A. Tomlinson).

http://dx.doi.org/10.1016/j.engfracmech.2015.12.007
0013-7944/

Nomenclature

c	critical value
G	energy release rate
K	stress intensity factor, $MPa\sqrt{m}$

time consuming and it is quite difficult to achieve a fatigue crack in a brittle material without unwanted fast fracture. Additionally, for testing of plastics (E1820), the shape of the notch is strictly defined, whereas in fracture testing of metals (ASTM E399 [1] and ASTM E1820 [5]), the production of the notch is less restrictive.

If the notch and the pre-crack are not introduced correctly and consistently then this has a detrimental effect on the fracture parameters determined, therefore accurate, repeatable specimen preparation is vital. Fracture specimen preparation is more challenging in brittle, polymer materials, since very little energy is required to propagate a crack in such materials, thus more controlled procedures are needed.

The aim of this paper is to evaluate critically the methodologies for introduction of pre-cracks recommended in the fracture testing standards for polymeric materials, particularly focusing on ease of use and repeatability. A more efficient, repeatable method to generate a pre-crack of specified length is then developed.

2. Development of methodology

It is observed in BS ISO 13586:2000 [3] that it is vitally important to use specimens containing a sharp, pre-crack in order for the Linear Elastic Fracture Mechanics (LEFM) theories to be valid. Good experimental practise dictates that several tests should be performed. The standard states that these specimens should have similar crack lengths to within 0.5 mm of each other. The current hand-held technique used to introduce a pre-crack into a test specimen utilises a razor blade and some skill is needed in avoiding manufacturing a pre-crack length in brittle materials that is too long, or fracturing the specimen completely.

Although it is possible to possess the necessary skill to propagate a pre-crack, it is still very difficult to achieve a repeatable natural crack length using a razor blade. Fig. 1(a) shows how the blade is positioned by the operator into the machined notch and tapped vertically to propagate a crack. The tapping force needed is very subjective depending on the material and the operator. This procedure requires good coordination and bi-lateral stable positioning to achieve a natural crack. Holding a razor blade at the correct angle and tapping the hammer simultaneously is challenging and has associated risks. Therefore, a prototype rig was designed to introduce some control into the procedure.

2.1. Prototype pre-crack rig

The prototype pre-crack rig was designed to aid in creating a natural crack onto the test specimen presented in Fig. 1(b). The rig clamps the specimen and holds the razor blade within the notch fixed in the x–y plane. The razor blade is positioned just touching the tip of the notch, then the top of the fixture is tapped with a hammer by the operator. The guide springs ensure that there is no rotation of the razor blade about the z axis or y axis and also ensures that no compressive force is applied to the notch surface apart from the operator's tapping force.

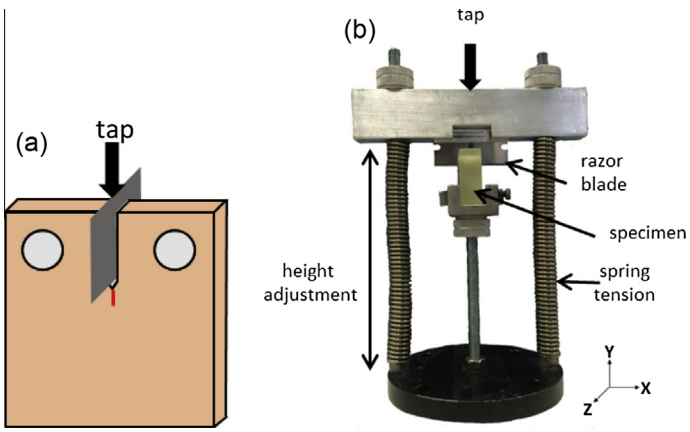

Fig. 1. (a) Pre-cracking with a razor blade and (b) prototype pre-crack rig.

Although the pre-crack rig was able to tackle the operator's coordination problems, and hence out-of-plane cracks are prevented, it was not possible to achieve complete control of the length of the pre-crack produced using this rig. The applied tapping force still depends on the operator's consistency and the material properties. Additionally, producing a repeatable pre-crack is more challenging in polymers containing toughening particles or short fibres due to the unpredictability of such material. Finally, the risks of using a razor blade have been reduced, but not completely eliminated. Therefore, an alternative method was investigated.

2.2. Further development

A technique for "growing" a pre-crack in a brittle material was proposed by Tamura et al. [6]. This general method is illustrated in Fig. 2, where a pre-crack is generated by applying loading in two directions. An initial compression load is applied in the transverse direction, normal to the surface of the specimen, ahead of the manufactured notch and a secondary tension load is applied with a tensile test frame via loading pins in the direction to open the crack. Tensile loading commences the growth of the pre-crack until the required length is achieved, the compressive load causing crack arrest. Tamura et al. described results in a variety of brittle materials but did not supply enough experimental detail to allow easy replication of the method. They also noted that crack fronts of variable shapes were observed and appeared not to be controllable.

This basic theory has been developed into a simple practical method to grow cracks of a repeatable, defined length; without the use of a razor blade, thus increasing the safety of the preparation method.

2.2.1. Application of the loads

The application of the compressive load was investigated using modified Arcan-type specimens [7,8] made from an untoughened epoxy resin used in aerospace composites. Two clamps, a G clamp and simple tool-makers clamp (T-clamp) were used to apply the compressive load and these generated very different crack front shapes. The G-clamp produced a curved crack front, whereas the T clamps generated a very straight crack front.

Fig. 3 illustrates the key differences between the G-clamp and T-clamp compressive force contact areas. The G-clamp applies a Hertzian-type contact of a ball on a plane, resulting in a small circular contact point; whereas the T-clamp is a larger, flat, rectangular contact area. Hence as the crack meets the area under load, the y-direction dimension of the T-clamp is much larger than that of the G-clamp. In some cases, the contact area of the G-clamp was not sufficiently big to arrest the crack which propagated around the contact area. Additionally, the T-clamp generated a uniform stress through the thickness of the material, hence generating a straight crack front when compared with the crack front from the G-clamp. Therefore, the T-clamp was chosen to apply the compressive loads.

3. New methodology

The new methodology requires a tool-makers clamp to apply a compressive load ahead of the notch, and a tensile load is applied to achieve the desired pre-crack length. The apparatus is shown in Fig. 4.

3.1. Determination of optimum compressive load

An experiment was conducted to determine the compressive load required for production of a pre-crack of known length. The compressive load was applied using a 0–5 N m slipper torque wrench on the T-clamp. The compressive load applied to

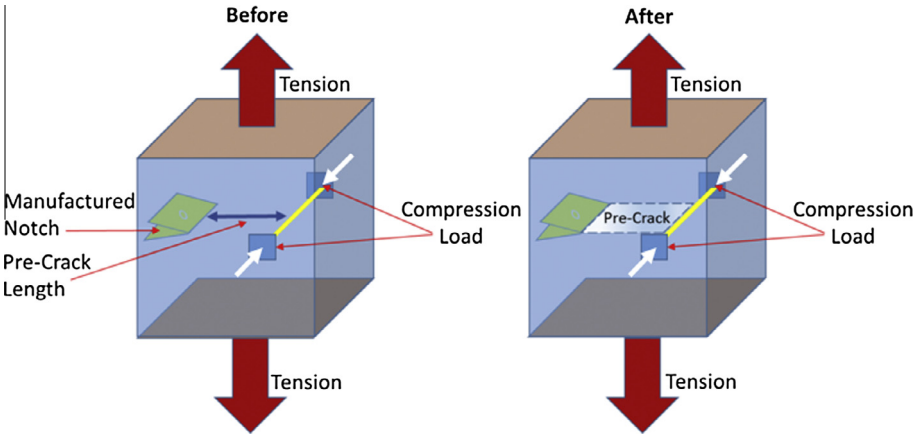

Fig. 2. Pre-crack growing principle without using a blade.

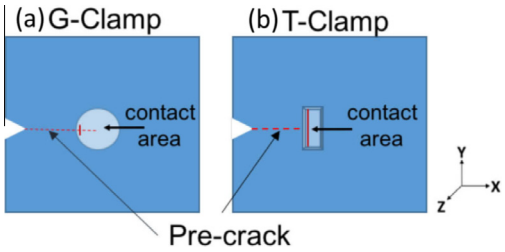

Fig. 3. Contact areas of the compressive load of (a) the G-clamp and (b) the T-clamp.

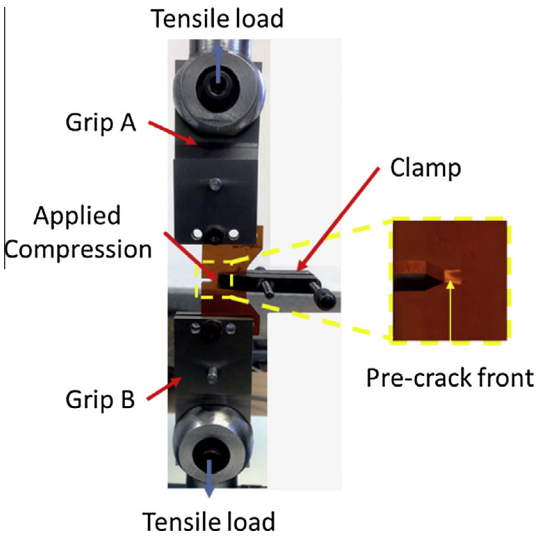

Fig. 4. Pre-crack growing principle without using a blade.

the specimen per unit torque on the clamp was determined by compressing a calibrated load cell with the clamp; 0.5 N m of torque resulted in 100 N of force.

A compressive load of 100 N was applied to an untoughened epoxy modified Arcan specimen using the apparatus in Fig. 4. The tensile load was increased slowly until the crack started to propagate and then the load was removed immediately since the crack grew rapidly. The arrest point of the crack was observed. The compressive load was increased in 100 N steps and the experiment repeated on a new specimen at each step.

The desired point of arrest of the crack was the front edge of the clamp. Fig. 5 illustrates the behaviour of the pre-crack in the modified Arcan specimens with variation of transverse compressive load. If the load was insufficient then the pre-crack either propagated fully through the specimen or arrested further than the desired point. If the load was adequate then pre-crack arrested at the desired point. If the compressive load was too large, then the tensile load needed to initiate the crack was also large and the result was that the pre-crack travelled along the axis and then bifurcated and propagated perpendicular to the pre-crack axis as shown in Fig. 5(c).

The optimum compressive load for this material using a 4 mm thick specimen was 300 N and approximately 300 N tensile load was also required to initiate the crack.

Following the removal of the compressive load, each specimen was observed in a dark field circular polariscope [9] to evaluate the effect of compressive loading. The polariscope allows a visualisation of the residual strains.

By observing Fig. 6, a qualitative comparison of the residual strains can be made in specimens where cracks have been propagated using the T-clamp method (Fig. 6(a)) and the razor tapping method (Fig. 6(b)). The specimens in Fig. 6(a and b) were manufactured using a CNC machine; the specimen in Fig. 6(c) was manufactured using traditional machining techniques. The traditional machining methods clearly introduce large residual strains, whereas the specimen in Fig. 6(a) shows that the CNC machining eliminates all machining strains. The razor tapping method introduces a small amount of residual strain at the notch, and also at the crack tip; however the compressive load in the T-clamp method does not cause any residual strain to remain in the specimen. This is important because if residual stresses remained this will have a detrimental effect on the accuracy of the subsequent fracture toughness test.

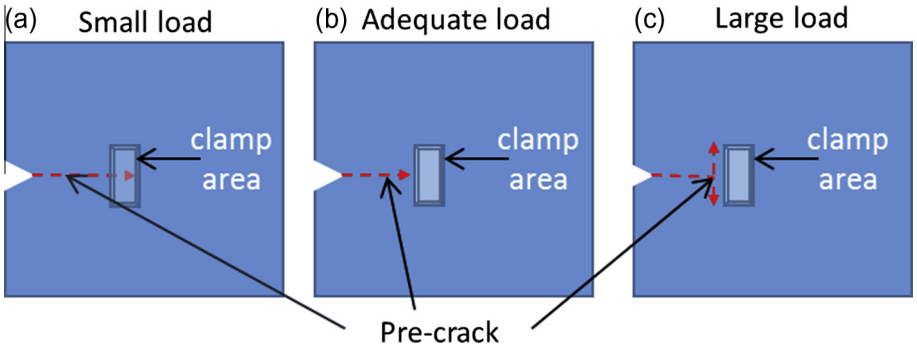

Fig. 5. An illustration of pre-crack "grown" with varying transverse compressive loads on an untoughened epoxy resin.

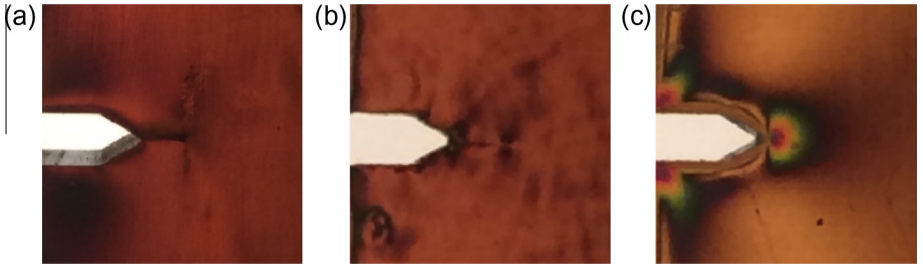

Fig. 6. Showing residual strain CNC-machined specimens with a crack introduced (a) using the T-clamp method; (b) using razor tapping; and (c) a specimen machined using traditional machining methods (notch only). The specimens were viewed in a white-light, dark field, circular polariscope [9].

3.2. Repeatability of the method

The pre-crack experiment was repeated on 40 identical untoughened epoxy modified Arcan specimens, with the front edge of the T-clamp positioned at exactly 2 mm from the notch. The T-clamp applied 300 N of compressive force and 300 N tensile force was applied to initiate the crack. The length of both sides (A and B) of the subsequent pre-crack which propagated was measured using a calibrated microscope and the results are shown in Fig. 7.

35 of the 40 pre-cracks were exactly 2 mm in length to an accuracy of 10 μm. The high repeatability is attributed to the ability of the flat faces of the clamp to apply an appropriately distributed compressive force to arrest the crack at a given distance.

4. Discussion

The specimens prepared by the several different pre-cracking methods were used in fracture toughness tests and the images of the fractured pairs of crack faces are shown in Fig. 8.

When using a razor blade, it is quite common to obtain a crack where the length varies through the thickness. Fig. 7(a) illustrates this and shows a 1.51 mm difference in crack length through the thickness.

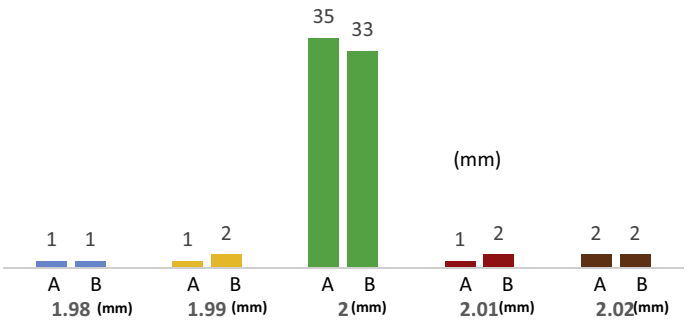

Fig. 7. An illustration of the repeatability of the pre-crack with the new methodology with measurements taken from both sides (A and B) of each specimen.

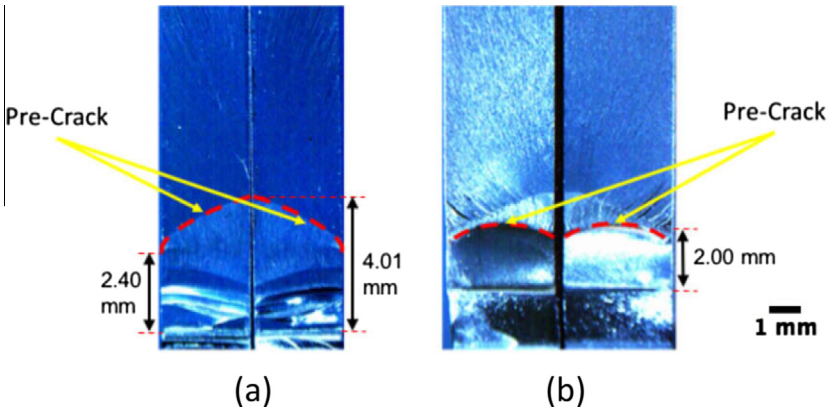

Fig. 8. An image of a specimen pre-crack generated with (a) pre-crack razor blade rig and (b) the new T-clamp method.

The T-clamp method has proved to reduce this through-thickness variation; as shown in Fig. 8 the crack lengths are the same on both sides of the specimen, with only a small curvature of the crack front. This slight curvature is common in metallic pre-cracking and is due to the constraint of the material.

If the crack length changes through the thickness, then the calculation of the fracture toughness will use an average of measured crack lengths.

The current methodology has been developed for use in Digital Image Correlation experiments [10,11]. The image of one side of the specimen is recorded at increments of load during the fracture test and strain maps determined from these images. The Williams series is then fitted to these strain maps in order to determine the stress intensity factor and fracture toughness. If the crack length is different on the front and rear faces of the specimen, then the stress intensity factor will vary. Tests are also being carried out on many different formulations of particle-toughened epoxy resins and it is good experimental practise to have identical specimen dimensions and only change the material in order to understand the material behaviour. Hence it is important to have a uniform pre-crack.

Although this method has been proved highly repeatable and controllable, the tests conducted here were for a single material of a single thickness. If the material thickness or formulation were changed, then the compressive load and tensile load required would vary. Hence it is recommended to use the procedure outlined in Section 3.1 to determine the optimum compressive load to arrest the crack and then use this load for subsequent pre-cracking. This approach was similarly conducted by Tamura et al. [6] to identify adequate loading condition for pre-cracking.

In addition to the repeatability and control afforded by the new method, razor blades are no longer needed thus reducing risks to the operator. The new method also reduces material and time wasted due to accidentally fracturing specimens during the pre-cracking process which is common with the un-controlled razor blade method.

5. Conclusion

A simple procedure for generating pre-cracks in brittle polymeric materials has been developed from the technique proposed by Tamura et al. [6]. The new methodology achieves highly repeatable, controllable pre-crack lengths and shapes in specimens for the investigation of fracture parameters, with significantly reduced waste of time and materials.

Acknowledgements

The authors would like to thank Cytec Engineered Materials and the Engineering and Physical Sciences Research Council for their financial support and also Mr Richard Kay for his assistance and support in specimen preparation.

References

[1] ASTM. Standard test method for linear-elastic plane-strain fracture toughness K_{Ic} of metallic materials. In: ASTM stand. E 399-12e3. p. 33
[2] ASTM. Standard test methods for plane-strain fracture toughness and strain energy release rate of plastic materials. In: ASTM stand. D5045, no. 14; 2014. p. 10.
[3] Standard B. Plastic – determination of fracture toughness (GIC and KIC) – linear elastic fracture mechanics (LEFM) approach. British Standard International Standard Organisation, International Standard Organisation; 2000.
[4] ASTM. Standard test method for determining J–R curves of plastic materials. In: ASTM stand. D 6068-10, no. 10. p. 8.
[5] ASTM. Standard test method for measurement of fracture toughness. ASTM stand. E 1820-13; 2013. p. 54.
[6] Tamura Tamura K, Hasjimoto S. A precrack introducing method in CT-specimens for measuring K_{IC} values of brittle materials. In: 15th International conference of experimental mechanics. ICEM15. Portugal; 2011. p. 7.
[7] Banks-Sills L, Arcan M, Bortman Y. A mixed mode fracture specimen for mode II dominant deformation. Engng Fract Mech 1984;20(1):145–57.
[8] Jones S. An experimental investigation of the fracture behavior of particulate toughened epoxies. Thesis; 2013. p. 224.

[9] Tomlinson RA, Kuppusamy N. Repeatable fracture specimen preparation for 2D and 3D digital image correlation. In: 16th International Conference of experimental mechanics. Cambridge (UK): ICEM; 2014. p. 2.
[10] Michael J-JO, Sutton Hubert A, Schreier W. Image correlation for shape, motion and deformation measurements – basic concepts. In: Theory and applications. Springer; 2009.
[11] Yates JR, Zanganeh M, Tai YH. Quantifying crack tip displacement fields with DIC. Engng Fract Mech 2010;77(11):2063–76.